2022-06

HIGH-SPEED ROTOR TIP CLEARANCE MEASUREMENTS IN A TRANSONIC COMPRESSOR

Magno, David M.

Monterey, CA; Naval Postgraduate School

NAVAL POSTGRADUATE SCHOOL

MONTEREY, CALIFORNIA

THESIS

HIGH-SPEED ROTOR TIP CLEARANCE MEASUREMENTS IN A TRANSONIC COMPRESSOR

by

David M. Magno

June 2022

Thesis Advisor: Anthony J. Gannon
Co-Advisor: Walter C. Smith

THIS PAGE INTENTIONALLY LEFT BLANK

REPORT DOCUMENTATION PAGE			*Form Approved OMB No. 0704-0188*

1. AGENCY USE ONLY *(Leave blank)*	**2. REPORT DATE** June 2022	**3. REPORT TYPE AND DATES COVERED** Master's thesis

4. TITLE AND SUBTITLE HIGH-SPEED ROTOR TIP CLEARANCE MEASUREMENTS IN A TRANSONIC COMPRESSOR	**5. FUNDING NUMBERS** JON RMNP6
6. AUTHOR(S) David M. Magno	
7. PERFORMING ORGANIZATION NAME(S) AND ADDRESS(ES) Naval Postgraduate School Monterey, CA 93943-5000	**8. PERFORMING ORGANIZATION REPORT NUMBER**
9. SPONSORING / MONITORING AGENCY NAME(S) AND ADDRESS(ES) Office of Naval Research, Arlington, VA	**10. SPONSORING / MONITORING AGENCY REPORT NUMBER**

11. SUPPLEMENTARY NOTES The views expressed in this thesis are those of the author and do not reflect the official policy or position of the Department of Defense or the U.S. Government.

12a. DISTRIBUTION / AVAILABILITY STATEMENT Approved for public release. Distribution is unlimited.	**12b. DISTRIBUTION CODE** A

13. ABSTRACT (maximum 200 words)

Performance of a gas turbine compressor is directly dependent on the size of the region between the rotor blade's tips and the surrounding casing, the tip clearance, which dynamically changes with rising rotor speed due to rotor blade radial growth from centrifugal loading. Too large a tip clearance introduces disruptive air flow that will lower compressor efficiency and lead to stall conditions, whereas too small a tip clearance will increase the risk of blade tip rubbing with the casing inner wall and may lead to catastrophic failure. This experiment is a part of a program of research that characterizes the Naval Postgraduate School Military Fan (NPSMF) in the Turbopropulsion Lab's (TPL) Transonic Compressor Rig (TCR). This study involves the design, creation, and use of two benchtop rigs with a capacitive proximity probe blade tip clearance measurement system to develop mathematical methods to post-process capacitive probe output signals for calibration and tip clearance measurements. The mathematical methods developed in this study are validated against the tip clearance measurement system manufacturer's method, showing improvement. A comparison of the different calibration rigs' resulting calibration curves is discussed. The post-process method is then applied to high-speed tip clearance measurements of the NPSMF in the TCR and the results are compared to a model.

14. SUBJECT TERMS Transonic Compressor Rig, tip clearance, tip gap, capacitive probe, frequency modulation, gas turbine, compressor, Fast Fourier Transform, signal-to-noise ratio	**15. NUMBER OF PAGES** 239
	16. PRICE CODE

17. SECURITY CLASSIFICATION OF REPORT	**18. SECURITY CLASSIFICATION OF THIS PAGE**	**19. SECURITY CLASSIFICATION OF ABSTRACT**	**20. LIMITATION OF ABSTRACT**
Unclassified	Unclassified	Unclassified	UU

NSN 7540-01-280-5500

Standard Form 298 (Rev. 2-89)
Prescribed by ANSI Std. 239-18

THIS PAGE INTENTIONALLY LEFT BLANK

Approved for public release. Distribution is unlimited.

HIGH-SPEED ROTOR TIP CLEARANCE MEASUREMENTS IN A TRANSONIC COMPRESSOR

David M. Magno
Lieutenant, United States Navy
BS, University of Washington, 2014

Submitted in partial fulfillment of the
requirements for the degree of

MASTER OF SCIENCE IN MECHANICAL ENGINEERING

from the

NAVAL POSTGRADUATE SCHOOL
June 2022

Approved by: Anthony J. Gannon
Advisor

Walter C. Smith
Co-Advisor

Garth V. Hobson
Chair, Department of Mechanical and Aerospace Engineering

THIS PAGE INTENTIONALLY LEFT BLANK

ABSTRACT

Performance of a gas turbine compressor is directly dependent on the size of the region between the rotor blade's tips and the surrounding casing, the tip clearance, which dynamically changes with rising rotor speed due to rotor blade radial growth from centrifugal loading. Too large a tip clearance introduces disruptive air flow that will lower compressor efficiency and lead to stall conditions, whereas too small a tip clearance will increase the risk of blade tip rubbing with the casing inner wall and may lead to catastrophic failure. This experiment is a part of a program of research that characterizes the Naval Postgraduate School Military Fan (NPSMF) in the Turbopropulsion Lab's (TPL) Transonic Compressor Rig (TCR). This study involves the design, creation, and use of two benchtop rigs with a capacitive proximity probe blade tip clearance measurement system to develop mathematical methods to post-process capacitive probe output signals for calibration and tip clearance measurements. The mathematical methods developed in this study are validated against the tip clearance measurement system manufacturer's method, showing improvement. A comparison of the different calibration rigs' resulting calibration curves is discussed. The post-process method is then applied to high-speed tip clearance measurements of the NPSMF in the TCR and the results are compared to a model.

THIS PAGE INTENTIONALLY LEFT BLANK

TABLE OF CONTENTS

LIST OF FIGURES

LIST OF TABLES

LIST OF ACRONYMS AND ABBREVIATIONS

AM	Additive Manufacturing
AFBP	Average Fraction of Blade Passage
BPF	Blade Pass Frequency
BTC	Blade Tip Clearance
BCTR	Benchtop Calibration and Testing Rig
COM	Common
cRIO	Compact Reconfigurable IO Module
DAS	Data Acquisition System
DRO	Digital Read Out
FBP	Fraction of Blade Passage
FM	Frequency Modulated
GND	Ground
IO	Input Output
kHz	Kilo-Hertz
MHz	Mega-Hertz
NI	National Instruments
NPS	Naval Postgraduate School
NPSMF	Naval Postgraduate School Military Fan
OPAMP	Operational Amplifier
OPR	Once Per Revolution
PFI	Programmable Free Interface
RSL	Rugged Sensor Laser
SMA	SubMiniature version A
SMB	SubMiniature version B
SOP	Standard Operating Procedure
TCR	Transonic Compressor Rig
TPL	Turbo Propulsion Laboratory
VDC	Volts Direct Current
VAC	Volts Alternating Current

THIS PAGE INTENTIONALLY LEFT BLANK

ACKNOWLEDGMENTS

I'd like to say a tremendous thank you to Dr. Anthony Gannon and Dr. Walter Smith for all their help in this research. I thank them for their advice and guidance, all the while allowing me the freedom to figure out challenges on my own, allowing me to grow and learn as an aspiring engineer. Prior to this research I had never used programs like MATLAB and ANSYS and had never worked in a machine shop. Their patience and willingness to teach me are invaluable and gave me a great starting point to take off into this research. Thank you to Mr. John Gibson, Mr. Dave Dausen, and the rest of the NPS Turbopropulsion Laboratory staff for their help and advice. Most importantly, thank you to my wonderful wife, Maria, for her unending support while I pursued my research. I could not have accomplished this major milestone without the support of all these amazing people.

THIS PAGE INTENTIONALLY LEFT BLANK

I. INTRODUCTION

A. MOTIVATION

An ongoing mission of the U.S. Navy is the constant effort to develop and enhance the performance of the systems and equipment used. Gas turbine engines are widely used on U.S. Navy ships, namely the General Electric LM2500 used in ship propulsion and the Rolls Royce AG9140 used in electrical power generation. Gas turbines are also used on U.S. Navy aviation platforms. In any attempt to optimize the performance of gas turbine engines, an engineer must understand and quantify the performance inhibitors that occur. A major design constraint of compressors faced by gas turbine designers is the blade tip clearance (BTC) that inherently causes engine performance losses if it becomes too large. The performance losses originate from air flows that are introduced from the gap region between the tips of a rotor's blades and the surrounding engine's casing. The flow of this air disrupts the main bulk axial flow of the compressor causing this performance loss. The instability of this flow may lead to stall conditions. The amount of flow disruption is directly proportional to the size of the BTC. Larger tip clearances will lessen the margin to stall of a gas turbine. Thusly, gas turbine designers look to reduce this area as much as practical to reduce its effects, though a working clearance between a rotor's blades and its surrounding casing is necessary for the engine to operate safely. The BTC dynamically decreases in size as the engine's rotor is radially strained by stresses caused by increased rotor speed. Too small a BTC will cause rubbing of a rotor's blade tip to the engine's casing which will lead to blade degradation, loss of integrity, and possibly catastrophic damage.

BTC is dependent upon the rotor's environment. In addition to radial strain of the blades from centrifugal forces, rotor material degradation and engine component degradation over engine life may also affect BTC. Furthermore, blade radial growth from high temperatures and blade deflections caused by vibrations from resonance and supersonic shock waves have a substantial effect on BTC. Therefore, a dependable means of determining BTC behavior under different conditions is required to effectively understand and determine engine performance. By identifying and fully characterizing the

BTC as it changes with varying loads and at near-stall conditions, optimization of gas turbine compressor performance can be accomplished.

This study is experimental and analytical in nature and its aim is to conduct a high-speed BTC measurement of the Naval Postgraduate School Military Fan's (NPSMF), shown in Figure 1, while also developing modified post-processing techniques for the data. This research uses a capacitive proximity probe-based BTC measurement system that principally operates via frequency modulation (FM) to develop analytical methods customized for this specific application. These methods were developed on an originally designed benchtop rig. An experimental program is created to verify the validity of the methods developed showing improvement when compared to an existing method. These methods were then used to measure the radial blade growth of the NPSMF BTC in a Transonic Compressor Rig (TCR). The experiment includes tip clearances measured at 70%, 80%, 85%, and 90% of the transonic rig's design speed at peak efficiency (near choke) flow.

Figure 1. Naval Postgraduate School Military Fan. Source: [1].

B. IMPORTANCE OF TIP CLEARANCE IN TURBOMACHINERY

There are various efficiency losses that occur due to the various flows in gas turbine machinery. Profile viscous losses along the rotor and stator blade surfaces, losses along the casing inner surface, and losses in the clearance spaces are some of the areas of flow that contribute to the efficiency losses. The required clearances within a gas turbine engine are unavoidable as there needs to be a gap between the stationary and rotary parts of an engine. This produces various secondary flows that are distinct from the main flow of air in a turbomachine. Some flows introduced in the clearances of gas turbine machinery include leakage flow at the blade tip for unshrouded blades, flow in the labyrinth region of a shrouded blade, stator root seals, and windage flows at the rotor disc walls. This study

focuses on the radial blade growth for an unshrouded rotor. Figure 2 provides a graphic displaying the location of the tip clearance for one stage of an unshrouded rotor.

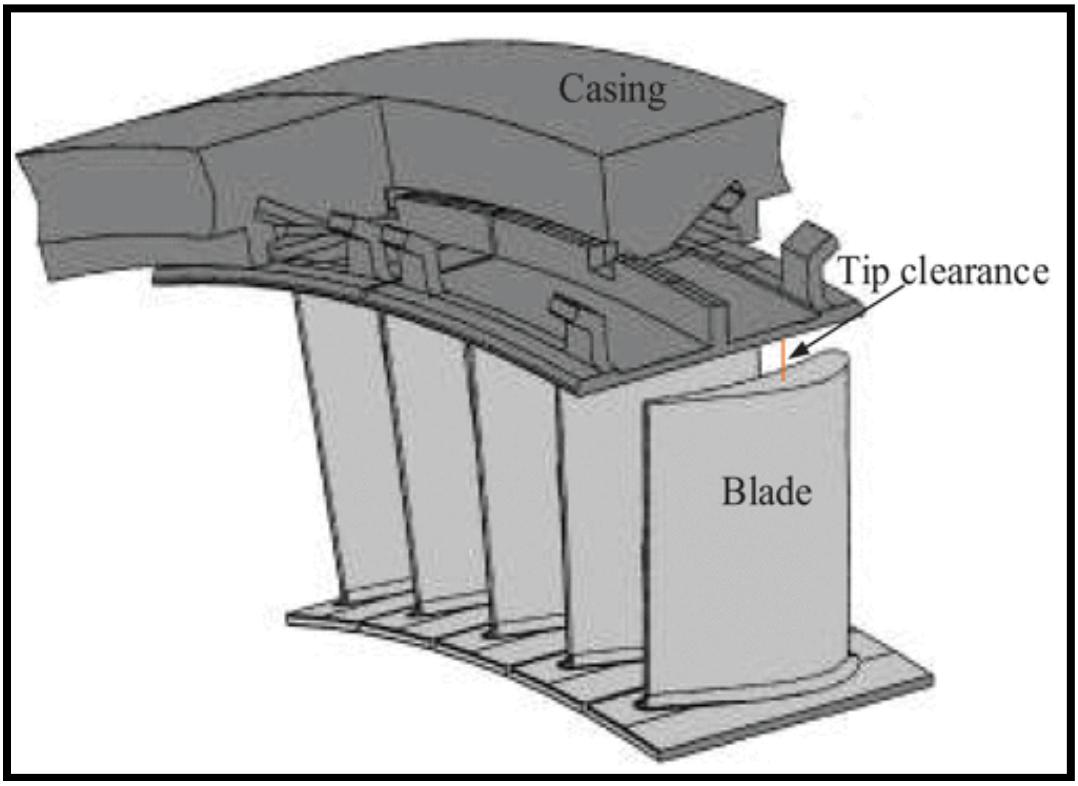

Figure 2. Location of the Tip Clearance Region of an Unshrouded Rotor Stage. Source: [2].

Leakage flows of a compressor's fan and cascade stages lower efficiency as these flows disrupt air flow due to the pressure difference of the suction and pressure side of the blade. In addition, the tip flows also reduce the margin to stall conditions as noted by both Lampart [3] and Adamczyk et al. [4]. Tip leakage losses apply to both compressors and turbines, though this experiment primarily focuses on compressors since the test rotor used is a compressor's turbofan, the NPSMF. It was found through measurements of pressure distributions along the casing of compressor rotors that tip clearance greatly effects the margin to stall due to flow instabilities developed. As this tip clearance size grew, the margin to stall lessened as noted in multiple experiments by Londoño [1], Adamczyk et al. [4], and Miller and Bailey [5].

As mentioned, the driving force behind the tip region's flow is due to a difference in pressure. As a compressor is driven by its motor, in the local region of an individual compressor blade, the side of the rotor blade in the direction of rotation experiences a relatively higher pressure than the side of the blade opposite the rotation. These are the pressure and suction sides, respectively. The tip leakage flow of the air is driven by the pressure difference of the sides of the compressor rotor blades. Leitner et al. [6].states the combination of this leakage flow with the main, axial flow of the bulk fluid causes disruption in the bulk fluid's boundary layer and flow in the main passage, which contributes to a large portion of the losses in a compressor. Figure 3 demonstrates this phenomenon for a compressor stage rotor blade. The tip flow wraps around the tip region of the rotor blade. The suction side experiences a vortex flow that is propagated by the main flow, causing blockage in the main axial flow which in turn causes flow instability, lowering the margin to stall conditions. Furthermore, the vortex created from the tip leakage will breakdown and expand as the ratio of the axial to flow to the rotor's speed decreases, blocking more area, considerably affecting the when the inception of stall will occur. An analysis of how flow originating from the tip clearance region interacts with the different air flows is explained in detail by Leitner et al. [6].

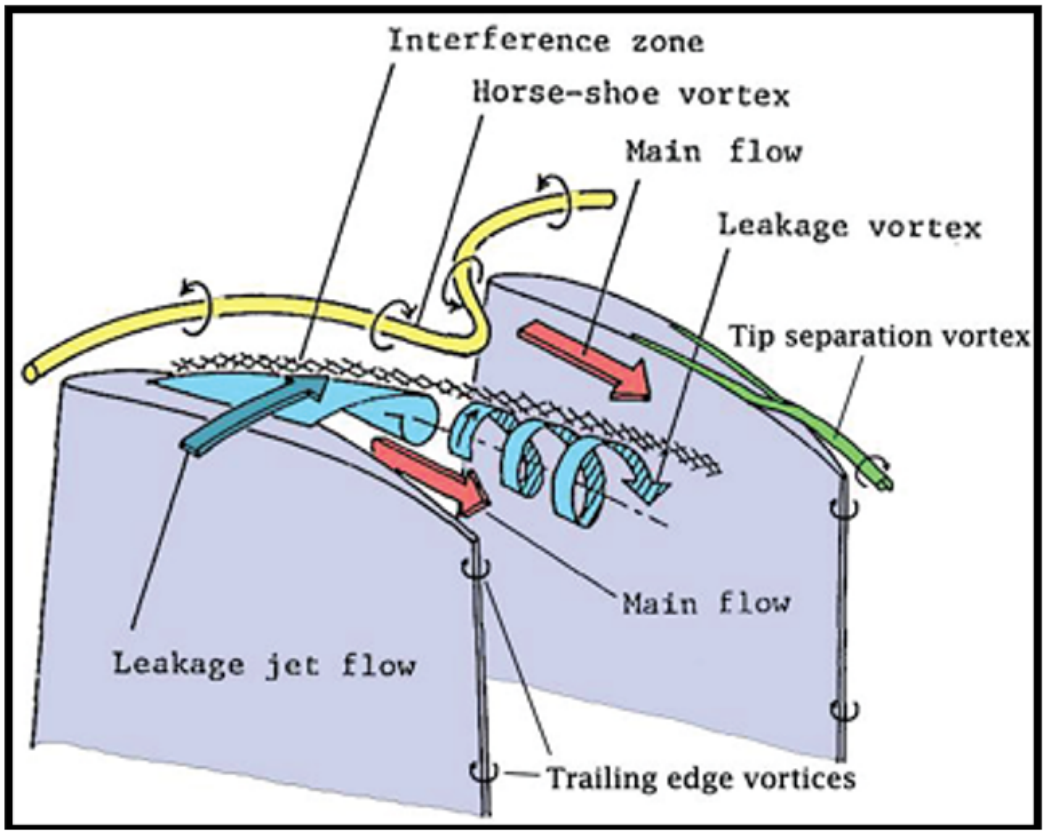

Figure 3. Secondary Flows Occurring in a Compressor Stage. Source: [6].

The extent to which the flow from the blade tip affects the rest of the main flow has been found to change with mass flow rate and rotor speed. A series of pressure measurements were taken along the inner wall of a compressor's casing by Miller and Bailey that looked at the blade passage shock system of the blade tips in a transonic rotor [5]. Figure 4 provides a contour plot of the shock system for both near-stall and choke conditions. Adamczyk et al. provided annotations in a later publication [4]. From choke flow the contours suggest that a series of oblique shock waves occur and the vortex path is not noticeable. The opposite occurs in near-stall conditions. At near-stall the shock wave is detached and turns into a bow shock wave. The contours are evidence of a tip vortex that occurs originating at the leading edge of the rotor blade's suction side. Where the vortex of the first blade meets the shock wave of the consecutive blade we see a strong interaction. This strong interaction causes the vortex to expand and behave as described earlier. The large pressure differentials created by these shock waves not only exacerbate the tip vortex

issue, but also deflect the blade tips, slightly increasing the tip clearance which creates larger vortices.

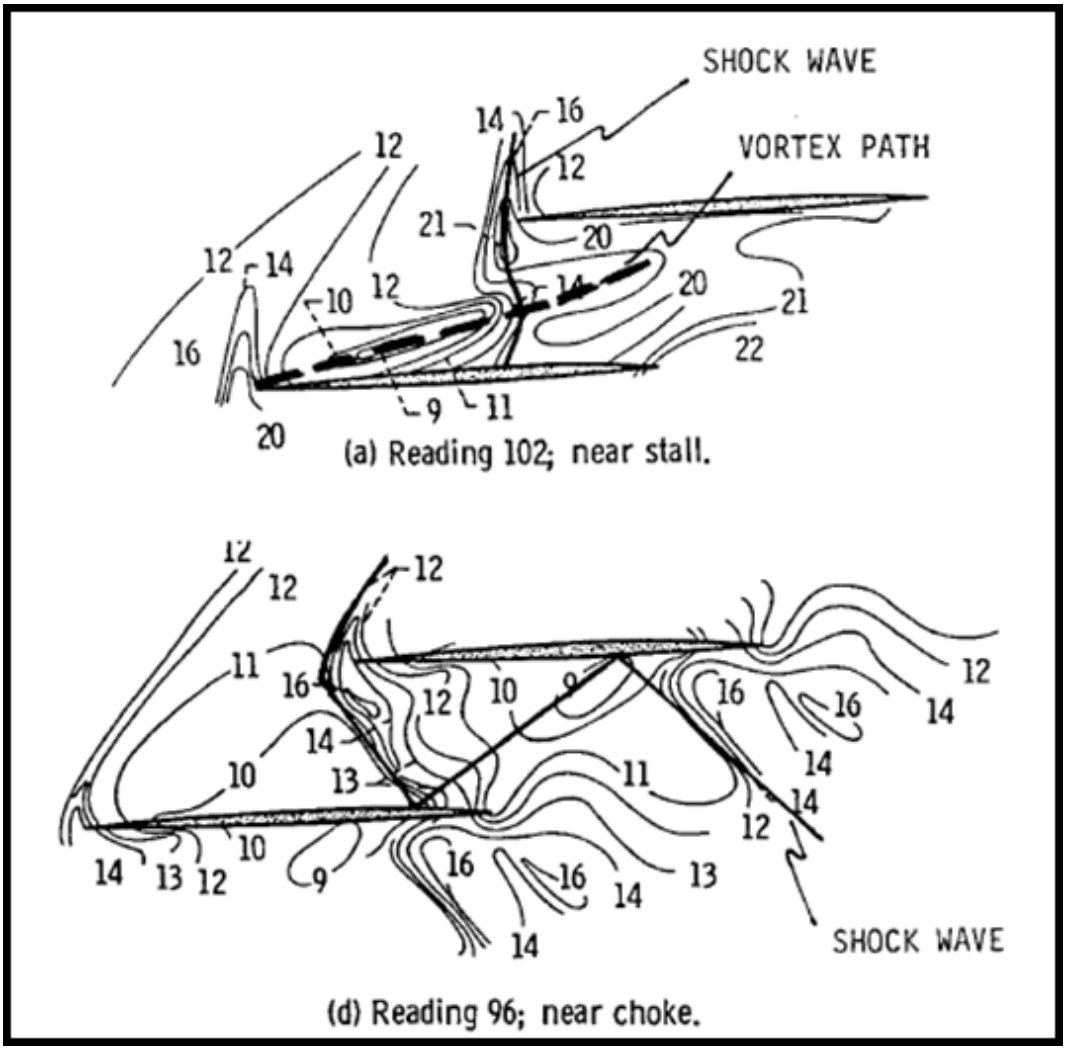

Figure 4. Contour Pressure Plot of Blade Tips for Choke and Near-Stall Conditions. Source: [4].

Londoño [1] used Kulite pressure probes embedded within the NPSMF's surrounding casing to examine the pressure distribution. The research took pressure readings at 70, 80, 85, and 90% of design speed for peak efficiency (near choke), close to stall, and near-stall conditions. It was determined that the normal shock wave, as described by Adamczyk et al. [4], is noticeable on the NPSMF when operating at 70% speed at near-

stall conditions. As the rotor was taken toward choking conditions, the normal shock wave turned into an oblique shock, again matching Adamczyk's explanation. The study also found that as rotor speed was increased, keeping the near-stall condition, this normal shock wave turns into an oblique shock wave. A tip vortex cross flow can be seen originating from the suction side of the leading edge, shown in Figure 5. The tip vortex originates at the leading edge since it is the leading edge that experiences the largest difference in pressure from the pressure and suction side of the rotor blade.

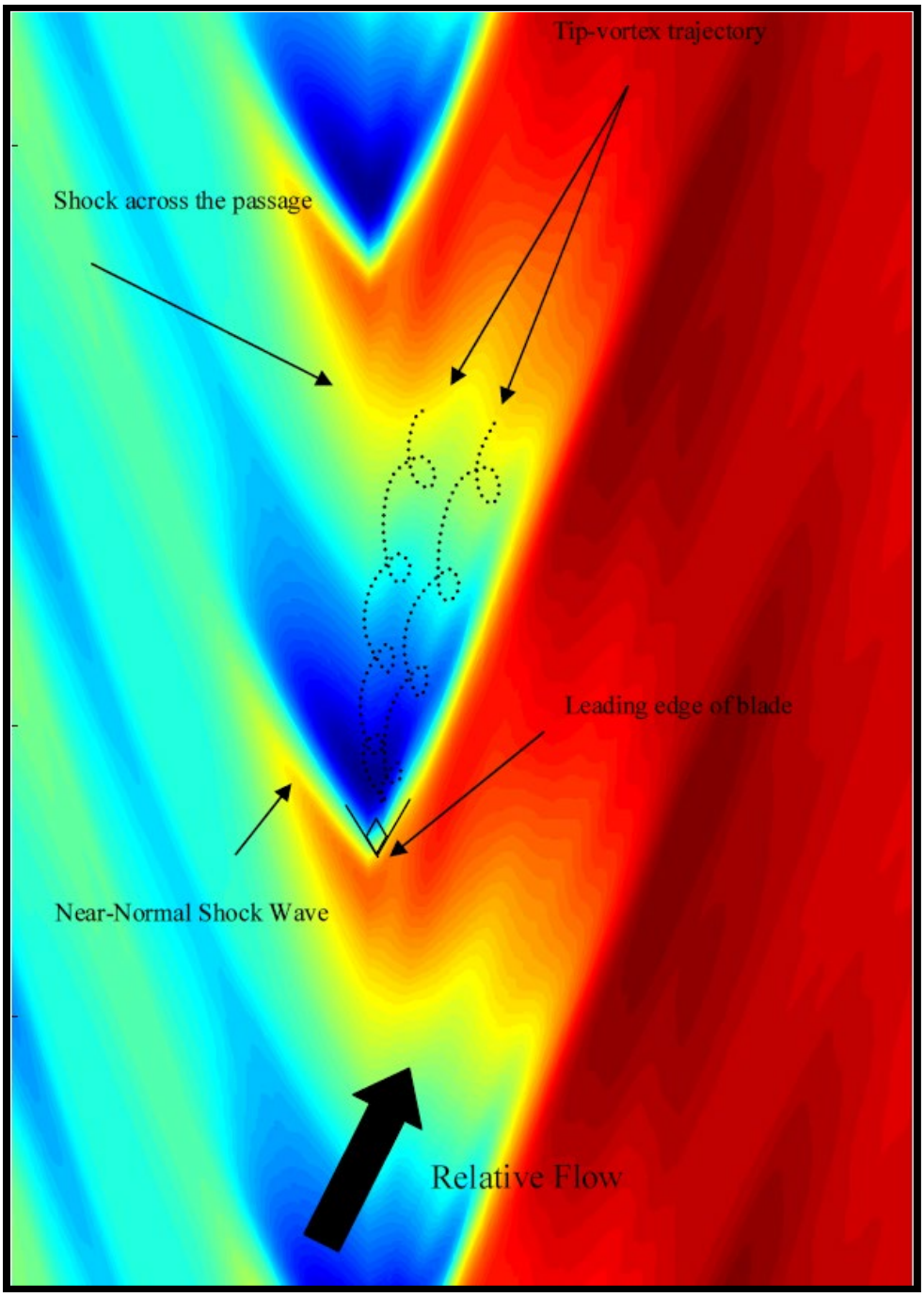

Figure 5. Pressure Distribution of NPSMF at Near-Stall Condition at 70% Rotor Speed. Source: [1].

The tip clearance clearly has a large effect on the flow characteristics of an axial compressor. The size of this tip clearance directly affects the magnitude to which these flow instabilities occur lessening the margin to stall. There is evidence that tip vortices do

occur with the NPSMF. Thus, it is paramount to characterize the tip clearance of the NPSMF.

The radial strain of a rotor's blades increases parabolically as the radial stress rises. Garcia et al. reports the results of an experiment examining an aircraft engine's compressor's first stage that the tip clearance decreased exponentially as the rotational speed of the engine increased linearly [7]. Figure 6 depicts a typical tip clearance change resulting from increasing speed.

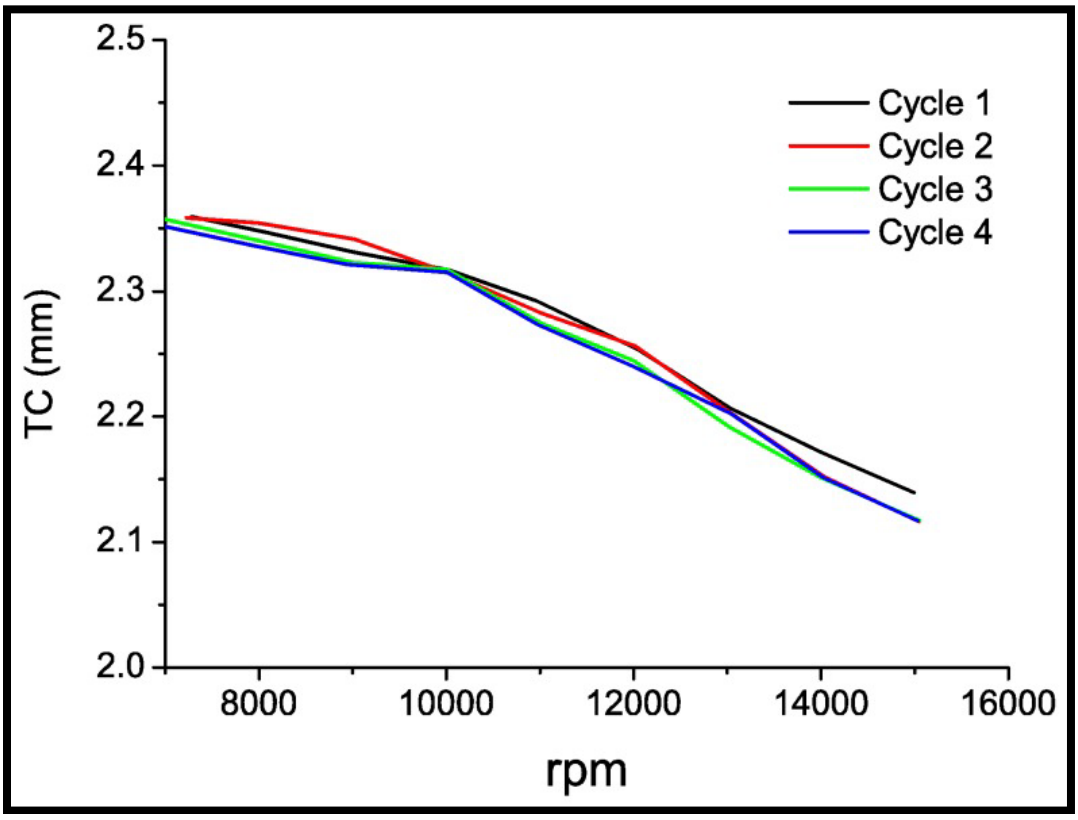

Figure 6. Example Reduction in Tip Clearance Due to Rising Centrifugal Load. Source: [7].

A finite element model simulation was conducted using the geometry of the NPSMF during this experiment with loading created by rotational speed. The model confirms this characteristic exponential reduction in the tip clearance region. This

simulation is further discussed in detail in a comparison to the results of the measured blade growth.

C. SURVEY OF TIP CLEARANCE MEASUREMENT METHODS

1. The Different BTC Measurement Methods

As tip clearance is an important parameter to design and monitor, multiple tip clearance measurement methods have been developed. Static methods of tip clearance include using a feeler gauge as a means of a routine check, though this only measures the cold BTC. The BTC will change as the rotor speeds up so a BTC measurement system is desired under dynamic conditions.

A common method of measuring dynamic BTC is by using proximity optical lasers and measuring the BTC by triangulation. Development of such a system is described by Ford et al. from the Pratt and Whitney Aircraft Group [8]. A recent use of such a system was used by Simmons et al. [9]. The work used these probes to not only monitor the minimum BTC but to also examine individual blades tip behavior. The experiment was also able to measure shaft vibration and displacement. A second BTC measurement method used is via inductance proximity probes which operate by measuring the effects of induced eddy currents on the passing rotor blades. The probes operate by measuring the change in inductance in planar spiral coils as detailed by Yu et al. [2]. A recent use of eddy current based system is documented by Wu et al. The research attempted to fix signal response issues with eddy current BTC measurement systems [10]. Other measurement systems include a tip timing method, microwave method, and optical fiber method which are reviewed by Yu et al. [2]. In this study BTC measurement via the capacitive method is used. A survey of the capacitive methods is provided in the following section. A description of the operational theory of the tip clearance system used in this study is provided in the next chapter.

2. Capacitive BTC Measurement System Survey

The capacitive BTC measurement system uses capacitive probes that measure the amount of distortion caused by the temporary capacitance developed between the rotor

blade and the capacitive probe. The original BTC measurement system using the capacitive technique was created by Chivers [11]. The system uses capacitive transduction via a capacitive probe in conjunction with an oscillator to produce an FM signal used to measure the BTC. Chivers' thesis provides details regarding this original BTC measurement system and provides system assessments on a test rotor, compressor, and turbine [11]. An operational description of the specific system used in this experiment is discussed in the following chapter. Chivers was successful in continuously measuring a rotor's average BTC. Sheard et al. conducted a series of work to develop a "blade-by-blade" tip clearance measurement system that can monitor the BTC of each individual rotor blade. The study incorporated the capacitive probe of Chivers into a stepper motor driven probe design [12].

Muller et al. [13] also had created a similar system to meet specific engine installation design requirements, using the probes to measure BTC for both turbines and compressors. The research's experimental design improved on earlier designs with the inclusion of a long flexible cable and was able to validate results against another capacitive BTC system. The work also was able to pinpoint the rotor axis' radial displacement by identifying a frequency in the first shaft order. Muller et al. [13] also was able to determine relative movement between the rotor shaft and the casing, as is done in this study. Sheard et al. further developed the system to where a probe can be calibrated in situ just prior to use on-the-line. The study also demonstrated the ability to incorporate a blade analyzer unit into the circuitry that can register blade numbers, and measure blade-by-blade tip clearances while the rotor spinning [14].

A major challenge in using a capacitive tip clearance system as opposed to other measurement methods is that the capacitive probes are susceptible to noise from temperature changes, electromagnetic interference, vibrations, or moisture resulting in a poor SNR due to their high sensitivity [11], [13], [15], [16]. Attempts to correct temperature susceptibility was conducted Sheard et al. [17] where a high temperature BTC measurement system was developed and tested. The work consisted of developing a method to lower the susceptibility to low frequency changes due to temperature changes. Sheard [14] stated having to use a pneumatic motor to drive a test rotor due to interference

of an electrical motor. This was taken into consideration for this study, which involved the use of a pneumatic motor as well.

Chivers [11] noted electromagnetic noise was of particular concern in this experiment as the probes are calibrated and used in direct electrical contact with the aluminum casing which is contrary to other setups which used electrically insulated probes. The RCap V BTC measurement system used in this study is provided by Rotadata, Ltd. The RCap V and its sister system, the RCap X, are commonly used BTC measurement systems and have resulted from a series of developments originating from the original design by Chivers [18]. A study was conducted in 2020 of the RCap V and RCap X BTC measurement systems by Stubbs [15] validating improvements made in noise reduction. The validation demonstrated that the systems have improved the capacitive probe signal-to-noise (SNR) that arise from the susceptibility to background noise. Although major improvements in noise cancellation have been made to the tip clearance measurement system [15], the susceptibility to noise hasn't been entirely eliminated, motivating the need for the post-processing methods developed in this paper.

Another issue with calibrating probes is the need of a probe to be calibrated and maintained with the same probe to channel configuration. Chivers [11] found that capacitive probes interact differently when paired with different data acquisition system (DAS) channels as the circuitry is different. Stubbs [15] explains that this dependence has been removed in the development of the newer systems. This experiment takes a conservative measure and ensures the probes remain paired to their corresponding channels.

Furthermore, it is common practice to calibrate capacitive probes using a calibration blisk. The manufacturer of the system used in this experiment provided a calibration blisk whose blade tips reflected the geometry of the NPSMF, shown in Figure 7.

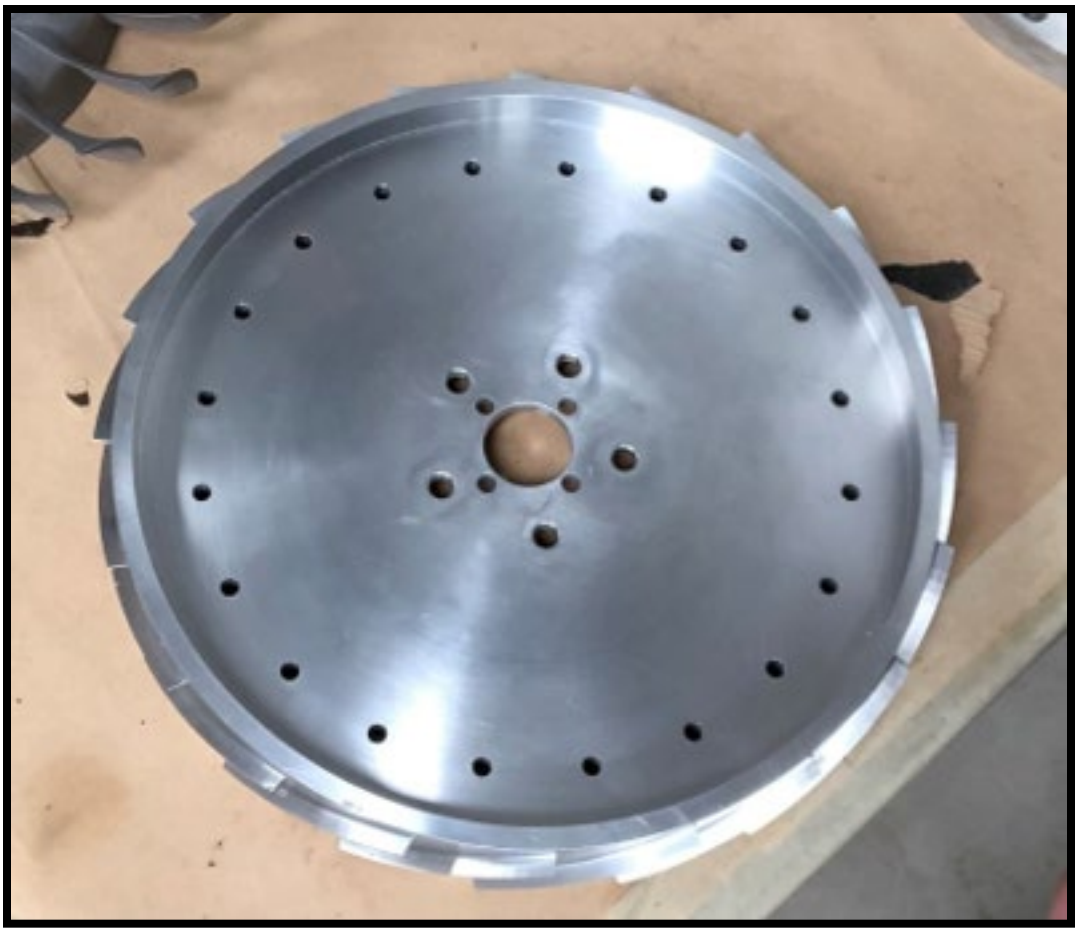

Figure 7. Rotadata Calibration Blisk Used for Initial Calibration.

Due to the probes' high sensitivity the different rotor geometry, different calibration mounting, and facility background noise may result in different calibration results. The different geometry and mass between the NPSMF and the supplied calibration blisk may result in a different probe response causing possible error in using a calibration curve from the calibration blisk for measurements on the NPSMF. This issue was addressed by Muller et al. [13]. The report had stated the deviation between the rotor geometries was their main source of uncertainty in the calibration process. Muller applied a correction factor to the capacitive probe output signal to adjust the tip clearance data accordingly. To avoid this uncertainty, this experiment conducted all calibrations on the NPSMF itself.

3. Current Research Program

This study is part of a larger program of research that is conducted at the Naval Postgraduate School's (NPS) Turbo Propulsion Laboratory (TPL) involving experiments on the NPSMF. The NPSMF is a solid titanium alloy turbofan consisting of 20 forward swept blades with a design speed of 30,000 RPM. The rotor's nominal diameter is 287.02 mm (11.3"). The fan is driven by the TPL's Transonic Compressor Rig (TCR), shown in Figure 8. The TCR is driven by an air turbine. The air is supplied by an Allis Chalmers, VA 312 compressor installed in a separate cell. The air is delivered to the TCR's test cell and moves the drive turbine which in turn drives the test rotor. Air is then exhausted through a series of exhaust piping.

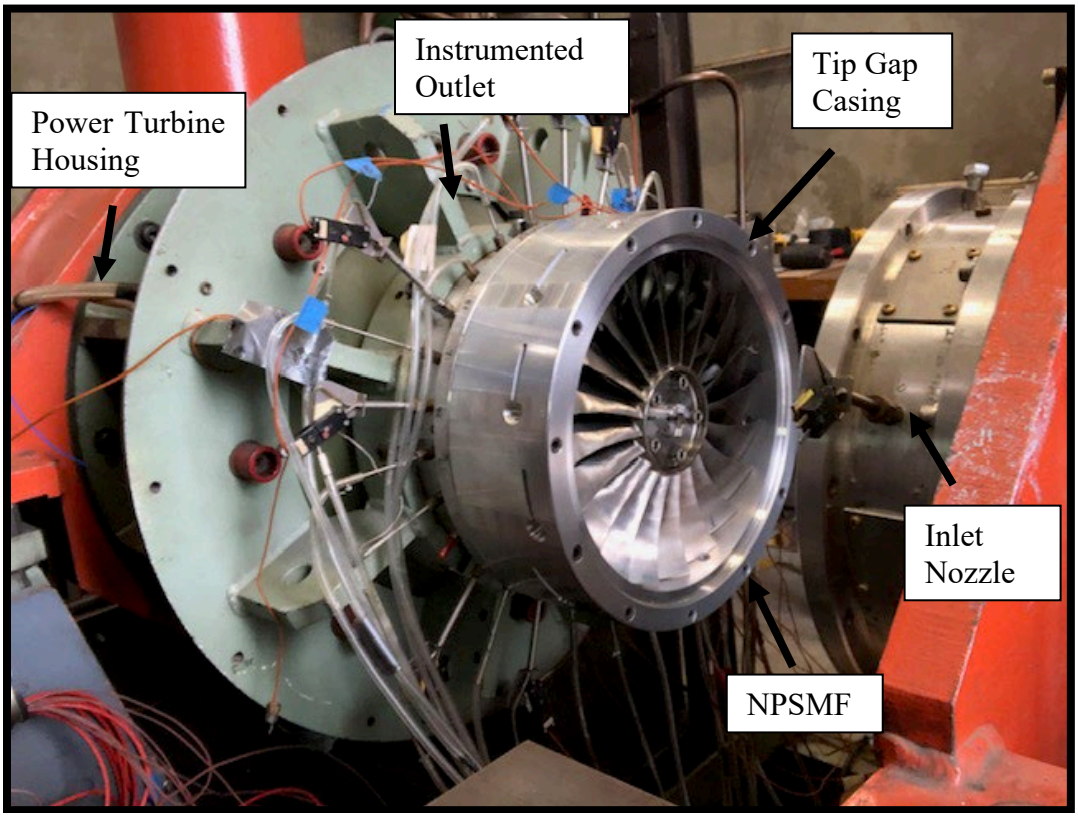

Figure 8. Transonic Compressor Rig with Inlet Nozzle Removed Showing NPSMF.

Previous works from NPS that relate to this study's experimental measuring of the NPSMF's tip clearance is covered by Londoño, Thornton, and Meinster's theses. Londoño [1] conducted a series of experimental measurements of non-periodic flow disturbances using an array of Kulite pressure probes in the tip clearance region. The thesis showed the behavior of pressure distributions for various rotor speeds and inlet mass flow rates to find causes for stall. The research was successful at experimentally identifying locations of tip leakage vortices which was found to originate at the leading edge of the tip of the NPSMF. The work characterized how the tip vortices behave as the margin to stall was lessened as well as the shock profiles in the vicinity of the blade tip.

Thornton [19] improved on previous CFD models of the NPSMF in the TCR by using a fluids structure interaction model. The thesis specifically addressed issues of modeling performance when using the rotor's "cold" geometry and proposed a model that takes into account blade growth, affecting tip clearance and therefore air flow. By coupling a fluid model for pressure with a structural model for rotor blade growth and deflection the study increased the reliability of NPSMF CFD modeling.

Meinster [20] further improved previous CFD models via a mesh sensitivity analysis to better examine flows of a single blade passage at near-stall. The thesis used ANSYS-CFX to examine flow for zero, narrow, and wide tip clearance cases. The research used flow visualizations to show the flow field around the tip region specific to the NPSMF and shows how a wide tip gap can create a stall-causing tip vortex. A graphic showing the simulation for a wide tip clearance nearing stall is shown in Figure 9.

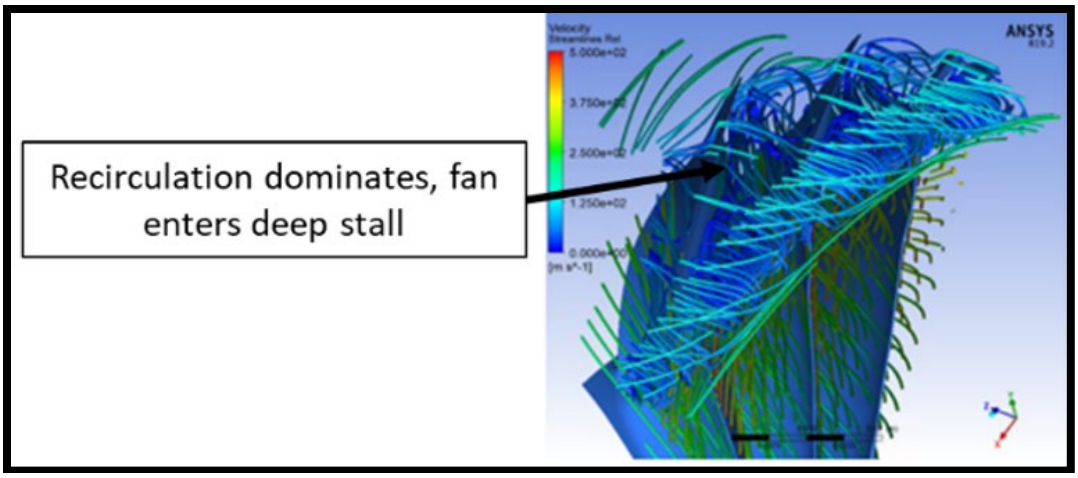

Figure 9. Simulated Tip Vortex from a Wide Tip Clearance for the NPSMF. Source: [20].

This string of research has examined pressure distributions and air flow models that originate from this tip clearance region. What is lacking in all these studies is the actual measurement of the NPSMF BTC. This study looks to finish this series of research and characterize the blade tip position behavior. By then referencing these previous studies with the results of measuring tip clearance, one can better understand the performance losses related to BTC within the TCR. The post-process methods described and used in this thesis are summarized by Magno et al. [21].

D. THESIS OVERVIEW

This paper documents the measurement of NPSMF's BTC behavior from the physical development and design of the testing rigs used, to the development of the mathematical methods used for probe calibration and BTC measurement and ends with the presentation of the NPSMF BTC measurement results. Chapter II discusses the theory and description of the instrumentation used for the experiment. Chapter III documents the description and use of a Benchtop Calibration and Testing Rig (BCTR) to develop the post-processing methods used in probe calibration and BTC measuring. Chapter III also validates the use of these mathematical methods. Chapter IV discusses the procedure used to calibrate the capacitive probes and use them to measure BTC in the TCR using the methods developed from Chapter III. Chapter V provides the results of the NPSMF BTC

measurements in the TCR and the results of rotor axial displacement measurements. Chapter VI summarizes and concludes the work conducted. The appendices provide supplemental information that is referenced in the main discussion of this thesis. The appendices include the calibration curves and tables used, NPSMF BTC resulting tables, calibration rig design description, detailed standard operating procedures, and the MATLAB coding used.

II. THEORY AND DESCRIPTION OF INSTRUMENTATION

In this chapter the overall operational theory of the capacitive probe BTC measurement system is explained. This is followed by descriptions of the individual instrumentation components used for the experiment.

A. BLADE TIP CLEARANCE SYSTEM OPERATION THEORY

The overall basic operation of the BTC measurement system used is similar to the original design as described by Chivers [11] and the design as described by Sheard [14]. Through the years improvements and changes have been made to this original design, increasing system performance, though the principal operation remains the same. The block diagram of the BTC measurement system used in this experiment is provided in Figure 10.

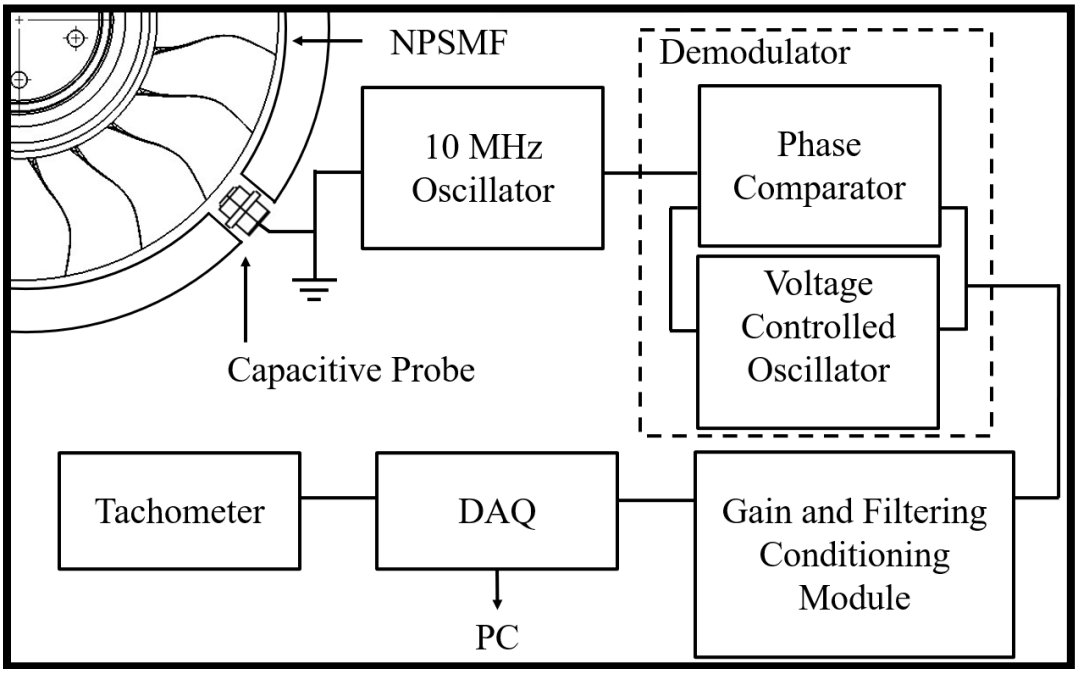

Figure 10. Operational Block Diagram of the BTC Measurement System.

The tip clearance measurement system uses FM techniques. In the system's most basic form the FM capacitive probe system consists of the probes, each consisting of an

electrode sensor, a frequency oscillator (nominally at 10 MHz), and a ground station. The capacitive probes are mounted into the casing's mounting ports. The probe outer sheath and compressor casing are in electrical contact with each other. Therefore, the casing is grounded to discharge any charge or interference developed in the casing so as not to interfere with the probe output signal. The principle of the capacitive probe measuring method is based on the changes in electrical capacitance developed between a sensing electrode and the rotor blade tip. The center plate, or the sensing electrode, on the probe's face serves as one plate of a crystal oscillator's capacitor. The rotor blade tip itself serves as the opposite electrode of the "capacitor."

A capacitance is developed across the two electrodes as each rotor blade passes by. The probe's oscillator is designed to react to the changing capacitance created from the blade's passing. To simplify the explanation, one can assume that the probe and blade tip behave as two plates of a parallel plate capacitor. The capacitance would behave per Equation (1). As the distance of the blade tip from the probe increases (enlarging the BTC) the capacitance between the two "plates" will decrease.

$$C = \frac{\varepsilon_o \varepsilon_r A}{d} \tag{1}$$

C is the capacitance, ε_o is the permittivity of free space, ε_r is the relative permittivity of the dielectric, A is the area of the "plate," and d is the BTC. The reaction from the oscillator to this capacitance change is exhibited as a modulation in the oscillatory frequency that drives the probe such that it correlates to a live capacitance gauged at the face of the probe. This FM signal is fed to a phase-locked loop (PLL) demodulator which uses a phase comparing circuit, a hardware filter, and a voltage-controlled oscillator (VCO). The phase comparator receives the FM signal from the capacitive probe and compares this to a reference line, outputting a voltage proportional to the phase difference between the two. This voltage is filtered and fed to the VCO. The VCO will then output a frequency proportional to this input voltage and this frequency is fed back to the input of the comparator's reference line. The comparator senses the frequency difference between the feedback output of the VCO and the process repeats. With the capacitance continually

changing due to continuous rotor movement, there will be a continually changing difference in phase, creating a continually changing voltage output from the comparator. The comparator's output behaves as a train of pulses whose amplitudes are proportional comparator's measured phase different which in turn is proportional to the proximity of the rotor tips. As the blade tip approaches the probe, the voltage pulse rises. As the rotor tip leaves the probe the pulse decays back to the DC line voltage. The peak-to-peak height of each pulse period is measured and corresponds to the tip clearance. Larger peak-to-peak DRO values indicate smaller BTC. Relative motion between the probe and rotor must exist for this pulse rise to occur due to the need of a difference in phase. Should the rotor stop, however, the output of the comparator will decay to the DC line voltage. Figure 11 shows an example of this output signal. Each data point occurs every 2 μsec corresponding to the probe's 500 kHz sampling frequency.

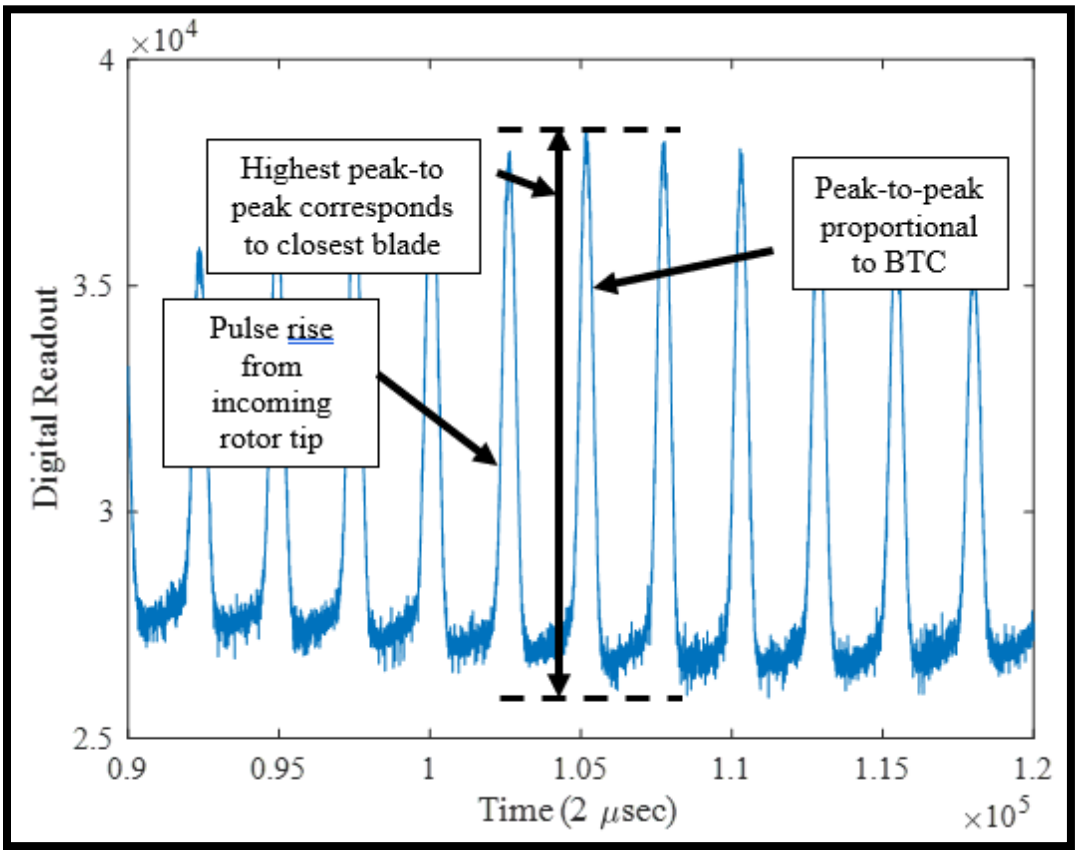

Figure 11. Example of Raw Capacitive Probe Signal Output.

This amplitude-varying analogue signal is hardware filtered and conditioned based on user specified settings and is then converted to a digital readout (DRO) in a conditioning module. This conditioned signal is then sent to the data acquisition system (DAS). A separate input to the DAS is the laser tachometer used to synchronize the data via a once-per-revolution (OPR) signal and number the rotor blades for use in the software's display. Both the raw data from the sensing probe and the tachometer sensing line are recorded in two separate files as either .csv files or .bin files.

B. INSTRUMENTATION

The following section discusses the instrumentation components used for both capacitive probe calibration and BTC measurements. The instrumentation was used on both a Benchtop Calibration and Testing Rig (BCTR) and the laboratory's Transonic Compressor Rig (TCR). A summary description of the operation of the BCTR is covered in the following chapters. Detailed discussion covering the specific design of the BCTR and incorporation of its various components as well as their specifications are discussed in Appendix C.

1. Capacitive Probe Description

Rotadata's MS1743 4 mm (0.157") low temperature capacitive probes are used in the BTC measurement experiments. The capacitive probe head consists of an outer sheath connected to ground and a center plate located at the front face of the probe. Ceramic insulation separates the inner electrode from the outer sheath. They are compact in comparison to an engine, with a max outer diameter of 14 mm (0.551"), a probe face diameter of 10 mm (0.394"), and an inner electrode face diameter of 4 mm (0.157"). The overall axial length is 13.6 mm (0.535"). They are connected via a 1 m (3.28 ft) long Teflon shielded coaxial cable that connects to a 7.5 m (24.6 ft) coaxial cable and terminates via an SMA plug and connect to one of two SMA jacks on the corresponding conditioning module. The probes can operate up to 180 °C (356 ºF) and their connector maximum operating temperature is 160 °C (320 ºF). When mounted into the compressor casing's ports they are flush with the casing's inner wall. Figure 12 provides a SolidWorks rendering of the capacitive probes used. Full specifications of the probe are provided in Appendix C.

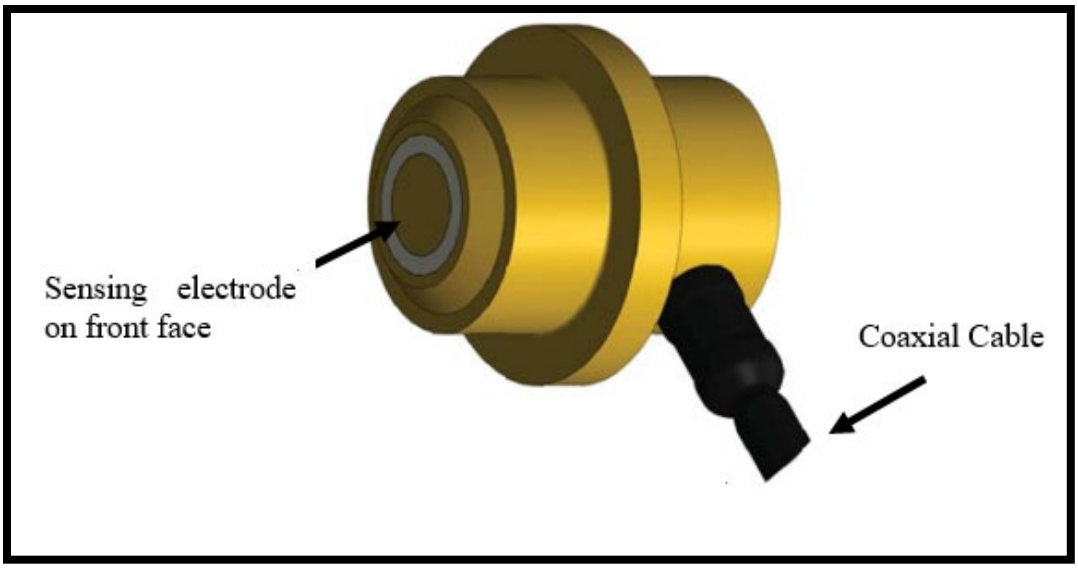

Figure 12. Rotadata Low Temperature, 4 mm (0.157") Electrode Capacitive Probe.

2. Conditioning Module

Rotadata supplies their own signal conditioning model using the module case of a standard National Instruments module that easily plugs in and out from the DAS. Demodulation and analogue signal gain and filtering for the demodulated signal are done within the conditioning module. The DAS has 4 slots to input up to 4 signal conditioning modules. The conditioning module houses the 10 MHz oscillator. It has a sampling frequency of 500 kHz. The user can adjust the analogue gain and filtering circuitry housed within the conditioning module through the RCap V software. Gain can be adjusted to 1 (no gain), 2, or 4, and up to 4 filtering stages can be used. The filtering options available are:

- No filtering
- 5 kHz 4 pole lowpass filter
- 20 kHz 4 pole lowpass filter
- 50 kHz 4 pole lowpass filter

Each module contains two channels, corresponding to 2 capacitive probes. The maximum of 4 modules allows for a max of 8 probes that can record BTC simultaneously. A total of 4 probes connected to 2 modules were used for this experiment. Although they have a SMA jack for the capacitive probes, the modules also feature a port for oscilloscope monitoring for each channel for live signal viewing as needed. Further specifications can be found in the RCap V User Manual [22]. A conditioning module is shown in Figure 13.

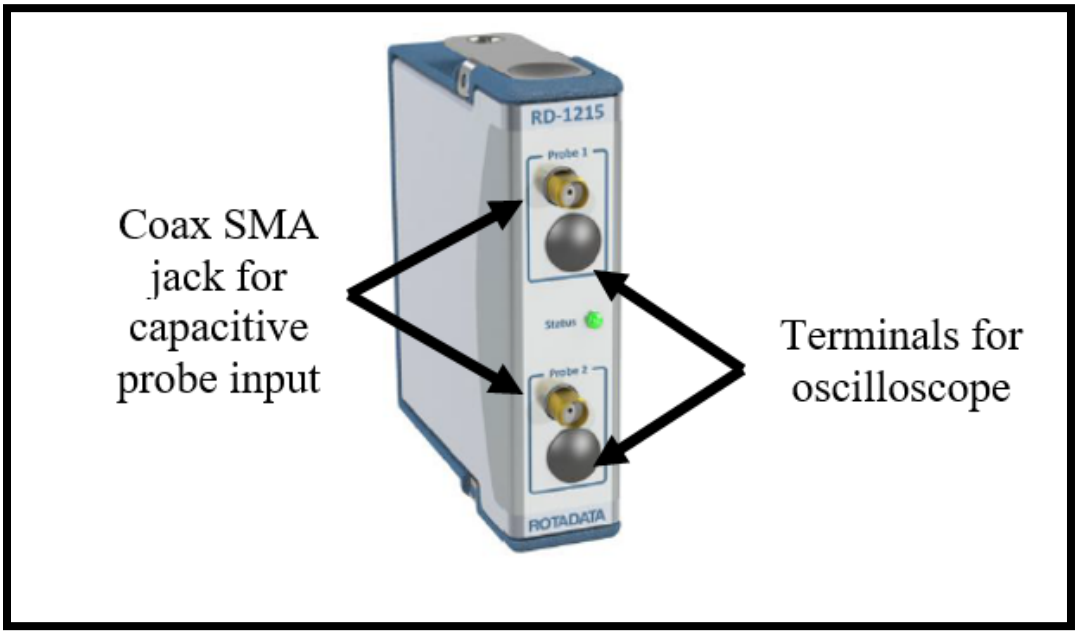

Figure 13. RCap V Conditioning Module.

3. Data Acquisition System

The data acquisition used is the National Instruments cRIO-9042 chassis, shown in Figure 14. It is the standard chassis used by Rotadata for their tip clearance measurement instrumentation. The DAS is based on a 1.6 GHz quad-core CPU. The chassis is a compact, high performance control system that can fit up to 4 signal conditioning modules, which gives a total of 8 measurement channels that can record simultaneously. The DAS requires an external computer to interface with and store the data collected. The system communicates to the external computer via ethernet. The DAS has a measurement

bandwidth of up to 1.2 MHz. For relevant specifications and dimensions refer to Appendix C. For full specifications refer to the cRIO specification sheet [23].

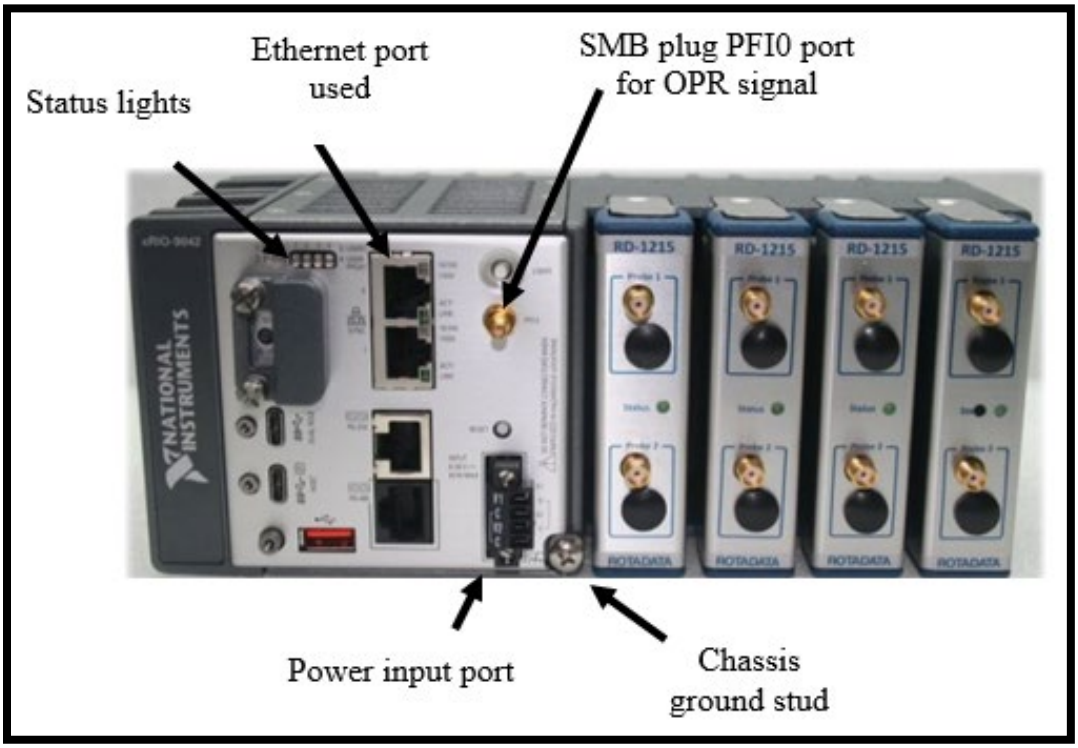

Figure 14. cRIO-9042 DAS Used with the RCap V BTC Measurement System.

It also features a PFI0 port with an SMB plug terminal to supply an OPR signal for data synchronization. It is a 5 V TTL I/O terminal and has a 5 V input maximum prior to there being risk of electronics damage. The power supply for the tachometer must be kept to less than 5 V. The max positive going threshold is 2.28 V and the minimum negative going threshold is 0.86 V, therefore a minimum of 2.28 V is required as a power supply for a tachometer to show a positive pulse on the DAS. 4.95 V was used for this experiment.

The ports included on the DAS front panel include a USB Type-A and USB Type-C and multiple ethernet ports, though only one of the ethernet ports is used to interface with the PC, the top port. Status LED lights are provided. A terminal to plug in the 24 V power supply and ground connection for the chassis are also provided. A separate 24 V

volt power supply (not shown) is also provided with the chassis. The 24 V power supply is powered via a standard 120 V connection to the facility. The ground connection wires into this power connection's ground terminal. The casing ground wire connects to this stud.

4. RCap V Software

The RCap V software runs on Windows 10 and later PCs. It enables the ability for one to view the raw DRO of each probe in real-time as well as real-time clearance measurements with a user assigned calibration file. This enables a user to watch BTC behavior live at different speeds and transients. The software also allows the user to interface with the DAS to select different gain and filtering settings to optimize the hardware. Furthermore, the ability to change the averaging technique is available. The filtering and gain settings are chosen during the calibration process into a calibration file. When this file is used, the DAS will configure to the calibration file's gain and filter settings.

The software contains multiple different tabs, each containing a separate function. The main tab, or the configuration tab, is shown in Figure 15. It provides the ability to specify the amount of blades on the rotor, set the probe debounce time, specify if readings should be as DRO or read in μm, and set the OPR signal's RPM and number of pulses (for more than one pulse per revolution). The debounce times are in units of 2 μsec. The user can also specify how many revolutions are averaged at a time to be displayed on the live, average tip clearance histogram plots. The averaging also dictates the number of revolutions to average at a time for calibration. Per the RCap V manual [22], calibrated digital readout of a specified calibration distance is the average of these averages. Further the user can specify which probes are active and choose whether raw data can be displayed or not in the raw data tab. The ability to choose the calibration file to use is available. A default calibration file is provided for the user for initial use. Whichever file is used, the gain and filter settings used in that calibration will be displayed. The user can also choose where to save calibration files and raw data files as well as choose to save them as a .csv, .bin or .tdms file.

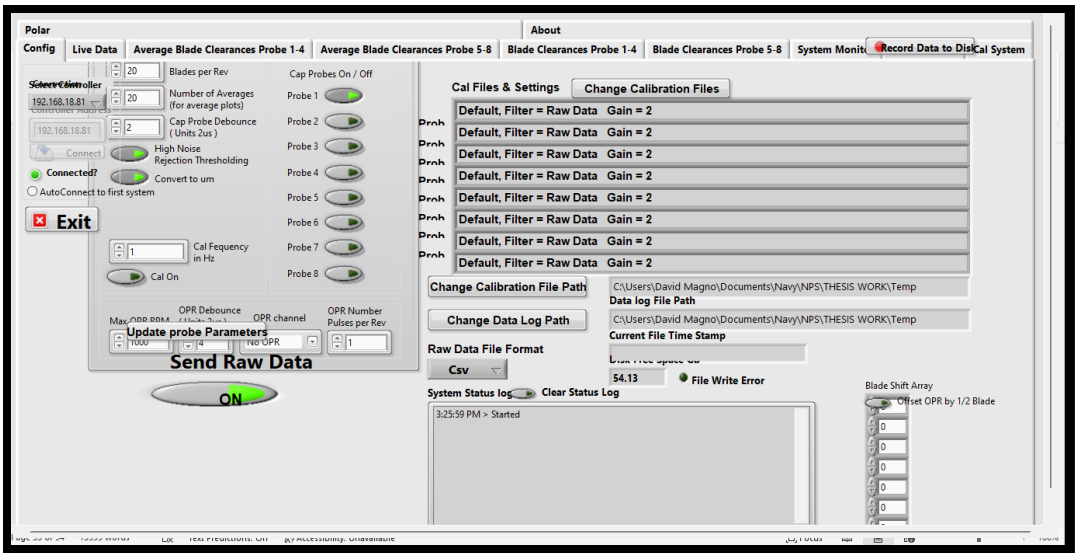

Figure 15. RCap V Configuration Tab.

The live data tab is available once raw data is enabled from the configuration tab. Up to two separate channels can be displayed simultaneously, to include the PFI0 input as an additional channel to the 8 probe channels. Channels are selected from a drop-down menu. Automatic or manual scaling can be done by the user as well. The data that is displayed has the calibration file settings for filter and gain applied. A display of the number of dropped packets is available to show the amount of data loss occurring in the case of lacking computer resources. Figure 16 provides a graphic of the live data tab for both a capacitive probe (above) and the output of a OPR signal (below).

Figure 16. Live Data Tab Showing Live Capacitive Probe and Tachometer Signals.

The following 4 tabs provide histograms for average and live data that are displayed in either DRO or µm. Each page shows up to 4 channels. RPM is also available in this tab. An example is shown in Figure 17.

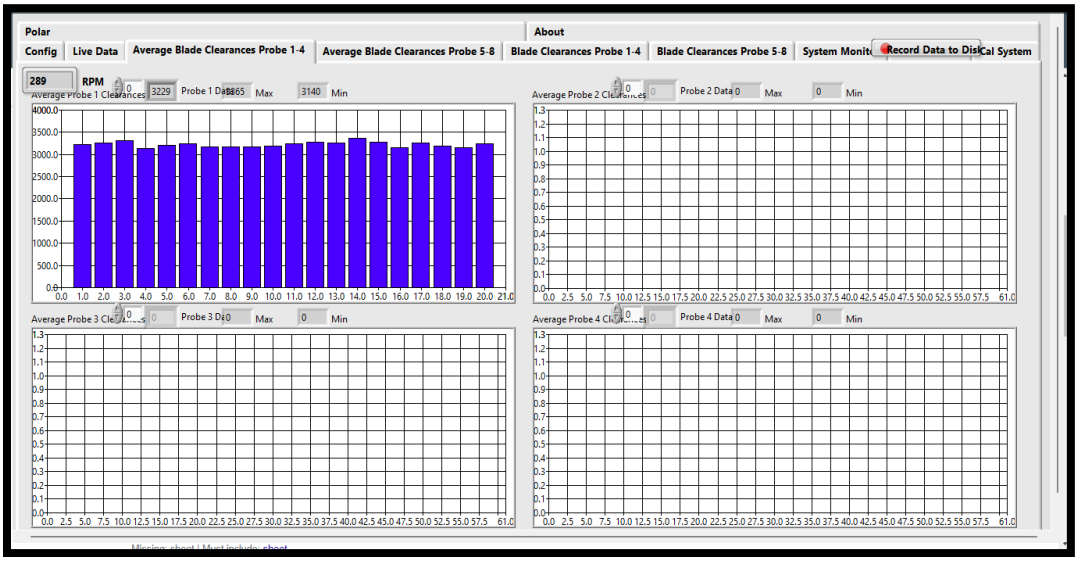

Figure 17. Histogram of Average Blade Tip Clearance.

A system monitoring tab (not shown) is available to show performance of the hardware. A calibration file editor tab is available to load and edit a calibration file without corrupting it due to formatting issues. Next, a calibration tab, Figure 13, is available to the user to provide a user interface for live calibration. A Cal Points file can be loaded or the user can specify their own calibration points. Rotadata provides the user with a default Cal Points file that can be loaded in. The RCap V user manual [22] provides instruction to conduct a calibration, though the software's calibration procedure is guided on the software making it user friendly. As previously mentioned, the user specifies the amount of gain and filtering to be used for calibration. The user positions the probe to the specified calibration position from the rotor tip and measures an average DRO value that it assigns to that calibration point. The user specifies the number of averaged points that are used for each calibration point. The software will calculate an average DRO at revolution intervals specified by the user. This is adjusted in the configuration tab. These averages are then averaged for the calibration position's DRO assignment. Therefore, the calibrated values from the RCap V software are an "average of averages." The software computes a live "signal quality" ranging from 0–100%. This signal quality pertains to the signal's SNR. It is displayed for the user to see the quality of the signal used. Only 100% quality data is recorded. Should the SNR become too poor a "Blade SNR Too Low" warning will display, as shown in Figure 18.

During this experiment, a self-developed calibration procedure was used using MATLAB as opposed to using the RCap V software to enable more user freedom in how calibrations are calculated, be able to record data past the low SNR limitation and analyze data quality for data loss. A detailed description of the procedure is available in Appendix D.

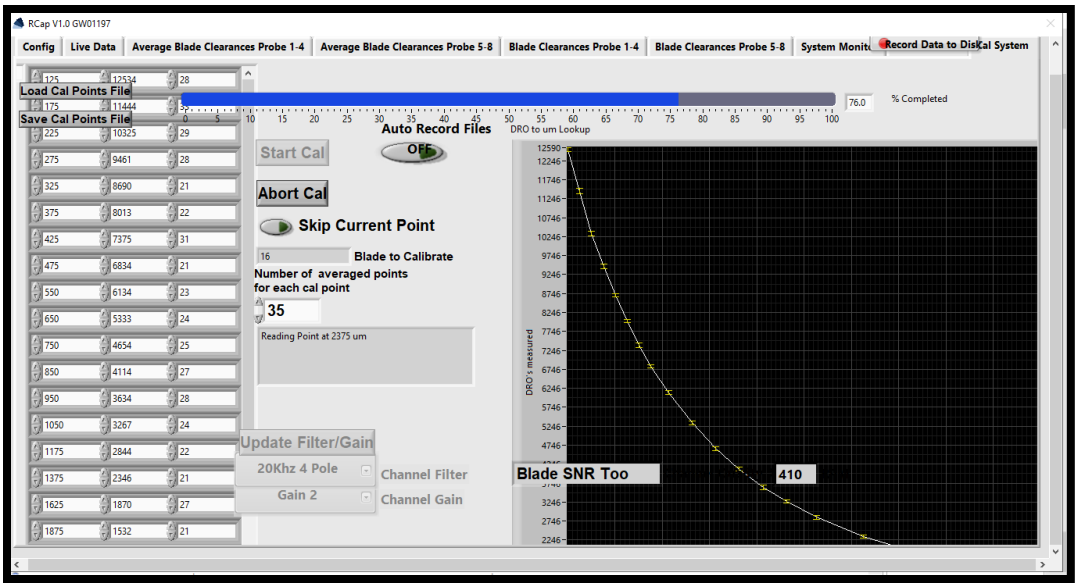

Figure 18. Calibration Tab with Low Quality Warning.

The software also provides a polar view tab, which gives a top-down view of the clearances for a different orientation view. When recording, the software will create multiple files to include a raw data file, an OPR files (if used), a full data file of capacitive probe BTC, and an average probe BTC file. For further information of how to use the RCap V BTC Measurement System software, refer to the manual [22].

5. Tachometer

A Monarch Instrument Optical Rugged Laser Sensor was used as a once-per-revolution (OPR) tachometer. The TCR and BCTR each have their own laser sensors. The BCTR tachometer is shown in Figure 19. It operates by emitting and then sensing a reflected 1 mW (max) red laser, outputting pulsed signal. The laser sensor can sense speeds up to 250,000 RPM. The tachometer is available from the manufacturer with open wire ends that can be spliced and connected as needed or can come as a 3 pin 3.5 mm (1/8") phone plug. Cable termination for the BCTR was chosen as an open-ended wire for flexibility in wiring configuration, whereas the TCR uses a previously installed 3.5 mm (1/8") phone plug. The wiring configuration and diagram are discussed in the following chapter describing the BCTR components.

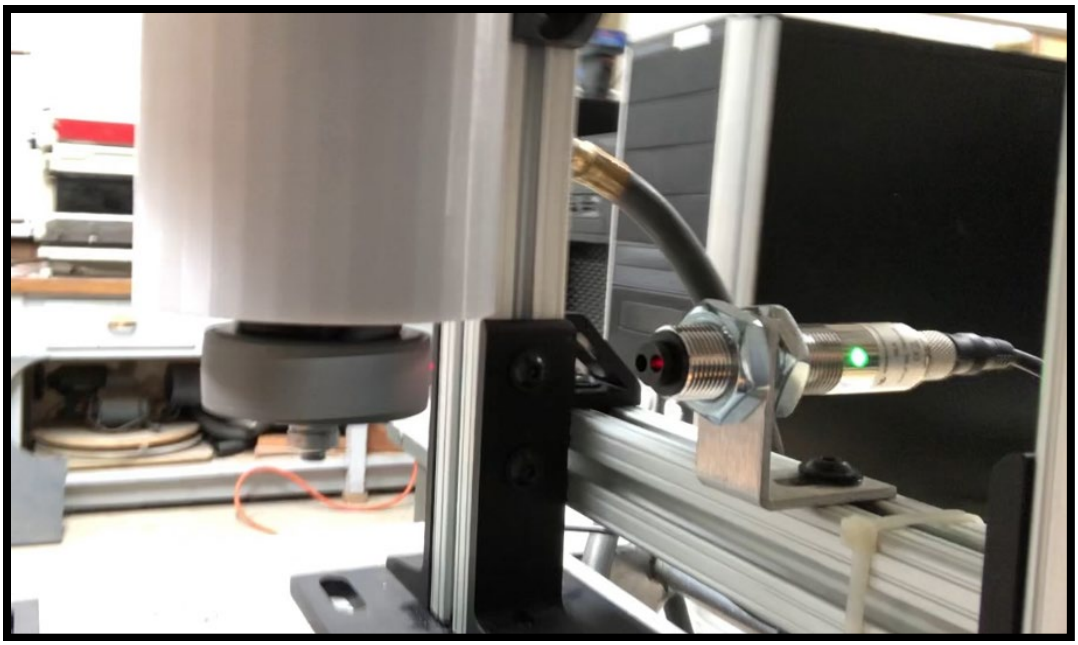

Figure 19. RLS Tachometer.

The tachometer's OPR signal is displayed as a 1V square pulse as shown previously in Figure 16. The tachometer features an "on target" indicator via a green LED light that turns on when the signal pulses high, shown lit in Figure 19. This provided a visual queue for the operator that the pulse signal was firing when required in the absence of an oscilloscope. A voltage greater than 4 V was required to create the output signal from the tachometer. The instrument is powered by a 4.9 volt DC power source. The voltage was chosen so as to ensure the signal was well above the 2.28 volt TTL threshold of the cRIO-9042 DAS, but with a large enough margin so as to not exceed the 5 volt maximum of the PFI0 fitting.

The terminal of the tachometer featured four open wires, a voltage in, a common ground, a sensing signal output, and an unused wire. This was connected to a coaxial wire with an SMB female terminal to plug into the cRIO-9042 DAQ PFI0 SMB fitting. The outer wire of the coaxial wire was connected to the same common as the laser sensor. The inner wire was used for the pulse signal from the sensor. Prior to connection to the cRIO-9042 DAQ the signal was verified under the 5 V maximum via oscilloscope for an added

safety measure. Further detailed discussion about wiring and probe mounting configuration is discussed in Appendix C.

6. Translation Stages and Measurement Devices

The calibration rig used two separate translation stages to support two different casings that differed in weight that will be discussed in the following chapter. The two different translation stages and their accompanying position measurement devices are described in this section.

a. Piezo Driven Translation Stage and Digital Dial Indicator

A Thor Labs PD1 piezo driven translation stage, Figure 20, is used to traverse a small casing element forward and back to each of the probe's calibration points. The stage is positioned via open or closed loop operation, commanded remotely via software or manually by a local control panel on its KIM001 motor controller. The stage is positioned to move the mock casing radially from the rotor's center. Total travel length is 20 mm (0.787"), though only up to 3 mm (0.118") is needed for calibration. Typical step size is 1 μm (0.000039") with 20% variability based on environment conditions as presented by Thor Labs, Inc. [24]. To account for the variability, distance is measured with a digital dial indicator. An optical encoder is not available for the PD1 model used. The list of relevant specifications and design parameters are discussed in Appendix C.

Figure 20. Thor Labs PD1 Translation Stage. Source: [24].

The stage is controlled by a separate motor controller. A KIM001 K-Cube Piezo Inertia motor controller is what is compatible with the PD1 stage. The controller offers the user control on its top panel by use of a scroll wheel. This motor controller houses only a single channel. Another compatible motor controller, the Thor Labs KIM101 motor controller, holds up to four channels, though this wasn't needed for this experiment. Figure 21 displays the PD1 stage and KIM001 motor controller mounted onto the calibration rig. Further specifications are provided in Appendix C.

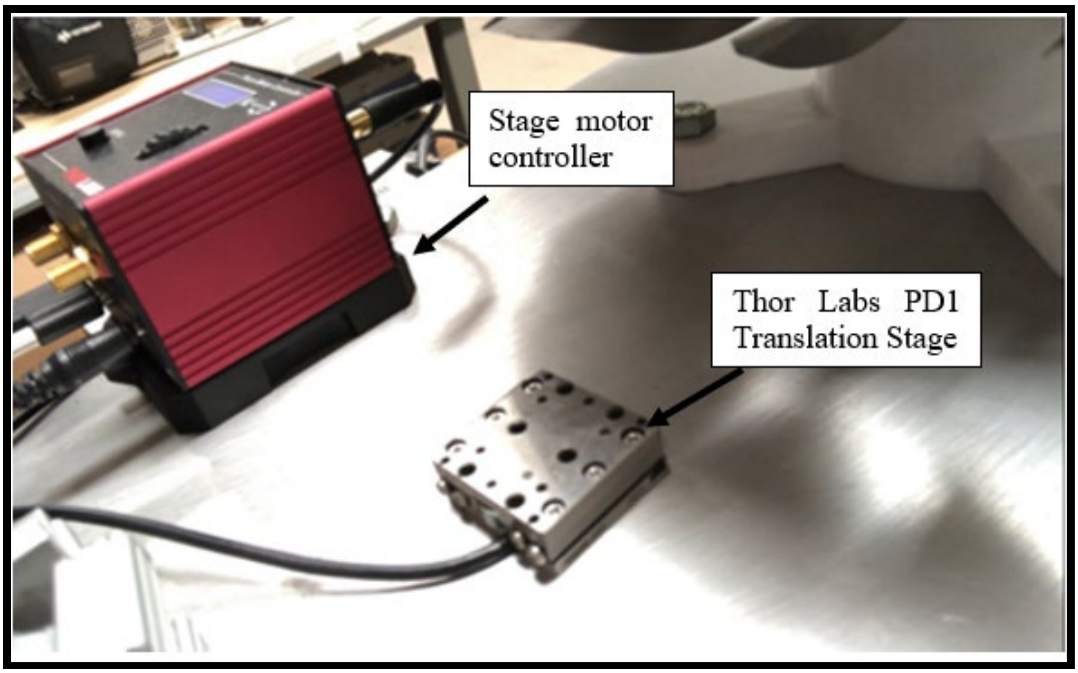

Figure 21. Piezo Translation Stage and Motor Controller.

Thor Labs provides remote operation of the stage by use of their software, Kinesis. The KIM001 motor controller is connected to a PC via USB cable. The software provides the ability to set the stage speed, set step size, command the stage to a specified location via closed loop or open loop, and to jog forward and back. Figure 22 provides a graphic of the software's user interface. Although the user interface provides a distance readout, a digital dial indicator was used instead to ensure repeatable results as there appeared to be errors within the PD1 stage.

Figure 22. Kinesis Software Interface. Source: [24].

The digital dial indicator used in the BCTR measured the amount of distance the probe traveled from its zero position. By experiment it was found that the distance readout in the Kinesis software did not match the actual movement of the casing. Therefore, a Series 543 Mitutoyo Digimatic Indicator (ID-C) was used in tandem with the mock casing to determine the distance traveled from the zero position. The dial indicator position accuracy is +/- 0.0001 in. [25]. It is shown in Figure 23.

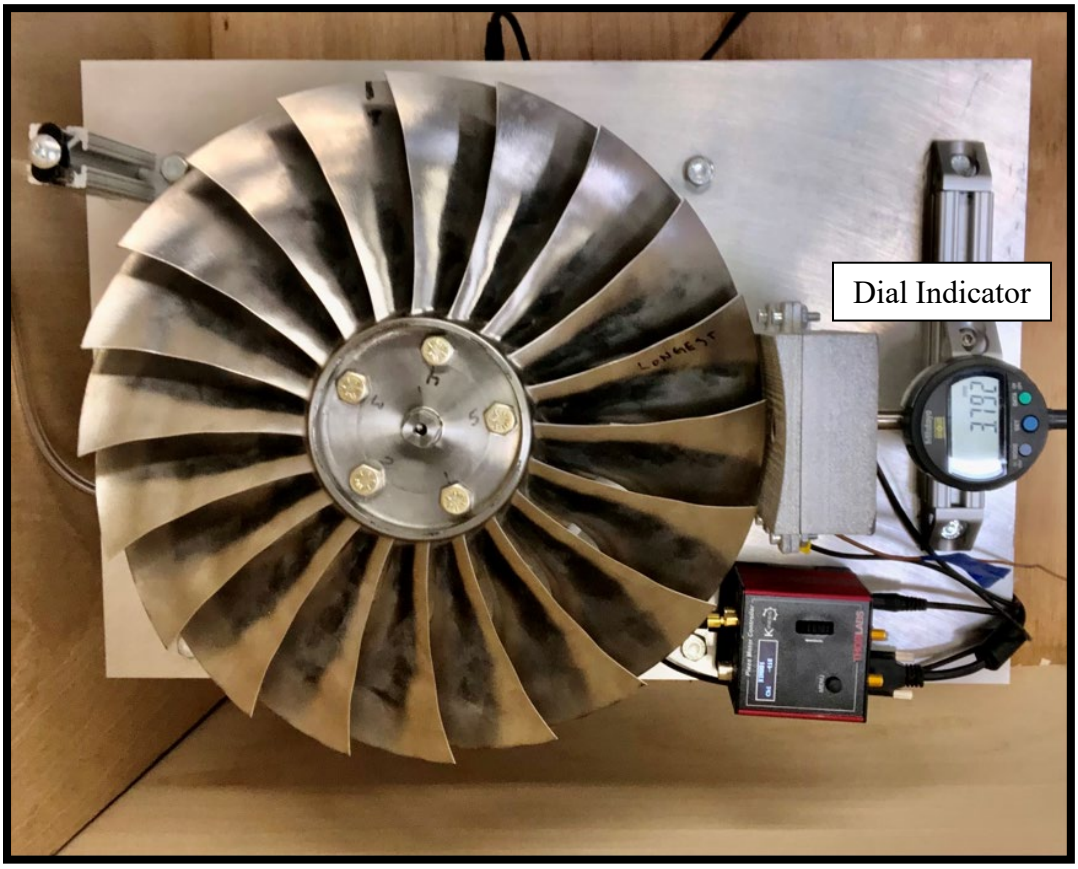

Figure 23. Dial Indicator Measuring Distance of Probe Travel.

b. Stepper Motor Stage and Magnetic Linear Encoder

As will be discussed in the following chapter, the BCTR later required modification to conduct probe calibration on a much heavier casing. This required a larger translation stage that had a higher loading rating. A Velmex BiSlide stage driven by a stepper motor with a built-in magnetic linear encoder was used. The magnetic linear encoder's measured

position is shown on a digital VRO encoder display. Both the stage and VRO encoder display are shown in Figure 24.

Figure 24. Velmex BiSlide with Built-In Encoder (left) and Encoder Display (right). Source: [26].

The stage operates by moving a mounting carriage via a precision lead screw controlled by a Vexta PK266 stepper motor. The magnetic linear encoder has an accuracy of 0.025 mm/100 mm (0.001"/3.94") as presented by Velmex, Inc. [26] and has a repeatability of 0.01 mm (0.000394"). The encoder resolution is 1 μm (0.000039"). When the carriage reaches the limit switch, the carriage depresses a button signaling the carriage to stop movement. A serial port from the stage motor controller and from the VRO display enable the user to interface the devices via PC. For this experiment, both the VRO encoder display and the stage were remote controlled using a MATLAB GUI. Port configuration, detailed specification, and calibration rig design incorporation are discussed in Appendix C.

III. POST-PROCESSING METHOD DEVELOPMENT AND CAPACITIVE PROBE CALIBRATION

This chapter discusses the development of the methods used to calculate the NPSMF BTC. To develop these methods and conduct probe calibration, two versions of a Benchtop Calibration and Testing Rig (BCTR) were created. The rigs' descriptions and an explanation of the signal post-processing methods used to process the rigs' data are provided in this chapter. A comparison is made between the calibration curves created with the original calibration rig and the modified rig. A determination is made as to which set of calibration curves is to be used for the TCR BTC measurement experiment. A detailed description of the design of the BCTR and its component specifications is covered in Appendix C.

A. BENCHTOP CALIBRATION AND TESTING RIG

The casing used to mount the probes for use in the TCR experiment is referred to as the "tip gap casing." The first version of the BCTR, however, utilized 3D printed aluminum mock casings which served to validate the geometry design of the tip gap casing and verify that the BTC measurement system can operate within this aluminum casing. The manufacturing process for the final tip gap measurement casing was initiated. During this wait period the post-process methods were developed using the mock casings and an initial calibration was done. A modification was then done to the BCTR to install the newly received tip gap casing. A second calibration was conducted with the larger tip gap casing using the same methods developed to validate the mock casing calibration.

1. BCTR (Mock Casing) Description and Operation

The BCTR was created to calibrate the capacitive probes in an environment that closely reflected the TCR. The rig also was used to identify potential issues prior to ordering the actual casing to be manufactured. The rig served to develop the mathematical post-processing methods used for calibration and analysis prior to use on the TCR while the tip gap casing was being manufactured. Furthermore, it enabled the ability to determine if the probes will function properly and not fail due to noise when in electrical contact with

an aluminum casing. Finally, the BCTR itself was an experiment to see if 3D printed aluminum casings are an accurate substitute for the actual tip gap casing used in the TCR. The Benchtop Calibration and Testing Rig (mock casing) with the RCap V BTC measurement system connected is shown in Figure 25.

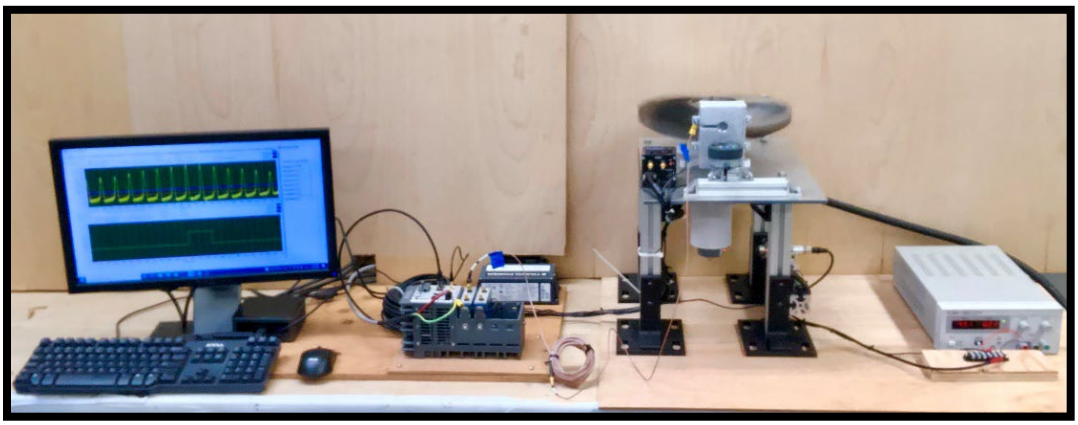

Figure 25. Benchtop Calibration and Testing Rig (Mock Casing).

Figure 26 provides a simple operational diagram showing the overall operation of the BCTR. As mentioned, the rig uses 3D printed aluminum mock casings. The mock casings were printed using the Xerox ElemX printer located at the NPS TPL. 3 separate casings are used, with mounting ports in 3 different monitoring locations: the leading edge, mid-chord, and the trailing edge. The capacitive probes are mounted into the 3D printed aluminum mock casing. The mock casing is mounted onto the Thor Labs piezo driven translation stage via a plastic mount that is commanded locally by a motor controller's top panel or remotely by PC software to move the casing back and forth radially in reference to the rotor's rotation axis. This allows repositioning of the probes for calibration while the rotor remains spinning. The plastic casing mount also serves as an electrical air gap between the mock casing and rest of the apparatus. A digital dial indicator is used in tandem with the mock casing to measure the distance traveled with an uncertainty of +/- 2.54 μm (+/- 0.0001") as presented by Mitutoyo [25]. The NPSMF is pneumatically driven by the TPL's 100 psi pressurized air system via a hose applying the air directly onto the rotor

blades. The NPSMF is coupled to a vertical shaft that is supported by 2 pairs of angular contact bearings, housed within a bearing housing fastened to a base plate.

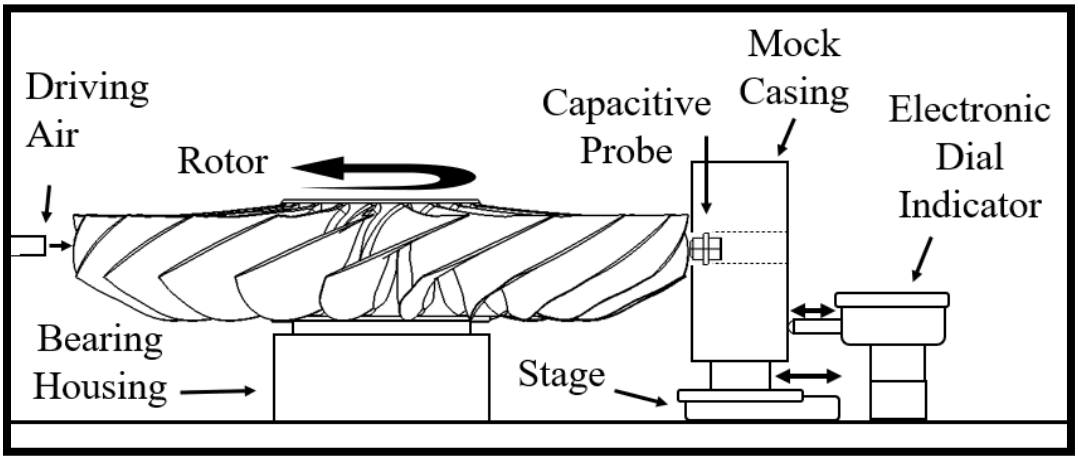

Figure 26. Operational Diagram of the BCTR (Mock Casing).

Below the bearing housing is a laser tachometer (not shown) that measures the shaft speed with a disc attached to the shaft that has a section of reflective surface. The tachometer outputs 1 pulse per revolution. To prevent buildup of charge in the mock casing, a grounding strap is attached that connects the casing to the ground stud connection on the DAS. The capacitive probe signal is fed through a coaxial cable into the DAS which is connected to a dedicated workstation PC. The BCTR is designed to run at low speeds. Above 600 RPM the BCTR experiences vibrations that cause the digital dial indicator's output display to change excessively, causing a large amount of uncertainty. The majority of the calibration and testing done on the BCTR was kept between 300–500 RPM. Detailed design descriptions and specifications of the BCTR (mock casing) are given in Appendix C.

2. BCTR (Tip Gap Casing) Modifications Description and Operation

The tip gap casing was then installed on the BCTR and a second calibration was done using this casing to verify the validity of calibration using the mock casings. The addition of the larger casing required modification of the BCTR. Figure 27 shows the

modified rig, the BCTR (tip gap casing), with the RCap V BTC measurement system connected.

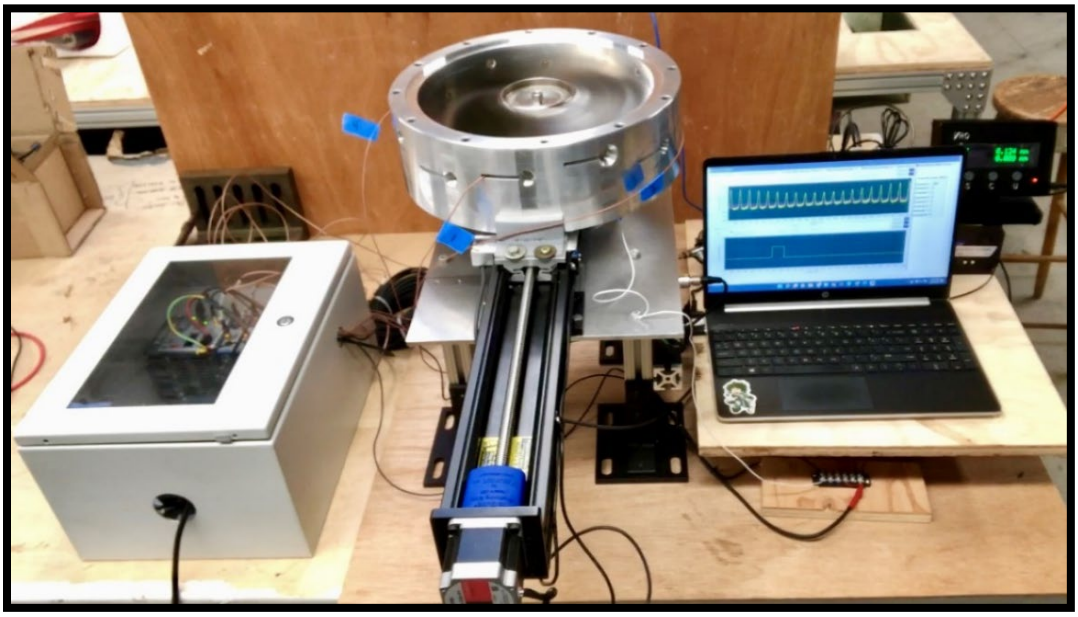

Figure 27. BCTR (Tip Gap Casing) with RCap V BTC Measurement System.

Due to the increased weight of the casing, a larger translation stage was required. The piezo driven stage was replaced with a larger stepper motor driven translation stage, previously described in Chapter II. The digital dial indicator was replaced by a magnetic linear encoder that is built-in to the translation stage. The linear encoder is repeated with an encoder digital display for the user.

Figure 28 displays an operational diagram of the BCTR (tip gap casing). Dimensions of the components in the figure are simplified and are not representative of the actual rig. The principle of operation is the same as the BCTR (mock casing). The four capacitive probes are instead all mounted into the tip gap casing mounting ports at one monitoring position simultaneously. Two plastic mounts hold onto the tip gap casing and couple the casing to a translation stage and guiding slide. The tip gap casing has a grounding wire attached to discharge any charge buildup just as in the mock casing version. The stage is remote controlled using MATLAB and allows motion of the tip gap casing

while the rotor spins. The stage carriage's current position is displayed on the encoder and relayed to the user on MATLAB as well.

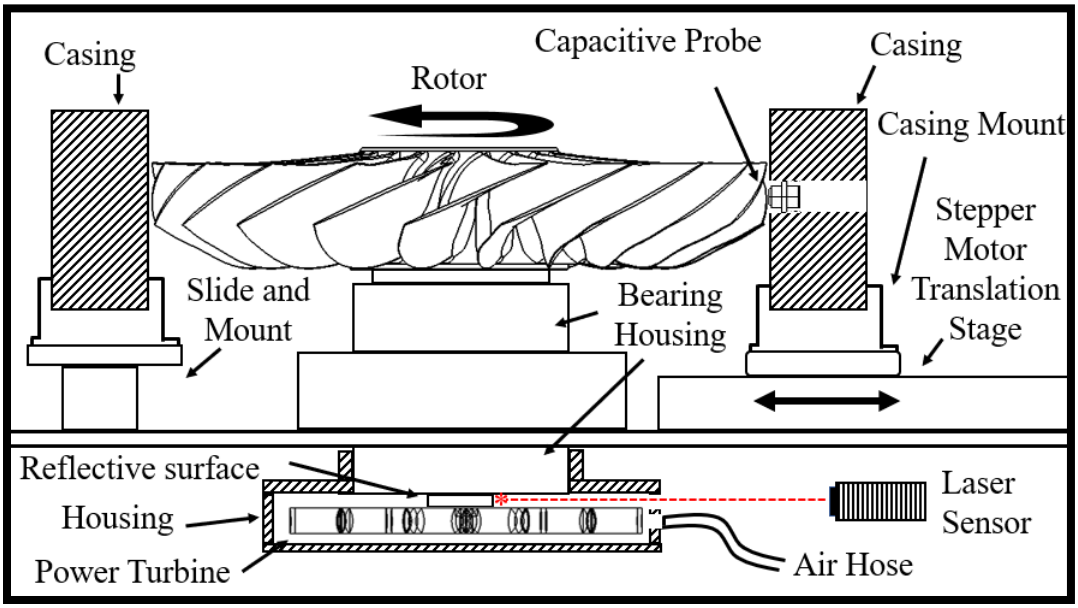

Figure 28. Operational Diagram of the BCTR (Tip Gap Casing).

The tip gap casing made it difficult to apply air directly onto the NPSMF at an angle to obtain the same speed as with the mock casing design. Therefore, a power turbine assembly was created and mounted under the bearing housing. The NPSMF is driven by a 3D printed PLA power turbine located under the base plate. The turbine is housed in a 3D printed turbine housing that has an inlet port for 689.5 kPa (100 psi) air to drive the turbine. A window in the housing allows the laser tachometer to sense shaft RPM.

During calibrations, the limit switches stop the stepper motor stage to prevent the inner wall of the tip gap casing to rub against the rotor. The bearing housing and DAS connections are the same as was used in the BCTR (mock casing).

3. Benchtop Calibration Rig Calibration Procedure

This section provides an abbreviated description of the calibration method used on the BCTR. A detailed standard operating procedure (SOP) is provided separately in Appendix D. Capacitive probes and conditioning module channels are maintained paired

together for the experiment. The capacitive probes are labeled 1–4 and were calibrated with channels 1–4, respectively. The casing is mounted onto the carriage of its respective translation stage. The Thor Labs translation stage is used for the mock casing, and the larger Velmex translation stage is used with the tip gap casing. The probe to be calibrated is then mounted into the probe mounting port and secured in place using a M20 - 2.5 (¾"-10) nylon screw. A second nylon screw is then fastened behind the first screw to prevent loosening from vibrations. The probe, ethernet cable, and tachometer are connected onto the DAS's corresponding jacks and all equipment is powered on.

A MATLAB GUI, referred to as the Tip Clearance App, is then started. A picture of the application's calibration tab is shown in Figure 29. It was created to streamline the calibration process. Initially, the data file recording path is specified by the user using the GUI. Parameters such as probe location, probe number, intended RPM, file type, and which rig is used are selected for file recording organization. The specification of these parameters will dictate the naming convention of the folders and files created for consistency.

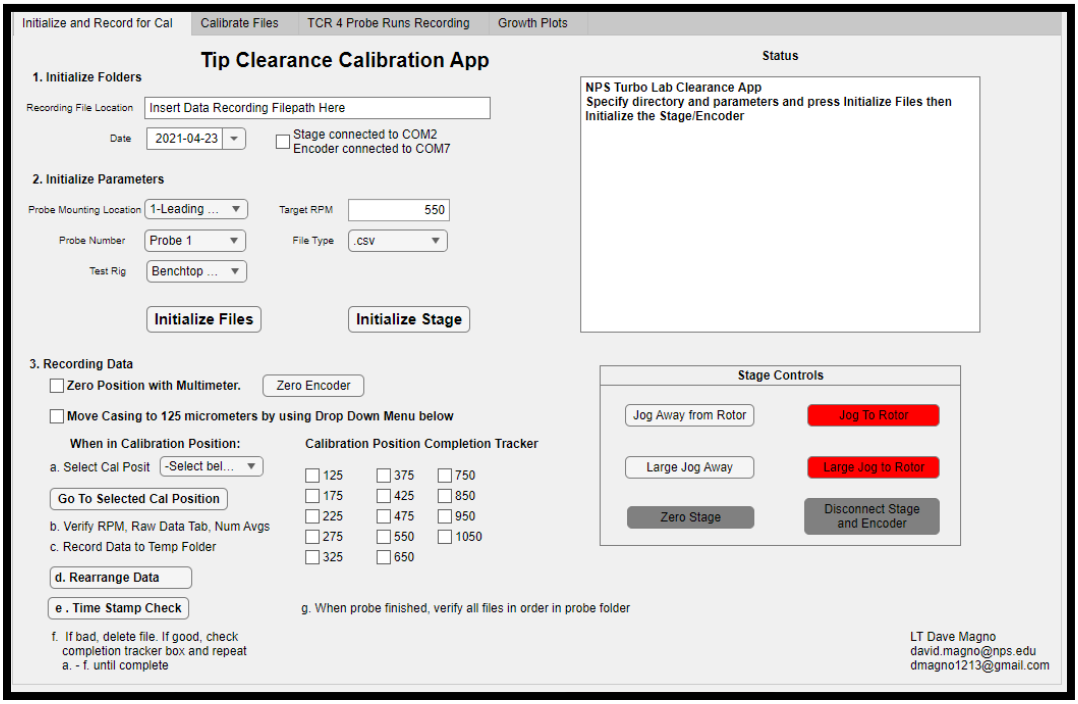

Figure 29. Tip Clearance App in MATLAB.

The RCap V program is then started and is used to establish the PC connection to the DAS. The RCap V configuration page, previously shown in Figure 14, is used to specify:

- Max expected RPM
- Capacitive probe debounce time
- OPR debounce time and which probe(s) are enabled
- File type to save data
- Number of averages needed to update the histograms

Data loss can be minimized by reducing the amount of computational resource used. The amount of revolutions used to average data for the histograms displays is increased to its maximum value to lower computation time to average data. Furthermore, the live data graphic displays are disabled. The translation stages are then setup for remote operation.

A multimeter is connected to the rotor and the casing in “forward bias” mode. To zero the position of the stage, the stage is slowly jogged forward while simultaneously slowly spinning the rotor by hand. After reach rotation of the NPSMF, the stage is jogged closer an additional step. When the rotor blade just touches the casing the zero point is reached. An audible alarm by the digital multimeter indicating contact is used as a queue. The audible sound must come from the rotor spinning freely, as any slight bend coming from the user’s hand on the rotor isn’t representative of the zero position. The distance measurement device, either the dial indicator or linear encoder, is then zeroed and the stage is jogged to its first calibration position, 125 μm (0.0049").

The air cutout valve is then slowly cracked open. Air is applied to the NPSMF. The rotor is slowly brought up to the desired speed by throttling open the air cutout valve. After the probe output signal’s proper behavior is verified via the live data tab on the RCap V software and the NPSMF is spinning at the desired RPM as shown in the histogram tab, the data is recorded for approximately one minute.

Upon finishing recording the data, the files are rearranged and sorted using the Tip Clearance App. The remaining data is then checked for excessive data loss or if the OPR and data are out of synchronization. This data loss and synchronization check is described in the following "Initial Processing" section.

Once data has been deemed useable with no data loss, the stage is then moved to the next position and the process repeats. A total of 25 calibration positions were used in this experiment. All 25 positions were used to validate the calibration method against the manufacturer's method. Only the first 14 positions were used for creating the calibration curves to be used in the TCR as the additional calibration distances were far beyond the cold clearance of the tip gap casing with the NPSMF. The designed cold clearance of the NPSMF in the tip gap casing is 889 μm (0.035"). The calibration positions used are as shown in Table 1. The rest of the calibration procedure is post-processing the data to create a calibration reference curve and table.

Table 1. Calibration Points Used in Procedure

Calibration Point	Distance (μm)	Calibration Point	Distance (μm)
1	125	14	1050
2	175	15	1175
3	225	16	1375
4	275	17	1625
5	325	18	1875
6	375	19	2125
7	425	20	2375
8	475	21	2625
9	550	22	2875
10	650	23	3125
11	750	24	3375
12	850	25	3625
13	950		

B. DATA PROCESSING METHODS

The following sections discuss the initial processing and post-processing methods used for capacitive probe output signal processing, probe calibration curve creation, digital

readout to micrometer conversion, and calculating rotor axial displacement. The program MATLAB was used for the computations discussed in this chapter. All functions and scripts are provided in Appendix A. The detailed step-by-step procedure for using the MATLAB GUI is provided in the procedures in Appendix D.

1. Initial Processing

The initial processes consist of organizing the recording file paths, recording the data, and checking for data loss.

a. Initializing Files and Recording Data

The RCap V software supplied by Rotadata, Ltd. offers the ability to directly record raw capacitive probe signal DRO data and the OPR data into separate .csv or .bin files to a user specified folder location. Their software also has the ability to directly record tip clearance and an average tip clearance when used in conjunction with a calibration file. For this experiment, only the raw capacitive probe and OPR data files are used. The other files outputted by the RCap V program are removed.

The Tip Clearance App is used to specify the recording locations for the files. Upon pressing the "Initialize Files" push button, a folder is created with a naming convention based on the parameters selected in the GUI. The recorded files will be automatically moved into this folder to store the calibration data files in one location. A folder for the eventual calibration table is also created and a folder for figures corresponding to that data set is created. The parameters set by the user in the app dictate the folder and file naming convention. A typical data set for calibration will have 12 folders corresponding to the 4 probes in their 3 different monitoring locations and the calibration and figure folder.

The Tip Clearance App also features an "Initialize Stage" push button that connects the Velmex stage and encoder to MATLAB. This is only used for the modified calibration rig. Next, the user continues to follow the calibration procedure as previously discussed, zeroing the casing position then moving to the first calibration position. The data is then recorded using the RCap V software.

If data is saved as a .csv file, the user can open the file and examine multiple parameters including the raw DRO readouts. The raw data files come in multiple rows of 5006 columns. The first column provides the channel the data is coming from, 2nd is the UNIX time stamp, 3rd is current time in units of 2 μsec. The 4th is the RPM recorded at the timestamp, the 5th is data packet size and the 6th column through the 5,006th is the recorded is the DRO recorded every 2 μsec (corresponding to the 500 kHz sampling rate) and the next row is started. Therefore, each row has nominally 10,000 μsec worth of data drawn from the capacitive probe. The sampling frequency is governed by a crystal oscillator and has an approximate 50 ppm band of deviation from the nominal 500 kHz sampling frequency. The OPR signal is similarly created except it records 10,000 points of data per row as opposed to the 5,000 from the capacitance probe. The OPR data is written into the .csv file as 1's and 0's for when the pulse is on or off, respectively. Figure 30 shows an example of the raw data in a .csv file recorded straight from the RCap V software.

Channel No.	UNIX Timestamp	Time (2 micro sec)	Rotational Speed	Data Packets	DROs (2 micro sec)	DROs (2 m	DROs (2 m	DROs (2 m	DROs (2 m	DROs (2 m	DROs (2 m	DROs (2 m
5	3654583470	800539	33595	128187	31442	31852	32096	32078	31909	31790	31833	31951
5	3654583470	820539	33595	128188	29150	29338	29516	29712	30068	30404	30605	30798
5	3654583470	840539	33595	128189	31649	32103	32460	32743	33060	33464	33851	34137
5	3654583470	860539	33708	128190	36110	35837	35562	35298	34918	34390	33636	32619
5	3654583470	880539	33708	128191	28386	28414	28322	28254	28291	28318	28306	28414
5	3654583470	900539	33708	128192	31723	31794	31830	31703	31427	31227	31147	31019
5	3654583470	920539	33708	128193	29438	29524	29639	29921	30396	30965	31546	32036
5	3654583470	940539	33708	128194	29100	29413	29792	30360	31103	31878	32567	33148
5	3654583470	960539	33860	128195	30211	30637	30899	31074	31262	31422	31543	31632
5	3654583470	980539	33860	128196	32236	32306	32503	32584	32374	32092	31925	31662

Figure 30. Example Raw Data File. Source: [22].

b. Automated Organization and Data Loss Check

The rearrangement of the data files is achieved using the "Rearrange Data" push button on the Tip Clearance App. Each file is named following a similar naming convention as the parent folders. They are arranged in a particular order to streamline the process.

The data then is reviewed for data loss. When the "Time Stamp Check" push button is pressed a function will analyze the .csv file for errors by examining the time stamps. Time stamp information is only available for .csv files. If files are saved as a .bin file this step is skipped. Majority of data taken in this study was recorded as a .csv file to allow the ability to check time stamps. All data used for calibration was recorded as a .csv file.

The function finds the folder where the data is stored then finds the .csv files and extracts data from both the raw probe data and the corresponding raw OPR data using MATLAB's "*dlmread.m*" command into matrices. Referring to Figure 30, the UNIX timestamps (sec) of the 2nd column are added together with the time stamps of each row (μsec) of the 3rd column into a vector. The differences of each value in the vector are then calculated using MATLAB's "*diff.m"* function. Nominally, each of these should be the 10,000 μsec between each row of capacitive probe data and 20,000 μsec for OPR data. The amount of deviation from the nominal time value is then determined from each row of data and then added to find a total amount of deviation in time. Normally, less than a hundred microseconds are lost per calibration point. The small loss in time is due to the imperfect crystal oscillator that times that circuitry housed within the DAS.

A calculation is then conducted to find time differences between each row greater than 10,000 μsecs (or 20,000 for the OPR data). A difference greater than 10,000 indicates a whole row of data missing, which can occur if the RCap V software is saturated (high refresh rates). After the capacitive probe data has been checked for data loss, an equivalent check is then done for the OPR data. A true/false statement is used to produce a 1 if one or more rows of data is missing in the .csv file, or a 0 if not, and is displayed to the user.

The difference in data loss between the raw probe data and OPR data is then calculated to see the degree of data loss synchronization. Normally less than 10 μsec of microdata is lost between raw probe data and OPR data and is not noticeable. A summary page of the information is then outputted by the function for review by the user. An example of this summary is shown in Figure 31.

RAW DATA
Time Error in Raw Data? (T/F): 0
Rows skipped of Raw Data: 0
microsec of Raw Data Lost: -5.983353e+01

ONCE PER REV
TimeError in OPR? (T/F): 0
Row Skipped of OPR Data: 0
microsec of OPR Data Lost: -6.330490e+01

BLADE PASSING INTERVAL INFO
Total Revs Recorded: 646
Average Period of Blade Pass: 5.063436e+03 microsec
Raw Data Percent Time of Lost of the Average Blade Period: -1.181678e+00%
Once-Per-Rev Percent Time of Lost of the Average Blade Period: -1.250236e+00%
Raw Data Time Lost - OPR Time Lost = 3.471375e+00 (microsec). If positive RD shifts to right relative to OPR intervals.

Figure 31. Data Loss Summary Example.

Finally, a check is done to verify the raw capacitive probe data is properly synchronized with the tachometer's OPR signal. An arbitrary blade is singled out of the data. The index of this blade's output signal's maximum is determined for each revolution in reference to the OPR signal. The peak location is expressed as a fraction of the individual blade's passage by dividing the peak's index by the total number of points in the revolution. The function produces a scatter plot of the peak location for each revolution, as shown in Figure 32.

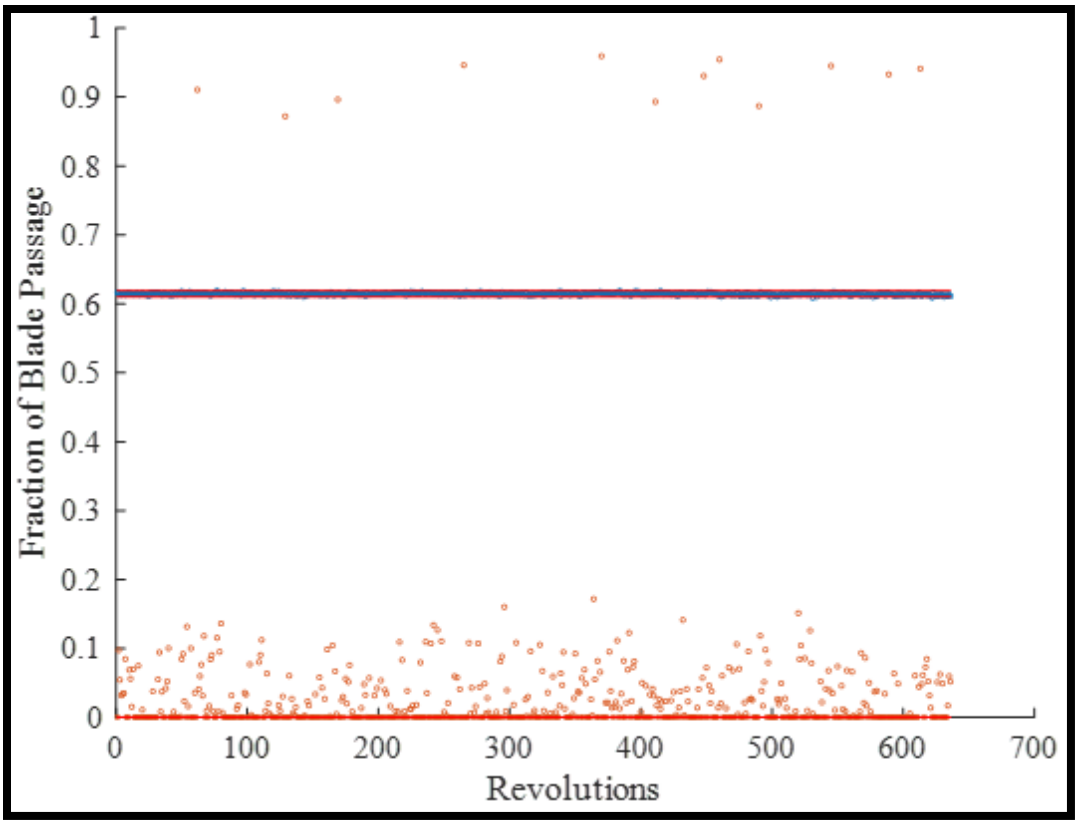

Figure 32. Data OPR Synchronization Check Showing Nominal Result.

A blade fraction of 0 indicates that start of the rotor blade tip passing the capacitive probe and a fraction of 1 indicates the end of the blade passing event. The figure shows the maximum peak of the output pulse occurs at ~61% of the blade passing event, on average, and the minimum occurs near the beginning of the blade passing event. The expected result is that the maximum location remains in the same location, as shown. If data loss or loss of synchronization were to occur, the user will find the location of the peak will trend in reference to the OPR signal over time as shown in Figure 33. If excessive data loss in either the raw capacitive probe data or OPR raw data exists, or if there's issue with OPR synchronization, the data is thrown out and that calibration point is rerecorded. Once the data has been verified to have none of the data deficiencies described, the calibration procedure continues to the next point. Once all calibration points have been recorded, the data is then processed for either calibration and/or analysis.

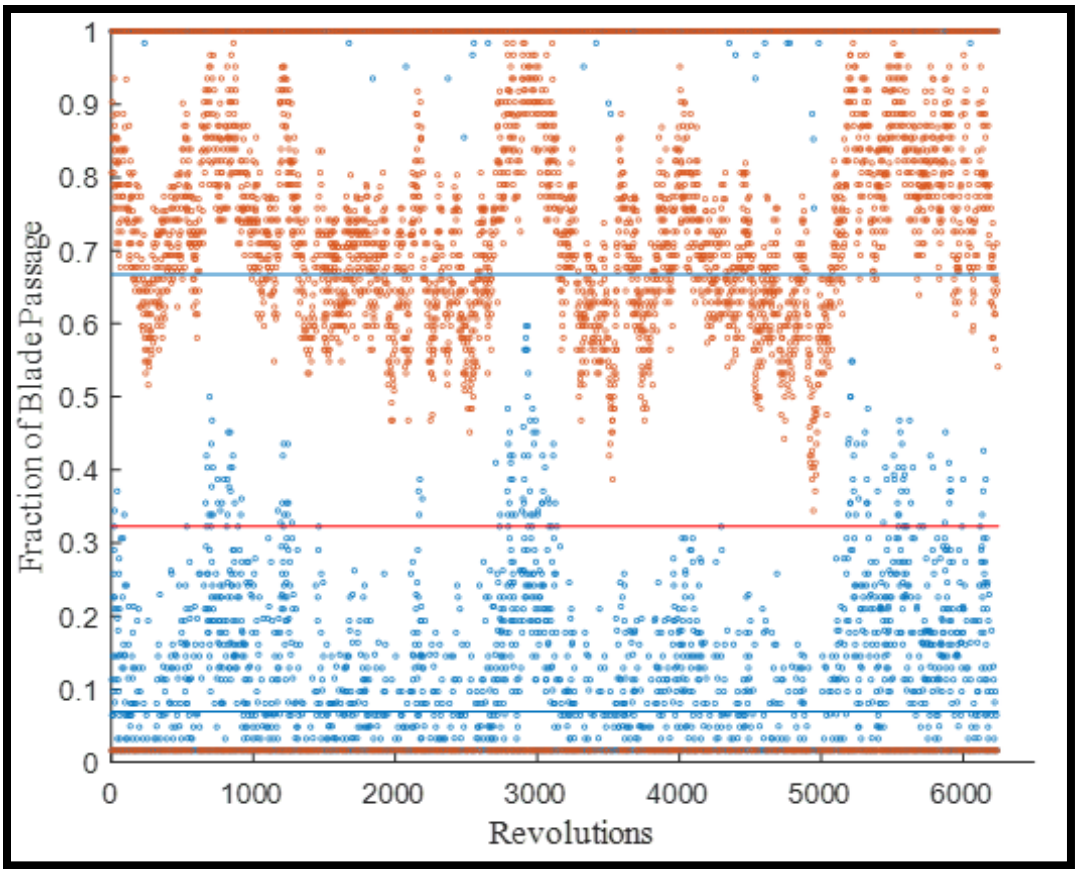

Figure 33. Data OPR Synchronization Check Showing Loss of Synchronization with OPR Signal.

2. Resampling and Filtering Data

a. Data Extraction and Rearrangement

Once all 14 calibration points are recorded and quality checked, the user uses then begins the post-processing calibration. The function processes each pair of capacitive probe data and OPR data. If the data was recorded as a .csv file the paired capacitive probe and OPR raw data are imported into MATLAB using the program's "*dlmread.m"* function, creating a matrix within the random-access memory. The columns involving the timestamp, channel, and data packet information are removed leaving only the raw data readings. Each row of data is then rearranged from their matrixed organization and rearranged into a continuous row vector.

If the files were recorded instead as a .bin file, the data is already recorded in a vector and does not need rearranging. The .bin files are stored as *uint16* and must be read as such. A plot of a portion of the raw capacitive probe data and OPR raw data are shown in Figure 34. The raw OPR data is amplified for visual purposes.

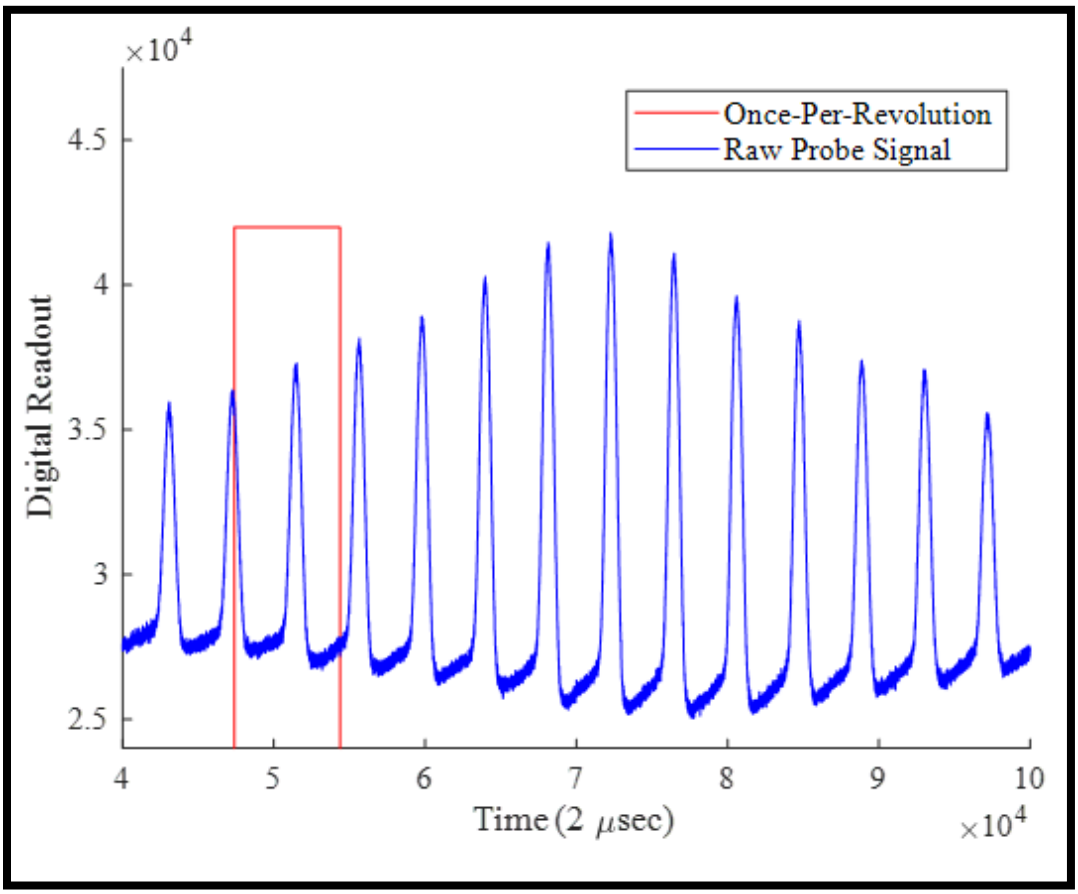

Figure 34. Sample Interval of Raw Capacitive Probe Data and Amplified OPR Data Overlaid.

As described in Chapter II, the peak-to-peak DRO value of the raw capacitive probe signal is proportional to tip clearance distance. Larger peak-to-peak values mean a smaller clearance. As mentioned, the sampling frequency is 500 kHz meaning each data point is recorded every 2 μsec.

b. Resampling the Data and Transferring to Spatial Domain

The BCTR and TCR are driven by their respective pressurized air source. The air is pressurized with an air compressor, either the facility 100 psi shop air, or the Allis Chalmers compressor on the main test rig. The compressors are controlled to maintain the pressure within a pressure band. This band of pressure causes a corresponding band of shaft RPM. Figure 35 provides an example of how the RPM behaves over the course of a minute due to the pressure band maintained by the air compressor. Each revolution's average RPM is found by finding the amount of data points between each pulse rise of the OPR raw data. The pulse rise indices can be located by using the MATLAB "*find.m"* and "*diff.m"* functions to find all times when the difference in the individual points of the OPR's square wave signal are greater than zero. By then knowing each sample point is taken every 2 μsec and inverting the period of each revolution, this average RPM is found.

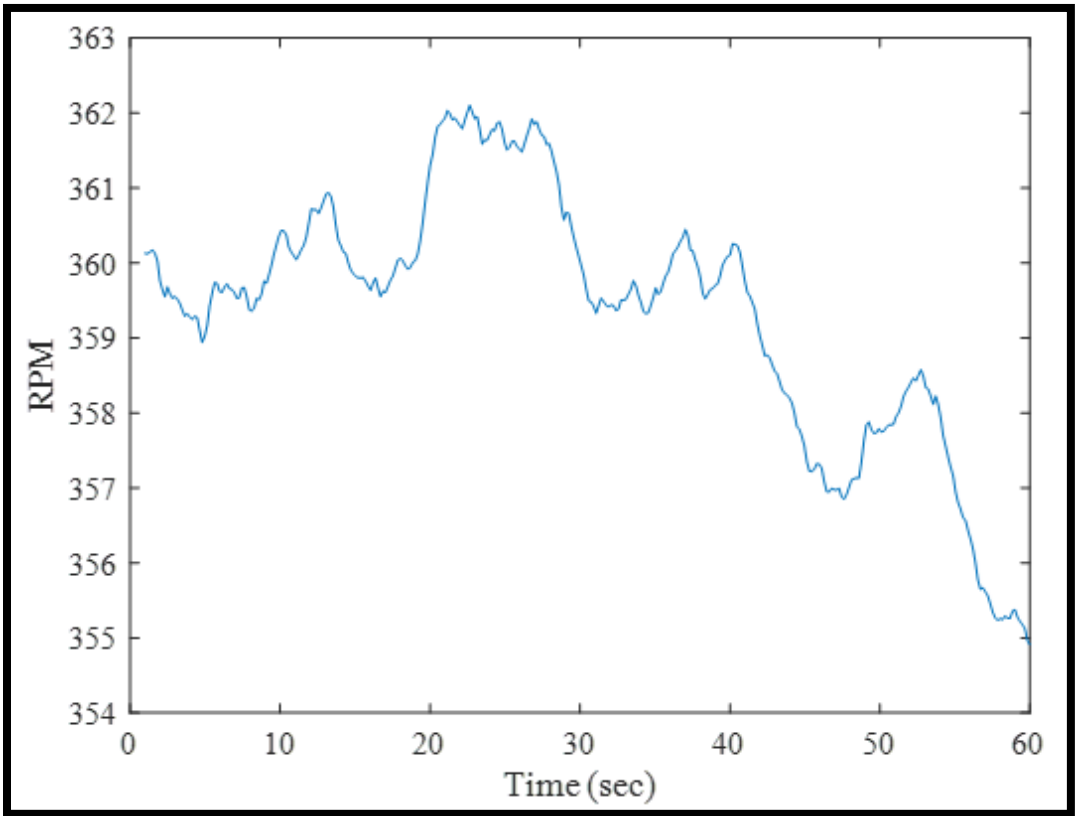

Figure 35. Variance in RPM Due to Compressor Pressure Changes.

The difference in speed causes there to be more frequencies present in each data set as shown in a Fast Fourier Transform (FFT) analysis discussed later. If there was no speed variance, a better FFT can be produced. The variance in speed causes the amount of sample points within each revolution to be different. To remove the effects of varying speed the data is resampled with each revolution interpolated with a uniform amount of data points. This transforms the time data to spatial data.

It was found that a lowpass filter's output was different when passing through data from the benchtop rig and transonic rig. A considerably larger amount of power was taken out of the raw signal from the benchtop rig as compared to the transonic rig. To create a signal that's comparable to the TCR's signal at its highest speed, the data is "under-sampled" to mimic the calibration rig spinning at 27,000 RPM.

Taking the OPR data, the indices of the pulse rises are located and stored. The amount of resampling to be done between each of these pulse rises is set to the amount of samples that would be taken at a 500 kHz sampling frequency if the rig were to spin at 27,000 RPM. The sampling amount is then increased to the nearest integer divisible by 20. Increasing to the next number divisible by 20 enables the revolution to be divided into 20 equal intervals for blade-by-blade analysis.

The raw data is resampled via linear interpolation so that each revolution has this same number of data points. The interpolation is done using a loop that takes the indices of the start of each revolution, determined from the OPR signal, and resamples each revolution using the "*interp1.m"* MATLAB function. This essentially creates an artificial sampling frequency. Under-sampling with a uniform amount of data points for each revolution keeps the RPM uniform, removing the RPM swings previously discussed. Figures 36 and 37 show the effects of interpolating the raw capacitive probe data. Figure 38 is extrapolated from TCR data at 27,000 RPM and is given as a comparison.

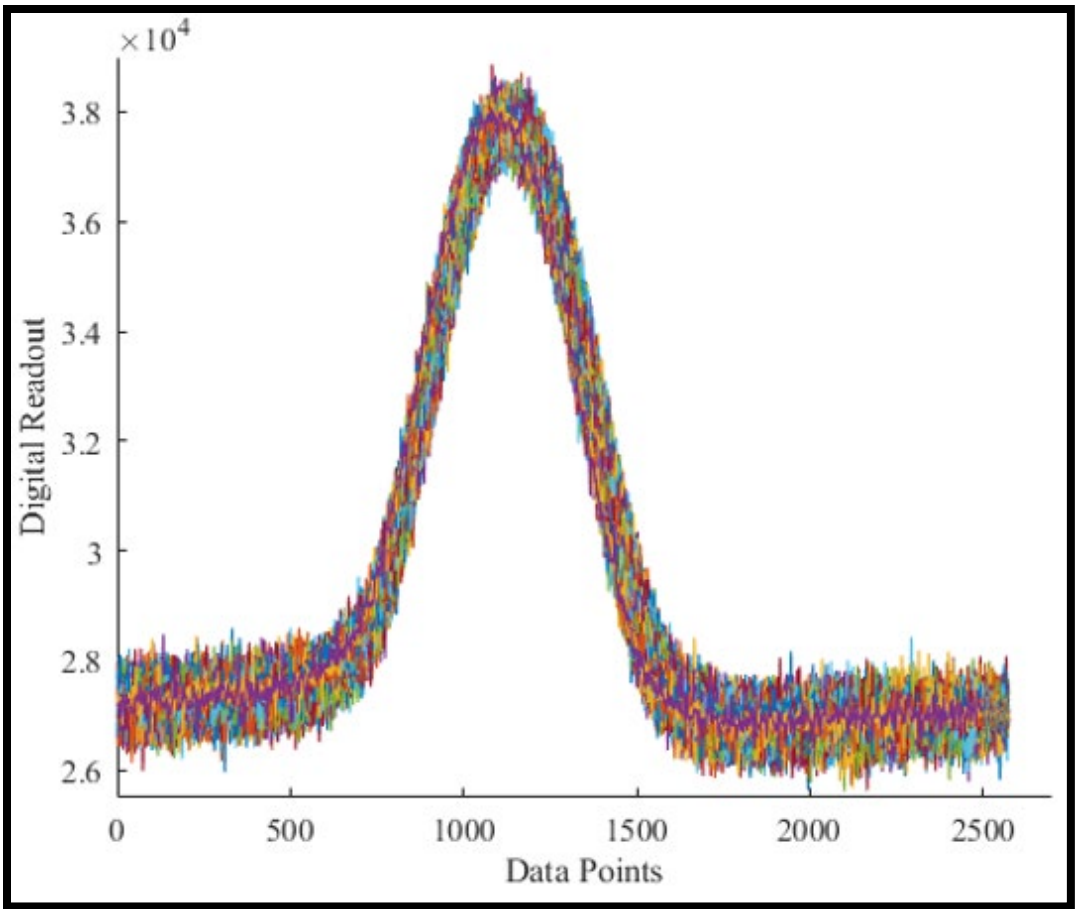

Figure 36. Overlaid Plots of a Single Blade Prior to Resampling.

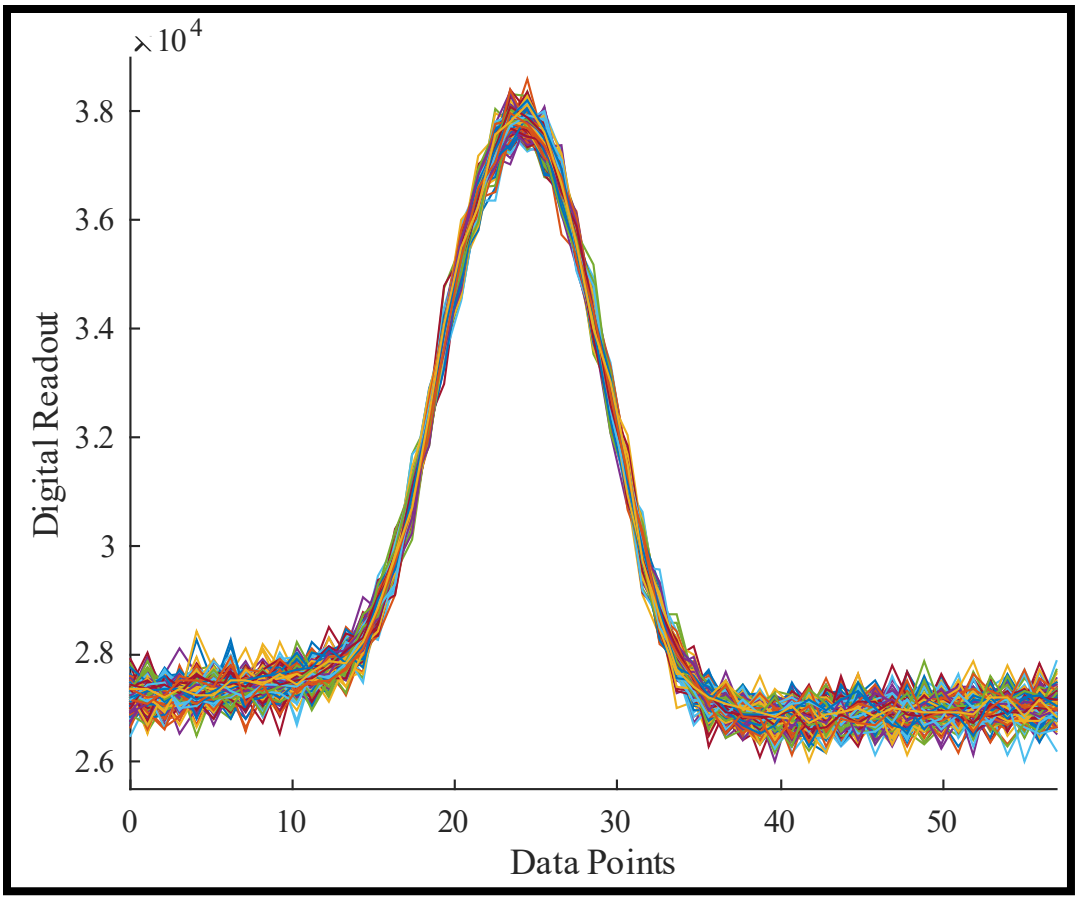

Figure 37. Overlaid Plots of a Single Blade Post Resampling.

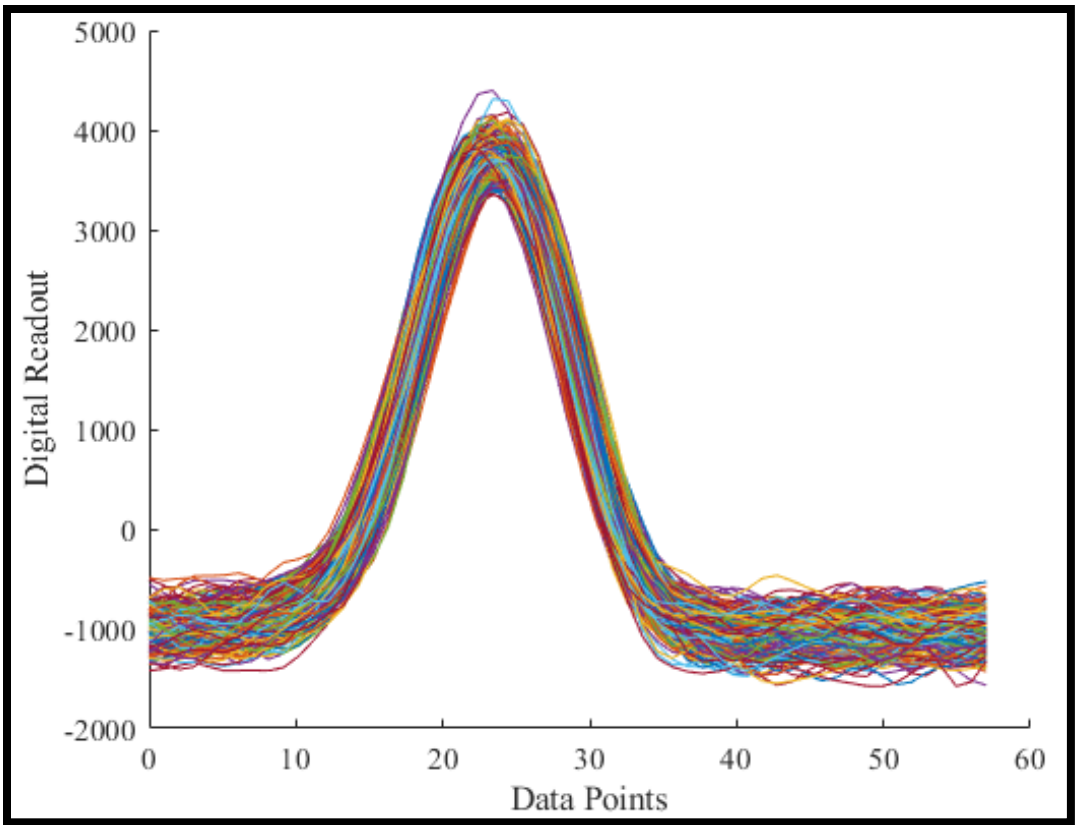

Figure 38. Overlaid Plots of a Single Blade Bon TCR.

Figures 36 through 38 show a representative blade's signal overlaid over 550 revolutions. The difference in speed of the non-resampled data can be inferred from the "width" of the overlaid plot (taking into account the x-axis scale in comparison). The significance of resampling the data with a uniform number of sampling points is that it improves the frequency resolution of the data and reduces the range of frequencies in the frequency spectrum, overall improving the SNR. This significance can easily be shown with a FFT analysis. Furthermore, by reducing the amount of sample points to mimic the signal that would be produced from running the TCR at its 90% speed makes the filtering effects of the two methods comparable.

c. Fast Fourier Transform

A FFT is run on the data to find an appropriate passband for the lowpass filter and to visualize the increased frequency resolution. The data is first detrended since when it is

recorded the signal is imposed on a DC line voltage. The detrending is done using MATLAB's "*detrend.m"* function. A Blackman window is applied to the data. Then MATLAB's "*fft.m"* command which applied a Fast Fourier transform to the data set is used. When running the FFT, frequency is converted into the shaft order domain by creating a time vector where each sample point is the inverse of the uniform resampling amount. The resulting FFT plot is shown in Figure 39. The figure also provides a comparison to an FFT run on unprocessed raw data.

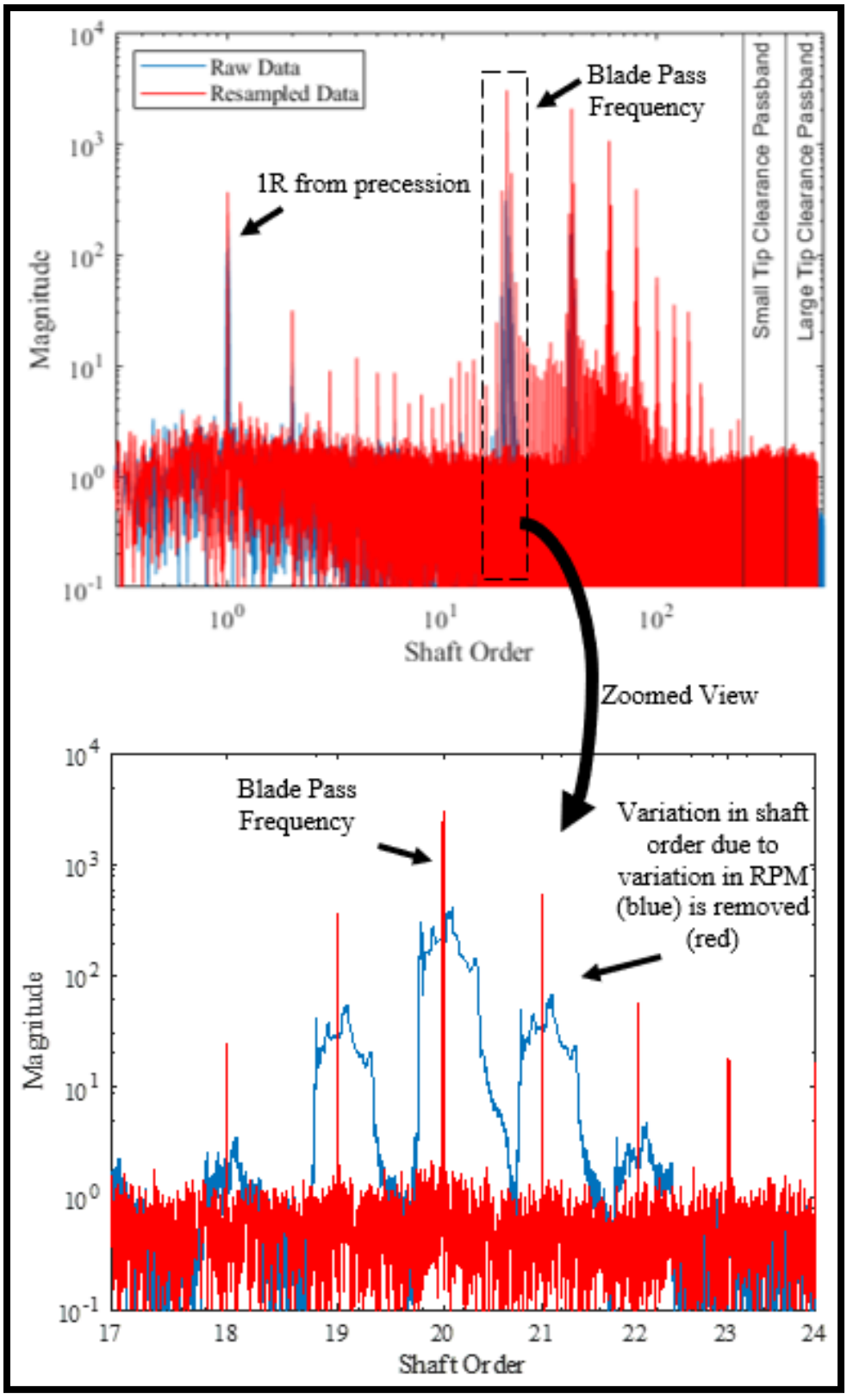

Figure 39. FFT Analysis with Zoomed-In View Showing Resampling Effect.

The peak occurring at order 1 corresponds to a frequency occurring once every revolution and can be attributed to rotor eccentricity or shaft precession from the rotor being improperly centered. This can be seen in the raw data (refer to Figure 34). Order 20 shows the blade pass frequency, corresponding to the 20 rotor blades. The raw data (blue) shows the deviation in speed when viewing the zoomed-in plot. It is evident that resampling the data has removed the variance in speed which translates to removal of variance in shaft order (red). These sharper peaks mean that the frequency resolution of the data is improved. The taller red peaks are a result of their being less frequencies present in the data set, signifying an improved signal-to-noise ratio (SNR). The significance of the better frequency resolution provides better filtering when this signal is passed through an adaptive lowpass filter (LPF).

d. Low Pass Filter

The output signals are passed through an adaptive LPF based on the rotational speed of the rotor (order domain). The frequencies present in the order domain of interest are all low values. Therefore, a LPF was desired as opposed to a high pass or band pass filter. The adaptive lowpass filter (LPF) has 2 different passbands that depend on the tip clearance size. For small tip clearances the passband includes up to order 400. Large tip clearances include orders up to order 250. These are shown previously in Figure 39. The small and large tip clearances were chosen by the author based on how well the output signal was smoothed. A large tip clearance is defined as a tip clearance that is equal to or larger than 950 μm (0.037"). The noisier large tip clearance raw data benefitted from excluding extra frequencies, while the better SNR smaller tip clearance data required a larger band to better shape the output signal.

The stopband is 1.3 times the passband. The passband attenuation is set to 1 and the stopband attenuation is set to 100. The LPF sampling frequency is set to the number of sample points per revolution calculated previously, which changes between each data set. A Butterworth IIR filter was used. The general shape of the filter envelope is shown in Figure 40.

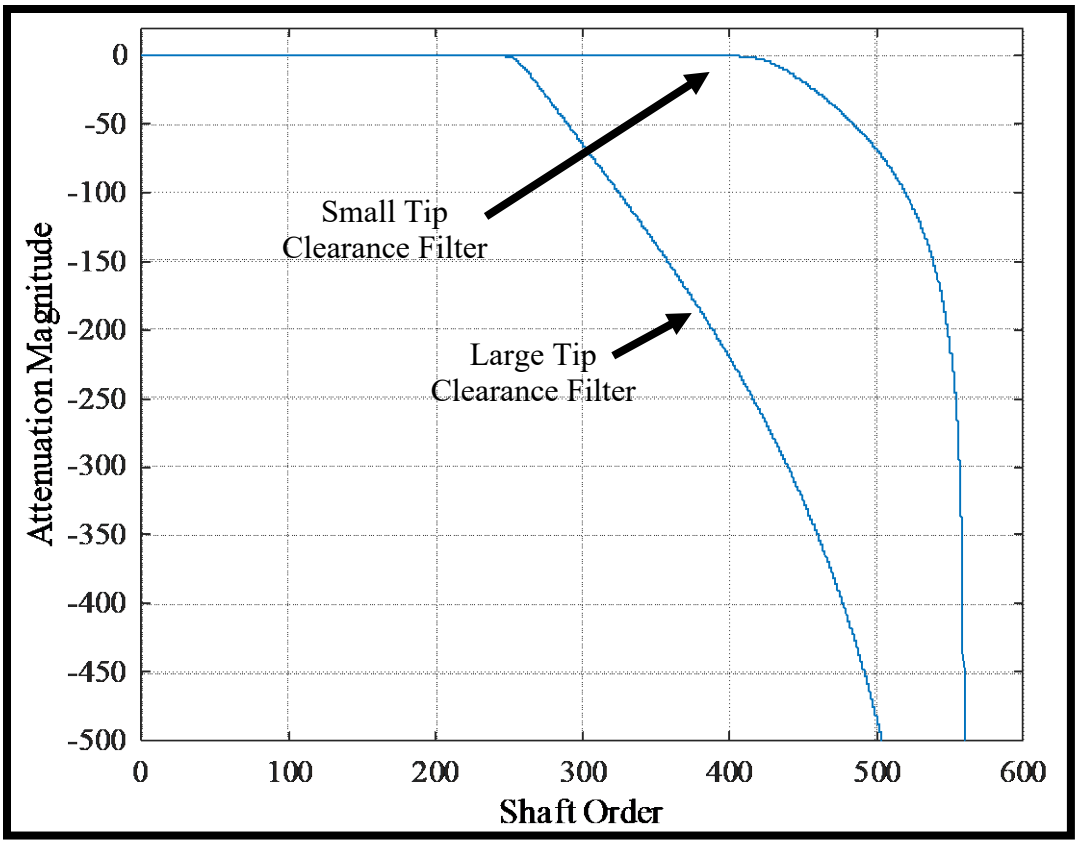

Figure 40. Lowpass Filter Envelopes.

Running the signal through the digital LPF causes the signal to lag by a certain amount. To correct the lag, the MATLAB function "*xcorr.m"* was used to find the cross-correlation between the detrended resampled raw data and its resulting lowpass filtered data. The "*xcorr.m"* function outputs both a vector of the cross-correlation and a vector of the lag. The index of the maximum of the absolute value of the cross-correlation vector then is found. The delay is found by finding the lag located at that calculated index. This delay is used to readjust the resampled, detrended data and the filtered data back in phase. The lag correction is done to remove the non-useable zeros generated at the ends of the vectors from the filter and also serves as a tool for a visual comparison to determine the effectiveness of the filter. Figures 41 and 42 show comparisons between the data before and after filtering for the smallest and largest tip clearance.

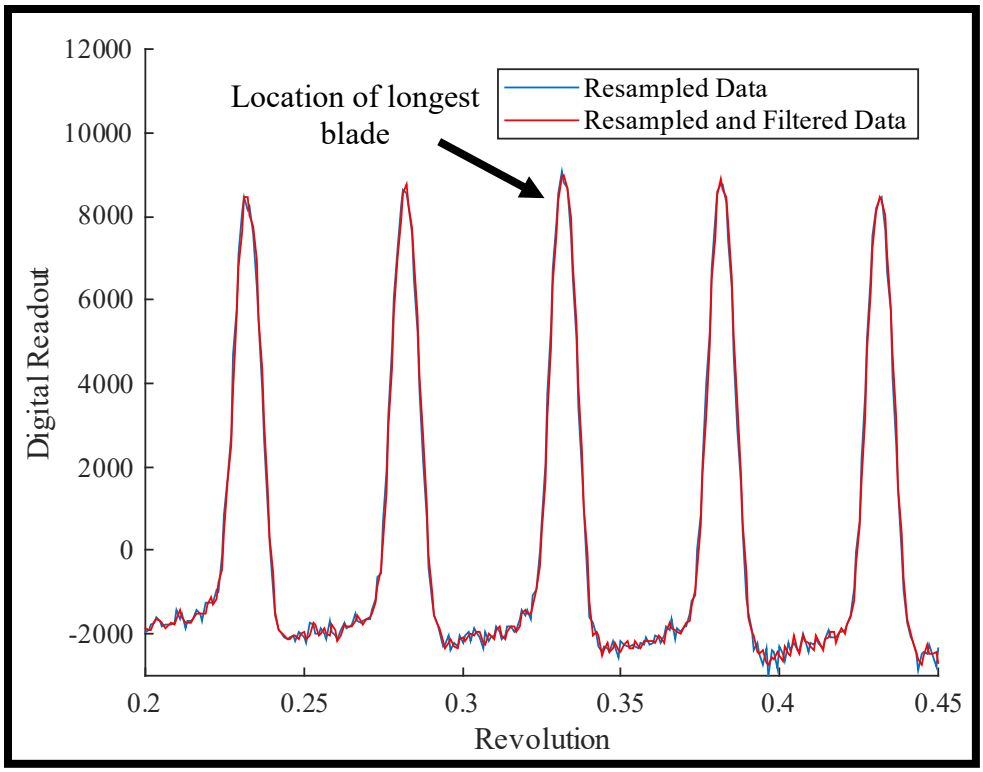

Figure 41. Filtered Data Comparison for 125 µm (0.00492").

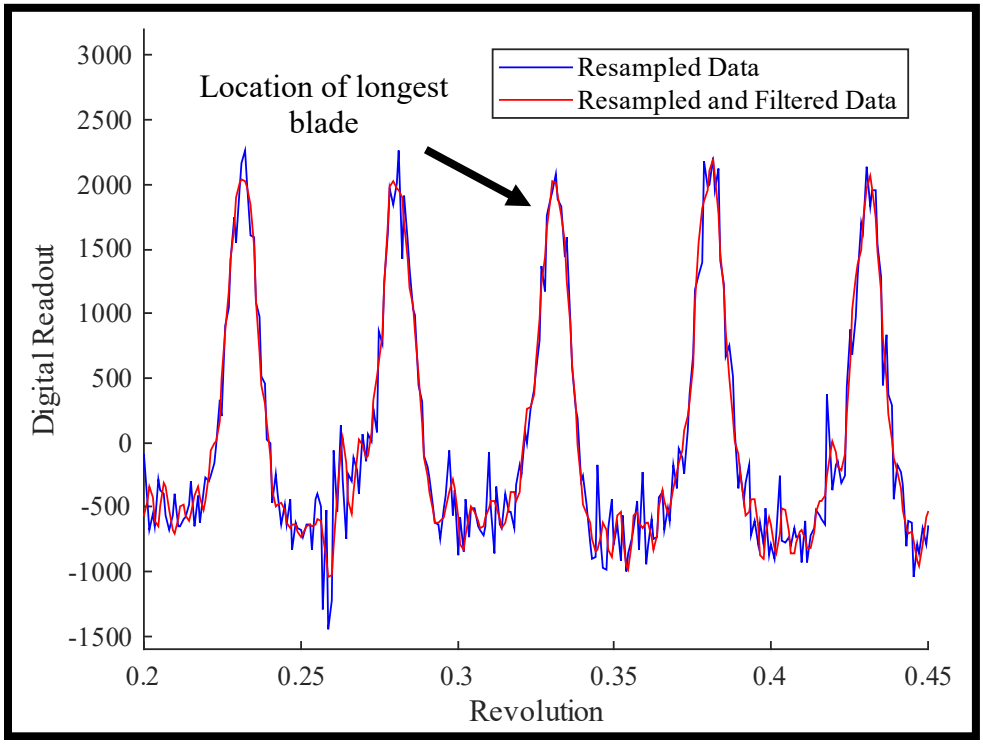

Figure 42. Filtered Data Comparison for 1050 µm (0.0413").

It is evident that the tip clearance dependent adaptive LPF raises the SNR for both small tip clearances and noisy large tip clearances. The closer tip clearance plot's filtered and unfiltered data are near the same since resampling the data already improves the SNR greatly. One can see in the larger tip clearance plot has a weaker peak-to-peak DRO and a smaller SNR. The larger tip clearances with the poorer SNR benefit most from the filter. The two plots were created using the same parameters, only differing in tip clearance size. One can also see that prior to filtering, finding the longest blade to calibrate against is more difficult due to the noise present. This is not as much an issue for the closer tip clearances.

e. Creating Indices for Blade-by-Blade Analysis

The revolutions are uniformly spaced by a set amount of data points, which was previously chosen to be divisible by 20. This allows for blade-by-blade analysis of the rotor. A table of indices is created. The table consists of 21 columns corresponding to blade number. The consecutive blade numbering starts at the beginning of the OPR's signal. Each row corresponds to a consecutive revolution. Beginning with the number 1, the index at the beginning of each row is a multiple of the previously calculated uniform number of resampled points. Each column adds $1/20^{th}$ of the resample amount. Therefore, columns 1 through 20 correspond to the start of each individual blade's starting index, with the 21^{st} column being the end of that revolution. Using this table streamlines the ability to single out one or more blades at a time. Figure 43 is a plot of the filtered probe signal with vertical lines plotted at the indices from this index table. The index value at the first column of each row is plotted with the blue vertical lines. The 20 subdivisions are shown in black.

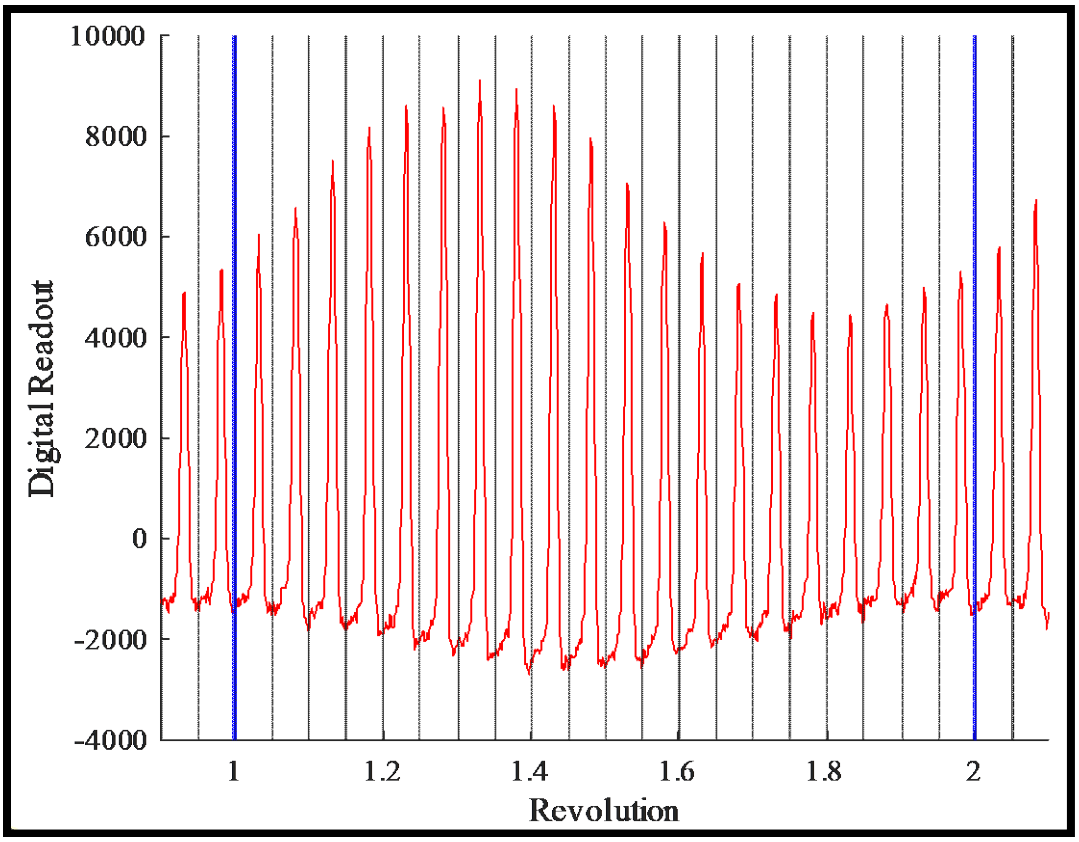

Figure 43. Filtered Data with Index Lines Isolating Blades.

3. Determining the Longest Blade to Calibrate Against

Imperfections in the rotor geometry or rotor precession can result in one blade consistently being closest to the capacitive sensor. The blade that on average outputs the largest peak-to-peak DRO output is referred to as the "longest blade." To determine the longest blade, each blade passing event for a specified number of revolutions is analyzed using the table of blade indices. When each blade is isolated, the filtered peak-to-peak digital readout (DRO) is calculated. The peak-to-peak values are stored in a "Revolutions x 20" matrix. The mean of the filtered peak-to-peak DRO values of all the specified number of revolutions for each individual blade is then calculated by taking the mean of each column. These mean values are then compared. The blade that on average displays the highest peak-to-peak DRO value is labeled the longest blade.

4. Creating the Calibration Curve

The BTC of each blade passing is proportional to the peak-to-peak DRO value of the signal produced. The same filtered peak-to-peak table is used from the longest blade determination. The mean of the data of the longest blade's column is calculated along with the standard deviation of those data points. The mean value and standard deviation is used for the calibration table for the calibration distance it was recorded at. The standard deviation is calculated using MATLAB's "*std.m"* function and is weighted by N = 1. The process is repeated for all 14 calibration points (25 points for the method comparison experiment). An error bar plot showing an example of a calibration curve is shown in Figure 44.

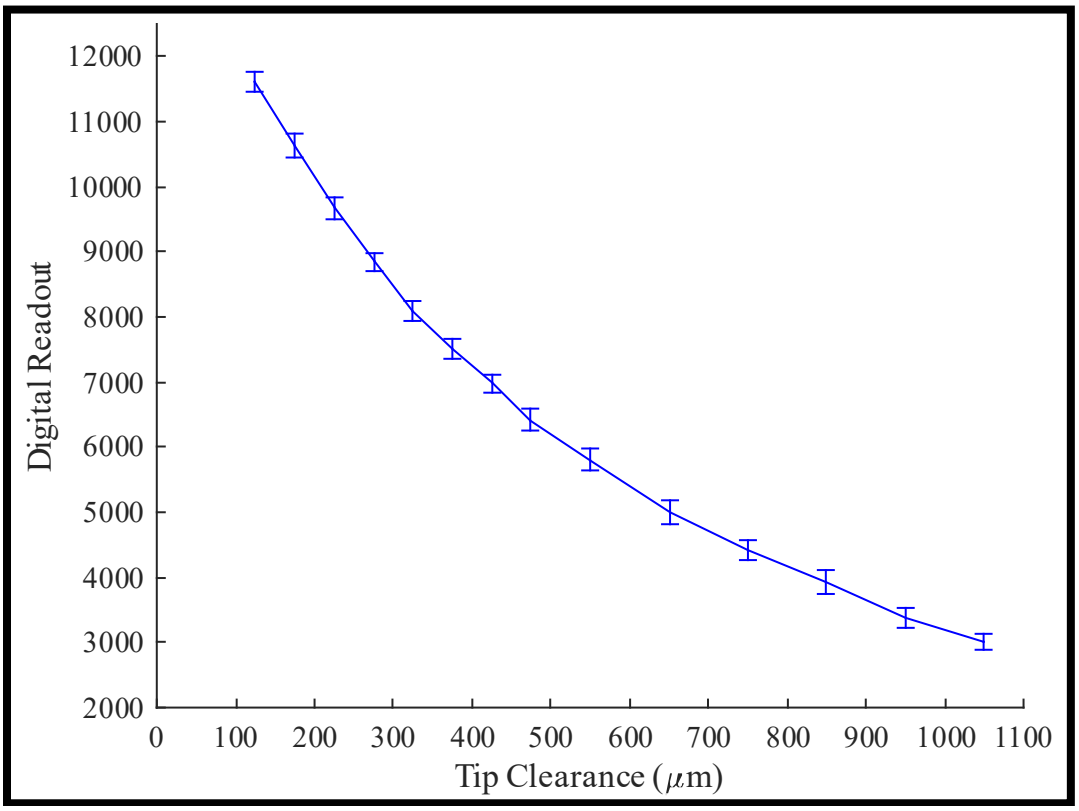

Figure 44. Calibration Curve Produced from Presented Method.

The BTC is plotted as the independent variable since it is the parameter the user changes during calibration. When converting DRO to BTC during an actual measurement,

the independent variable becomes the digital readout. Therefore, the graph's axes are inverted. This calibration curve is then curve fitted using the MATLAB curve fitting toolbox. The equation type was selected as "exponential" with 2 terms for a total of 4 coefficients with 95% confidence bounds. A nonlinear least squares method is used. The equation that is used for the fit is shown in Equation (2), where *x* is the digital readout and *f(x)* is the tip clearance. The *a*, *b*, *c*, and *d* are constant coefficients.

$$f(x) = ae^{bx} + ce^{dx} \tag{2}$$

The curve is then fitted using the MATLAB "*fit.m"* command with the mentioned fitting parameters which outputs the coefficients used to create the curve. The coefficients are extracted and inputted into Equation (2) which is evaluated from a digital readout of 0 to the maximum digital readout of the calibration set. The R-square values for the curve fits are typically about 0.9993 – 0.9999. Figure 45 provides a graph of this fitted curve overlaid on an error bar curve from the calibration set data.

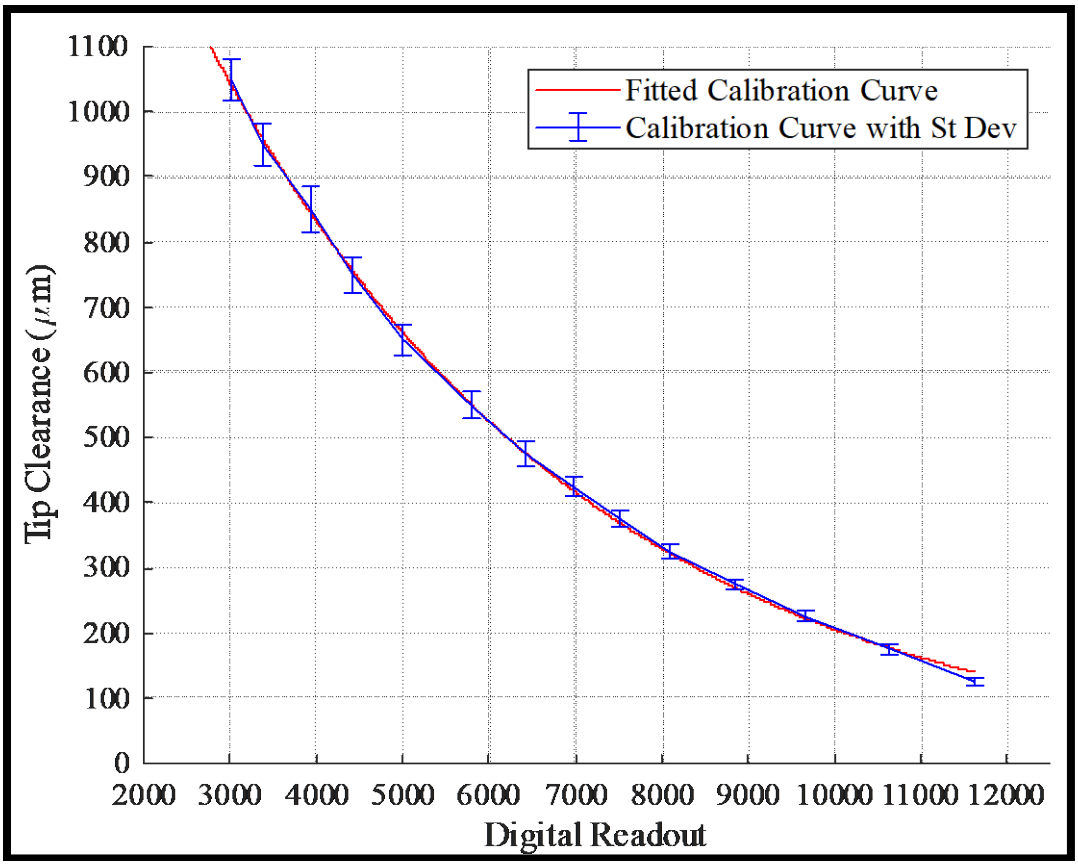

Figure 45. Fitted Calibration Curve Overlaid on Experimental Calibration Error Bar Curve.

Since the axes were inverted from Figure 44 to 45, the standard deviation bars were converted as well. These were calculated by evaluating equation (3) for all corresponding calibration points.

$$st.dev\ (\mu m) = f(x) - f(x + \Delta) \tag{3}$$

The variable x is the calibration point's average peak-to-peak DRO and Δ is the standard deviation in DRO of that calibration point. Function f is from Equation (2). The converted error bars decrease as digital readout increases since evaluating Equation (2) at larger tip clearances has a shallower slope as shown in Figure 45. The resulting calibration curves used in the TCR BTC measurement experiment are provided in Appendix A.

5. Measuring Tip Clearance Using the Calibration Curves

After the calibration curves and tables are made, measurements of blade tip clearance can be done. For tip clearance measurements, all four capacitive probes are mounted into the casing simultaneously recording. The Tip Clearance App is used again to create the recording folders and rearrange recorded files as necessary. The time stamp check is conducted on each probe's corresponding file. Next the recorded data is resampled and filtered in the exact same process as in calibration. The passband for the LPF was dependent on the calibration distance during the calibration process. Since the probe to tip distance is unknown prior to the measurement, the maximum and minimum of the entire data set's population are determined, and the difference is taken. This rough peak-to-peak value is compared to its corresponding calibration curve. If the peak-to-peak is less than the DRO at 950 μm (0.0374"), the larger passband of up to order 400 is used and if larger the passband is up to order 250. After the signal is passed through a LPF with an appropriate passband, the peak-to-peak DRO values are calculated mirrored to the method used in calibration.

A "Revolution x Blade" sized matrix is made and the filtered peak-to-peak values of each blade's passing are recorded, again similar to the calibration method. This allows any individual blade's peak-to-peak value to be converted to micrometers for every revolution. The filtered peak-to-peaks are inputted into Equation (2) for conversion. A scatter plot is then created showing an individual blade's tip clearance for each revolution. An example of a converted data set taken at 125 μm (0.00492") using probe 1 mounted in the mid-chord monitoring position is shown in Figure 46.

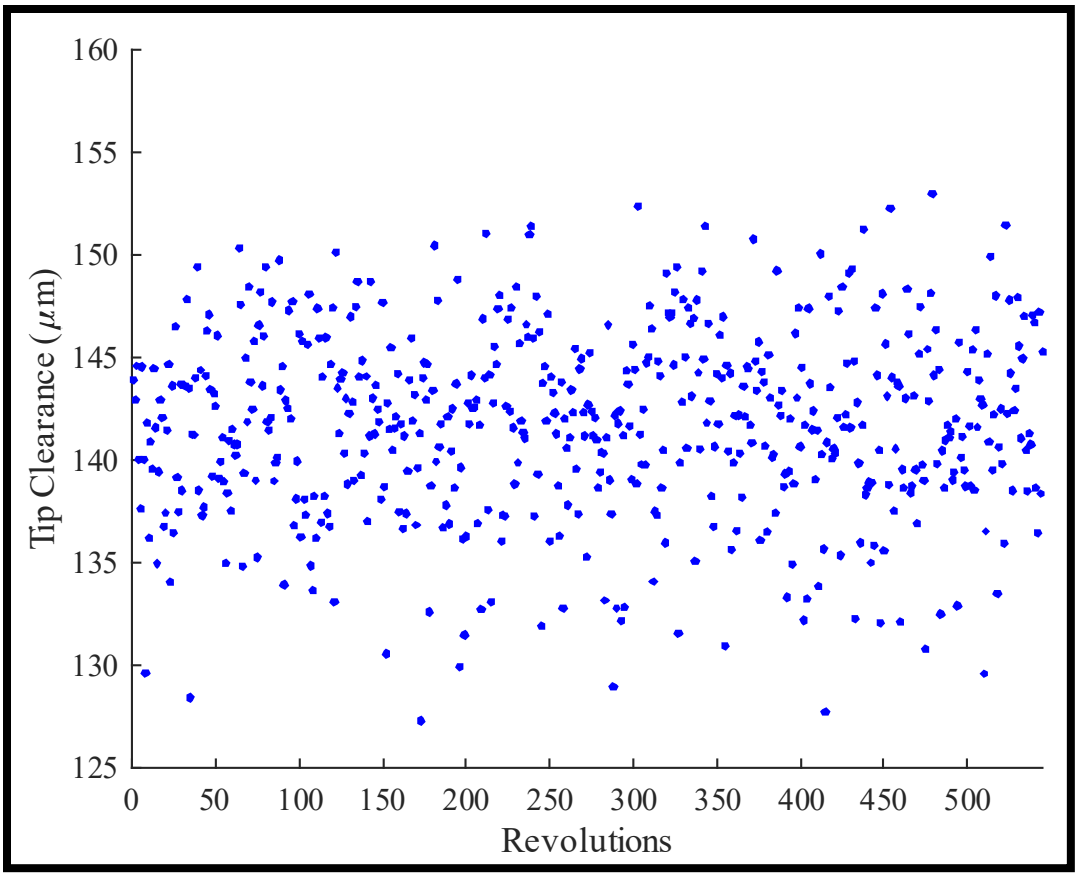

Figure 46. Converted Tip Clearance Values Using the Calibration Curve.

The data used in Figure 46 was from a calibration file, where the exact position of the probe is known. In an ideal situation, when using the exact same post-processing methods, the conversion should output the same value, 125 μm (0.00492"), but in this case the converted average is 141 μm (0.0056"), a deviation of 16 μm (0.0006") from the known value. This can be attributed to how well the curve is fitted. In this particular case the R-square value for this specific calibration curve was 0.9993. A similar plot can be made, but for all 20 rotor blades by instead plotting each converted peak-to-peak converted value on its corresponding blade number, shown with Figure 47. With this plot one can see the distribution of tip clearance values for each blade.

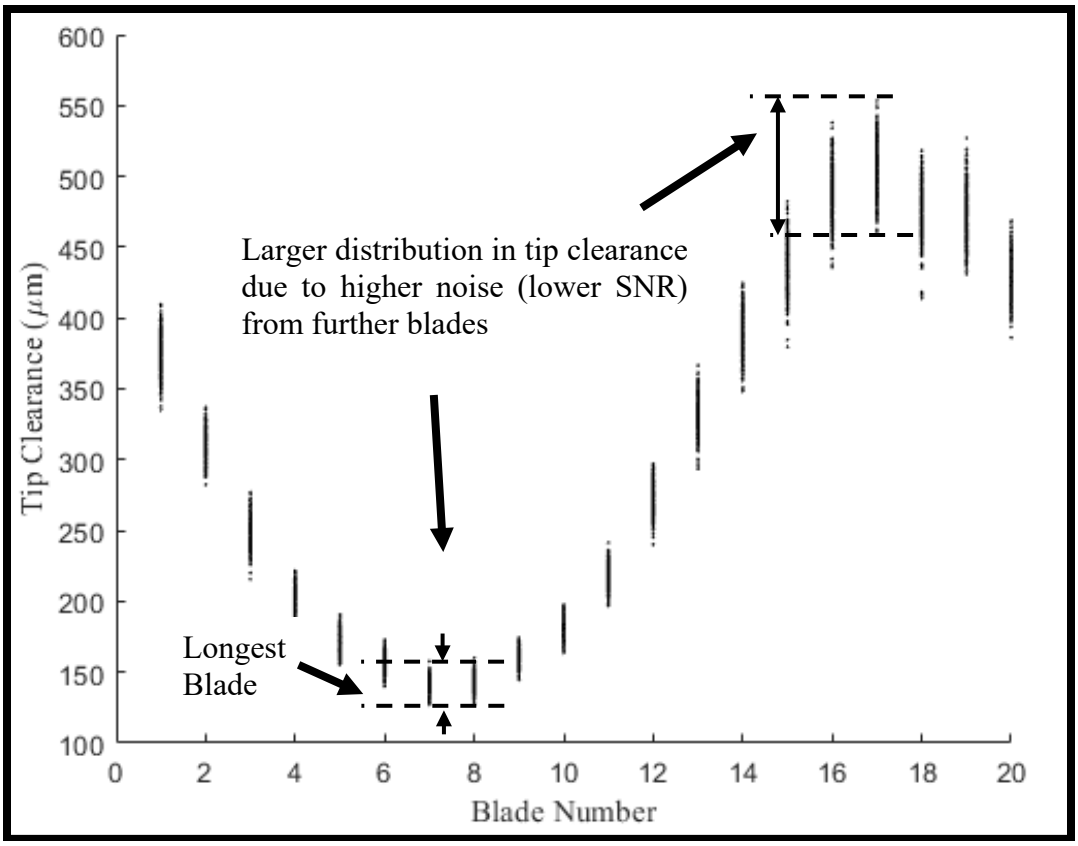

Figure 47. Blade-by-Blade Tip Clearance at 125 μm (0.00492").

The longest blade shown in the plot is blade 7 in probe 1's reference to the OPR. The range of tip clearance values for a single blade is attributable to rig vibration and capacitive probe background noise. One can see that for closer tip clearances, the range of tip clearance values in each revolution is smaller than for the blades that showed larger tip clearances. This can be attributed to a noisier signal at larger tip clearances. Furthermore, this graph explains the peak at shaft order 1 in the FFT plot discussed earlier (Figure 39). One can see there is either some eccentricity to the rotor, or the shaft's axis may have some precession on a once-per-revolution basis. These plots are used for the results of the blade tip growth tests.

C. VALIDATING THE POST-PROCESSING METHODS

1. Validating Proposed Calibration Method Against Manufacturer Calibration Method

A test was conducted to compare the effectiveness of the calibration using the data post-process methods presented in this research against the RCap V software's built-in calibration program. The parameters set regarding this test program are as follows:

- The mock casing version of the BCTR was used
- The gain was set to 2 for all calibrations
- All 25 calibration points (Table 1) are used
- 5 recording sessions were done for this test, one for each of the following filter options:
- The resampling with filtering method previously presented
- 5 kHz lowpass filter, 4 poles
- 20 kHz lowpass filter, 4 poles
- 50 kHz lowpass filter, 4 poles
- Raw data (no filtering)

The calibration using the RCap V software determines the maximum and minimum peak-to-peak values between each OPR signal (each revolution). It takes an average of the peak-to-peak DRO values at a user specified interval. It then takes the mean of the recorded averages and assigns this value to the calibration distance recorded in a calibration reference curve. For example, if an average is taken at intervals of 10 revolutions, for 100 total revolutions, 10 separate averages are taken. This results in a lower standard deviation than the method presented in this study. For the data processing methods presented by the author, the average of the bulk population is used, as previously discussed. To ensure an accurate comparison, however, the calibration averaging in this specific experiment was

adjusted to match the RCap V software's "average of averages." The averages were taken every 20 revolutions, each for a total of approximately 360 revolutions.

The RCap V software will only record data that exhibits 100% "quality," which includes a measure of the signal's SNR. The calculation of signal quality in the RCap V software is unknown to the author. Should a signal's quality consistently be low, the RCap V calibration software will not be able to record, and the calibration cannot be completed.

The results of the validation test comparing the data processing methods of this study against the RCap V software are presented. It is proven that the methods presented enhance the capability of the currently existing calibration method that is available with the manufacturer's software. The presented method provides comparable uncertainty as shown with the standard deviations. Also, the limits imposed by poor signal quality (low SNR) of the RCap V software are exceeded, showing greater dynamic range. The sensitivity is near the same as the slopes of the graphs are similar. The resulting calibration curves are shown in Figure 48. The raw data and 5 kHz filter calibrations using the RCap V software are omitted. The raw data calibration produced the exact same result as the 50 kHz lowpass filter and was therefore redundant. The 5 kHz filter caused the output signal's shape to behave as a stepped sine wave. The RCap V software immediately signaled "SNR Too Low" when using this 5 kHz lowpass filter. Thusly, only the 50 kHz and 20 kHz lowpass filtered calibration comparisons to the methods created by the author are shown.

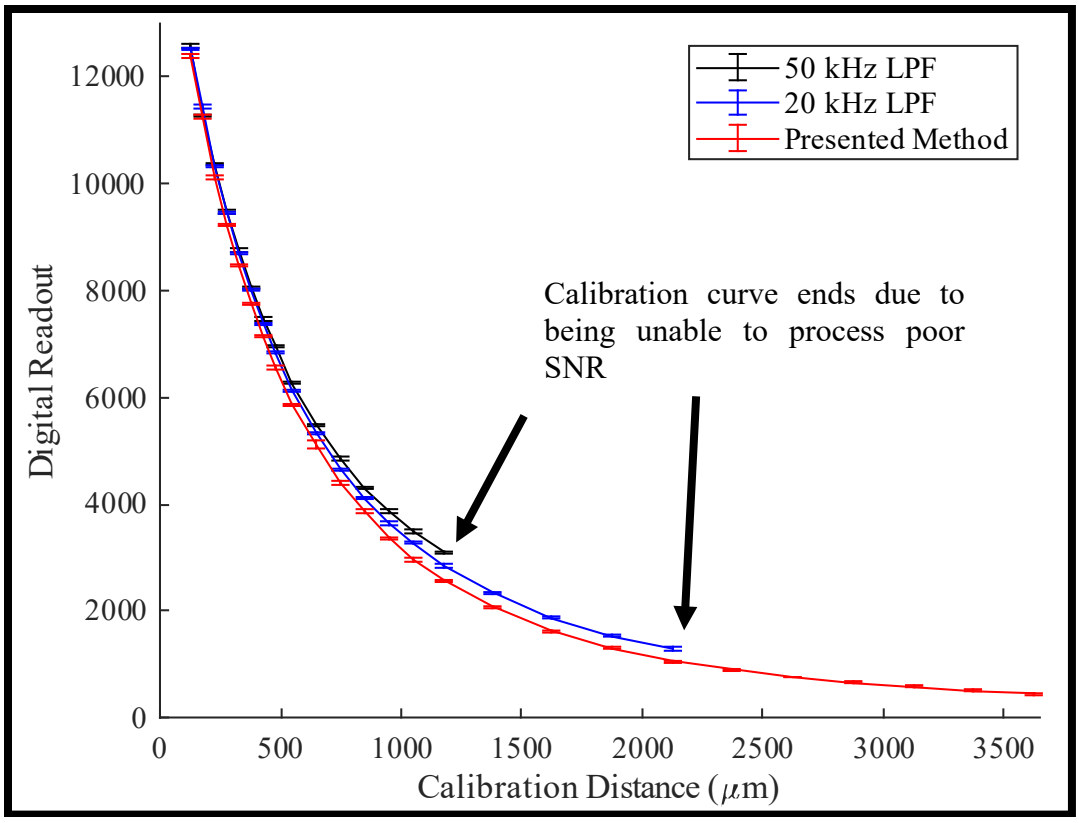

Figure 48. Comparison of RCap V Calibration Software Results to Calibration Method Presented.

Both the 50 kHz and 20 kHz lowpass filtered calibrations could not complete the full 25 calibration distances. The 50 kHz filter's signal quality was too poor to record at 1325 µm (0.0522") and therefore its curve stops at the 1175 µm (0.0463") point. The 20 kHz lowpass filtered signal quality was too low at 2375 µm (0.0935") and therefore its curve stops at the 2125 µm (0.0837") point. The methods created in this study were able to complete the calibration and still show a negative slope, showing curve sensitivity, and therefore calibration curve usefulness even at high tip clearances. This proves that the methods presented show larger dynamic range.

A standard deviation for the data used at each calibration point is calculated weighted normalized to the number of observations, N, and not N-1. They are calculated with MATLAB's "*stdev.m*" function. The standard deviation of each calibration point is represented by the error bars in Figure 48. These are recorded and averaged. The average

standard deviations of the points in each curve are shown in Table 2. The method presented shows a smaller standard deviation than the 50 kHz filter. The uncertainty is about the same as the 20 kHz filter.

Table 2. Standard Deviations of Filtered Calibrations Compared

Type of Calibration	Standard Deviation (μm)	Standard Deviation (in.)
50 kHz	28.0667	0.0011"
20 kHz	25.2105	0.001"
Method Presented	25.47	0.001"

Resampling the data uniformly removes speed variance when recording, which reduces the number of frequencies present in the data, improving signal quality and raising the SNR. Under-sampling the data reduces the "jaggedness" of the signal, also improving the SNR. This was shown with the FFT plot in the shaft order domain. By then using set shaft orders to pass through a lowpass filter a better calibration is achieved. This enables the TPL to characterize the NPSMF with better accuracy and range. Furthermore, this is significant in that calibrations and data runs can be done without the SNR limitation from the manufacturer's RCap V software. Capacitive probes can potentially be positioned further away from the rotor tips and still provide tip clearance data when using the methods proposed. Furthermore, they are proven to be able to operate in areas of higher background noise as shown with the effective filtering.

2. Validating Sensitivity by Testing Ability for Probes to Detect Small Blade Deflections

A second test was done to determine effectiveness of the post-processing methods. This involved wedging a foam block in between one set of rotor blades, blade 16 and 17, and used a tie to further pull the blades apart. The tie put tension on blade 16 away from 17 and tied around blade 8 and 9. The amount of deflection is measured using a vernier caliper between the leading edge forward most tips of blade 16 and 17. A deflection of 0.85 ± 0.05 mm (0.0335 +/- 0.002") was measured. This specific experiment was done with the

rotor rotating in the clockwise direction over 360 revolutions. Figure 49 show a diagram depicting the setup of this experiment.

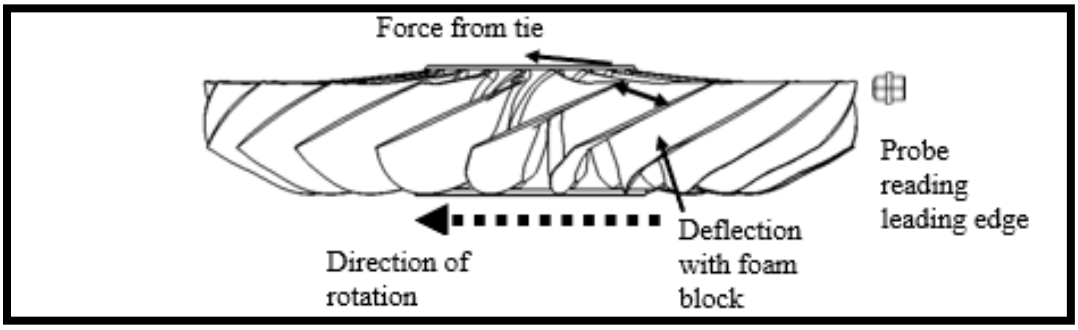

Figure 49. Diagram of Deflection Detection Experiment.

The deflection is measured by locating the indices of the peaks in each blade, over each revolution. A blade deflecting to the left, in relation to Figure 49's orientation, would have peaks that would occur sooner and vice versa for deflections to the right.

The basis of the blade deflection experiment is to prove the accuracy of finding the locations of the DRO peaks. Normally, the DRO peak locations have a relatively high uncertainty due to the noise in the raw signal as shown in Figure 50. In the figure one can see the real maximum location (as determined in red) isn't represented correctly when noise is present. Since the noise is mostly removed with the post-processing method proposed, the uncertainty in peak location is possibly low enough to where slight deflections of a blade can be determined. After 360 revolutions were recorded using the aforementioned procedure on the BCTR, a comparison is made between the peak locations of the NPSMF with and without the blade deflections physically imposed. The average of these peak locations is shown in Figure 51, showing the location of the maximum peak for each individual blade passage.

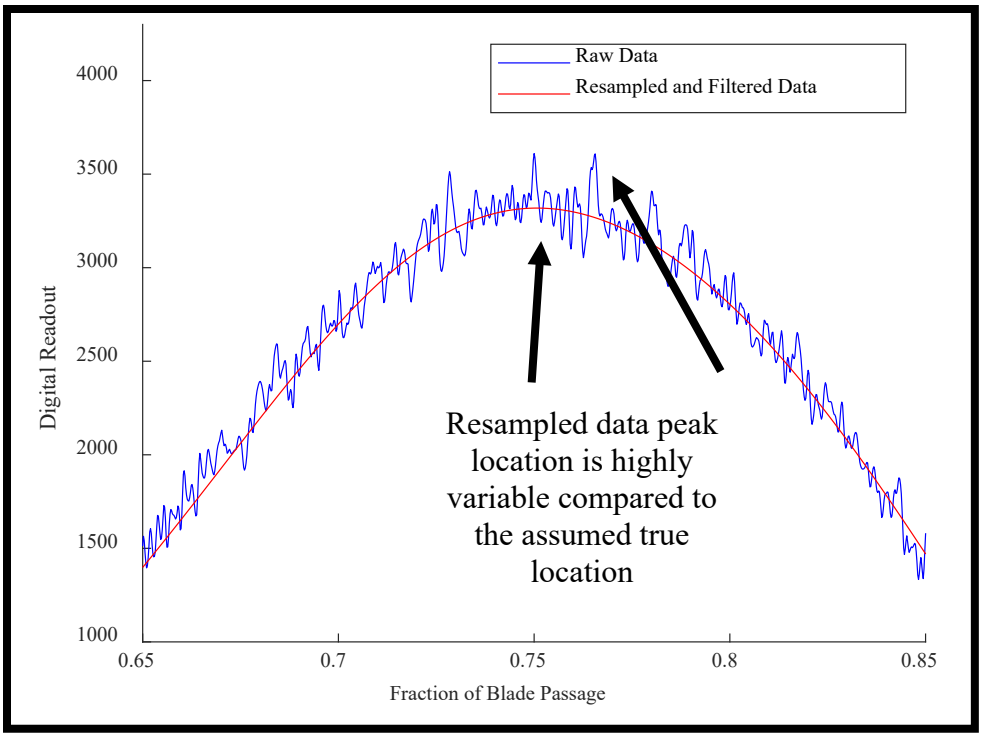

Figure 50. Peak Location Difference Between Filtered and Non-Filtered Signal.

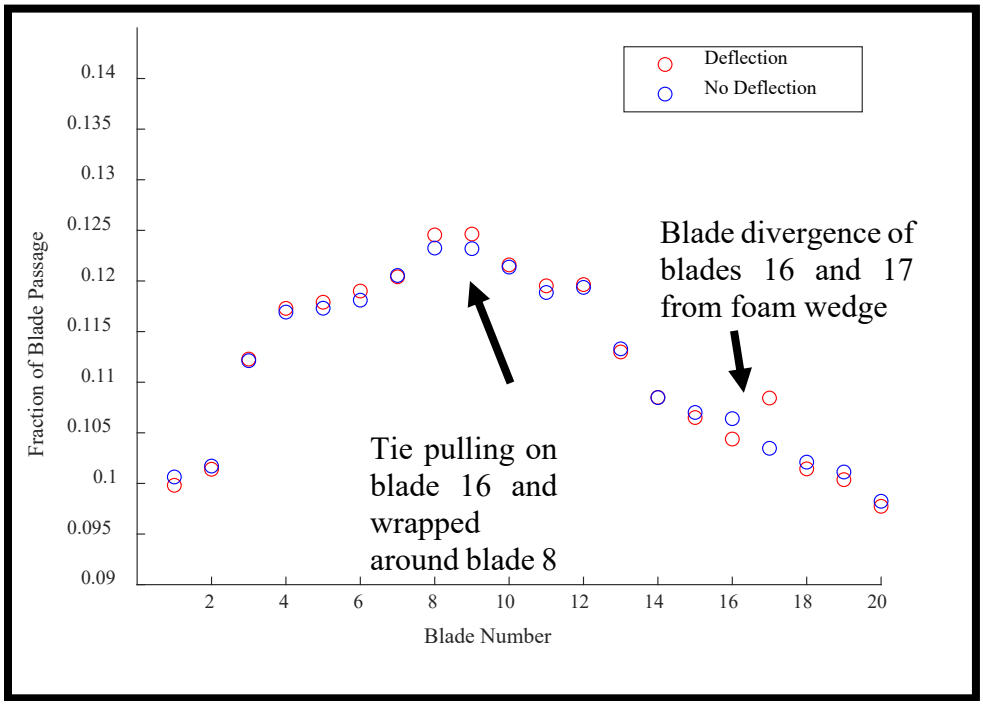

Figure 51. Scatter Plot Showing Blade Deflection Detection.

Figure 51 shows that the removal of the uncertainty due to noise in the capacitive probe's output signal has increased sensitivity enough that it can detect small deflections in the rotor blades. One can see that since the foam block deflected blade 16 to the left with the rotor spinning clockwise (right to left in the frame of the capacitive probe) experienced a maximum sooner than with no deflection. The opposite can be said for blade 17 which was deflected the opposite direction. The tie that put tension on blade 16 to the left further caused this peak to occur at a sooner fraction of the blade 16 passage on average. The tie placed stress on blades 8 and 9 is it rested on top of the blades and pulling them to the right. This caused their peaks to occur later in comparison to the non-deflected state. The other blades were not given a deflection, but it's seen that there is some difference between the average points. Although these non-stressed blades show some difference, they are small in comparison to the blades that were put under some kind of deflection. The degree of difference for the blades put under deflection were much higher as shown.

The significance of this experiment's results is that the accuracy and sensitivity from using the proposed post-processing is accurate enough to detect blade deflection of less than 1 mm (0.0394") (0.85 mm (0.0335") was used for this experiment as previously discussed). Furthermore, this opens the possibility of using the capacitive probes for a different application. By using the tip clearance probes to not only measure the peak-to-peak DRO values, but also the indices of the peaks, one can detect if blade deflection were to occur. While maybe not accurate enough to determine the exact deflection amount, or the cause of the deflection, this experiment can be used as an indicator to operators of a potential issue. This may possibly be able to be used in engine health monitoring for blade degradation. Overall, the post-processing methods proposed are validated in that it not only enhances the BTC measurement system's current capability, but also provide potential for new application.

D. VALIDATING MOCK CASING CALIBRATION AGAINST TIP GAP CASING CALIBRATION

1. Mock Casing Calibration Curves

The BCTR (mock casing) calibration plot of probe 1 at the mid-chord monitoring position is created using the methods described in the previous sections. Figure 52 shows the tip clearance in μm as a function of the capacitive probe output's resampled and filtered digital readout (DRO). These were calculated as described in the data processing methods section. The figure also shows the fitted curve created using MATLAB's curve fitting toolbox. Table 3 shows the tabulated values of the error bar plot in Figure 52. The tabulated values also show the standard deviation at each calibration point in both DRO and μm. The R-square value resulting from the curve fit and the corresponding coefficients used in Equation (2) to create the fit curve are also included.

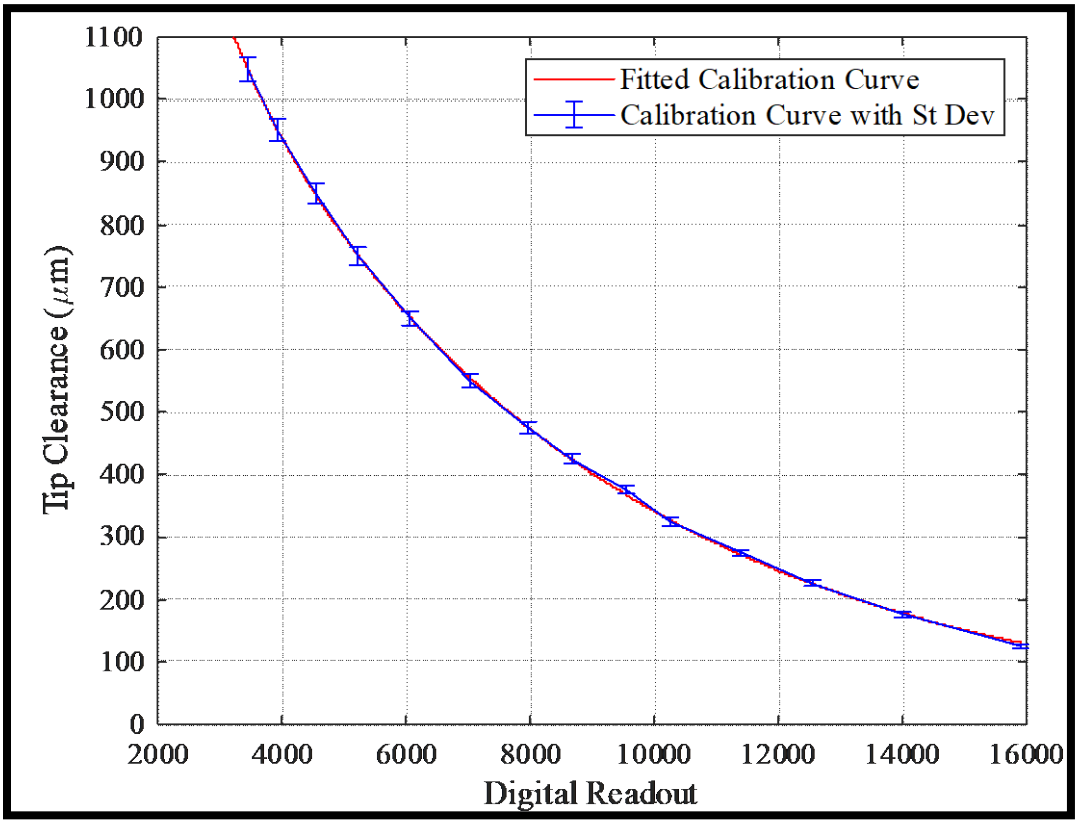

Figure 52. Calibration Curve, BCTR (Mock Casing), Mid-Chord Probe 1.

Table 3. Calibration Table, BCTR (Mock Casing), Mid-Chord Probe 1

Calibration Distance (µm)	Average Value (DRO)	St. Deviation (DRO)	St. Deviation (µm)	Curve Fit Parameters
125	15900.41	122.3734	2.572661	R-square = 0.9998
175	14012.9	121.5834	3.479002	a = 2393.761
225	12543.82	125.759	4.572716	b = -0.00109
275	11370.14	115.0316	5.071411	c = 1744.346
325	10242.45	124.5901	6.60103	d = -0.00016
375	9557.358	114.5225	6.795371	
425	8682.288	111.9834	7.678905	
475	7968.016	113.0434	8.732657	
550	7027.484	114.1216	10.35582	
650	6056.688	106.7371	11.57003	
750	5228.955	108.3097	13.91809	
850	4557.64	102.7432	15.5624	
950	3924.707	97.57242	17.89135	
1050	3447.769	87.13239	19.11333	

2. Tip Gap Casing Calibration Curves

The BCTR (tip gap casing) calibration plot (Figure 53) is created in the same manner. Only the resulting curve for the mid-chord, probe 1 calibration is shown for brevity. Figure 53 shows the tip clearance in µm as a function of the capacitive probe output's resampled and filtered digital readout (DRO). Table 4 shows the tabulated values of the plot and is created in the same manner as before.

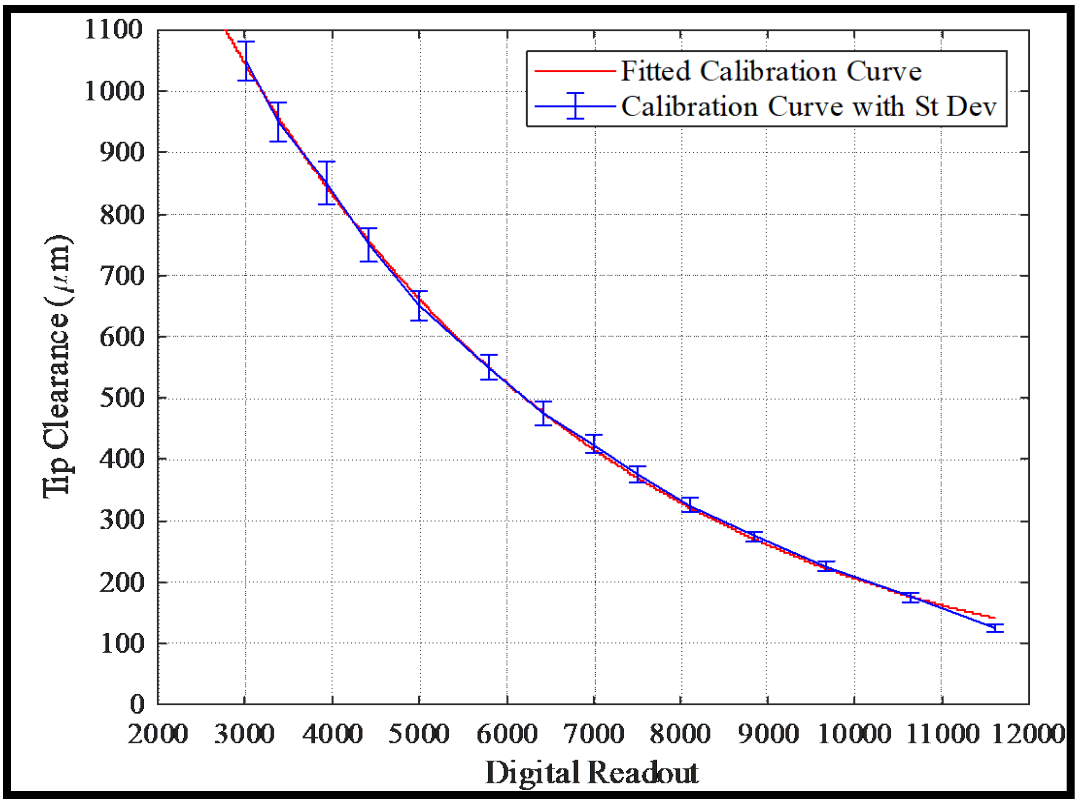

Figure 53. Calibration Curve, BCTR (Tip Gap Casing), Mid-Chord Probe 1

Table 4. Calibration Table, BCTR (Tip Gap Casing), Mid-Chord Probe 1

Calibration Distance (µm)	Average Value (DRO)	St. Deviation (DRO)	St. Deviation (µm)	Curve Fit Parameters
125	11617.76	160.9831	5.273733	R-square = 0.9993
175	10636.33	176.4919	7.259931	a = -933982
225	9671.388	155.9229	8.045783	b = -0.00027
275	8847.587	142.3172	8.897949	c = 936024
325	8101.021	148.3603	11.00505	d = -0.00027
375	7510.705	159.4597	13.52179	
425	6988.576	135.8832	13.01277	
475	6417.071	169.5182	18.41072	
550	5808.17	166.5498	20.76003	
650	5001.659	168.8638	25.21489	
750	4414.62	161.5679	27.51779	
850	3942.755	181.5238	34.248	
950	3374.586	146.7332	31.49441	
1050	3013.124	136.0939	31.65435	

3. Comparing Calibration Curves

Plots are created for comparison between the two rig designs. Figures 54, 55, and 56 are plots of both rigs' fitted calibration curves for the leading, middle, and trailing edges, respectively. All four probes' calibration curves are overlaid into one plot.

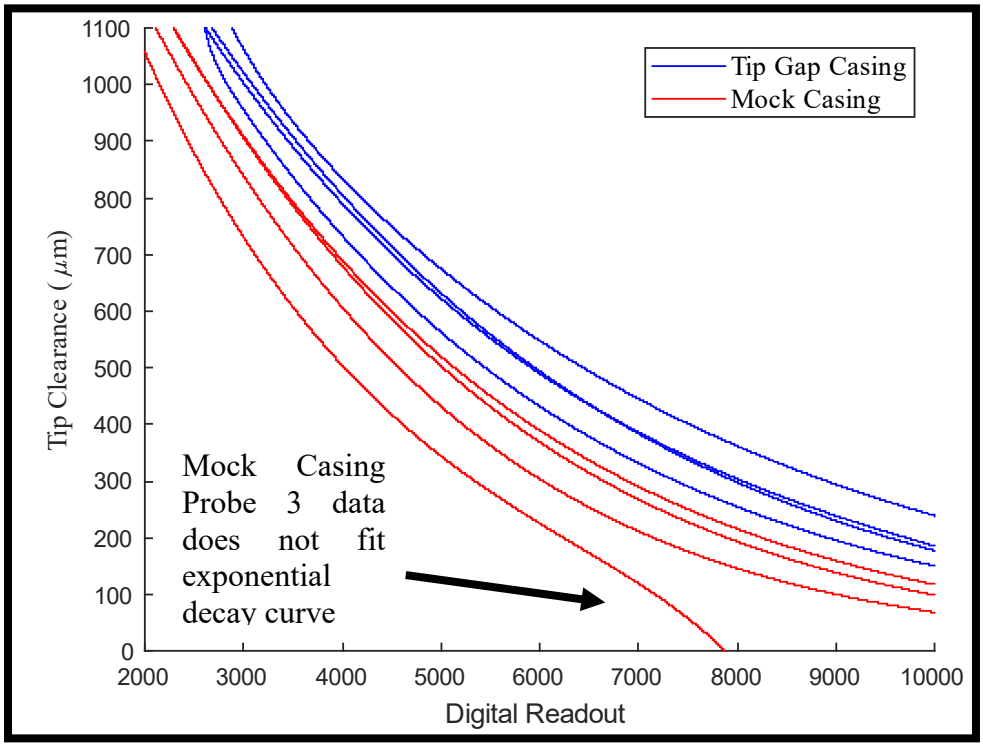

Figure 54. Mock Casing to Tip Gap Casing Comparison, Leading Edge.

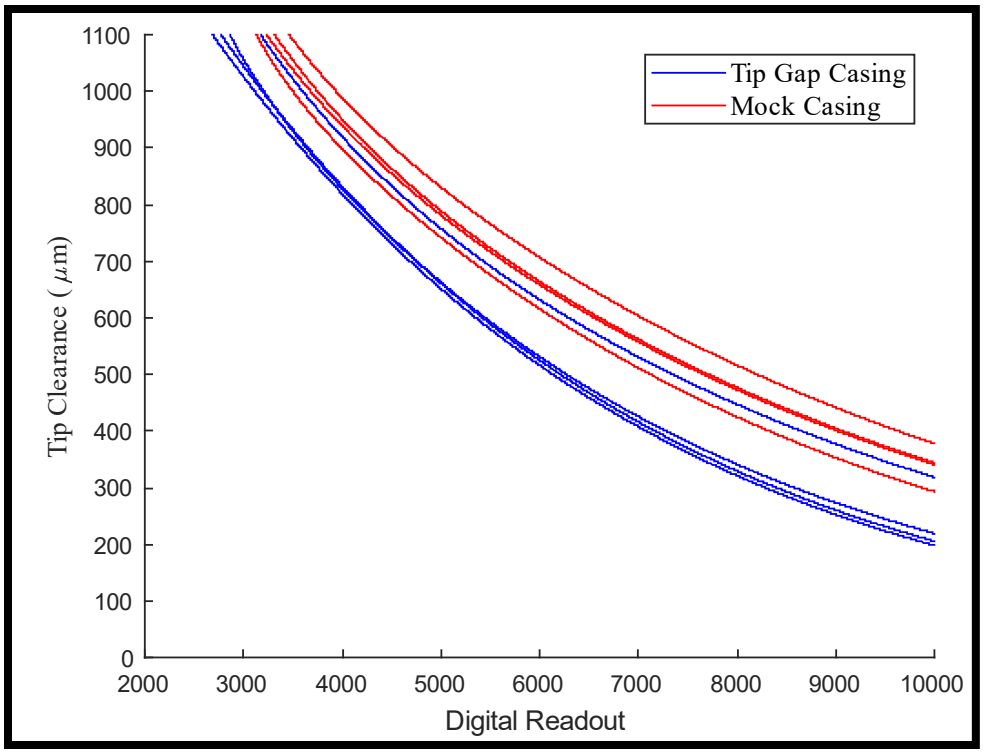

Figure 55. Mock Casing to Tip Gap Casing, Mid-Chord.

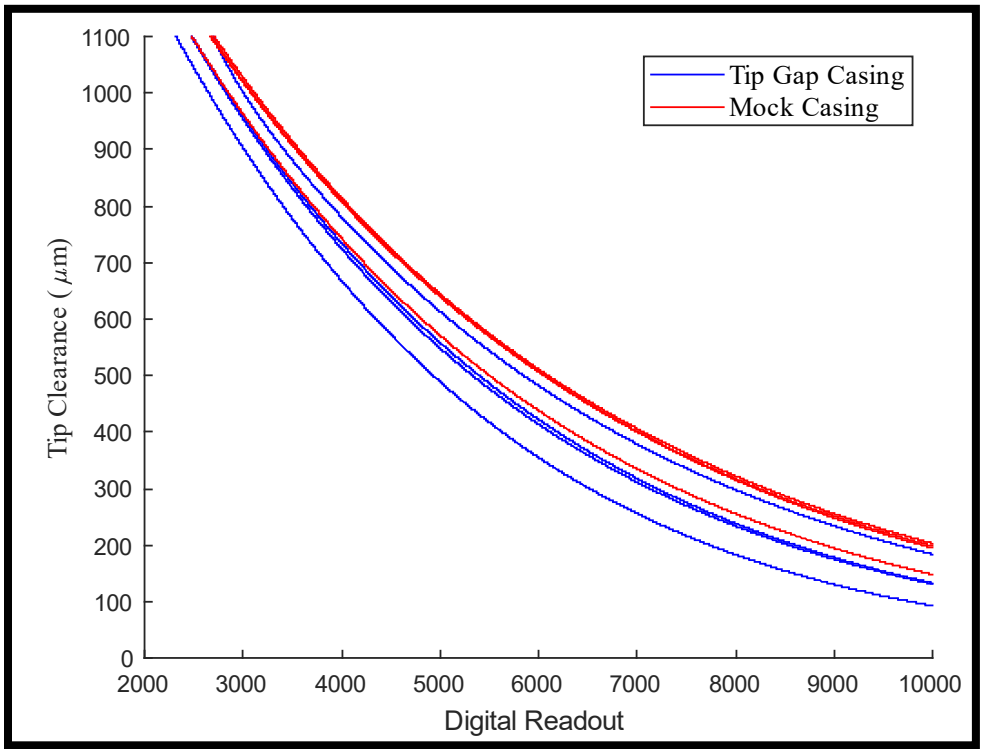

Figure 56. Mock Casing to Tip Gap Casing, Trailing Edge.

Both calibration rig designs have curves that behave as an exponential decay as evidenced by R-square values ranging from 0.9992 to 0.9997. The calibration curve is effective in that the curve maintains a negative slope throughout the range of expected tip clearance. The average standard deviation of all calibration points for all four probes for all probe mounting positions is shown in Table 5. The table shows results in digital readout. Each standard deviation was also converted into μm and averaged.

Table 5. Average Standard Deviation of Calibration Curves

	Avg St. Dev (DRO)	**Avg St. Dev (μm)**	**Avg St. Dev (in.)**
Mock Casing	121.4556	17.7694	0.00070"
Tip Gap Casing	131.0221	16.0487	0.00063"

The mock casing calibration shows slightly smaller standard deviations in DRO. This may be attributed to the fact that all 4 probes were in electrical connection with each other when using the tip gap casing. When using the mock casing, each probe was mounted alone. It may also be due to the fact that all probes in the tip gap casing are connected to a much larger piece of aluminum, which can interact with background interference more. Although tip gap casing DRO standard deviations are larger the converted micrometer standard deviation is smaller. This may be attributed to a difference in curve sensitivity. Overall, the average standard deviations between the two rigs are comparable to each other.

Another item to note is that the standard deviation lowers as tip clearance increases. This may indicate that the capacitive probes are affected by axial vibrations of the rotor. When referring to the slopes of the curves in Figures 52 and 53, At smaller tip clearances the DRO to BTC ratio gets larger. The calibration curve sensitivity dependency on tip clearance causes a larger change in digital readout for rotor axial vibrations at smaller tip clearances. As the rotor moves away (increasing tip clearance), the curve sensitivity lessens, lower the standard deviation. This lowering standard deviation is shown in both the mock casing and tip gap casing calibrations on the BCTR.

When comparing all the mock casing calibration curves to the tip gap casing curves it is difficult to find a constant correlation between the two. A glaring lack of consistency is evidenced by the smaller tip clearances for a given DRO of the mock casing curves than the tip gap casing curves for the leading edge. This may be attributed to the fact that the blade tips at the leading edges are much thinner than the rest of the blade tip giving rise to error. The calibration curves for the mid-chord and trailing edge plots show that the tip clearance for a given DRO is lower when using the tip gap casing curves. Additionally, the mock casing probe 3 curve for the leading edge calibration curves did not follow the characteristic exponential decay making the "set" unusable.

Also, the tip gap casing curves all show probes 1, 2, and 4 are all consistently close to one another in DRO values and behave very similarly. The probe 3 calibration curves for the tip gap casing consistently show higher than the rest, meaning probe 3 in channel 3 is more responsive than the others. This consistency between probes isn't seen between the mock casing calibration curves. When considering a constant mounting position, the mock casing calibration curves do not all start at the same value, nor do they share a similar pattern to the tip gap casing curves where the third probe is highest and the others are nearly the same.

Furthermore, imperfections of the ElemX Xerox printer created a rough surface where the lines of material extrusion created "steps" in the curved inner wall face of the mock casing. As such, the probes were not exactly flush with the casing inner wall as they were with the tip gap casing, causing the probes to be slightly further away from the blade tips compared to the tip gap casing results. Since the curve is more sensitive (steeper slope) at the lower tip clearances (refer to Figure 16), this would cause a larger distribution in DRO for the tip gap casing calibration and a smaller distribution in DRO for the mock casing.

The slope of the curve can be directly correlated to how sensitive the curve is. The mock casing curves do not show any correlation to each other whereas the tip gap casing curves do. Considering the slope of the line between the 125 μm (0.00492") and the 175 μm (0.00689") calibration points only for all the curves we can make the following

comparison. Table 6 shows the linear slope of these first two points on each calibration curve.

Table 6. Linear Slope of First Two Points of Calibration Curve

Location and Probe	Mock Casing (DRO/µm)	Tip Gap Casing (DRO/µm)
Leading Edge Probe 1	-9.571739214	-17.99403586
Leading Edge Probe 2	-14.10541042	-20.18441642
Leading Edge Probe 3	-13.31722405	-27.40407193
Leading Edge Probe 4	-15.30952222	-21.52313688
Middle Edge Probe 1	-37.75023951	-19.62863032
Middle Edge Probe 2	-34.67055703	-21.89043399
Middle Edge Probe 3	-37.66957736	-29.28442898
Middle Edge Probe 4	-29.70279699	-18.87912967
Trailing Edge Probe 1	-17.85943283	-16.03371213
Trailing Edge Probe 2	-21.5625975	-16.41465295
Trailing Edge Probe 3	-20.97498947	-21.99490281
Trailing Edge Probe 4	-21.30452731	-15.94285505

On average, the two rigs produce comparable slopes. With the exception of the third probe for the tip gap casing, which shows a consistently higher slope, the tip gap casing Probes all show a repeated correlation in slopes. Probes 1, 2, and 4 are all similar and within 2–3 DRO per µm from each other. The probe 3 slopes are about 6 DRO/µm more negative than the other probes for a given probe location. The mock casing calibration curves do not show any pattern or correlation between the different slopes other than the leading edge curves were less sensitive than the others. Human error in calibrating, and vibrations from a smaller, less inertial casing may cause this inconsistency.

The goal of using the BCTR (mock casing) was to develop signal post-processing methods while the tip gap casing was being manufactured and to determine whether 3D printed mock casings could be a substitute for the actual tip gap casing. The result of a

successful experiment would be that the probes could be calibrated separately from the tip gap casing so the casing would not need to be disassembled from the TCR. Based on these findings we see that although the BCTR (mock casing) calibration curves are somewhat similar to calibrations done with the tip gap casing, their inconsistency proves these calibration curves are not useable. The process of creating the curves with the mock casing version of the BCTR, however, did prove useful as it resulted in the methods developed, expediting the experiment process upon receipt of the tip gap casing. The higher accuracy, evidenced by the smaller standard deviations in both DRO and μm, is attributed to less noise, which is most likely due to the smaller surface area that can interact with background interference. Furthermore, the lack of 4 probes all electrically connected, possibly interfering with one another, may attribute to this lower standard deviation. The mock casing rough surfaces affecting the zero position of the calibration is also a major point of contention. For the TCR radial growth measurement experiments, the calibration curves from the BCTR (tip gap casing) were used. The complete set of calibration curves and their lookup tables are provided in Appendix A.

THIS PAGE INTENTIONALLY LEFT BLANK

IV. EXPERIMENTAL SETUP

The following chapter describes the facility and experiment for the NPSMF BTC measurements in the TCR. The SOPs used in this experiment are provided in Appendix D.

A. TRANSONIC COMPRESSOR RIG WITH TIP GAP CASING DESCRIPTION

The TCR's casing is segmented to allow for component interchangeability in testing. It consists of a filtered flow straightening pipe leading to an inlet nozzle. This then leads to an instrumented inlet casing section, inlet guide vanes, and then a variable rotor casing, which for this experiment was the tip gap casing that contains the mounting ports for the capacitive probes. This is followed by an instrumented rotor outlet casing. The outlet casing allows for installation of a stator as needed for various experiments. A SolidWorks model of the assembly is shown in Figure 57 for clarity. The instrumented inlet casing is made transparent for the viewer to understand the location of the NPSMF within the tip gap casing.

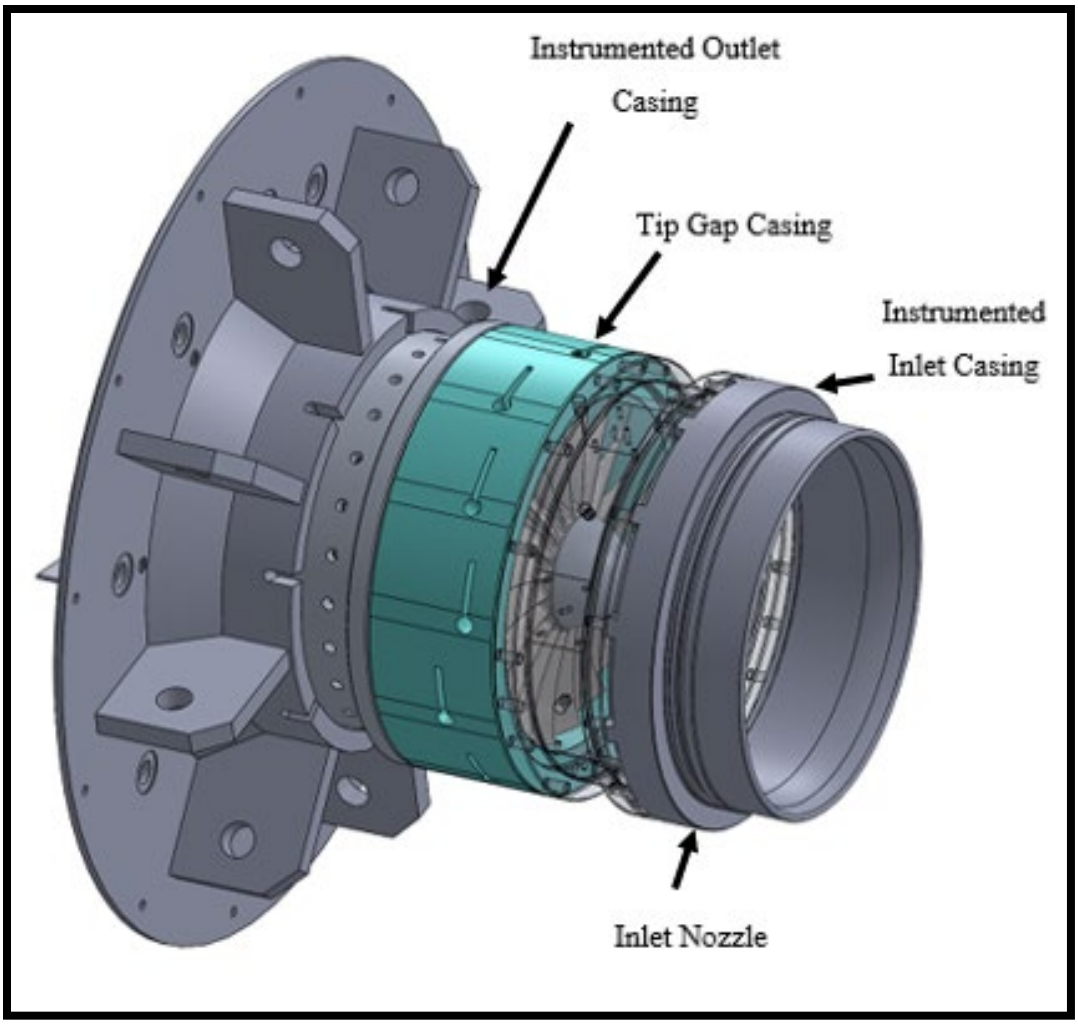

Figure 57. SolidWorks Model of the Tip Gap Casing and Surrounding TCR Components.

An aluminum rotor casing was fabricated to mount the capacitive probes. Unlike other casings used in TCR experiments this casing does not have an abradable lining and has a larger tip gap. The casing has 4 sets of 3 probe ports. They are positioned to monitor the leading edge, mid-chord, and trailing edges of the rotor tips consecutively, each 30 degrees offset from each other about the casing's circular axis. The leading edge ports are 90 degrees from each other as are the mid-chord and trailing edges. The multiple ports allow for simultaneous recording of BTC measurements to be taken. Wire guides are cut out of the casing as well to accommodate the probe wiring since the wires protrude 90 degrees from the probe face. When calibrating using the tip gap casing, probes are kept in

their designated mounting locations. The mounting locations are labeled with an engraving with a probe number, 1–4, and a letter designating mounting position, either “L,” “M,” or “T” for leading edge, mid-chord, and trailing edges, respectively. For example, probe 3 at the trailing edge monitoring position is labeled “3T.” For the remainder of this paper, the probes will be referred to by this naming convention.

Furthermore, a grounding wire is connected to the casing by fastening the wire’s open end into a vacant probe port with a nylon screw. The grounding strap is earthed to the main ground connection of the TCR. Figure 58 shows the tip gap casing mounted onto the TCR with a zoomed view of port 3T’s engraved labeling. Figure 59 shows the tip gap casing’s probe port positions when mounted on the TCR.

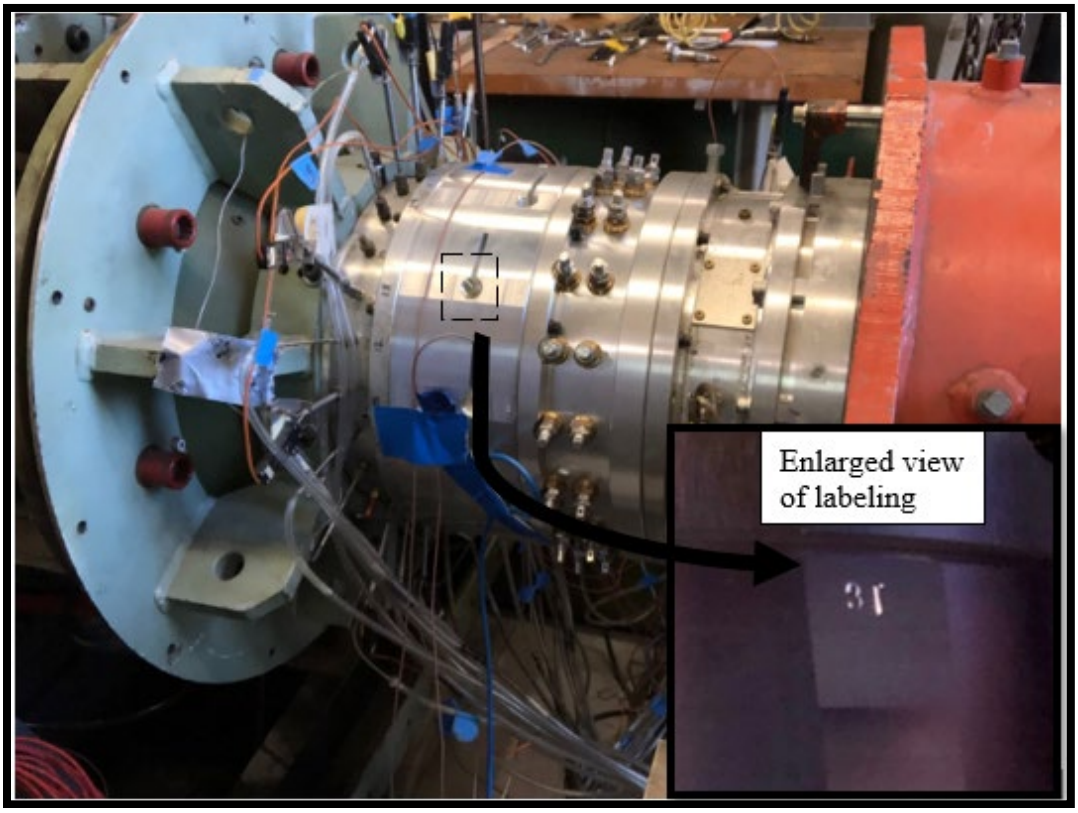

Figure 58. Tip Gap Casing Side View Showing Mounting Ports.

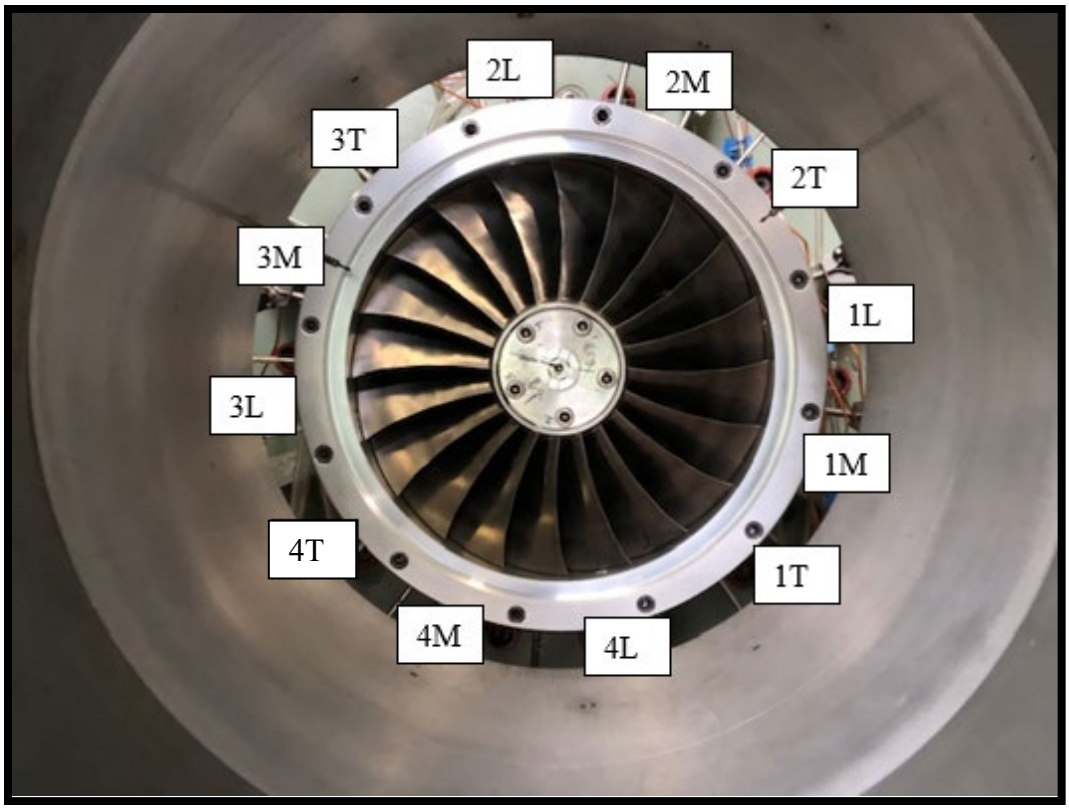

Figure 59. Axial View of Tip Gap Casing Showing Probe Mounting Locations.

The cold tip clearance between the rotor's closest point to the tip gap casing is designed to be 0.889 mm (0.035"). The probe is to be mounted flush with the inner wall of the casing. The probe has a section of a larger diameter that rests on a shoulder of the casing's probe port. An M20 - 2.5 (¾" –10) threading is cut in the probe port entry way. Two hexagonal driven headless nylon screws are used in tandem to hold the probes in place. The second screw ensures that the screws lock so TCR vibrations do not loosen the screws. A C-shaped 3D polycarbonate 3D printed clamp is attached onto the back of the capacitive probe. This is used to provide a distance margin between the nylon and back of the probe to prevent probe damage. A cross section view of a capacitive probe port is shown in Figure 60. Further specification is provided in Appendix C.

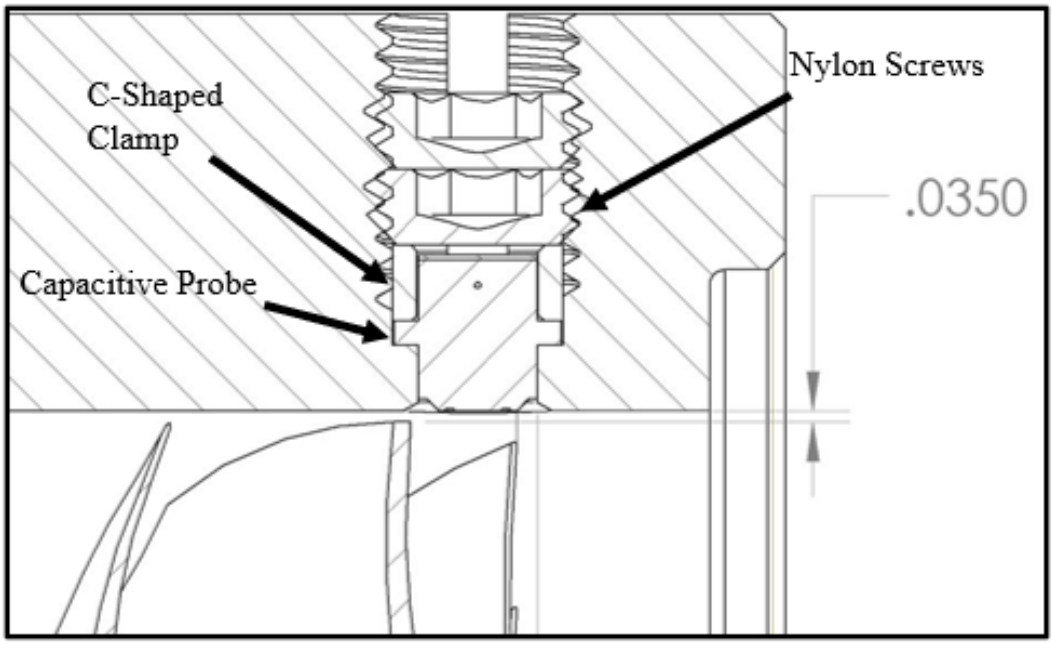

Figure 60. Cross Section View of Probe Mounted Into Port Showing Cold Tip Clearance.

B. VALIDATING BCTR CALIBRATION USE ON TCR

An experiment is done to validate if the calibrations conducted on the BCTR can be successfully transferred onto the TCR. The basis of the experiment consisted of moving the casing horizontally left and right and see if the amount of distance traveled detected by the capacitive probes matches within tolerance. The 4 capacitive probes were mounted in the mid-chord monitoring position. When viewing the TCR down the axis, the casing is first moved to the right by 91.44 μm (0.0036") from the center position as measured by a feeler gage and an initial tip clearance recording is done at 4000 RPM. Next the casing is moved 175.26μm (0.0069") to the left and another recording is done. The capacitive probe outputs are subtracted from one another and converted from DRO to inches. They are then compared to the expected 175.26 μm (0.0069") of casing horizontal travel. The 4 probes' measured differences in tip clearance from moving the casing are shown in Table 7.

Table 7. BTC Measurements from Calibration Validation Experiment

Probe	Measured Movement (μm)	Measured Movement (in.)
1M	-166.166	-0.00654
2M	-30.734	-0.00121
3M	156.972	0.00618
4M	37.846	0.00149

In reference to Figure 59, probes 1M and 3M are nearly horizontal and should read closest to the 175.26 μm (0.0069") of travel, which was observed. Probes 2M and 4M should see a smaller amount of BTC change as they are near vertical in relation to the NPSMF. Probes 1M and 2M should see the BTC decrease as the casing moves to the left and the opposite for probes 3M and 4M, which was observed. With this experiment it is determined that the calibration on the BCTR is valid for use on the TCR. The probe movement was correct within a fraction of a thousandth of an inch.

C. MEASURING BLADE GROWTH OF NPSMF AT DIFFERENT SPEEDS

The characterization of radial growth of the NPSMF under high-speed loading is conducted in this test. Three separate data runs were done, each with 4 probes monitoring either the leading edge, mid-chord, or trailing edge positions. Each of these data runs were conducted at 7 different speeds: 500 RPM, 3,000 RPM, 12,000 RPM, and 70%, 80%, 85%, and 90% design speed of the TCR. The probes are mounted such that all 4 probes monitor the same location of the blade tip. The inlet guide vanes are kept at 70% and the inlet piping is attached.

The probes are first mounted and connected to the data acquisition as well as the tachometer. In the RCap V configuration page, capacitance debounce times are kept to 2 μsec. The number of averages is kept to 10,000 (maximum) to alleviate software computational resource. All four probes are enabled as well as the PFI0 connection and are checked for proper signal response by hand rotating the rotor. The 500 RPM run is conducted using 100 psi shop air to drive the power turbine. This run is done for a “zero growth” starting point. Running at 500 RPM also creates a similar capacitive probe output signal to the calibration signal that was run at that speed.

The Tip Clearance App is used to keep the recording files organized during testing. After the 500 RPM data run has been completed, the Allis Chalmers compressor system is started and the TCR is brought up to 3,000 RPM. Each recording is done for approximately 10 seconds. After each recording, a data loss and OPR synchronization check is done. Recordings with data loss are discarded. Upon completion of data recording the process is repeated for the other 5 speeds. Upon completion of the data run, the TCR is brought to a stop and the capacitive probes are moved to the next monitoring position. The raw recorded data is then processed. The results of the NPSMF BTC are shown in the following chapter.

THIS PAGE INTENTIONALLY LEFT BLANK

V. RESULTS AND DISCUSSION

A. TRANSONIC COMPRESSOR RIG TIP CLEARANCE RESULTS AND ANALYSIS

The results are presented for the tip clearance measurements in the transonic compressor. Tip clearance was measured from the TCR at 7 different speeds all at peak efficiency flow (near choke):

- 500 RPM
- 3,000 RPM
- 12,000 RPM
- 21,000 RPM (70% Design Speed)
- 24,000 RPM (80% Design Speed)
- 25,500 RPM (85% Design Speed)
- 27,000 RPM (90% Design Speed)

Multiple runs were taken at each speed, each recorded for approximately 10 seconds. The peak-to-peak DRO values of the longest blade with respect to the probes' position in reference to the tachometer's OPR signal are calculated and then converted into micrometers and inches. Each probe's measured BTC is then averaged. Next, the difference of each respective probes' measured BTC is taken between the different speeds. This corresponds to the decrease in tip clearance as the rotor speeds up and is synonymous to rotor radial blade growth. An average of all 4 probes' growths are then taken for each speed. Next a curve is fitted to these average growth values using the curve fit MATLAB tool. A 2nd order polynomial with 3 coefficients is used forming Equation (4). A 2nd order polynomial is used as the expected growth behavior of the rotor is parabolic.

$$f(x) = p_1 x^2 + p_2 x + p_3 \tag{4}$$

The function, *f,* is the radial growth of the blade in inches and the variable, *x*, is the rotor speed in RPM. The terms p_1, p_2, and p_3 are constant coefficients. The 3rd coefficient, p_3, is constrained to equal zero to start at zero blade tip growth. The fitted curve shows small growth from 0 to 500 RPM. The probe radial growths' and average growths are adjusted to start at the result of the data run's Equation (4) value at 500 RPM to account for this initial growth. Any precession of the rotor's axis or rotor eccentricity is taken into account by averaging all 4 probes' growth, taken 90° from each other. The tabulated values of the calculated tip clearances are given in Appendix B.

Figures 61 through 63 are the resulting blade growth plots in inches for the leading edge, mid-chord, and trailing edge positions, respectively. Each plot displays each individual probes' measured blade growth and an average growth shown with a dashed line. Tables 8 through 10 provide the tabulated values from the plots. The probes are referenced by their position naming convention as described previously.

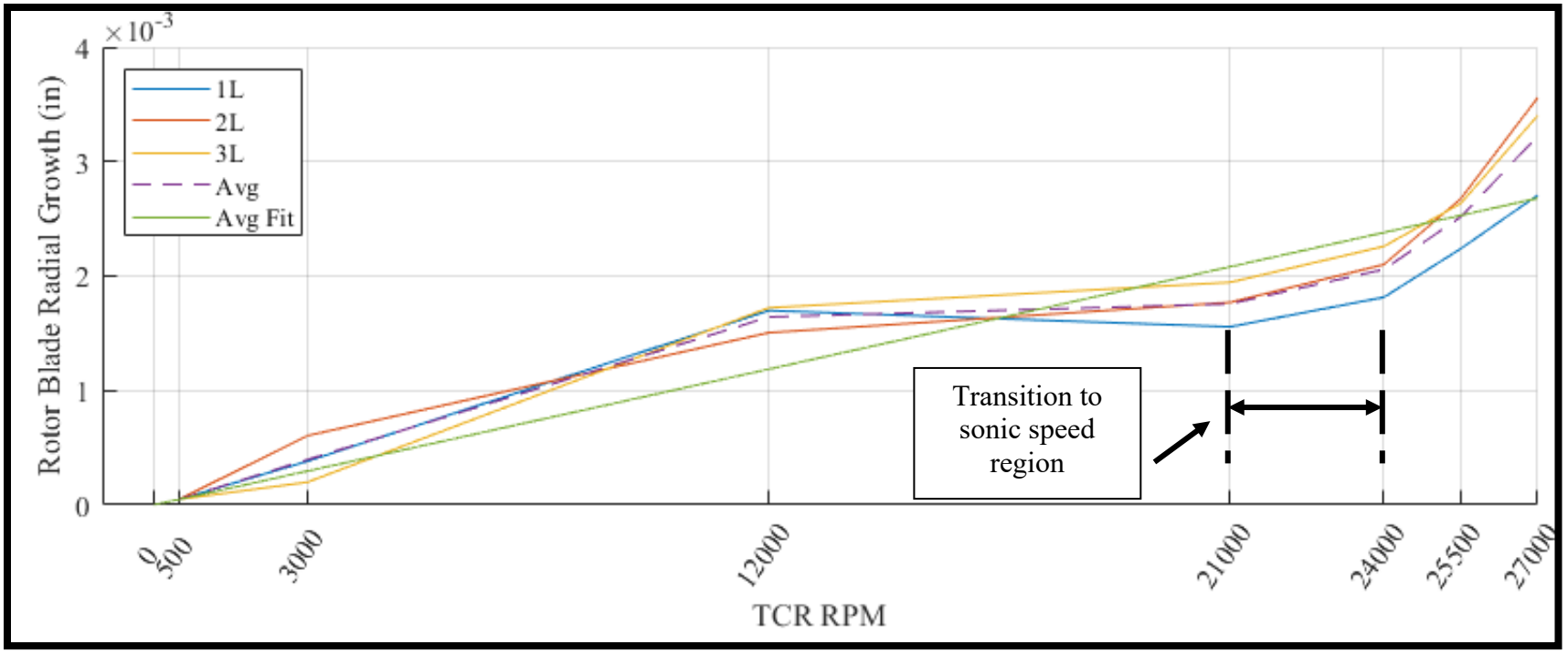

Figure 61. NPSMF Radial Growth, Leading Edge.

Table 8. NPSMF Radial Growth, Leading Edge

RPM Range	500-3k	3k – 12k	12k –70%	70 – 80%	80 – 85%	85 – 90%	Total
Avg Growth (in.)	4.92E-05	0.000395	0.001642	0.001757	0.002058	0.002516	0.003222

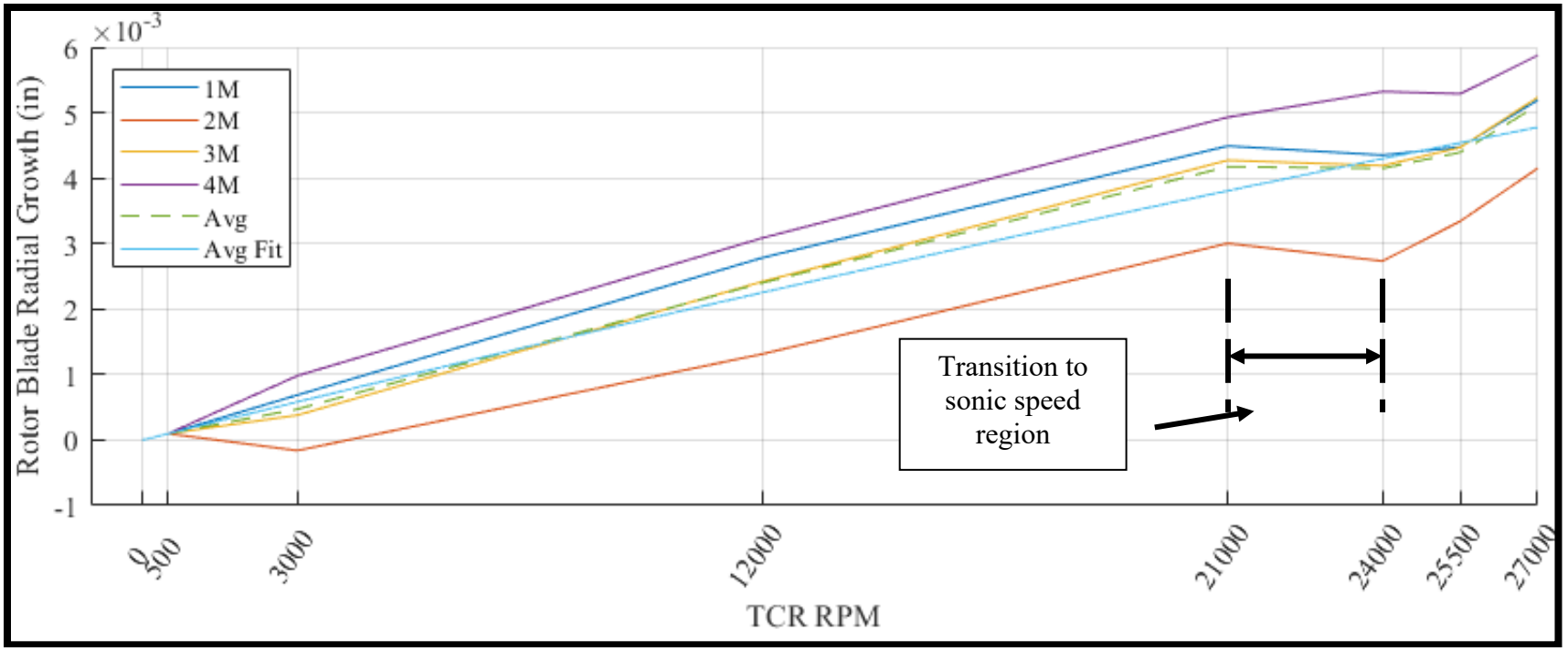

Figure 62. NPSMF Radial Growth, Mid-Chord.

Table 9. NPSMF Radial Growth, Mid-Chord

RPM Range	500-3k	3k – 12k	12k –70%	70 – 80%	80 – 85%	85 – 90%	Total
Avg Growth (in.)	9.78E-05	0.000472	0.002401	0.004174	0.004149	0.004392	0.005112

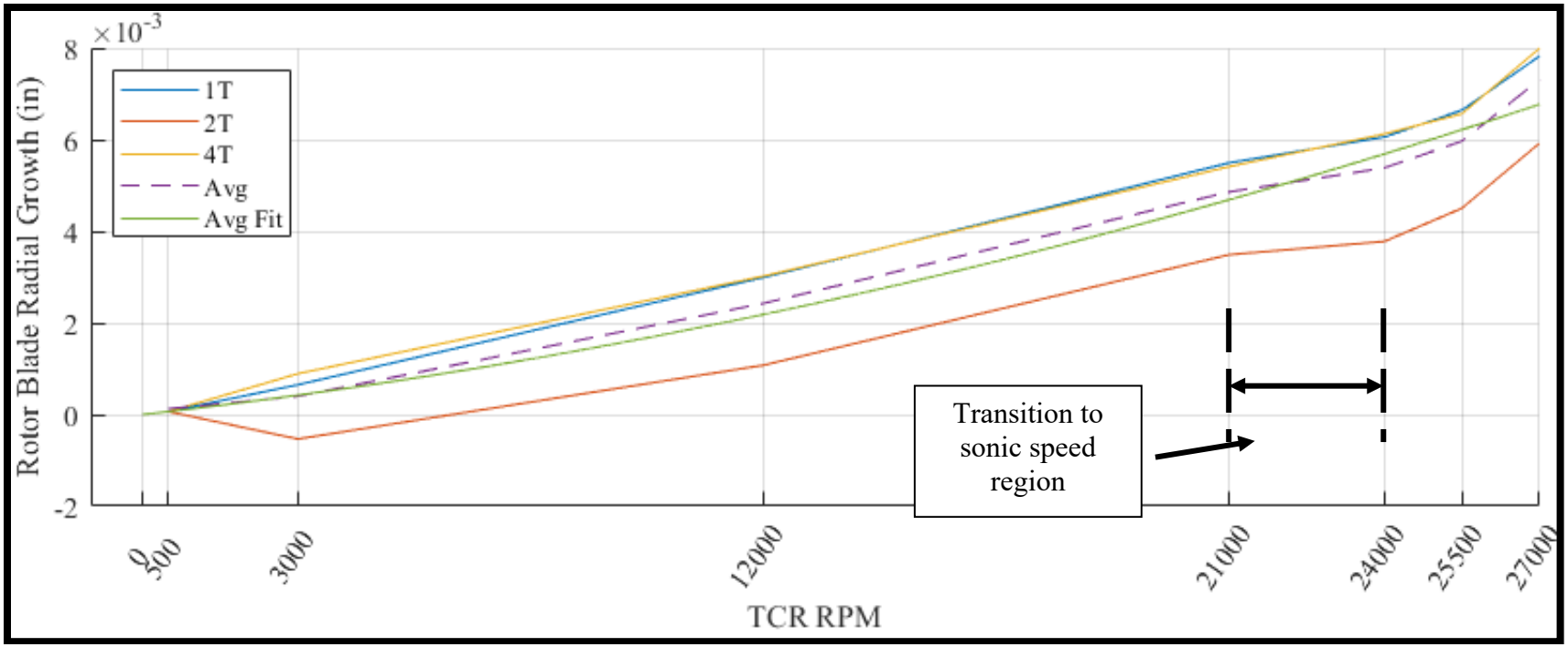

Figure 63. NPSMF Radial Growth, Trailing Edge.

Table 10. NPSMF Radial Growth, Trailing Edge

RPM Range	500-3k	3k – 12k	12k –70%	70 – 80%	80 – 85%	85 – 90%	Total
Avg Growth (in.)	6.01E-05	0.000331	0.002359	0.004793	0.005315	0.005899	0.007241

B. DISCUSSION

Based on these measurements it is determined that the trailing edge experiences the most growth with the maximum radial growth at 27,000 RPM being 183.90 μm (0.00724"). This is expected as the blades' curved surface, especially between mid-chord to the trailing side, will "unfold" in addition to the radial growth of the blades. This is confirmed in a structural model shown later. Probe 4L and 3T failed during the experiment and are omitted in Figures 61 through 63 and have been omitted in the average calculations.

1. Comparison to Simulation

A simulated model was created on ANSYS using a static structural analysis of the NPSMF. The geometry used in the simulation is adapted from the solid model of the fan. The selected material is Ti-6Al-4V. The mesh element size was kept below 1.25 mm. A mesh sensitivity study was done that found element sizes less than 1.25 mm showed negligible change on the order of 1E-5 m. A rotational velocity is applied to the model for the 7 rotational speeds done on the TCR. The thermal condition was set to 22 °C. A fixed support is imposed on the sides of each individual blade's base where the individual blades are inserted into the hub. A radial-directional deformation analysis was conducted on the simulation with the direction set as the x-axis to ensure only radial growth was being displayed. Figure 64 shows the modeled result of a total radial-directional deformation for the fan run at 27,000 RPM.

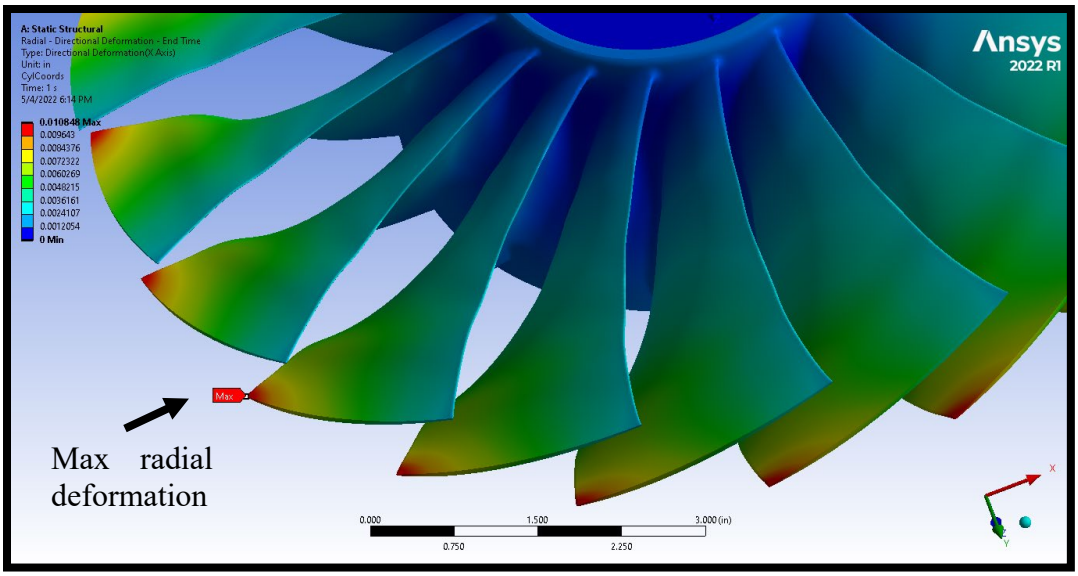

Figure 64. Radial – Directional Deformation Solution.

The maximum growth of the rotor in the radial direction occurs at the trailing edge's tip as shown in the figure in red, agreeing with the recorded behavior on the transonic rig. This confirms that the curved trailing side of the blade does unfold causing the radial growth throughout the blade to be non-uniform. The maximum simulated radial growth is 274.32 µm (0.0108") and is annotated in the figure. Majority of the growth occurs at the end of the rotor's blades and not in the main hub. This is because the speed of rotor increases radially outward for a given angular speed. Therefore, radial loading increases radially from the end wall to the tip. Tabulation of the blade growth in this simulation is given in Table 11 as well as the actual measured blade growth. The trailing edge simulation was taken at the very end of the blade tip and the leading edge was taken at the opposite tip. The mid-chord simulation was taken directly center of the blades' tips. The simulation data and measured data results for each of the 7 speeds are provided in Figure 65 for comparison.

Table 11. Simulated Data and Measured Data Max Growths

Blade Tip Position	Max Growth (μm)	Max Growth (in.)
Simulated Leading Edge	60.96	0.0024
Measured Leading Edge	81.28	0.0032
Simulated Mid-Chord	162.56	0.0064
Measured Mid-Chord	129.54	0.0051
Simulated Trailing Edge	274.32	0.0108
Measured Trailing Edge	182.88	0.0072

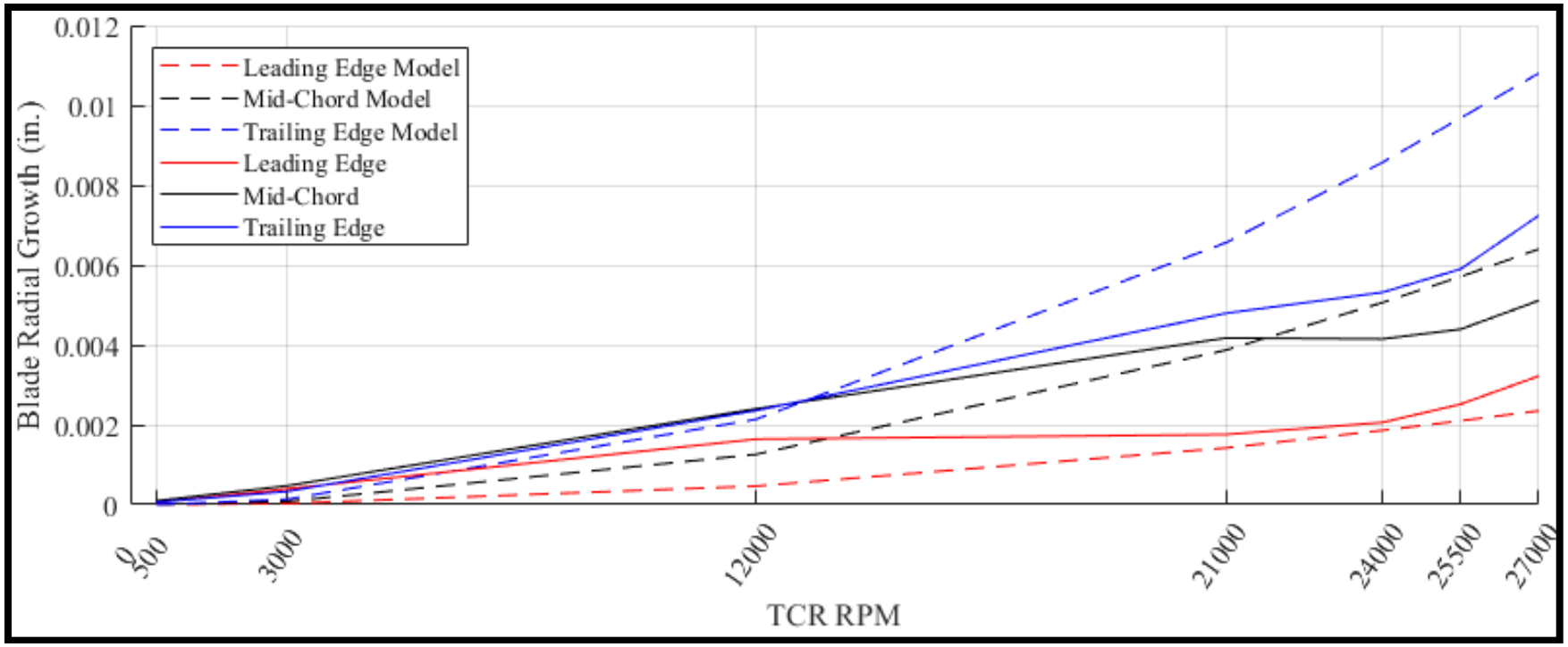

Figure 65. Simulated to Measured Data Radial Growth Comparison Plot.

It can be seen from Table 11 and Figure 65 that the mid-chord and leading edge's simulated and actual results for maximum growth are approximately 25.4 μm (0.001") from each other showing that the model and measured data nearly agree for those blade tip positions. All three blade tip positions' measured data show more growth than the modeled data from 500 to 12,000 RPM after which point their rate of growth drops below the modeled data. Another behavior noted is the drop in blade growth from 21,000 to 24,000 RPM for the trailing edge and mid-chord positions and from 12,000 to 21,000 RPM for the leading edge position. The effect is less in the trailing edge data but is severe enough in the mid-chord and leading edge data to cause a loss in blade growth. Possible reasons for this are discussed in the following section. If this "dip" in blade growth did not occur, the graphs suggest that the model and measured data would have better correlation.

The trailing edge shows the most difference in blade growth between modeled and measured data. The max difference between the simulated and measured trailing edge data is 91.44 μm (0.0036"). This is plausible when taking into consideration other factors than just radial blade growth from centrifugal loading. Other factors that can alter the BTC measurements are errors in probe calibration, thermal expansion differences between the rotor casing and the fan, pressure differences between the high and low-pressure sides of the fan causing the fan to flex upstream, large pressure differences from shocks occurring in the tip region, and the actual probe position compared to the model's measured position. A discussion of sources of possible error causing the difference between the actual measurements and the model is provided in the next section. The section following takes this error analysis into account, providing an adjusted comparison with an error band that includes factors from the discussion.

2. Possible Error Analysis

As the mid-chord and leading edge measured results were close to their simulated models, in-depth analyses of reasons for differing results for these locations are omitted. This discussion will focus on the trailing edge which provided the most interesting results. The principles covered in this section may be applied to the mid-chord and leading sections, though at a smaller scale.

a. Uncertainty Due to Calibration Curves

The individual probes have shown different sensitivities to the blade growth. Referring to the trailing edge results, Figure 63, probes 1 and 4 have shown a higher sensitivity to blade growth whereas probe 2 is lower. The opposite can be said for the leading edge, Figure 61. The inconsistency in the responses of the probes is a result of their dependency on how well the individual probes' calibration curves were created. This can also be attributed to the standard deviation band of the calibration curves.

On the calibration curves (Appendix A) changes at higher digital readouts result in smaller changes in tip clearances and vice versa. Therefore, uncertainty in tip clearance goes up as the tip clearances increases, which can be visibly seen with shrinking error bars as tip clearances is reduced. The cold tip clearance of the NPSMF in the tip gap casing is nominally 889 μm (0.035") and the most growth between the three monitoring positions is about 182.88 μm (0.0072"), meaning the smallest tip clearance will be 706 μm (0.0278"). Taking this range of 706 – 889 μm (0.0278 – 0.035"), then expanding this to the nearest calibration point, 650 and 950 μm (0.0256 and 0.0374"), respectively, the average standard deviation between all probes from all three blade tip monitoring positions is calculated as 19.73 μm (0.0008") or roughly 25.4 μm (0.001"). This uncertainty band of +/- 25.4 μm (0.001") means the actual maximum growth of the rotor blade's trailing edge could land between 157.48 μm (0.0062") and 208.28 μm (0.0082"). This band of uncertainty is confirmed with a scatter plot taken by probe 2T shown in Figure 66. In this run, the average standard deviation between all 20 blades was 24 μm, which equates to ~0.001".

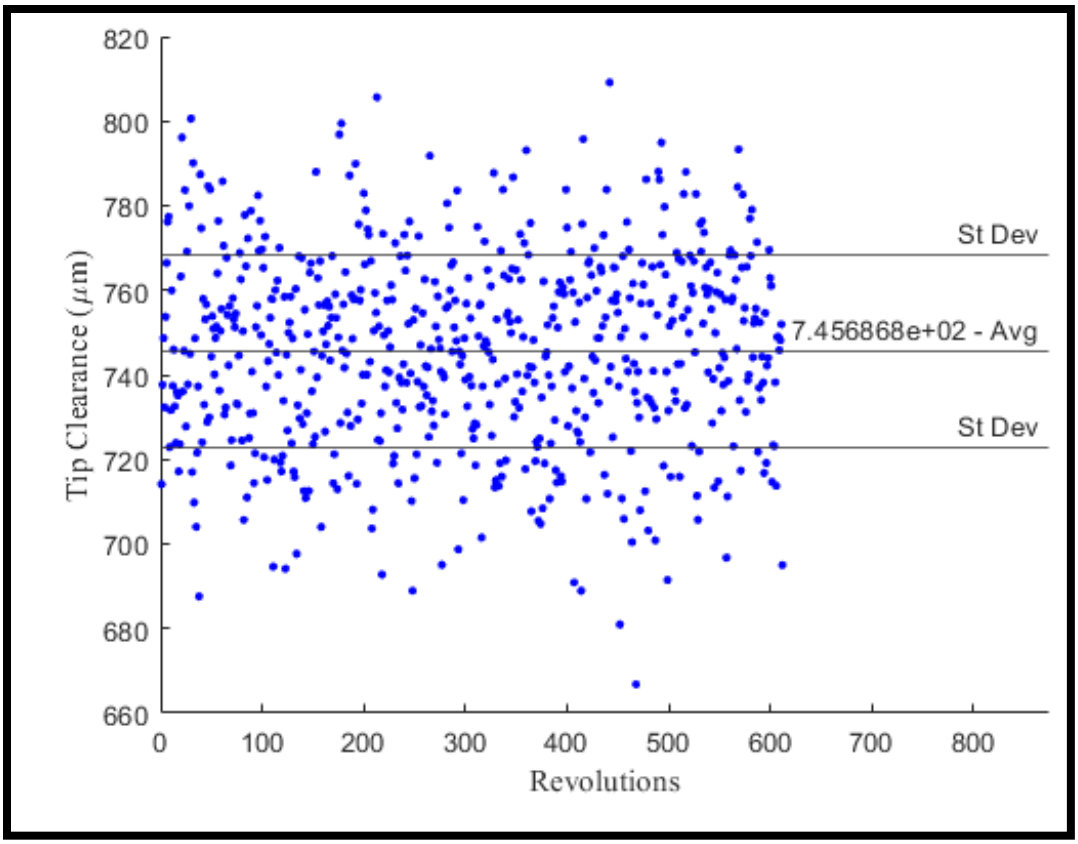

Figure 66. Scatter Plot of Tip Clearance, Probe 2T.

Additionally, the post-process method used on the TCR data produces a slightly different result than the calibration data from the BCTR. The difference in the output signals causes the measured growth to be slightly less than what is actually occurring. For example, a test was done on 2 similar tip clearances and speeds from probe 1M. Both data from the BCTR and TCR were run through the same data resampling and filtering as described in Chapter III. The resulting BCTR and TCR output data retained 96% and 98% of the original signal, respectively. Furthermore, at even higher speeds such as 27,000 RPM, this is further increased to 99%. This means that the data from the TCR appears to have a larger peak-to-peak than the calibration curve it uses for conversion. This means that the measured result is a slightly smaller tip clearance than what it actually is. When referencing probe 1M's calibration curve, a max difference of 3% in DRO for a tip clearance of 850 µm (0.0335") would lower the tip clearance to 824.94 µm (0.0325"), a difference of 25.06 µm (0.00099"). Therefore, the tip clearances being read from the TCR

data may be actually 25.4 μm (0.001") larger than what is being measured. Again, referencing the calibration curves in Appendix A, the change in tip clearance per unit change in DRO decreases at lower tip clearances. This means the TCR data exists in a slightly less sensitive portion of the calibration curve (further to the right) meaning that the radial growth being measured is less than what is actual conditions. Figure 67 shows an example calibration curve with annotations depicting this source of error. This could help partly answer why the trailing edge and mid-chord measurements are less than their simulated model. To take into account the curvature of the calibration curve, the derivative of the curve is taken then integrated for a 1000 DRO increase starting at 850 μm (0.0335") and starting at 824.94 μm (0.0325"). The difference in tip clearance growth is 5.08 μm (0.0002"). This can be factored into an overall error of on a growth of 5.08 μm (0.0002") in the positive direction. A thumb-rule can be made that a difference in BTC measurement of 25.4 μm (0.001") equates to a growth measurement difference of 5.08 μm (0.0002").

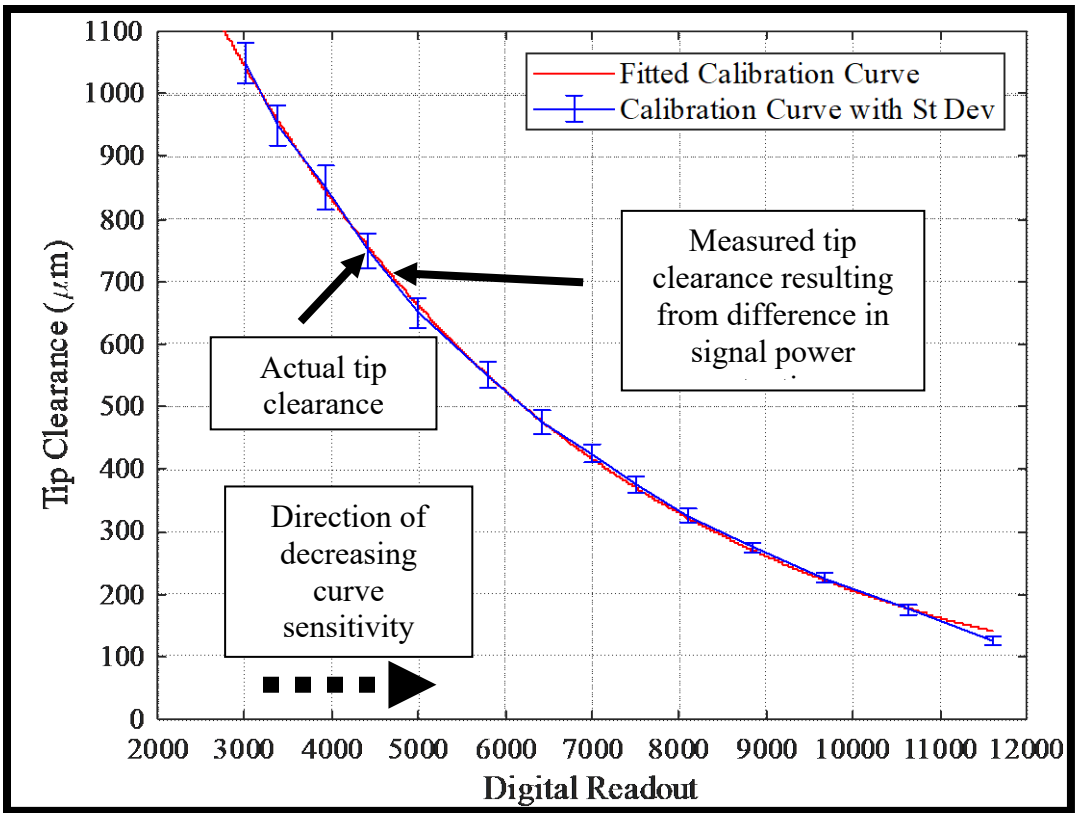

Figure 67. How Radial Growth Measurements are Affected by Calibration Sensitivity.

b. Uncertainty Due to Thermal Expansion

Another factor to consider is temperature changes in the TCR and how they affect thermal expansion. The tip gap casing's material, Aluminum 6061, is listed as having a linear thermal expansion coefficient, α_{Al}, of 26.6×10^{-6} °C^{-1} and the linear thermal expansion coefficient of Ti-6Al-4V, α_{Ti}, is 8.6×10^{-6} °C^{-1} [27]. The TCR typically can rise in temperature by approximately 44 °C at the blade tip region as shown in past performance runs. Therefore, the aluminum casing's percent expansion in length is approximately 0.1170% and the fraction change in length of the titanium rotor is approximately 0.0378%. As a rough estimate, without taking into account growth inhibitors such as fasteners and disregarding heat dissipation, a free-standing tip gap casing's inner radius of 144.40 mm (5.685") growth when compared to the rotor's 143.51 mm (5.650") radius will have a difference of approximately +0.1143 mm (0.0045"). This means that although the rotor may have grown from centrifugal loading and heat loading, the tip clearance measurement

may be short by a small amount since the casing will have moved away more than the rotor will have grown. An assumption is then made that the difference in thermal expansion of the rotor and casing isn't 114.3 μm (0.0045"), but only differs in expansion by approximately 10% of this amount, 12.7 μm (0.0005"). This is more realistic since there are fasteners and heat dissipation that will slow the casing outward growth. This means that the growth of the blades may be more than what was measured. This would equate to 12.7 μm (0.0005") of uncertainty in the positive radial growth direction.

c. Uncertainty Due to Pressure Differentials and Supersonic Shock Waves

Furthermore, there may be a slight change in tip clearance due to the bending of the fan's blades in the upstream direction. On a whole fan scale the upstream bending would be caused by the pressure differential between the low and high-pressure sides of the fan. The difference in pressure may cause there to be a moment developed on each of the blades causing them to flex upstream. Figure 68 portrays a graphic of how this could occur.

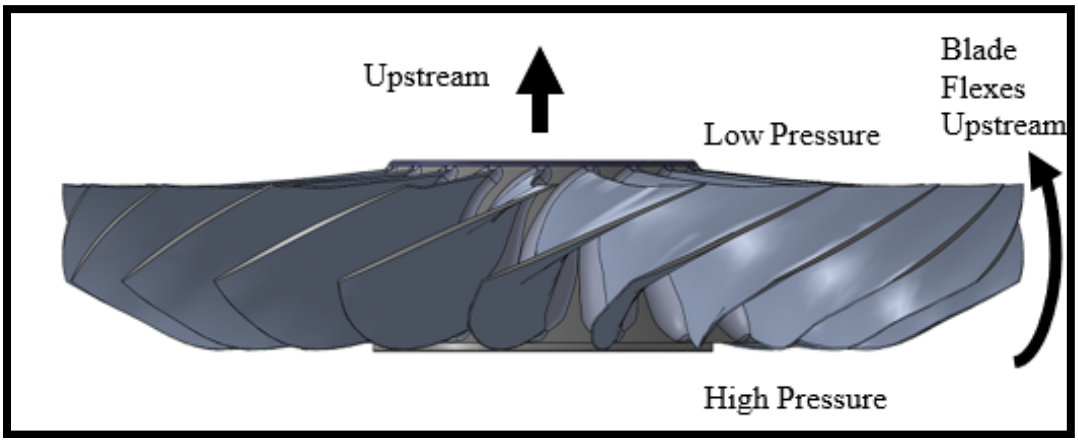

Figure 68. Upstream Bending of Fan Due to Pressure Differential.

Any bending of the blade will cause the closest distance of the blade to the capacitive probe to be further away. Although more than likely a negligible amount, this is a factor to consider in the uncertainty. An uncertainty of 2.54 μm (0.0001") is given in the positive growth direction.

On a blade-by-blade scale there may be blade deflection caused by shock waves after transitioning into sonic speeds. A phenomenon consistent between all three data runs is the drop in blade growth between 21,000 RPM to 24,000 RPM for the mid-chord and trailing edge position and between 12,000 RPM to 21,000 RPM for the leading edge. Assuming a perfect gas the speed of sound can be determined with Equation (5) [28].

$$a = \sqrt{\gamma g_c RT} \tag{5}$$

Where a is the speed of sound, γ is the specific heat ratio of air, g_c is the gravitational proportionality factor, R is the gas constant for air, and T is the temperature in Kelvin. Assuming an incoming air temperature of 300 K, the speed of sound within the TCR is 347 m/s. When transitioning from 21,000 RPM to 24,000 RPM the tip speed of the rotor changes from 316 m/s to 361 m/s, or Mach Numbers 0.91 to 1.04, transitioning into sonic speeds. The Mach numbers change slightly as temperature changes, though this estimate still holds true. Figures 61 through 63 have been annotated to show this region. This behavior in blade growth can be more easily compared between the 3 blade tip positions when viewing Figure 65. There may be some mechanism during this transition into the sonic region that is causing the blade growth to slow. Otherwise, if this stall in blade growth had not occurred, the growth line shape would behave more like the expected parabolic increase that the simulated model shows.

Meinster performed CFD analyses on the tip flow for various tip gaps and from his findings it is evident there exists a large pressure differential along the chord of the blade [20]. Figure 69 shows the simulated pressure distribution for peak efficiency flow developed across the length of the tip of the blade. The inlet air flow undergoes am oblique shock wave seen extruding upstream of the inlet and into the blade passage. We can see there is interaction between the blade passage's shock wave and the tip vortices from the leading edge. The results of Londoño's pressure measurement show similar results. The largest pressure differential occurs where the tip vortex is created at the leading edge of the blade on the suction side. On the pressure side of the blade, the distorted shock wave causes a pressure jump. In the figure the pressure differential at mid-chord is large, in this case approximately 41 kPa. Transitioning into sonic speeds may be introducing the formation

and collapse of the shock waves causing the rotor tip to bend and vibrate. The bending of the blade tip in this region would cause a change in tip clearance approximately equal to the cosine of the blade tip bend angle. When averages of the tip clearance for a vibrating blade, the result ends with a further tip clearance on average.

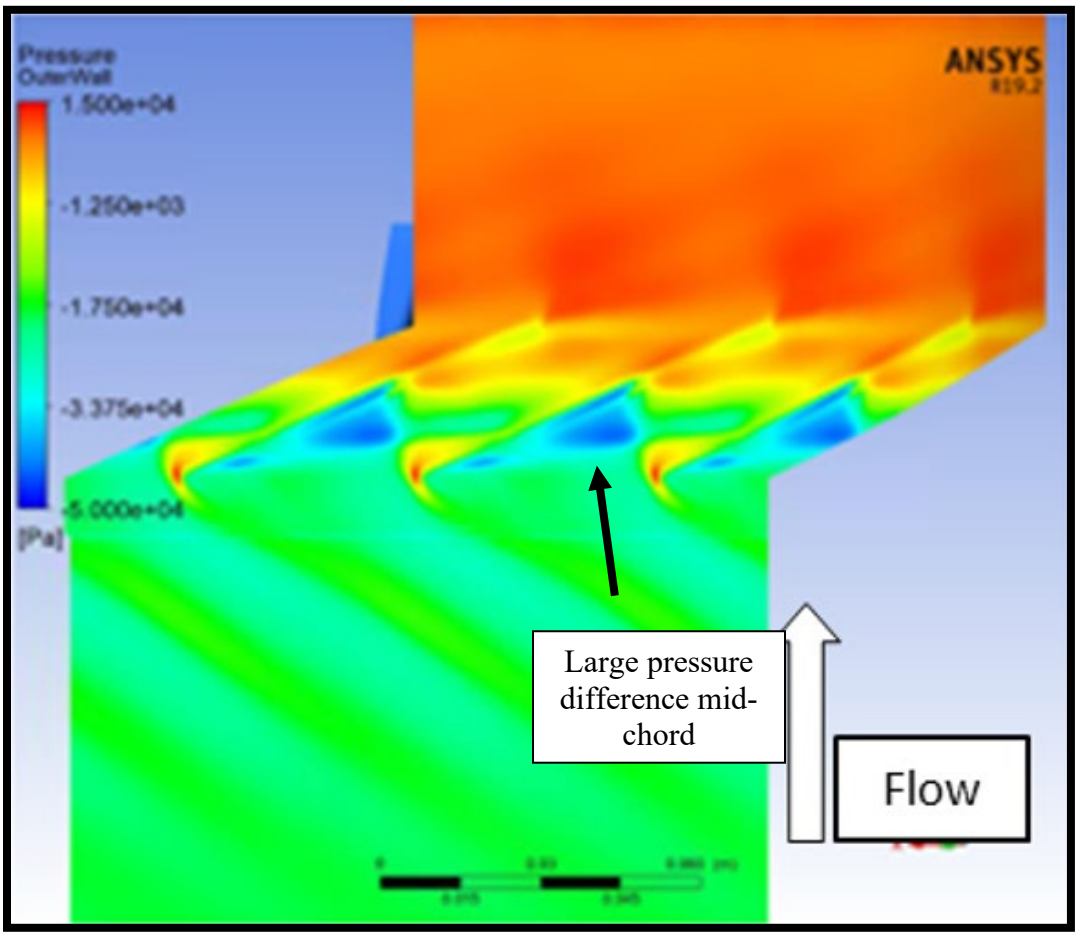

Figure 69. Casing Pressure in Tip Clearance Region Model. Source: [20].

The effect of the bending and vibrations from these shocks are better illustrated by plotting the location of the peaks over a number of revolutions. A comparison is made to show the widened distribution of the output pulse's peak location between a low-speed, low-vibration run, and a high-vibration, transonic run from the mid-chord position. The plot is made by taking the raw unprocessed data and recording the location of the longest blade's max peak in reference to its blade pass period. The deflection of the blade will

cause the location of the peak to occur either sooner or later in the blade pass period. Figure 70 is a comparison of the peak location distribution.

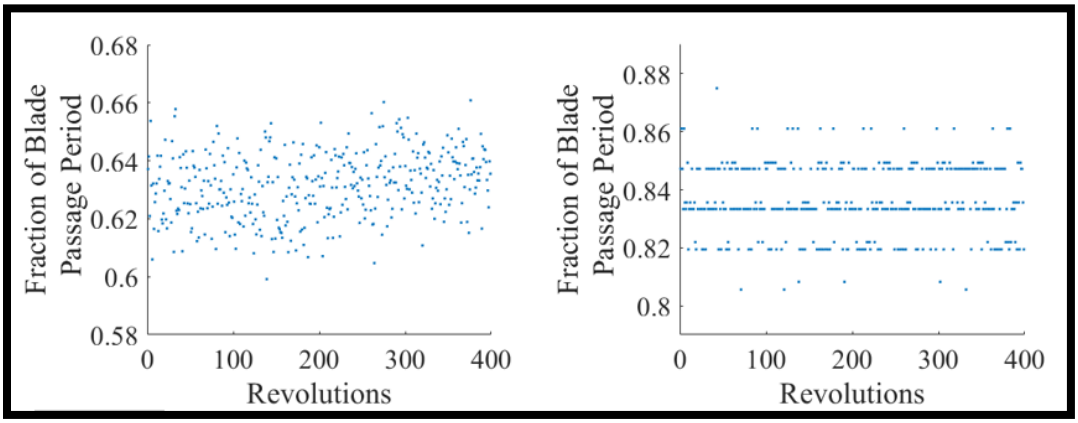

Figure 70. Location of Capacitive Probe Signal's Max Peak for 500 RPM (left) and 21,000 RPM (right).

The slow-speed run (left) has a standard deviation in units of fraction of blade passage period of .032 and the high-speed run has a standard deviation of .043. This means, on average, the high-speed run is measuring a lower tip clearance than it should be if compared to a no vibration run since it experiences the more deflection. Although this may be a small amount of deviation, it does mean that the actual tip clearance is closer than what is being measured and the blade should have "grown" more than what is measured. A more rigorous calculation of these uncertainty has not been conducted the author, though a margin of 2.54 μm (0.0001") is given in the positive growth direction.

d. Uncertainty Due to Probe Position

Finally, the actual probes' position in relation to the blade's tip as opposed to the simulated model is probably the largest factor to consider as to why the measured and simulated data do not exactly match. Only the trailing edge is considered in this analysis, though the argument can be applied to the leading, though at a smaller scale. The probe electrode is 4 mm (0.157") in diameter. Based on the solid model design of the transonic rig the sensing probe's center is 2.1048 mm (0.0829") in the fan's axial direction from the trailing edge's furthermost tip when the projection of the probe's electrode area is at a

maximum. This means that the amount of trailing edge deformation shown in the simulated data is not an accurate comparison to the TCR's measured data. Figure 71 shows approximately where the probes' actual position is. Using the legend in the figure, this corresponds roughly to a 228.6 µm (0.009") radial growth.

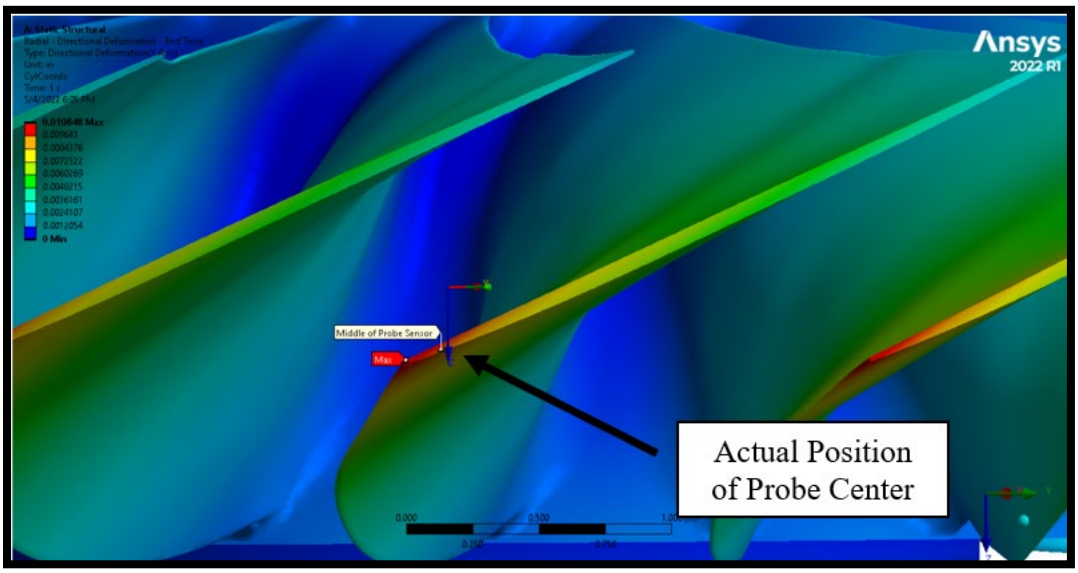

Figure 71. Zoomed View of Trailing Edge Radial Deformation Showing Actual Probe Position.

A more rigorous determination of the radial growth at this actual position is conducted. To account for this deviation from the model's simulated measurement location an extrapolation of the radial deformation data was taken by converting the ANSYS model into a stereolithographic model using Paraview. The radial distances of the surface along the tip of a single blade as a function of the axial position, z, are determined and the nominal rotor radius of 287.02 mm (11.3") was subtracted. All radii corresponding to the probes' actual position of 2.1057 mm (0.0829") in the fan's axial direction +/- the product of the radius of the probe electrode, 1.9939 mm (0.0785"), and the sine of the blade angle of, ~26 degrees, is then extrapolated. These values are the simulated radial growth of the rotor blade under the projection of the sensing electrode. The average is then calculated, resulting in an average radial growth at the proper probes' position of 244.856 µm (0.00964"), which is 89.3% of the maximum radial growth at the trailing edge's furthest tip. Figure 72

provides a solid model of the probes' actual measured position when the trailing edge passes through the middle of the sensing electrode. It shows the projection of the sensing electrode on the rotor blade.

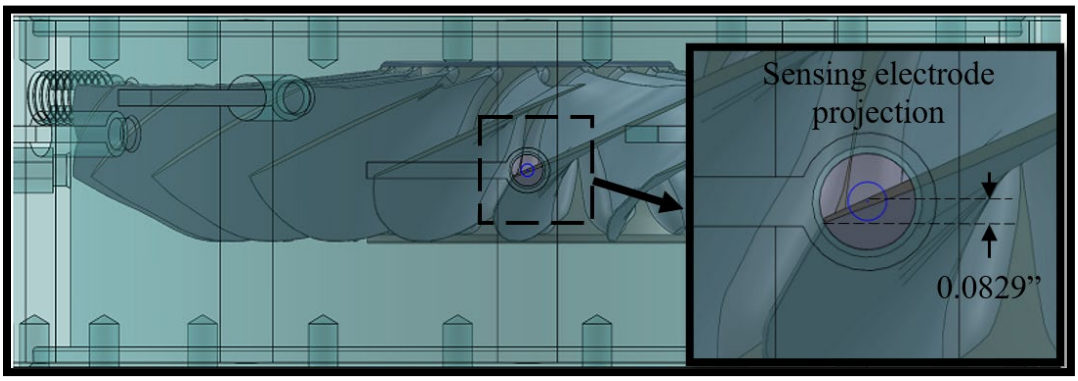

Figure 72. Sensing Electrode Projection onto Rotor Trailing Edge.

This error is further exacerbated in that in the actual TCR, the probe is positioned slightly more upstream than the solid model. This was because the TCR's components can be moved. Figure 73 shows a comparison of the SolidWorks model's probe position to the actual position on the TCR through the 2T position. By looking at where the NPSMF's trailing edge's furthest edge meets the edge of the probe hole, one can see the actual mounting of the fan is slightly further back by approximately 1.016 mm (0.04") in the axial direction as measured by a vernier caliper. This means the probe is monitoring further away from the trailing tip, resulting in a smaller radial growth being measured.

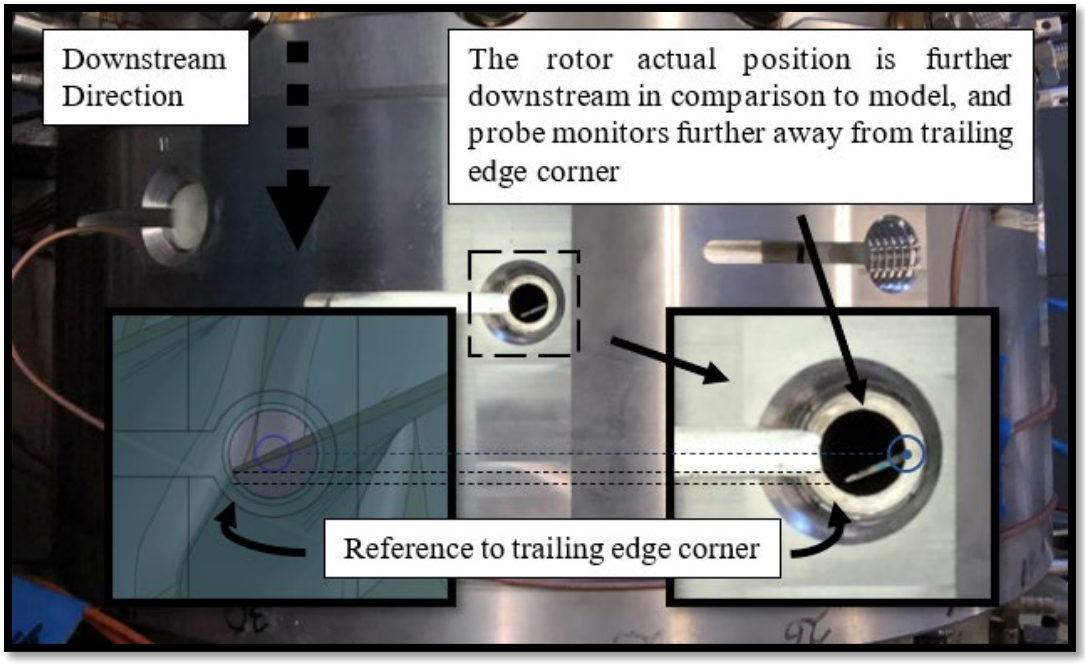

Figure 73. Comparison of Modeled Probe Monitoring Position to Actual Position.

After recalculating for this adjusted position using the same extrapolation method as earlier, the amount of radial growth at this radial position is 234.04 μm (0.009214"), or 85.3% of the 274.32 μm (0.0108") simulated max radial growth. Although a small change, this provides a more accurate comparison. Referring back to Figure 65 the opposite effect can be seen for the leading edge where the measured growth is more than the simulated result. The same principle described can be applied, though a rigorous calculation of this was not done as the measured and simulated result was within 25.4 μm (0.001").

e. Errors in Demodulator Circuitry Due to Rotor Speed

As mentioned in Chapter II, a 10 MHz signal is driven through the capacitive probe and the passing rotor blade tip will modulate this oscillating signal. The phase comparator of the demodulator will sense the phase difference, or the lag, between this modulated signal and a fed back reference signal. It is unknown to the author what the response time of the comparing circuit is, or the response time of its feedback loop (refer to Figure 10 for circuit block diagram), though at very high speeds there are very few oscillations of the 10

MHz oscillator that are passed through the circuitry for the blade passage. Possibly, there may not be enough time to give a proper response to the blades passing by.

The rotor's nominal radius is 287.02 mm (11.3"), giving a perimeter of 901.7 mm (35.5"). With the probe's electrode diameter of 4 mm (0.1575") (refer to Figure 72) and a speed of 27,000 RPM, the rotor tip will only be present in the vicinity of the probe's face for approximately 9.859 μsec. For a 10 MHz oscillating signal that gives approximately 99 oscillations every second. This oscillating signal is modulated during the blade passage, therefore even less cycles are passed through the comparing circuitry every second. The small number of cycles sensed by the comparator could potentially affect the voltage output of the comparator, giving a smaller peak-to-peak digital readout, and could potentially give reason to the "dip" seen in the blade growths.

The response of analogue circuitry is considered "near instantaneous", though in reality there is some lag within the circuitry. Although more than likely not a large source of uncertainty in the blade tip clearance measurements, there is merit to the circuit response time to measure the phase difference.

3. Adjusted Comparison to Simulation

The uncertainties and adjustments discussed in the previous section are not taken into account to create an adjusted model to measured BTC growth plot for the trailing edge. The positive uncertainty bound is calculated using Equation (6a) and (6b).

$$Growth\ Error\ (+) = \sqrt{A^2 + B^2 + C^2 + D^2} \tag{6a}$$

$$Growth\ Error\ (-) = A \tag{6b}$$

Where A is the average calibration curve standard deviation of the probes from 950 μm to 650 μm (0.0256"), which is 25.4 μm (0.001”). B is the 5.08 μm (0.0002") of error due to the power retention difference from post-processing. C is the 2.54 μm (0.0001") of uncertainty due to blade deflections and vibrations causing a larger tip clearance reading. D is the 12.7 μm (0.0005") of uncertainty imposed by the difference in thermal expansion of the casing and rotor. This results in an error bar of +28.956 mm / -25.4 μm (+ 0.00114" / - 0.00100"). The 85.3% factor is applied to all points of the simulated growth plot. The adjusted model and the measured BTC with the error bars are plotted for the trailing edge in Figure 74.

A difference of ~50.8 μm (0.002") between the max growth of the modeled data and the measured data still exists after the adjustment. The growth curve follows the model closely until approximately 21,000 RPM, then the TCR reaches transonic speeds. Possibly this may be due to human error in the calibration or measurement of the BTC. This may also be due to not having conducted a more rigorous calculation of the amount of deflection caused by the fluid pressure distribution when shocks are present. The deflection would cause there to be a smaller tip growth measurement. If the reduced growth from 21,000 to 24,000 RPM didn’t occur, it seems that the simulated result would be within the band of uncertainty of the measured result.

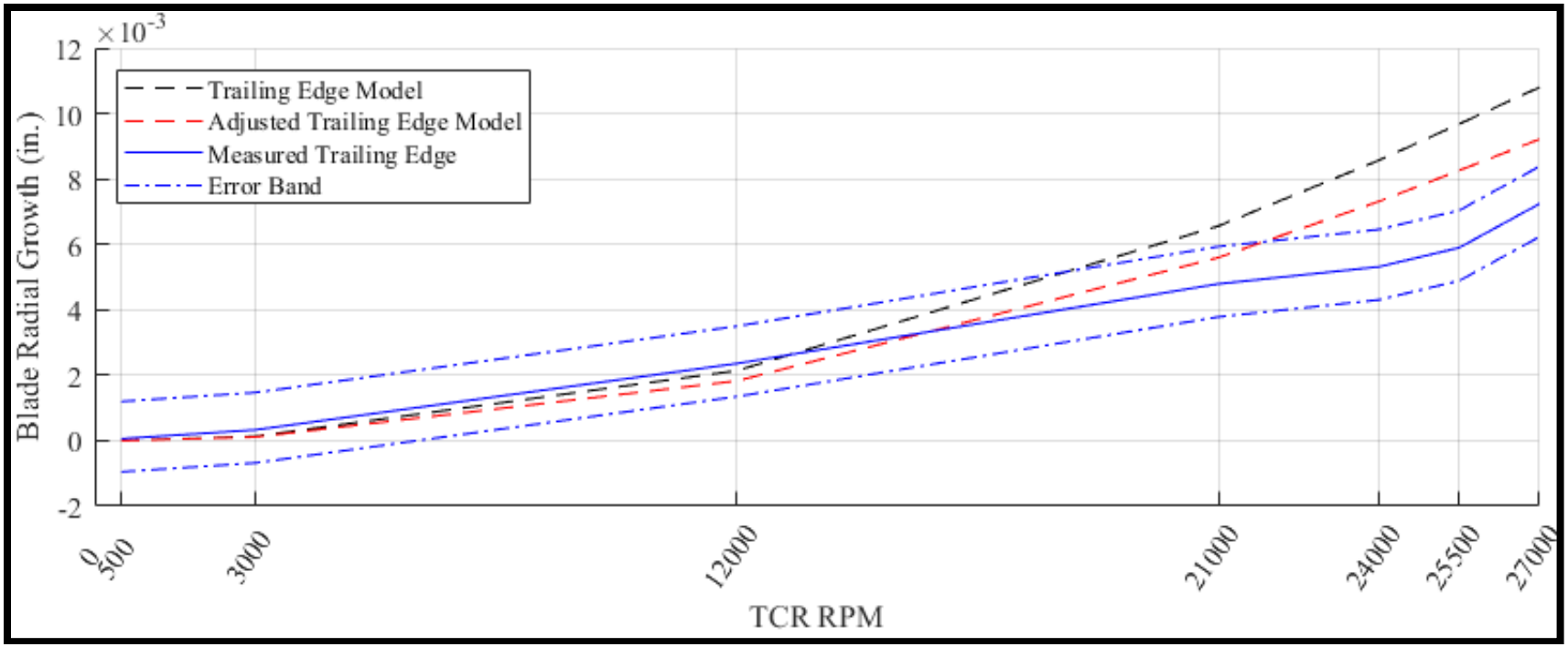

Figure 74. Adjusted Growth Plot for Trailing Edge.

4. Recommendations

The accuracy of the measured results is highly dependent on the proper calibration of the capacitive probes. A more stringent calibration with higher precision in distance measurements (better than the 0.025 mm/ 100 mm Velmex BiSlide) is recommended. Furthermore, because the BCTR capacitive probe output has much different characteristics than the TCR capacitive probe output signal, a calibration done on the TCR itself at higher speeds would also be beneficial. The higher speed would create a similar output signal shape to what will be measured. A new calibration casing that has a probe mounting port that can precisely translate the probes radial position is recommended. A calibration apparatus that can do what is described has been created by Sheard et al. [12]. In this calibration rig, a probe is stepped forward whilst the rotor spins until a touch probe, 10 μm (0.000394") further than the face of the capacitive probe, senses a spark discharge and is then stepped away from the rotor to a known amount to reach a zero position. This way a live calibration can be done just prior to actual tip clearance measurements ensuring the environment the probes are in is as close as possible to actual measurement.

Furthermore, a more rigorous search for a better filtering method could provide more accurate results. Different types of low pass filters and passband filters had not been explored in this paper. A simulation at numerous points along the edge of the blade should be conducted as well to provide a tip growth profile to give more points for comparison. Also, ensuring that the probe is axially positioned in the same location as the model will lower uncertainty in measurements.

Finally, a model that takes into account the air flow pressure distribution at peak efficiency at multiple speeds in conjunction with the model used for radial blade growth would give a more accurate comparison. A model that can show the blade deformation due to air pressure differentials would be more accurate. Next, a near-stall model and measurement would also provide interesting results as the rise in shock waves may cause larger deflections, affecting BTC. Finally, modeling the small radial expansion changes due to temperature would further increase the accuracy of the model.

THIS PAGE INTENTIONALLY LEFT BLANK

VI. CONCLUSION

A novel calibration and testing rig has been created to calibrate capacitive probes of a blade tip clearance measurement system in the TPL. A signal post-process method has been created using this calibration and test rig that involves the normalization of the data to a once-per-revolution signal and a tip clearance adaptive lowpass filter. Normalizing to a once-per-revolution signal is common in signal processing, but it has not been done for this application. The post-process method has been tested to show improved capacitive probe capability without altering already existing hardware. Using these methods a measurement of the tip clearances of the NPSMF in the TCR has been conducted at multiple speeds. The NPSMF blade growth simulation model was then created and compared to the measured result. An error analysis has been conducted with recommendations for future work.

THIS PAGE INTENTIONALLY LEFT BLANK

APPENDIX A. CALIBRATION CURVES

A. BCTR WITH TIP GAP CASING CALIBRATION PLOTS

Figures 75 through 86 provide BCTR calibration curves and their fitted curves overlaid. Tables 12 through 23 provide the BCTR tabulated values for the calibration curve points, their standard deviations, and the parameters for the curve fit.

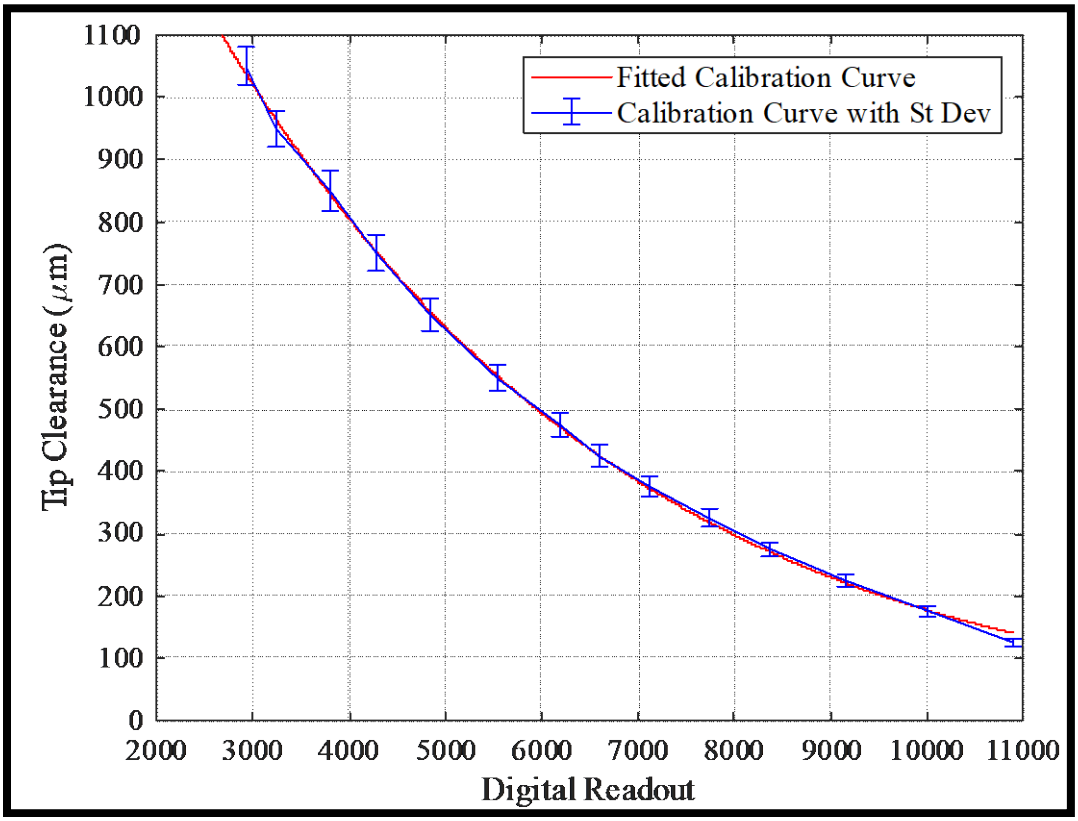

Figure 75. Calibration Curve, BCTR (Tip Gap Casing), Leading Edge Probe 1.

Table 12. Calibration Table, BCTR (Tip Gap Casing), Leading Edge Probe 1

Calibration Distance (µm)	Average Value (DRO)	St. Deviation (DRO)	St. Deviation (µm)	Curve Fit Parameters
125	10894.05	169.9357	6.152344	R-square = 0.9992
175	9994.343	173.3363	7.883402	a = 2617085
225	9159.009	173.1852	9.713581	b = -0.00031
275	8374.444	166.5973	11.35803	c = -2615086
325	7736.572	172.5139	13.73798	d = -0.00031
375	7131.021	172.1239	15.86818	
425	6598.239	182.8183	19.11641	
475	6188.16	170.9708	19.72295	
550	5542.5	161.3959	21.66424	
650	4847.654	163.8513	25.771	
750	4274.106	165.7516	29.6346	
850	3812.444	162.7154	32.20646	
950	3233.729	129.5992	29.15056	
1050	2932.553	126.1872	30.25072	

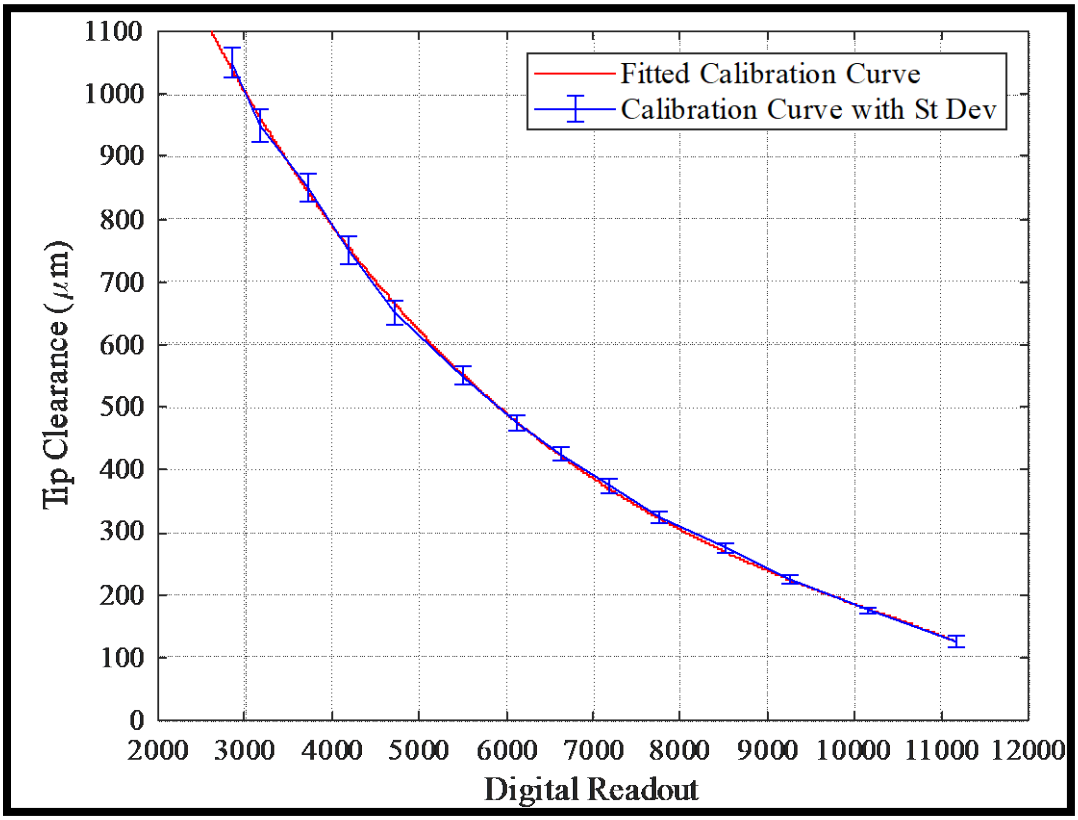

Figure 76. Calibration Curve, BCTR (Tip Gap Casing) Leading Edge Probe 2.

Table 13. Calibration Table, BCTR (Tip Gap Casing), Leading Edge Probe 2

Calibration Distance (µm)	Average Value (DRO)	St. Deviation (DRO)	St. Deviation (µm)	Curve Fit Parameters
125	11172.53	133.0681	8.304941	R-square = 0.9994
175	10163.31	128.7625	6.336737	a = -1.39E-06
225	9248.061	127.565	6.988315	b = 0.001465
275	8514.365	123.6475	7.893466	c = 2052.902
325	7758.87	131.8893	10.00742	d = -0.00024
375	7174.135	126.365	11.01411	
425	6631.441	124.7045	12.36837	
475	6116.373	117.814	13.22187	
550	5500.626	119.5431	15.53573	
650	4726.256	123.2892	19.26695	
750	4188.923	123.4443	21.93112	
850	3730.907	115.6364	22.93906	
950	3184.794	111.143	25.1315	
1050	2856.669	100.7533	24.66913	

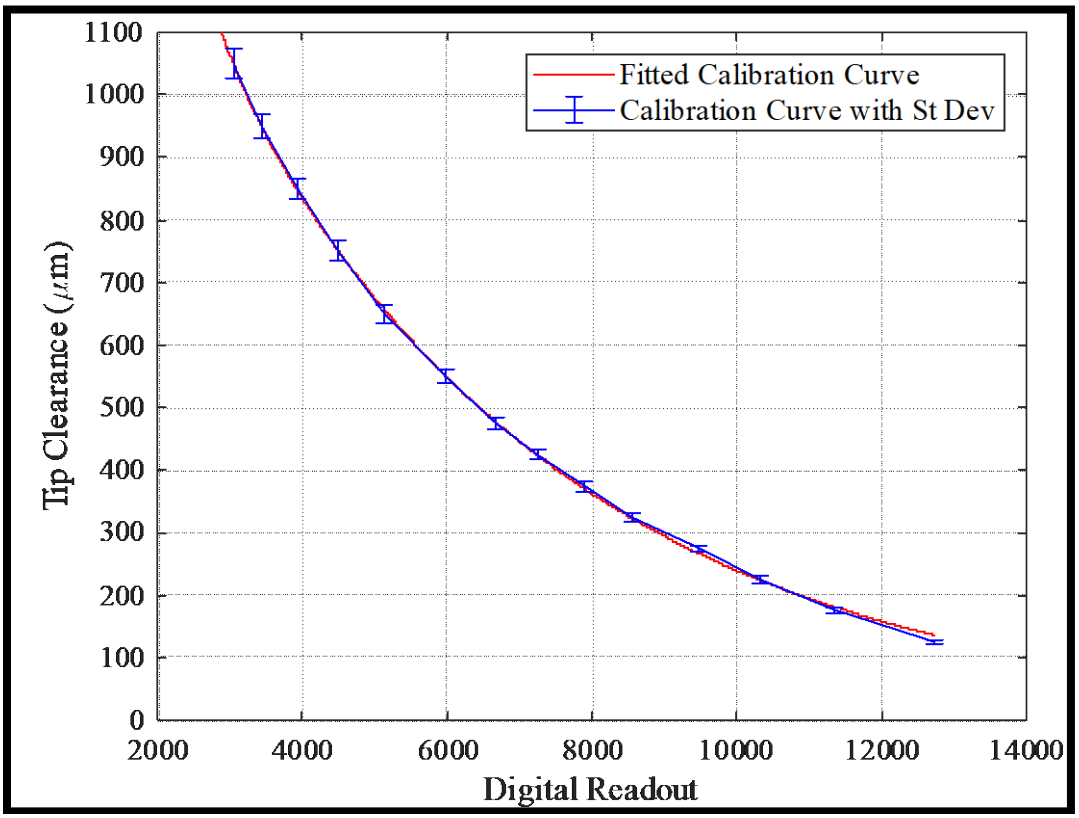

Figure 77. Calibration Curve, BCTR (Tip Gap Casing), Leading Edge Probe 3.

Table 14. Calibration Table, BCTR (Tip Gap Casing), Leading Edge Probe 3

Calibration Distance (µm)	Average Value (DRO)	St. Deviation (DRO)	St. Deviation (µm)	Curve Fit Parameters
125	12715.98	113.4928	3.165445	R-square = 0.9997
175	11345.78	107.671	3.992094	a = 2.63E+04
225	10322.67	113.3191	5.191264	b = -0.00214
275	9451.264	103.8647	5.705909	c = 1900.501
325	8554.151	102.3292	6.771816	d = -0.00021
375	7890.386	110.0381	8.34984	
425	7261.396	108.8862	9.415116	
475	6669.104	105.0014	10.27183	
550	5987.767	103.1792	11.63746	
650	5126.647	103.9912	14.09282	
750	4491.656	100.2658	15.74429	
850	3936.635	93.85128	17.23283	
950	3422.684	89.50436	20.18506	
1050	3044.475	88.8308	25.14617	

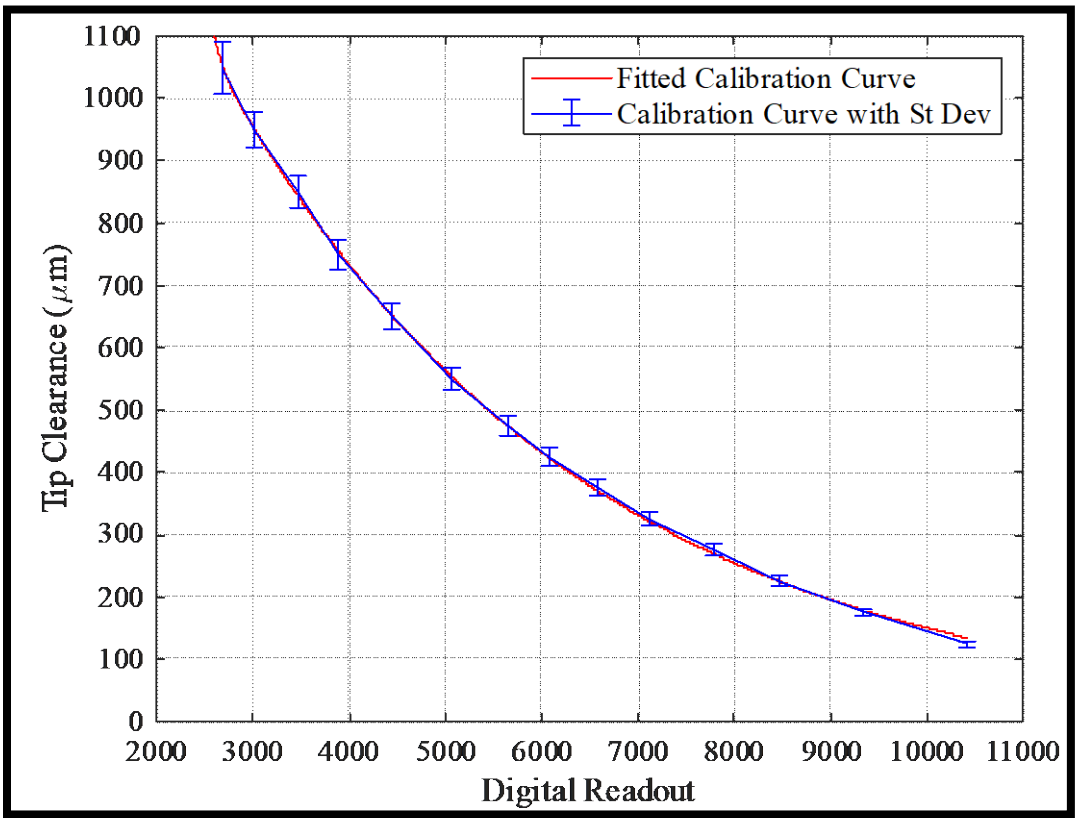

Figure 78. Calibration Curve, BCTR (Tip Gap Casing), Leading Edge Probe 4.

Table 15. Calibration Table, BCTR (Tip Gap Casing), Leading Edge Probe 4

Calibration Distance (µm)	Average Value (DRO)	St. Deviation (DRO)	St. Deviation (µm)	Curve Fit Parameters
125	10412.4	135.2712	4.726304	R-square = 0.9998
175	9336.245	134.1471	6.231037	a = 3.74E+15
225	8475.303	134.3096	7.833533	b = -0.01235
275	7775.254	131.1213	9.206778	c = 2111.498
325	7125.705	126.7298	10.57221	d = -0.00026
375	6577.209	125.5425	12.10993	
425	6084.813	131.7619	14.46565	
475	5639.921	129.9783	16.05526	
550	5060.689	124.6503	17.95849	
650	4438.358	124.8543	21.20529	
750	3896.094	124.7049	24.44629	
850	3463.887	118.8044	26.13072	
950	3016.414	118.6808	29.57561	
1050	2691.848	116.0226	41.82851	

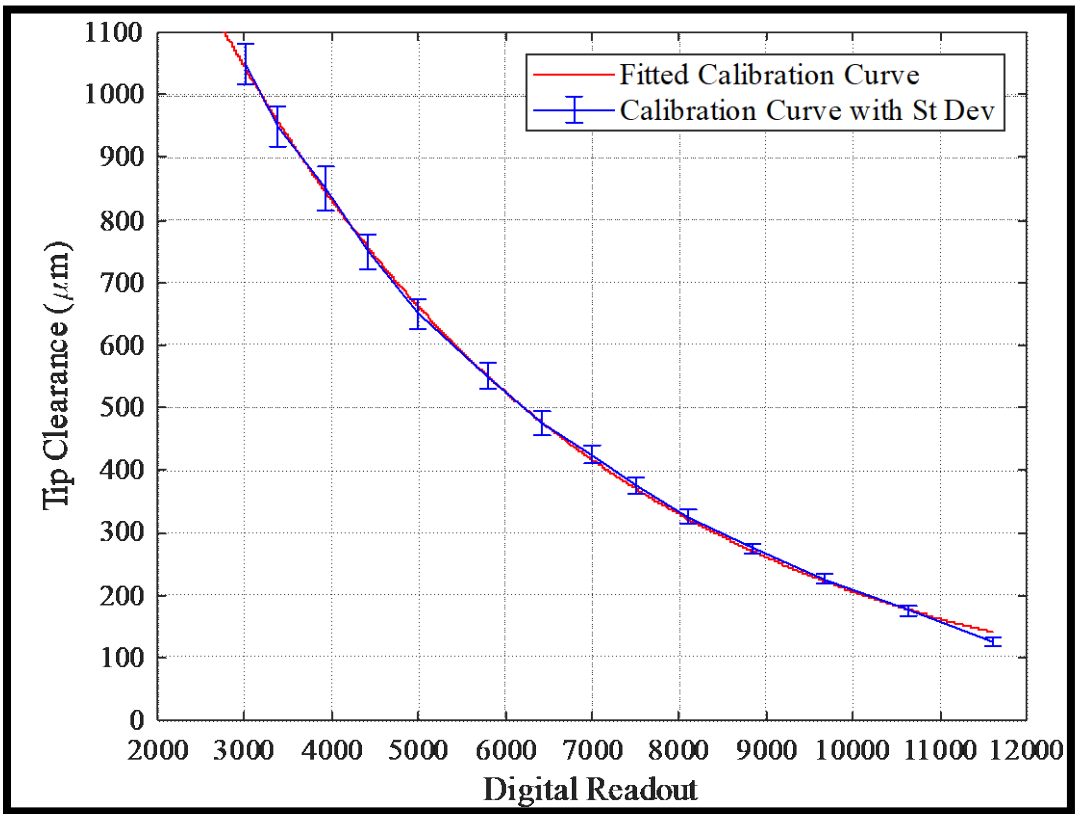

Figure 79. Calibration Curve, BCTR (Tip Gap Casing), Mid-Chord Probe 1.

Table 16. Calibration Table, BCTR (Tip Gap Casing), Mid-Chord Probe 1

Calibration Distance (µm)	Average Value (DRO)	St. Deviation (DRO)	St. Deviation (µm)	Curve Fit Parameters
125	11617.76	160.9831	5.273733	R-square = 0.9993
175	10636.33	176.4919	7.259931	a = -9.34E+05
225	9671.388	155.9229	8.045783	b = -0.00027
275	8847.587	142.3172	8.897949	c = 936024
325	8101.021	148.3603	11.00505	d = -0.00027
375	7510.705	159.4597	13.52179	
425	6988.576	135.8832	13.01277	
475	6417.071	169.5182	18.41072	
550	5808.17	166.5498	20.76003	
650	5001.659	168.8638	25.21489	
750	4414.62	161.5679	27.51779	
850	3942.755	181.5238	34.248	
950	3374.586	146.7332	31.49441	
1050	3013.124	136.0939	31.65435	

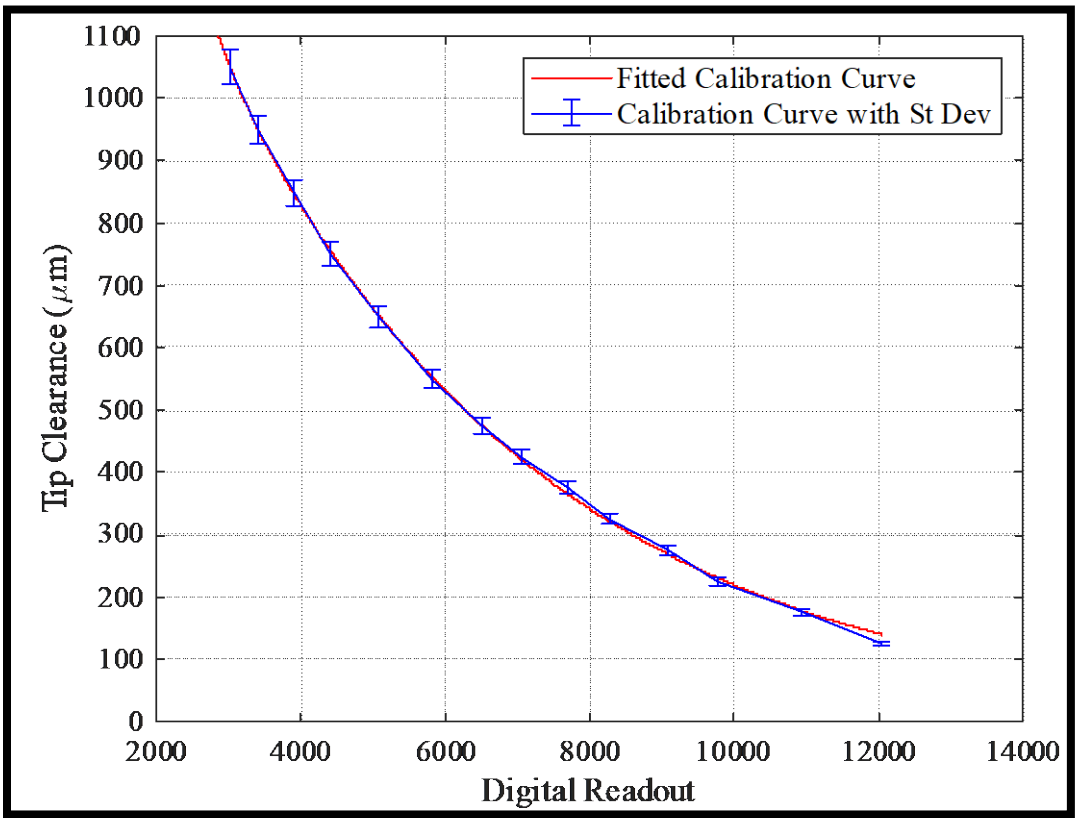

Figure 80. Calibration Curve, BCTR (Tip Gap Casing), Mid-Chord Probe 2

Table 17. Calibration Table, BCTR (Tip Gap Casing), Mid-Chord Probe 2

Calibration Distance (µm)	Average Value (DRO)	St. Deviation (DRO)	St. Deviation (µm)	Curve Fit Parameters
125	12035.19	117.2232	3.576215	R-square = 0.9996
175	10940.67	124.028	4.817166	a = 2.00E+03
225	9778.031	118.6752	5.96515	b = -0.00022
275	9073.884	123.0361	7.223639	c = 83040.5
325	8281.677	114.6104	8.025739	d = -0.0027
375	7684.922	111.0338	8.876426	
425	7061.44	120.8895	11.08211	
475	6499.131	113.3401	11.77696	
550	5825.414	115.7221	13.9566	
650	5056.753	114.7492	16.42883	
750	4415.598	115.4507	19.16331	
850	3907.463	110.1444	20.8669	
950	3405.468	98.63662	22.30513	
1050	3021.763	97.98455	27.48428	

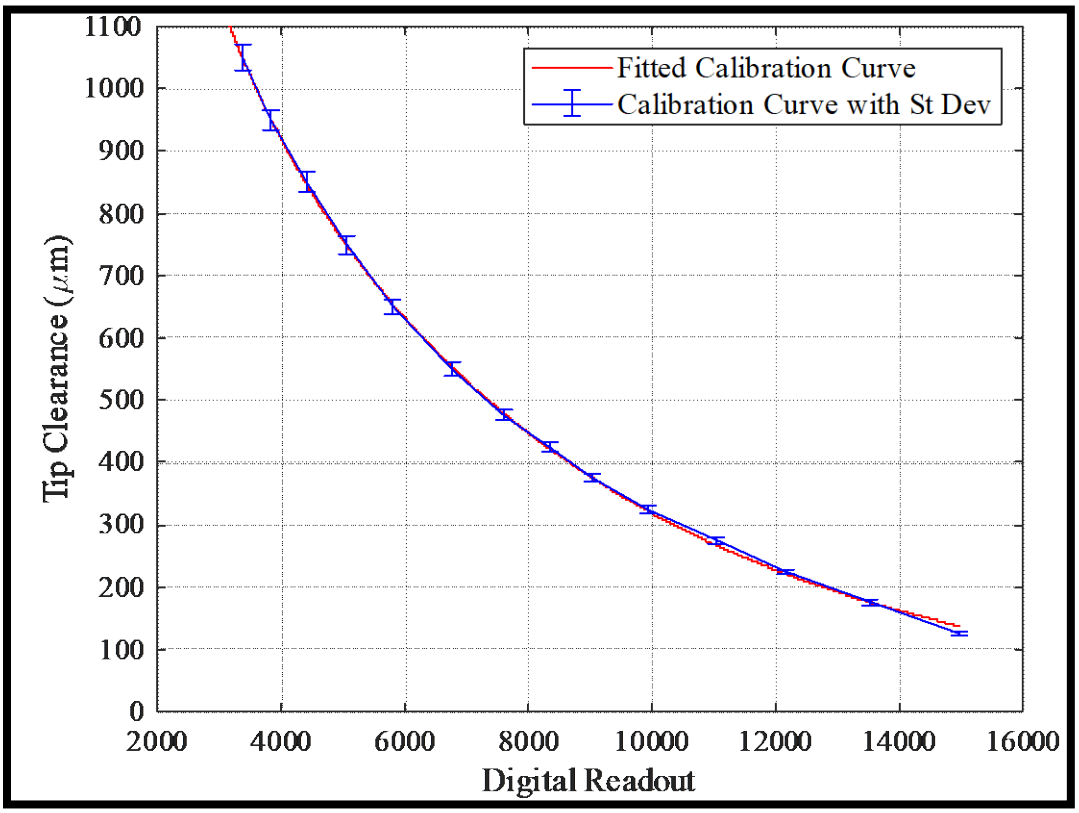

Figure 81. Calibration Curve, BCTR (Tip Gap Casing), Mid-Chord Probe 3.

Table 18. Calibration Table, BCTR (Tip Gap Casing), Mid-Chord Probe 3

Calibration Distance (µm)	Average Value (DRO)	St. Deviation (DRO)	St. Deviation (µm)	Curve Fit Parameters
125	14963.81	109.3034	2.516896	R-square = 0.9997
175	13499.59	112.2006	3.30734	a = 1.66E+03
225	12171.22	107.4337	3.965532	b = -0.00091
275	11027.9	110.376	4.943742	c = 1719.935
325	9928.168	108.1899	5.845251	d = -0.00017
375	9043.423	105.321	6.627475	
425	8339.565	106.9301	7.607875	
475	7609.753	100.3011	8.135669	
550	6769.868	103.597	9.825806	
650	5802.677	102.5406	11.83675	
750	5052.324	102.4025	14.05261	
850	4421.4	106.3637	17.25341	
950	3837.332	86.38401	16.85294	
1050	3373.871	86.67294	19.98621	

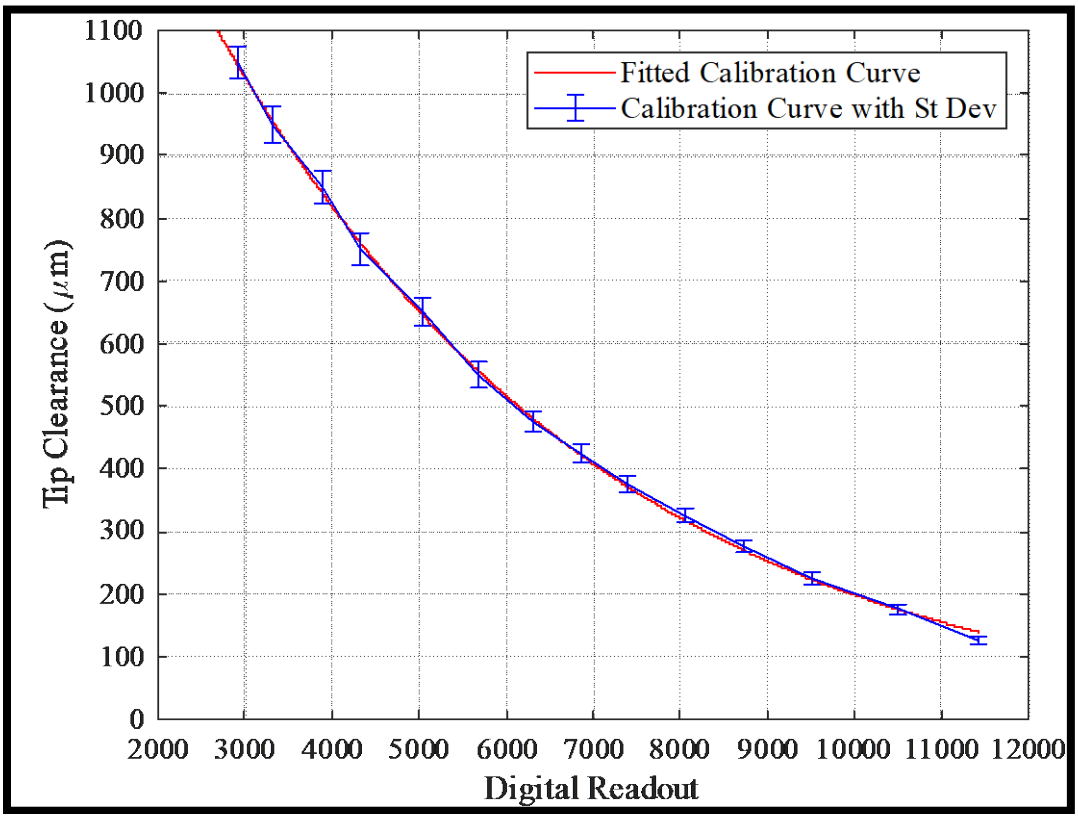

Figure 82. Calibration Curve, BCTR (Tip Gap Casing), Mid-Chord Probe 4.

Table 19. Calibration Table, BCTR (Tip Gap Casing), Mid-Chord Probe 4

Calibration Distance (µm)	Average Value (DRO)	St. Deviation (DRO)	St. Deviation (µm)	Curve Fit Parameters
125	11433.99	159.511	5.380809	R-square = 0.9994
175	10490.04	169.1717	7.140633	a = -1.38E+06
225	9509.018	160.9689	8.573009	b = -0.00029
275	8735.663	148.0622	9.459444	c = 1381186
325	8057.279	155.8081	11.63239	d = -0.00029
375	7393.076	156.2098	13.57355	
425	6852.771	150.4941	14.78636	
475	6307.723	141.7355	15.74874	
550	5684.209	154.8278	19.72007	
650	5034.013	152.6193	22.4066	
750	4317.731	149.9176	25.67195	
850	3883.674	141.8973	26.65204	
950	3316.809	135.0594	28.55897	
1050	2911.694	112.5888	25.92132	

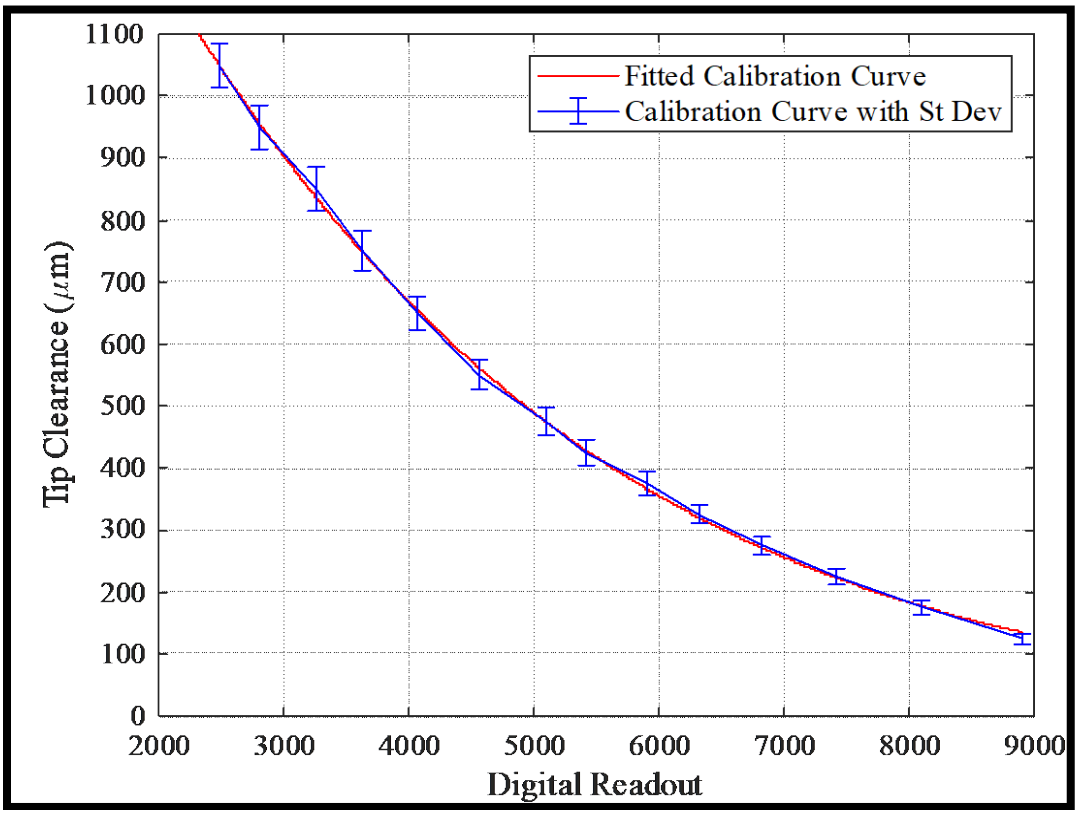

Figure 83. Calibration Curve, BCTR (Tip Gap Casing), Trailing Edge Probe 1.

Table 20. Calibration Table, BCTR (Tip Gap Casing), Trailing Edge Probe 1

Calibration Distance (µm)	Average Value (DRO)	St. Deviation (DRO)	St. Deviation (µm)	Curve Fit Parameters
125	8895.629	174.8658	7.837913	R-square = 0.9995
175	8093.943	173.9054	10.12046	a = 6.95E+05
225	7417.046	174.4714	12.60686	b = -0.00041
275	6827.325	160.4149	13.98306	c = -692494
325	6325.487	149.3672	15.23051	d = -0.00041
375	5899.133	159.0654	18.43809	
425	5422.859	159.7403	21.34668	
475	5098.823	152.6479	22.45885	
550	4560.351	144.0069	24.76535	
650	4069.433	138.8699	27.40964	
750	3620.433	145.8799	32.48301	
850	3249.386	145.3844	35.6836	
950	2797.557	126.2985	34.82987	
1050	2490.58	119.3559	35.48809	

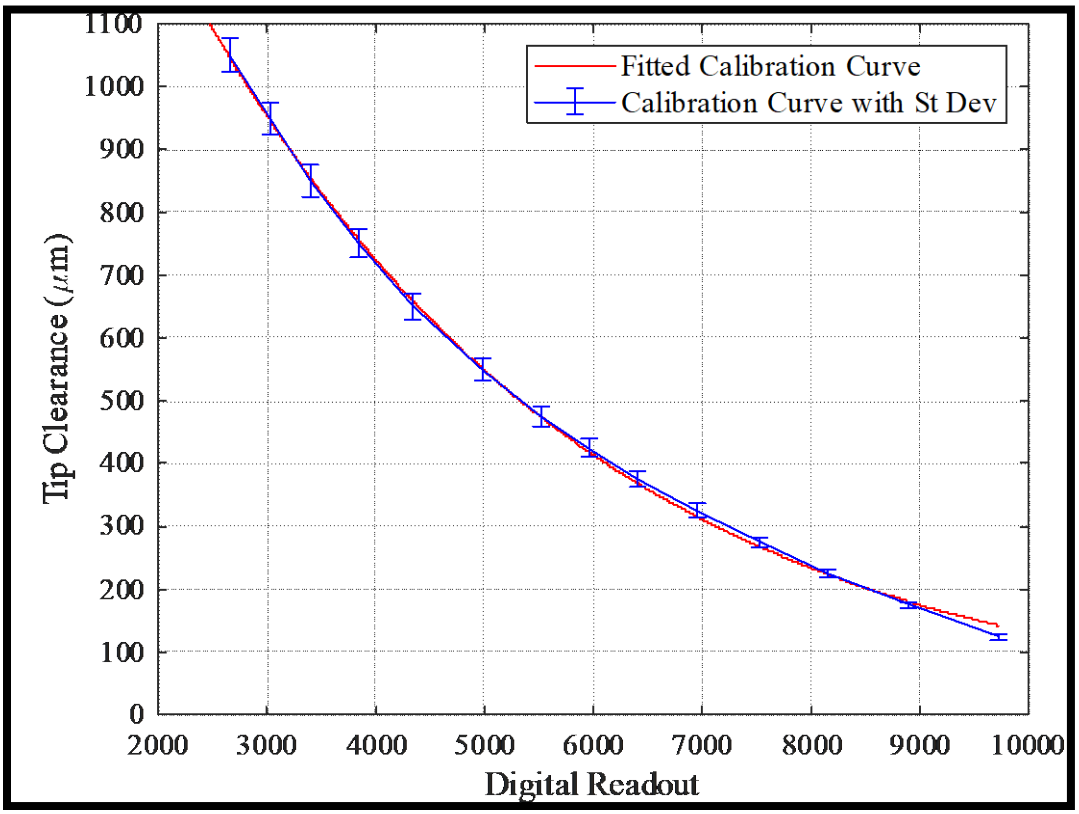

Figure 84. Calibration Curve, BCTR (Tip Gap Casing), Trailing Edge Probe 2.

Table 21. Calibration Table, BCTR (Tip Gap Casing), Trailing Edge Probe 2

Calibration Distance (µm)	Average Value (DRO)	St. Deviation (DRO)	St. Deviation (µm)	Curve Fit Parameters
125	9721.695	120.4243	4.8978	R-square = 0.9994
175	8900.962	115.0634	5.91297	a = -1.75E+06
225	8149.309	118.524	7.524713	b = -0.00034
275	7524.069	118.4636	8.95916	c = 1754742
325	6960.677	119.8627	10.59979	d = -0.00034
375	6401.449	114.3412	11.80842	
425	5959.092	118.7339	13.83533	
475	5514.789	113.5318	14.94263	
550	4976.461	110.841	16.88165	
650	4344.497	111.739	20.15636	
750	3841.468	108.8801	22.45297	
850	3404.846	107.4011	24.84665	
950	3031.556	97.90596	24.99568	
1050	2661.578	98.42518	27.64869	

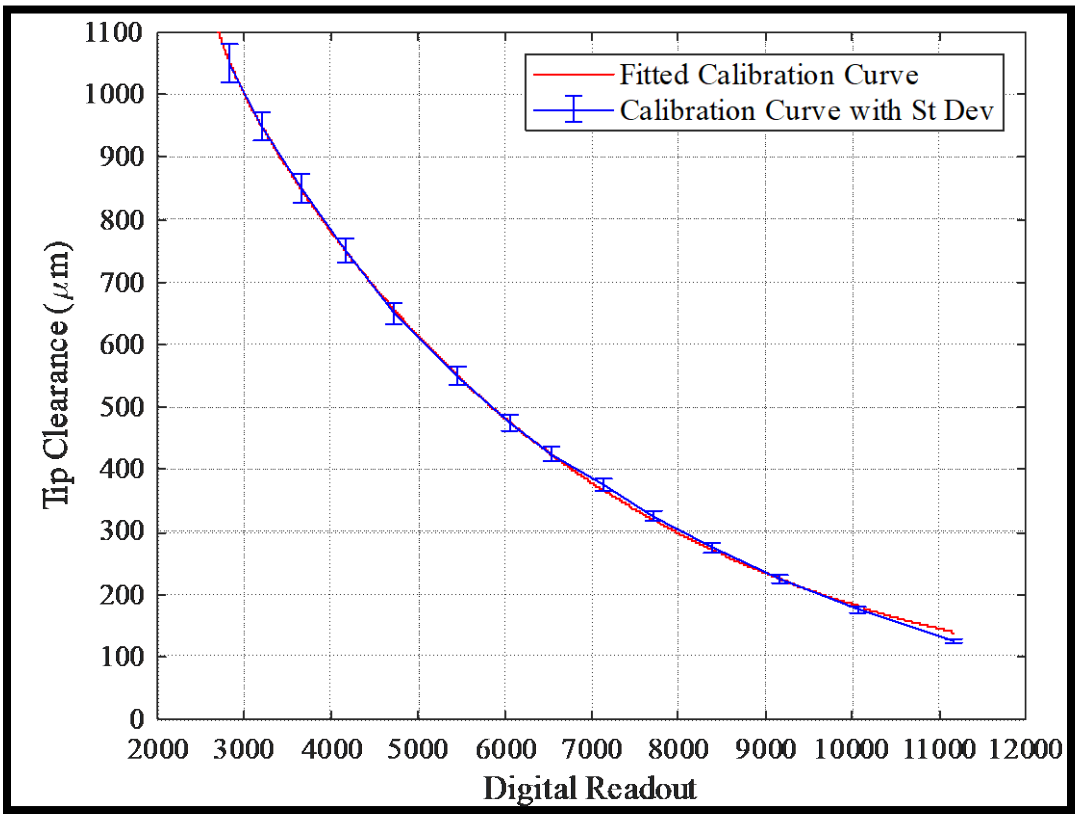

Figure 85. Calibration Curve, BCTR (Tip Gap Casing), Trailing Edge Probe 3.

Table 22. Calibration Table, BCTR (Tip Gap Casing) Trailing Edge Probe 3

Calibration Distance (µm)	Average Value (DRO)	St. Deviation (DRO)	St. Deviation (µm)	Curve Fit Parameters
125	11171.67	116.8654	3.849145	R-square = 0.9997
175	10071.92	111.7437	4.8	a = 5.95E+06
225	9171.324	121.3894	6.470411	b = -0.00449
275	8392.516	114.8849	7.393396	c = 2045.694
325	7702.875	110.0742	8.369096	d = -0.00024
375	7133.379	111.9788	9.76381	
425	6532.831	110.1599	11.10301	
475	6062.719	108.678	12.2695	
550	5456.519	111.8793	14.61169	
650	4722.481	108.6278	16.93958	
750	4152.995	103.9726	18.62463	
850	3658.119	108.1815	21.96899	
950	3196.605	96.19357	22.91405	
1050	2837.729	95.8241	29.64902	

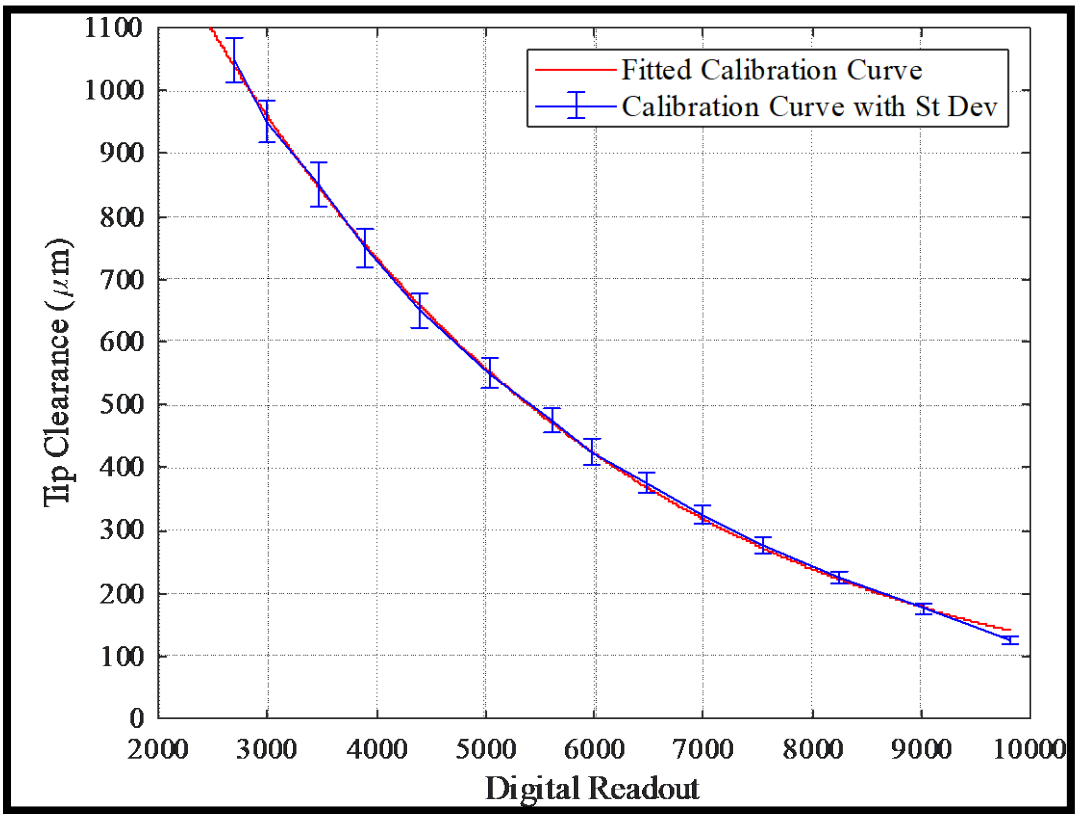

Figure 86. Calibration Curve, BCTR (Tip Gap Casing), Trailing Edge Probe 4.

Table 23. Calibration Table, BCTR (Tip Gap Casing), Trailing Edge Probe 4

Calibration Distance (µm)	Average Value (DRO)	St. Deviation (DRO)	St. Deviation (µm)	Curve Fit Parameters
125	9812.075	169.0352	6.838322	R-square = 0.9994
175	9014.932	162.5945	8.259592	a = -4.60E+05
225	8239.652	168.0189	10.6045	b = -0.00035
275	7550.287	166.9596	12.76005	c = 462332
325	7001.096	172.1187	15.28002	d = -0.00035
375	6472.515	165.8469	17.0037	
425	5987.675	166.1848	19.39765	
475	5603.651	157.773	20.40758	
550	5039.866	164.3542	24.60759	
650	4402.93	152.0891	26.8459	
750	3904.5	153.4254	30.68202	
850	3481.368	155.8094	34.56783	
950	2989.106	134.8711	33.77409	
1050	2695.482	131.6794	35.35395	

THIS PAGE INTENTIONALLY LEFT BLANK

APPENDIX B. TRANSONIC COMPRESSOR RIG TIP CLEARANCE RESULTS

A. CALIBRATION VALIDATION TABULATED RESULTS

As described in Chapter IV, an experiment was conducted to validate that the calibration curves and tables developed on the BCTR can successfully transfer to the TCR. The casing was moved from an initial position 175.26 μm (0.0069") towards probe 1M and away from probe 3M. The following Table 24 provides the tabulated measurements of the tip clearances from this experiment and the measured movement. For reference to where probes are positioned refer to Figure 59.

Table 24. Tip Clearance Measurements of TCR Calibration Validation

Probe Number	Tip Clearance Position 1 (in.)	Tip Clearance Position 2 (in.)	Measured Movement (in.)[1]
1M	0.03174	0.25202	-0.00654
2M	0.03080	0.02958	-0.00121
3M	0.03047	0.03665	0.00618
4M	0.02829	0.02978	0.00149

1 – The experiment had moved the casing 175.26 μm (0.0069"). Probes 1M and 3M were stationed near horizontal and should show near this amount of movement.

B. TABULATED VALUES OF TIP CLEARANCE MEASUREMENTS FOR BLADE GROWTH EXPERIMENT

Tables 25 through 27 are the measured tip clearances from the TCR blade growth experiment. The individual probe results are the average of all the data runs conducted at a maintained speed. Normally 5 data runs are recorded at each specified speed of the TCR. Table 28 is the tabulated values of the blade growths extrapolated from the values in Tables 25 through 27. The growths values in Table 28 include the adjusted 500 RPM zero value, as described in Chapter V. Table 29 shows the tabulated values of the blade growth from the modeled blade growth and includes the values from the adjusted model to account for probe position.

Table 25. Probe Averaged Tip Clearance Measurements, Leading Edge

Probe Number	500 RPM	3000 RPM	12000 RPM	21000 RPM	24000 RPM	25500 RPM	27000 RPM
1L (μm)	977.51	969.36	937.12	940.59	934.26	923.87	912.40
2L (μm)	874.57	860.95	838.90	832.42	824.32	810.23	788.61
3L (μm)	773.11	769.44	732.11	726.67	718.97	709.77	690.98
4L (μm)[1]							
Avg (μm)	875.06	866.58	836.04	833.23	825.85	814.62	797.33
Avg (in.)	0.03445	0.03412	0.03292	0.03280	0.03251	0.03207	0.03139

1 – Probe 4L showed erratic readings for some measurements and has been omitted from the data and calculations.

Table 26. Probe Averaged Tip Clearance Measurements, Mid-Chord

Probe Number	500 RPM	3000 RPM	12000 RPM	21000 RPM	24000 RPM	25500 RPM	27000 RPM
1M (μm)	780.21	765.77	714.39	672.59	676.02	672.98	655.48
2M (μm)	807.87	814.20	778.06	736.68	743.30	728.42	708.58
3M (μm)	847.42	840.51	790.52	745.16	747.16	740.36	721.60
4M (μm)	723.41	701.74	650.20	605.05	595.44	596.26	581.88
Avg (μm)	789.72	780.55	733.29	689.87	690.48	684.50	666.88
Avg (in.)	0.03109	0.03073	0.02887	0.02716	0.02718	0.02694	0.02626

Table 27. Probe Averaged Tip Clearance Measurements, Trailing Edge

Probe Number	500 RPM	3000 RPM	12000 RPM	21000 RPM	24000 RPM	25500 RPM	27000 RPM
1T (μm)	680.25	665.92	608.52	547.24	533.44	519.08	490.18
2T (μm)	731.32	745.98	706.53	647.43	640.35	622.58	587.81
3T (μm)[1]							
4T (μm)	713.83	693.59	641.41	582.87	565.39	554.59	519.61
Avg (μm)	708.47	701.84	652.15	592.51	579.73	565.42	532.53
Avg (in.)	0.02789	0.02763	0.02568	0.02333	0.02282	0.02226	0.02097

1 – Probe 3T showed erratic readings for some measurements and has been omitted from the data and calculations.

Table 28. Average Growth of Leading Edge, Mid-Chord, and Trailing Edge

RPM Range	500 – 3000 RPM	3000 – 12000 RPM	12000 – 21000 RPM	21000 – 24000 RPM	24000 – 25500 RPM	25500 – 27000 RPM	Total
Leading Edge (in.)	4.92E-05	0.000395	0.001642	0.001757	0.002058	0.002516	0.003222
Mid-Chord (in.)	9.78E-05	0.000472	0.002401	0.004174	0.004149	0.004392	0.005112
Trailing Edge (in.)	6.01E-05	0.000331	0.002359	0.004793	0.005315	0.005899	0.007241

Table 29. Simulated Growth of Leading Edge, Mid-Chord, and Trailing Edge

RPM Range	500 – 3000 RPM	3000 – 12000 RPM	12000 – 21000 RPM	21000 – 24000 RPM	24000 – 25500 RPM	25500 – 27000 RPM	Total
Leading Edge (in.)	0	0	0.0005	0.0014	0.0019	0.0021	0.0024
Mid-Chord (in.)	0	0.0001	0.0013	0.0039	0.0051	0.0057	0.0064
Trailing Edge (in.)	0	0.0001	0.0021	0.0066	0.0086	0.0097	0.0108
Trailing Edge Adjusted (in.)[1]	0	0.0001	0.0018	0.0056	0.0073	0.0083	0.0092

1 – Trailing edge is adjusted for probe position by a scaling factor of 0.853.

THIS PAGE INTENTIONALLY LEFT BLANK

APPENDIX C. BENCHTOP CALIBRATION AND TESTING RIG DESIGN AND SPECIFICATIONS

A brief description of the motivation and process leading up to the creation of the Benchtop Calibration and Testing Rig (BCTR) is discussed in this appendix. The design and specification of the components of the BCTR are described in detail.

A. MOTIVATION

The capacitive probes were delivered to the TPL previously calibrated by Rotadata, Ltd. The calibration blisk Rotadata fabricated and used is not representative of the full geometry of the NPSMF and did not have the same background noise present in the Turbo Propulsion Laboratory (TPL). This is a point of contention since the capacitive probes are highly susceptible to background noise and will create a different signal. Furthermore, the capacitive probes are designed to be installed in electrical contact with an aluminum tip gap casing. It is unknown if Rotadata conducted the calibration with the probes electrically insulated and this needed to be tested prior to start the tip gap casing fabrication process. Additionally, it was estimated that the tip gap casing would take several months to manufacture. Therefore, a mock casing was required to test if the probes could operate properly with their outer sheaths in electrical contact with one another and the casing and to start developing calibration methods and troubleshoot any issues during the months of wait time.

This also opened an opportunity to determine whether an aluminum 3D printed mock casing could be an acceptable substitute for a much larger casing. By using a BCTR, independent of the TCR, calibration could be conducted at a much faster rate as it involved only one operator and has less equipment required for operation. Finally, identification of any potential issues with the probes or post-processing methods could be determined in advance of tip clearance measurements on the TCR. For all these reasons, a separate calibration rig was created to calibrate the probes for use in the TCR and create the methods developed in Chapter III.

B. DESIGN REQUIREMENTS AND CONSTRAINTS

An aluminum mock casing was required to mount the probes in to mimic the aluminum tip gap casing. There would need to be 3 positions to monitor the leading edge, mid-chord, and trailing edge locations of the NPSMF's blade tips. Furthermore, operation of the capacitive probes required the rotor to be constantly spinning to create a voltage reading. Therefore, a rotor shaft accompanied with bearings, a housing assembly, and a means to rotate the rotor were required to create the rotary motion.

The TCR also uses a tachometer to produce an OPR signal and so the BCTR would need this as well to synchronize the raw data and develop a proper post-process method that applied to both the TCR and BCTR. Testing on the BCTR did not require high speeds, therefore a cost-effective, compact design would be achievable. For calibration, a means of moving the probe back and forth was needed to move the mock casing forward and backward radially from the rotor to either decrease or increase the tip clearance, respectively, in the order of micrometer. Therefore, a translation stage with adequate precision was required.

C. DEVELOPMENT OF CURRENT DESIGN

A previous design considered a horizontal shaft like the TCR. However, this was determined unfavorable as this design required multiple bearings to counteract the moment arm due to the weight of the rotor. A more simplistic vertical shaft design was then desired as it provided a more compact structure and the effects of moment arms would be a fraction of what they would be as compared to a horizontal shaft. Originally, the mock casing used to mount the capacitance probes was to be a quarter cut out of the whole casing so multiple probes could be mounted at the same time, though due to the weight requirement of the aluminum 3D printer, 2 pounds, this couldn't be done and was later changed to be only a 3 inch cut out.

The prime mover for the vertical shaft design was originally a repurposed AMT 369E-97 water pump motor that was vertically mounted under a baseplate. The bearings within the casing of the motor were used to account for any moment arms developed as the rotor spun. This provided an answer the requirement of rotational movement with limited

designing required. To provide variability in speed, a Frenic variable frequency drive was used. The pump motor was wired in its low-speed configuration. This initial rig is shown in Figure 87.

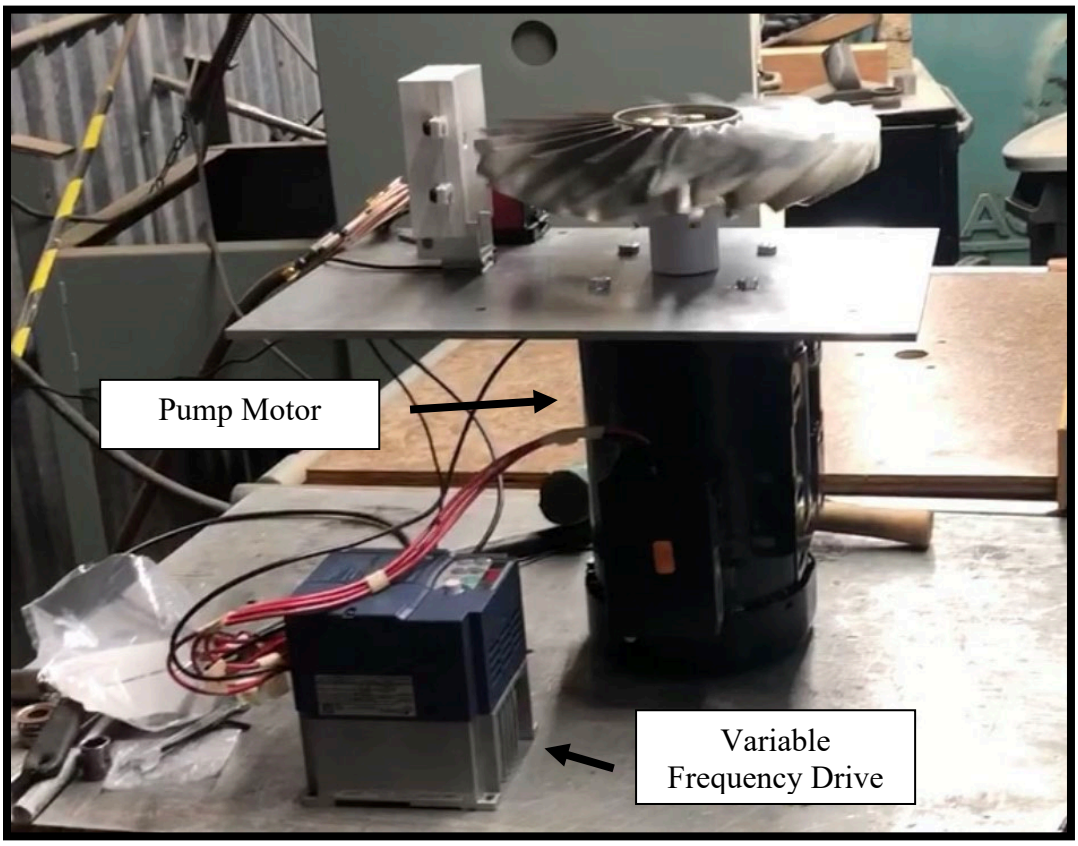

Figure 87. Initial BCTR Design with Pump Motor and Variable Frequency Drive.

This design proved ineffective as it was found the capacitive probes experienced excessive interference generated by the motor windings. The magnetic field of the motor causes significant distortion to the probe's output signal, as shown in Figure 88. The figure shows two probe outputs. The upper signal is from a probe mounted in an aluminum casing without electrical insulation, and a second probe that was held in place with insulation. The top graph shows that the interference picked up by the casing adversely affects probe performance. Insulating the probe reduces the noise, but the probe itself still is unacceptably affected.

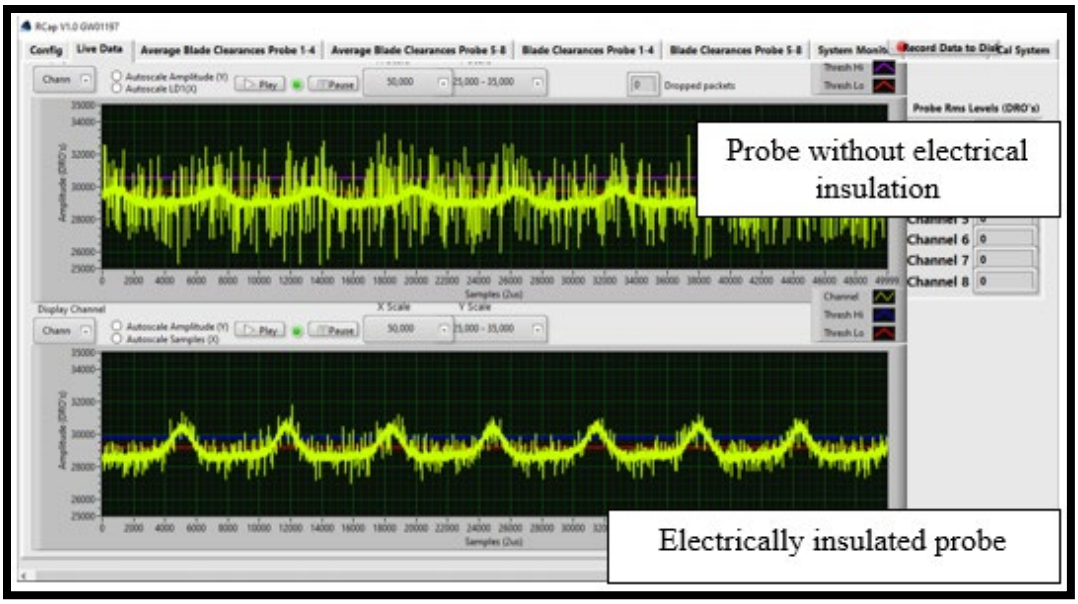

Figure 88. Excessive Noise from Pump Motor as Prime Mover.

It was then found residual voltage existed in the casing even when no power was applied, still causing unacceptable amounts of interference. It is advised that users move the rotor blade by other means, such as via a pneumatic motor as stated by Sheard et al. [14] who used an air motor for their calibration spin rig. The motor and variable frequency drive were therefore replaced with a polycarbonate shaft and housing driven by pneumatic means.

After the creation and use of the BCTR with the mock casing, a second calibration was proposed using the actual tip gap casing on the BCTR to validate the use of 3D printed mock casings. This led to augmenting the original design with a larger translation stage and power turbine to drive the fan. The two versions of the rig are referenced as the BCTR (mock casing) and BCTR (tip gap casing). The BCTR (mock casing) components are described in detail in the following section. The changes and replaced components are described in detail in the section after.

D. BTC MEASUREMENT SYSTEM SPECIFICATIONS

1. Capacitive Probe

The capacitive probes used were the Rotadata, Ltd. MS1743 4 mm (0.157") low temperature probe. The dimensions are given in Figure 88. The probe has a max operating temperature of 180 °C (356 ºF) and its wire connector's max operating temperature is 160 °C (320 ºF). The probe inner electrode face is 4 mm (0.157"), and the maximum diameter of the assembly is 14 mm (0.551"). The outer sheath around the electrode is 10 mm (0.394") in diameter. The mounting port of the casing matches this 10 mm (0.394") diameter. The probe has a 1 m (3.3 ft) long wire that terminates in a connector. A 7.5 m (24.6 ft) wire connects this terminal to the data acquisition.

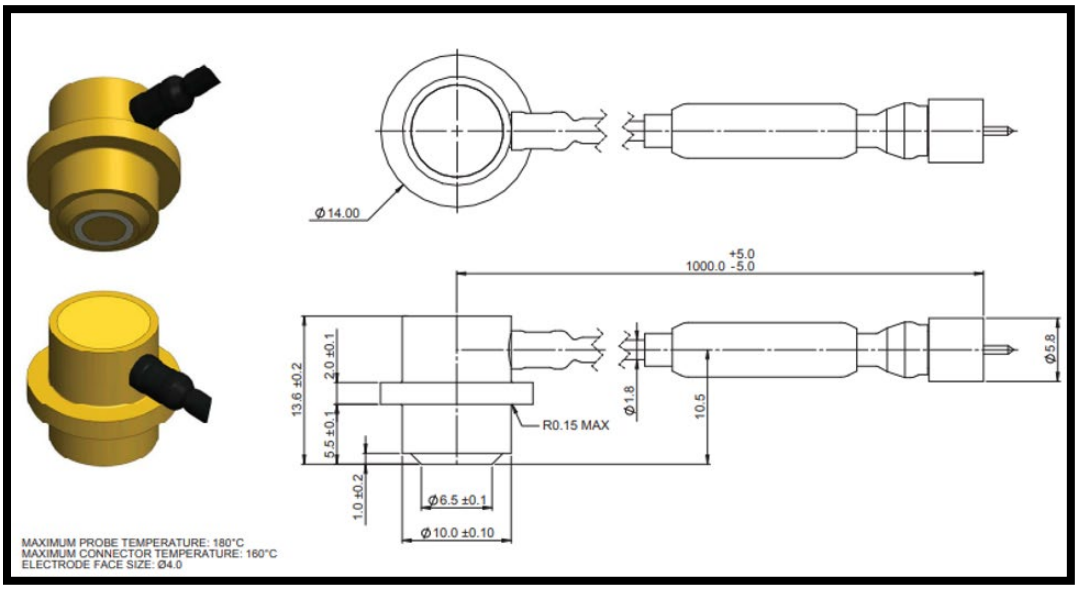

Figure 89. Capacitive Probe Dimensions (Units in mm). Source: [29].

2. Data Acquisition

Table 30 provides specifications for the National Instruments cRIO DAS used in the experiment. The RCap V manual [22] specifies which ports are not utilized in their system. The manual also specifies the IP address required to connect to the RCap V software. The data acquisition connects to a 120 VAC to 24 VDC power source shown in

Figure 89. The power source connects into the power input port of the data acquisition. The ground connection stud is located next to this power input port (annotated in figure). The BCTR casing is grounded to this stud.

Table 30. cRIO – 9042 DAQ Specifications. Source: [22], [23].

Function	Spec	Comment
Number of measurement channels	8	Automatically configured gain and filter settings
Derived OPR/key phasor	Various options	Software can be configured to utilize measurement channel as OPR. Alternatively, OPR can be derived from blade measurements. Dedicated single input highly recommended. Conditioning units can be integrated.
Sample rate	500 kHz	Simultaneous sampling
Measurement bandwidth	Up to 1.2 MHz	Dependent on optimum probe technology and signal conditioning
Temperature rating	5-60ºC	Automatic temperature compensation
Power supply	9 -30VDC	24 VDC 100 W recommended
Local interface		NA control and data storage required on separate PC. Pre-configured with RCAP DAQ and control software.
Local data storage		Required external to DAQ
Networked interface		Gigabit ethernet
Dimension	220x150x90	W x D x H (mm)

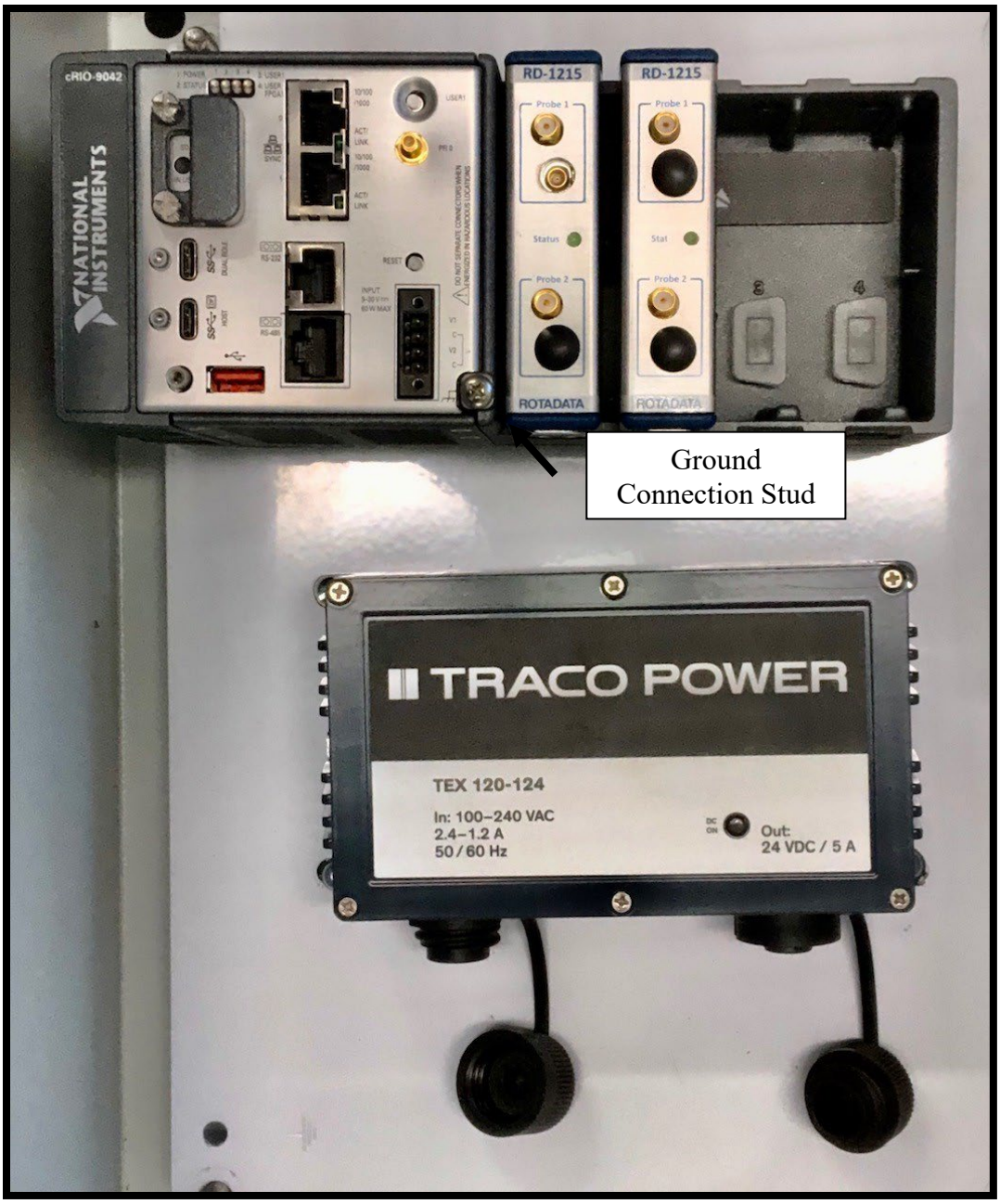

Figure 90. Data Acquisition and Power Source.

E. BCTR (MOCK CASING) COMPONENT DESCRIPTION

An overall view of the BCTR (mock casing) with annotated labels is provided in Figure 91. A zoomed view of the mock casing showing the front face of the probe is also provided in the figure.

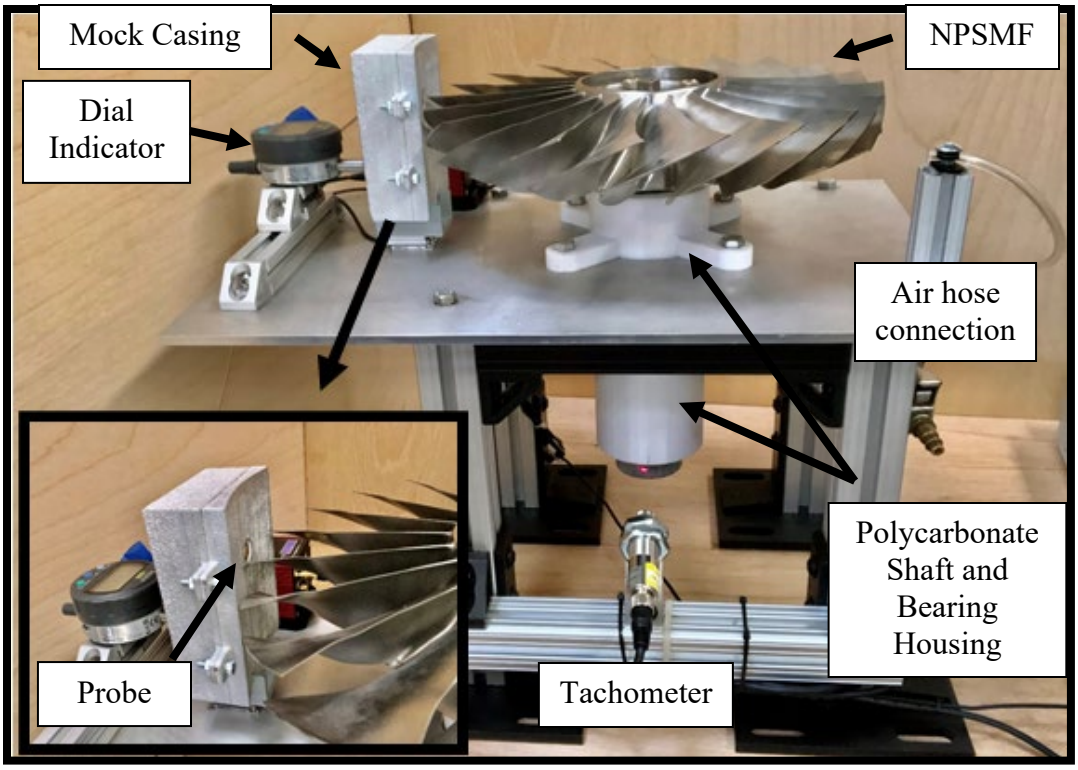

Figure 91. BCTR (Mock Casing).

1. Base Structural Material

The base structure, Figure 92, of the BCTR consists of an aluminum base plate, legs, and stretcher supports. The base plate dimensions are: 304.8 mm x 457.2 mm x 6.35 mm (12" x 18" x ¼"). Aluminum was chosen as it provided a lightweight base with the structural strength to hold a suspended electrical motor that previously drove the NPSMF (although the electrical motor was then replaced). Aluminum was also chosen for ease in drilling holes for mounting the various components of the BCTR since it is not as strong as steel. 80/20 15 series beams and their accessories are used as legs and stretchers to hold up the plate. An 88.9 mm (3.5") diameter hole is cutout of the base plate for insertion of the bearing housing. Holes for M8 (5/16") screws are cutout for the bearing housing fasteners and leg fasteners. The 80/20 legs were tapped with an M8 (5/16") thread for these screws.

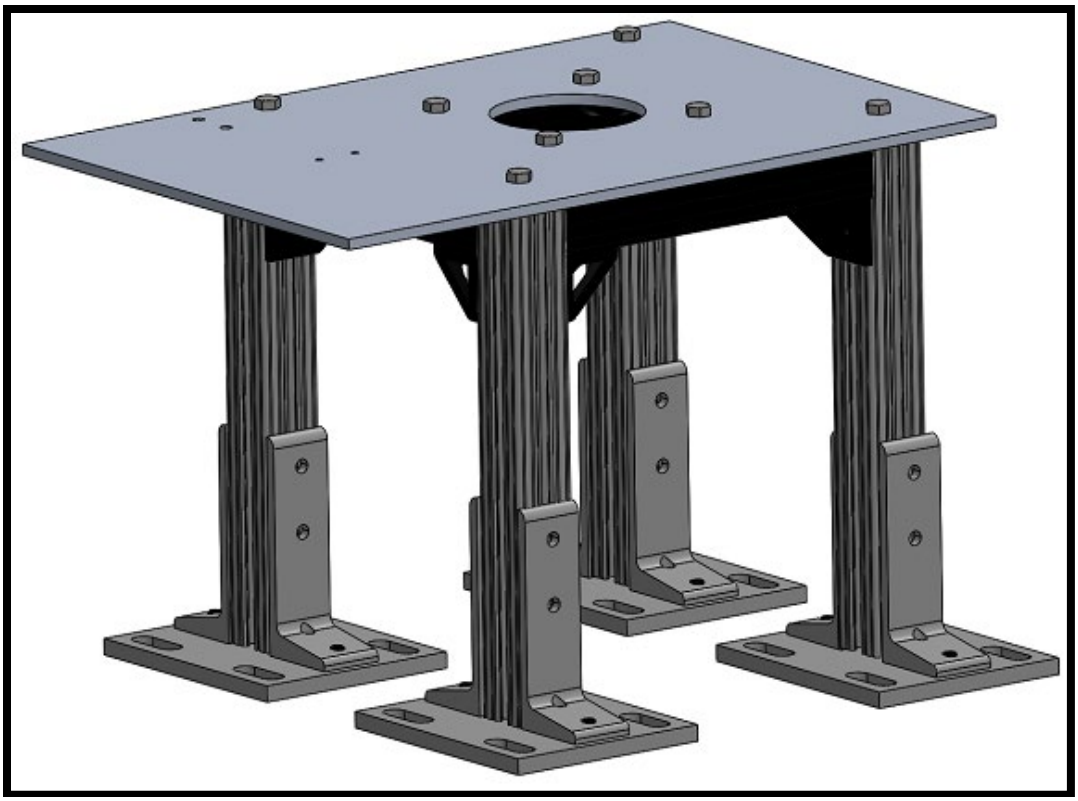

Figure 92. Base Structure of the BCTR.

2. Mock Casing

The BCTR (mock casing) uses alloy 4008 aluminum 3D printed mock casings. They were created using a Xerox ElemX printer. The printer prints by jetting molten aluminum droplets onto a base plate. They represent a 76.2 mm (3") cutout of the tip gap casing. Overhang limitations of the printer called for printing the mock casings in two separate pieces that are then bolted together. A wire guide is cutout for the probe's wire just like the tip gap casing. A SolidWorks rendering of this is shown in Figure 93.

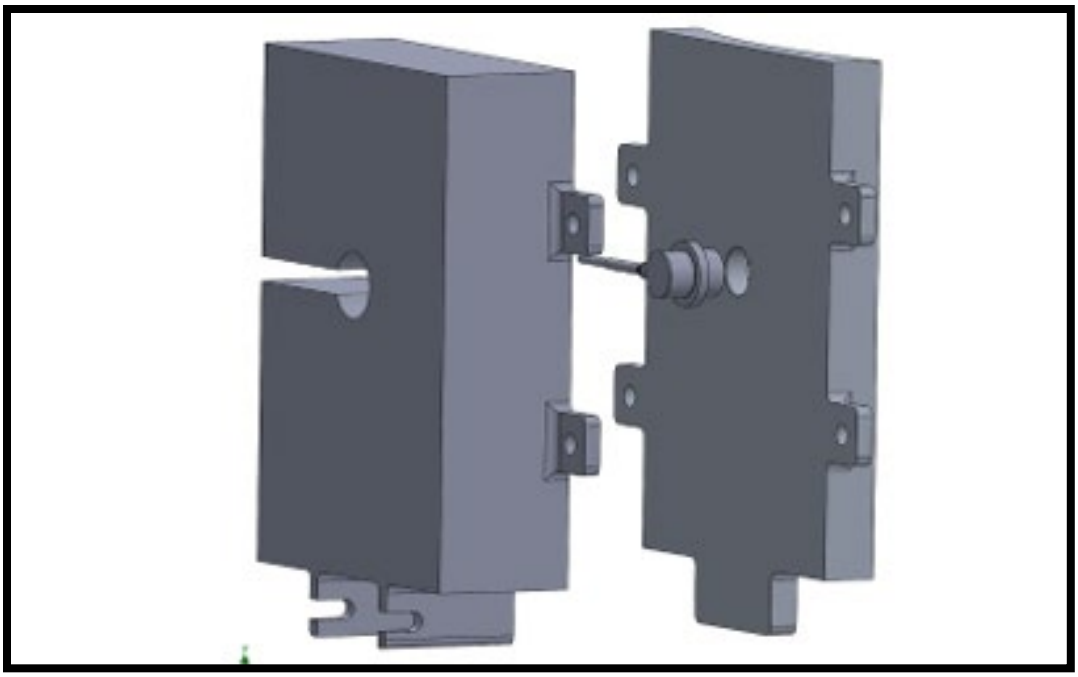

Figure 93. Mock Casing 3D Modeled.

The rear piece of the mock casing has a 15.875 mm (5/8") hole that was tapped with M20 x 2.5 (¾" -10) threads post-print. Figure 93 shows the rectangular cutout used on the rear piece to serve as the wire guide. The front piece has a 10 mm (0.393") diameter hole for the front face of the capacitive probe. The thickness of the front piece is such that when the probe is installed, the front face of the probe is flush with the front, curved face of the front part of the mock casing. The probe's 14 mm (0.5512") shoulder rests on the front piece. To hold the probe in place, two M20 x 2.5 (3/4" -10) nylon screws are fastened behind the probe. The geometry of the bottom of the front and back pieces are made to be inserted into a plastic gripping mount that fastens to the translation stage. The oval cutout of the connecting interface is sized for a M3 (4-40) screw to hold the casing to the plastic casing grips. Four M4 (8–32) screws and nuts are used to fasten the two pieces together. When mounted onto the BCTR, a grounding strap ring terminal is attached to one of the M4 (8–32) fasteners to discharge any charge built up during operation. The ground strap is connected to the DAS ground stud (Figure 91) to ensure the probe and casing share a common ground.

The 3D printer's jetted droplets create a rough surface texture when the prints were finished. This caused the front face of the capacitive probe to not be flush with the front face of the mock casing. The curved face of the front piece was sanded to smooth the surface as a result. 3 mock casings were printed, Figure 94, overall to install the probe in its 3 monitoring locations: the leading edge, mid-chord, and trailing edge (right to left in figure).

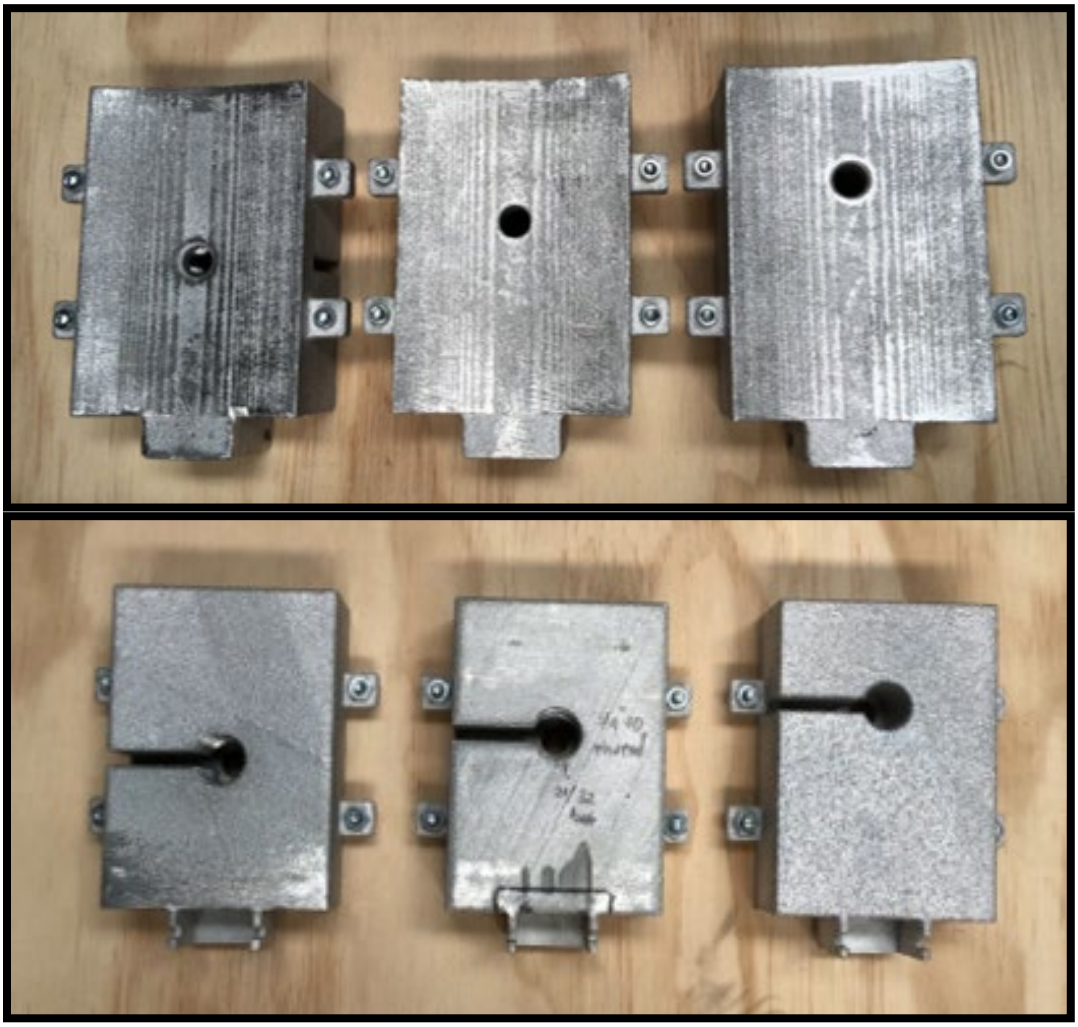

Figure 94. 3D Printed Aluminum Mock Casings.

3. Shaft and Bearing Housing Assembly

The NPSMF rotational motion was supported by a shaft and bearing housing assembly. For reference, the entire shaft and bearing housing assembly is shown in an exploded view in Figure 95 with annotations.

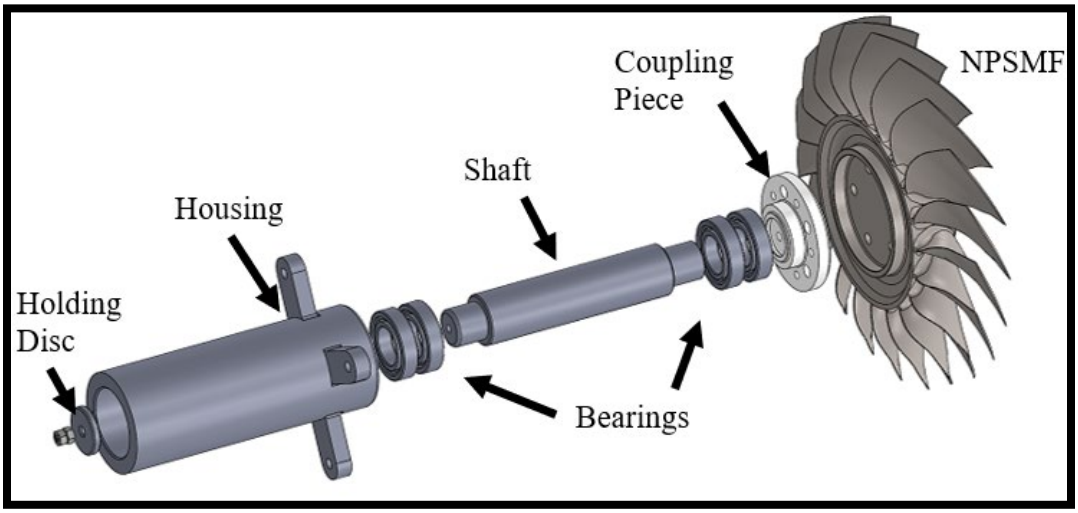

Figure 95. Exploded View of Shaft and Bearing House Assembly.

To connect the NPSMF to the shaft, a coupling device was used, Figure 96. The geometry is such that it forms an interference fit with the NPSMF's bottom recess fitting (refer to Figure 95).

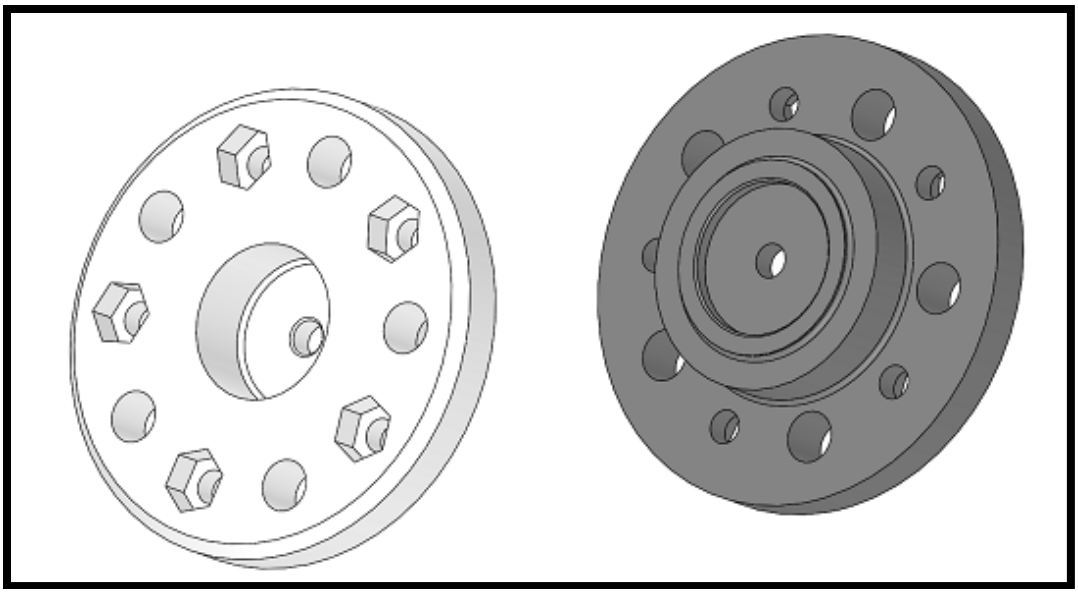

Figure 96. Top View (left) and Bottom View (right) of NPSMF to Shaft Coupling Piece.

The coupler is 3D printed out of polycarbonate. 5 holes are provided for the M8 x 1.25 (5/16") screws that hold the coupler together to the NPSMF. 5 M6 x 1 (¼"-20) hexagonal nut cutouts and M6 (¼") holes are present. The hex nuts are installed between the NPSMF and coupler in these recesses and remain in place during operation. When the coupler and NPSMF are to be separated, an M6 (¼") screw is used with these nuts to carefully separate the NPSMF from the couple in a circular pattern.

The shaft is 3D printed polycarbonate. As shown in Figure 97, the shaft has different diameters to account for the bearings. Both ends of the shaft are 29.972 mm (1.18") in diameter and are inserted into the bore of the bearings as an interference fit. An interference of 25.4 μm (0.001") by diameter was used. The larger, middle part of the shaft is 40.64 mm (1.6") in diameter and is larger than the inner bearing ring outer diameter, but less than the outer ring of the bearings. This ensures the shaft rotates with the inner ring while the outer ring remains stationary with the housing. The middle of the shaft has a minimum clearance of 6.35 mm (0.25") from the inner wall of the bearing housing. A 6.858 mm (0.27") hole runs down the middle of the shaft for the holding screw.

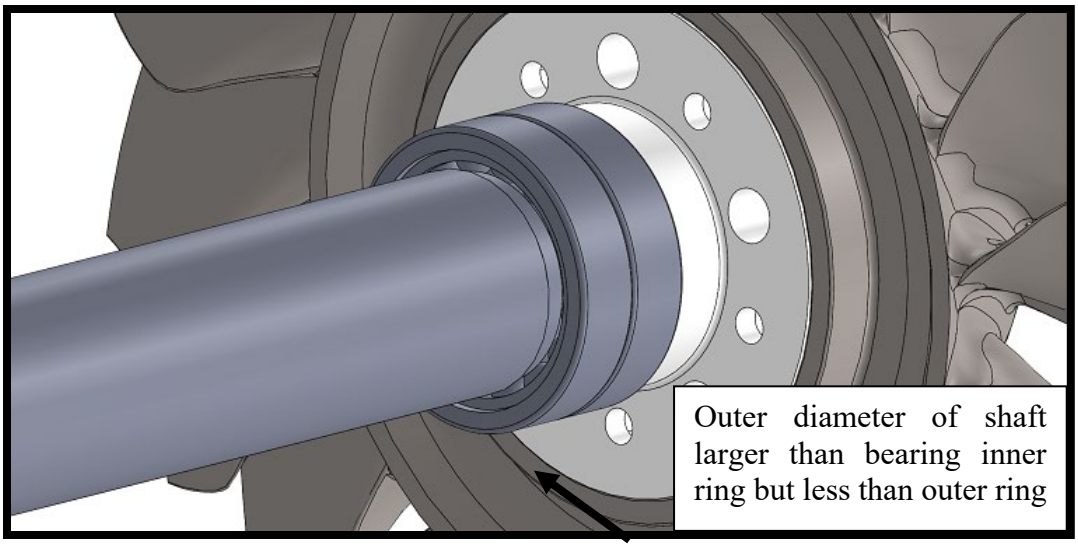

Figure 97. Rotor Shaft Insertion to Angular Contact Bearings.

The bearings used are GMN HY SM 6006 high precision angular contact ball bearings and are shown in Figure 98. The relevant specifications are provided in Table 31. The outer diameter of the bearings is made to make an interference fit with the bearing housing's inner diameter to provide pre-loading and secure the bearing in place. A pair of bearings are installed in both the top and bottom of the shaft. They are orientated such that they can support axial load in either vertical direction. The vertical separation of each pair of bearings allows for the bearings to support moments developed by the rotating shaft during operation.

Figure 98. GMN angular contact ball bearings

Table 31. GMN HY SM 6006 Ball Bearing Relevant Specifications. Source [30].

Parameter	Specification
Bore Diameter	30 mm (1.1811")
Outer Diameter	55 mm (2.165")
Bearing Width	13 mm (0.5118")
Dynamic Radial Load Rating	11,900 N (2675 lbf)
Static Radial Load Rating	4550 N (1023 lbf)
RPM Rating	58750 RPM
Light Pre-Load	60 N (13.5 lbf)

The bearing and shaft housing interference fits with the outer ring of the bearings. The diameters interfere by 25.4 μm (0.001"). Approximately an inch below the top of the bearing housing is a shoulder that protrudes inward 3.9878 mm (0.157") provides a stopping point for the bearing. A shoulder is not provided for the bottom pair of bearings. Below the bearing housing is a support disc whose diameter is larger than the outer diameter of the bearing inner ring. This rotates along with the shaft and serves as an end piece to hold the shaft together. Running along the axis of the rotor is a M6 x 1 (1/4”-20) headless screw. Two nuts are secured on either side of the assembly ends to hold the assembly together. The

additional nut on either side ensures that the nuts do not loosen during operation. A cross-sectional diagram of the assembly is provided in Figure 99.

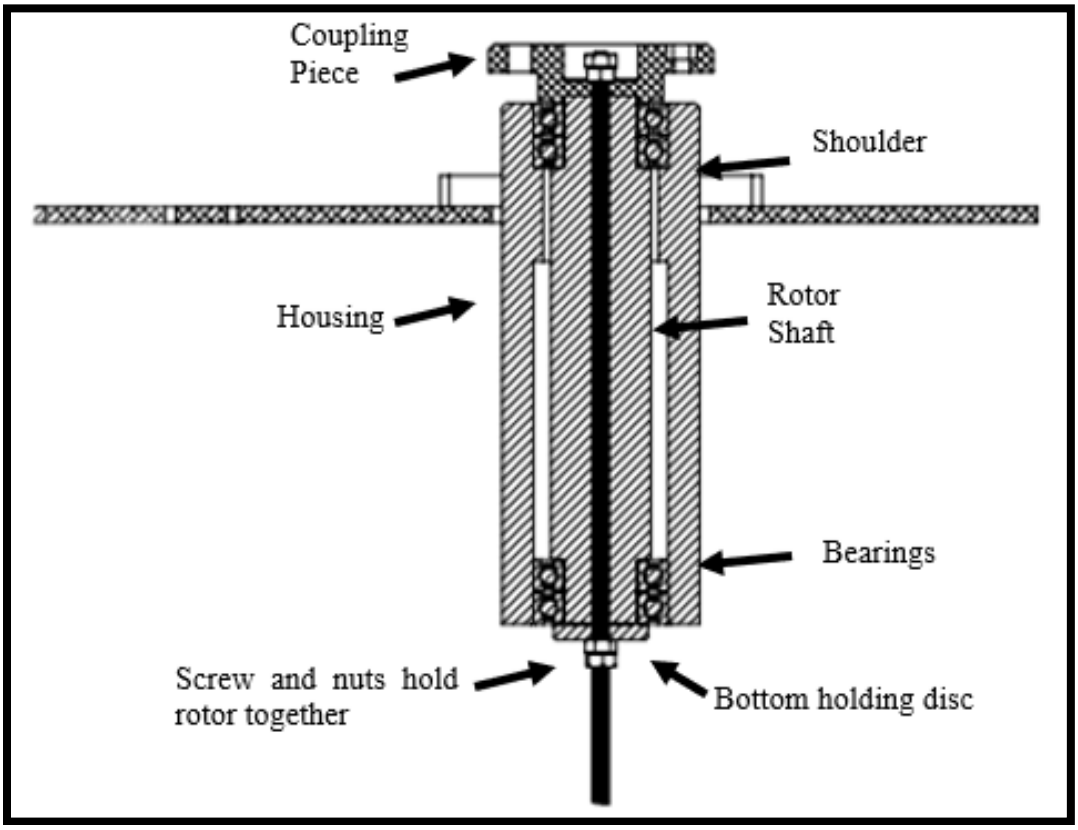

Figure 99. Cross-Sectional View of Bearing Housing Assembly.

4. Translation Stage

A Thor Labs PD1 piezo driven translation stage was used to traverse the casing forward and back to each of the probe's calibration points. The stage can be positioned via open or closed loop operation, commanded remotely via software or manually by a local control panel on its KIM001 motor controller. The stage is positioned to move the mock casing radially from the rotor's center. Total travel length is 20 mm (0.787"), though only up to 3.5 mm (0.1378") is needed for calibration. Typical step size is 1 μm (0.0000394") with 20% variability based on environment conditions. To account for the variability, distance is measured with the electronic dial indicator. An optical encoder is not available for the PD1 model used. A list of relevant specifications is provided in Table 32.

Table 32. Thor Labs PD1 Translation Stage Relevant Specifications

Parameter	Specification
Travel length	20 mm
Step size	Typical: 1 μm (0.00003937") Max: <3 μm (0.000118”)
Speed (continuous steps)	Up to 3 mm/s (0.000118"/s)
Horizontal capacity	3 kg (6.61 lbs)
Vertical load capacity	100g (3.5 oz)
Motor type	Piezo electric motor drive
Dimensions	32.5 mm x 32.0 mm x 11.5 mm (1.280" x 1.260" x 0.453")

M2.5 (3-56) or M4 (8–32) mounting screws can be used to mount the mock casing onto the mounting plate. The casing is coupled to the translation stage’s carriage via a plastic mount that grips onto the bottom of the casing. Two M4 (8–32) screws and accompanying nuts were used to fasten the plastic casing grip to the bottom of the mock casing. Figure 100 shows how the translation stage, casing grip mount, and mock casing connect with an exploded view Solid model rendering. The oval shaped cutouts out of the inserted portion of the mock casing and the oval shaped cutouts of the plastic mount create a hole for an M4 (8–32) screw to fit and fasten the two parts together.

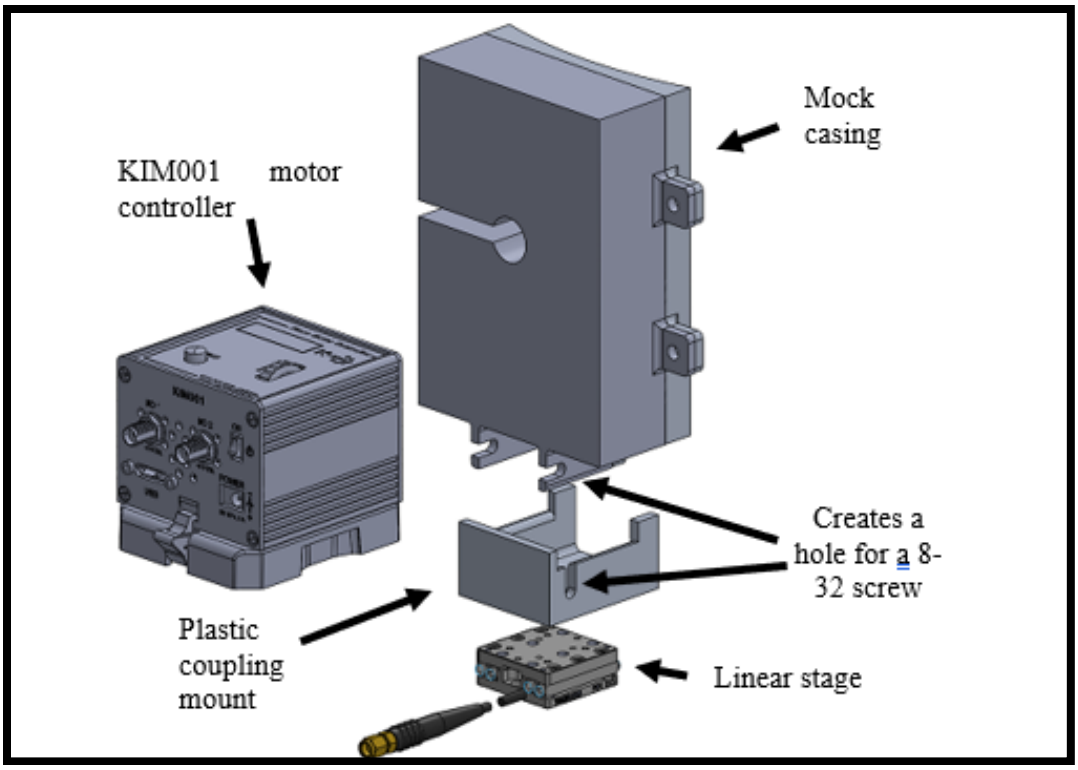

Figure 100. Exploded View of Translation Stage, Casing Grip Mount, and Mock Casing.

Thor Labs provides remote operation of the stage by use of their software, Kinesis. The software provides the ability to set the stage speed, set step size, command to a location via closed loop or open loop, and to jog forward and back. Figure 101 provides a graphic of the software's user interface. Although the user interface provides a distance readout, this was not used. It was found the actual movement of the stage did not match what was displayed on the screen.

Figure 101. User Interface of the Kinesis Software.

5. Air Hose

The air is supplied by the Turbo Propulsion Laboratory's 100 psi shop air system. The air hose nozzle terminates in a flexible hose held in place by 80/20 parts as shown previously in Figure 91. The hose is pointed to blow air directly onto the rotor blades. During operation rotor speed is controlled by throttling the air cutout valve.

6. Electronic Dial Indicator

Specifications of the dial indicator are provided in Table 33. 80/20 beams are used to secure the dial indicator in place, as shown in previously in Figure 91.

Table 33. Mitutoyo Digital Dial Indicator Specifications. Source: [25].

Parameter	Specification
Model Number	543-392
Range	0 – 12.7mm (0 - .5")
Resolution	0.001 mm or .0005"
Accuracy	+/- 2.54 µm (0.0001")
Measuring Force	< 1.5 N (0.337 lbf)

7. Tachometer

As mentioned, both the TCR and BCTR utilize a Monarch Instrument RLS. It is mounted onto the aluminum structure of the BCTR, perpendicular to the orientation of the rotor shaft. It is mounted onto the apparatus by using 80/20 15 series beams. An "L-shaped"

bracket with two M20 x 1.5 (3/4"-16) nuts hold the sensor in place. A square piece of reflective tape was placed onto a plastic disk under the bearing housing to monitor speed as shown in Figure 102.

Figure 102. Monarch Instruments Rugged Laser Sensor Tachometer.

The terminal of the RLS features four open wires: a voltage in, a common, sensor output, and an unused wire. The unused wire was electrically insulated. The sensor output and ground were connected to a coaxial cable wire with an SMB female terminal to plug into the cRIO-9042 DAQ PFI0 SMB male fitting. The outer wire of the coaxial cable was spliced with the same common as the RLS and the inner coaxial wire was spliced with the sensor output line. The voltage in line of the RLS was connected to a voltage power source. The DAQ PFI0 input port has a limit of 5 V to prevent circuitry damage. Prior to connection to the cRIO-9042 DAQ the signal was verified under the 5 V maximum via oscilloscope for an added safety measure. A simple wiring block diagram of the RLS and coaxial cable is provided in Figure 103. Table 33 provides all the relevant specifications of the tachometer. Figure 104 provides the physical dimensions of the tachometer.

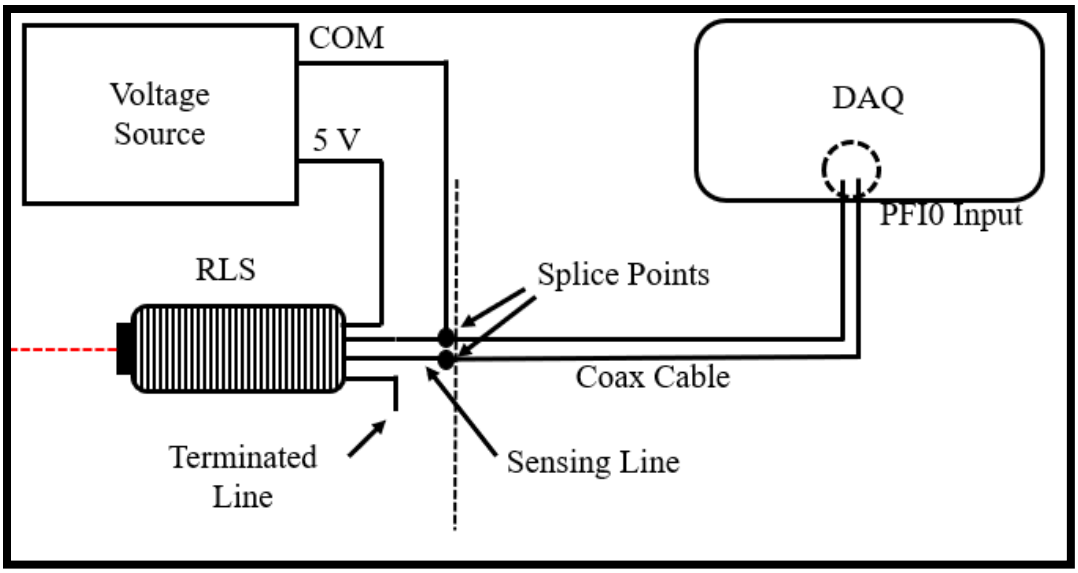

Figure 103. Electrical block diagram of RLS tachometer

Table 34. Rugged Laser Sensor Specifications. Source: [31].

Parameter	Specification
Speed Range	Up to 250,000 RPM
Laser	Class 2
Max Laser Output	1 mW
Pulse Duration	Continuous
Laser Wavelength	650 nm
Operating Range	Up to 25 ft
Max Temperature	50 °C
Max Voltage In	15 VDC

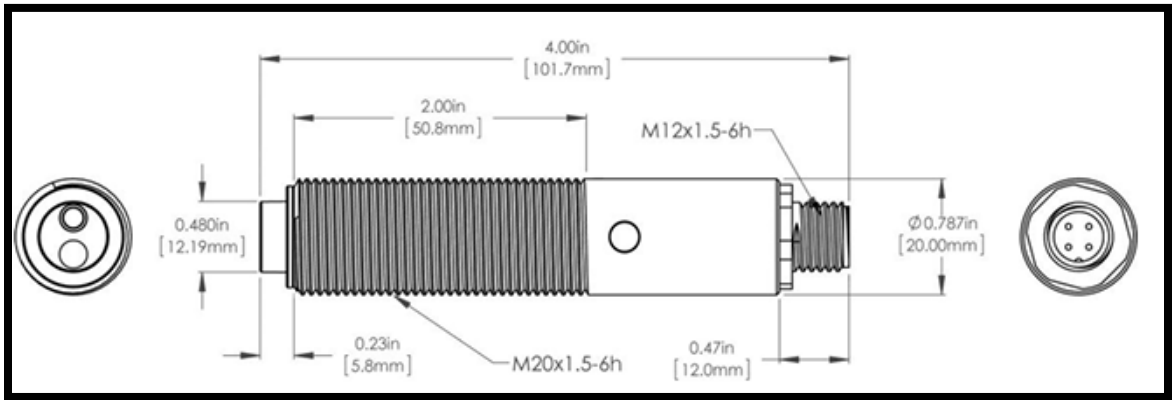

Figure 104. Dimensions of Monarch Instruments. Source: [31].

8. Possible Design Flaws/Issues

A number of design issues have been identified during the experiments. 3D printing the mock casing out of aluminum via material jetting produces a rough exterior affecting the achievable zero tip clearance. Furthermore, when printing, the product tends to be larger in the z-axis than specified with the STL model, making the mock casing slightly thicker than the actual casing. For both these reasons the mock casing's curved face needed to be sanded and smoothed. The imperfections of the rough texture also made fitting into the plastic casing grip mount difficult. Sanding both the mount and mock casing was required to make the fit. In the future, a larger tolerance of fitted pieces is recommended. Furthermore, vibrations from operation of the rotor caused the dial indicator to fluctuate in indication by approximately +/- 0.002 mm, increasing levels of uncertainty.

F. BCTR (TIP GAP CASING) COMPONENT DESCRIPTION

The tip gap casing version of the BCTR was needed to validate the calibration process of the original BCTR's use of 3D printed mock casings. The design built upon the mock casing design's existing parts. Only components that are different or have significantly changed are discussed in this section. Figure 105 provides a SolidWorks rendering of the BCTR (tip gap casing), annotating the new components created to account for the larger translation stage.

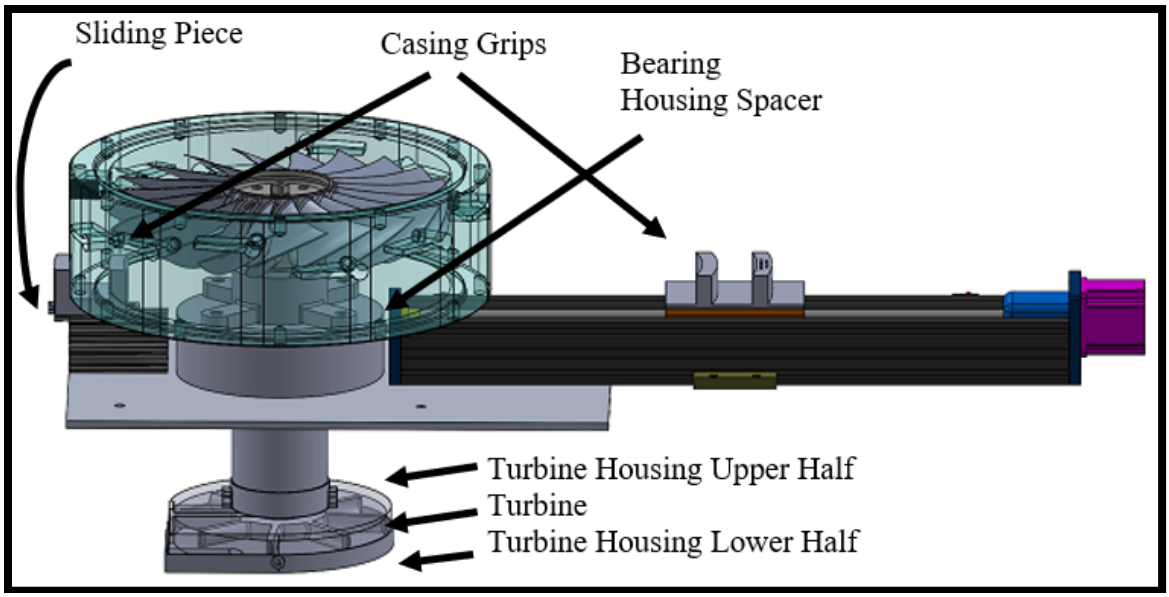

Figure 105. BCTR (Tip Gap Casing).

1. Tip Gap Casing

The tip gap casing replaces the mock casing used in the previous design. Overview of the tip gap casing is described in Chapter IV. The tip gap casing was created in the Halligan Hall machinery shop located at NPS. It is made of aluminum 6061. The dimensions (in inches) of the casing are given in Figures 106 and 107. The threading used to hold the capacitive probes in place are M20 x 2.5 (¾" -10) threads.

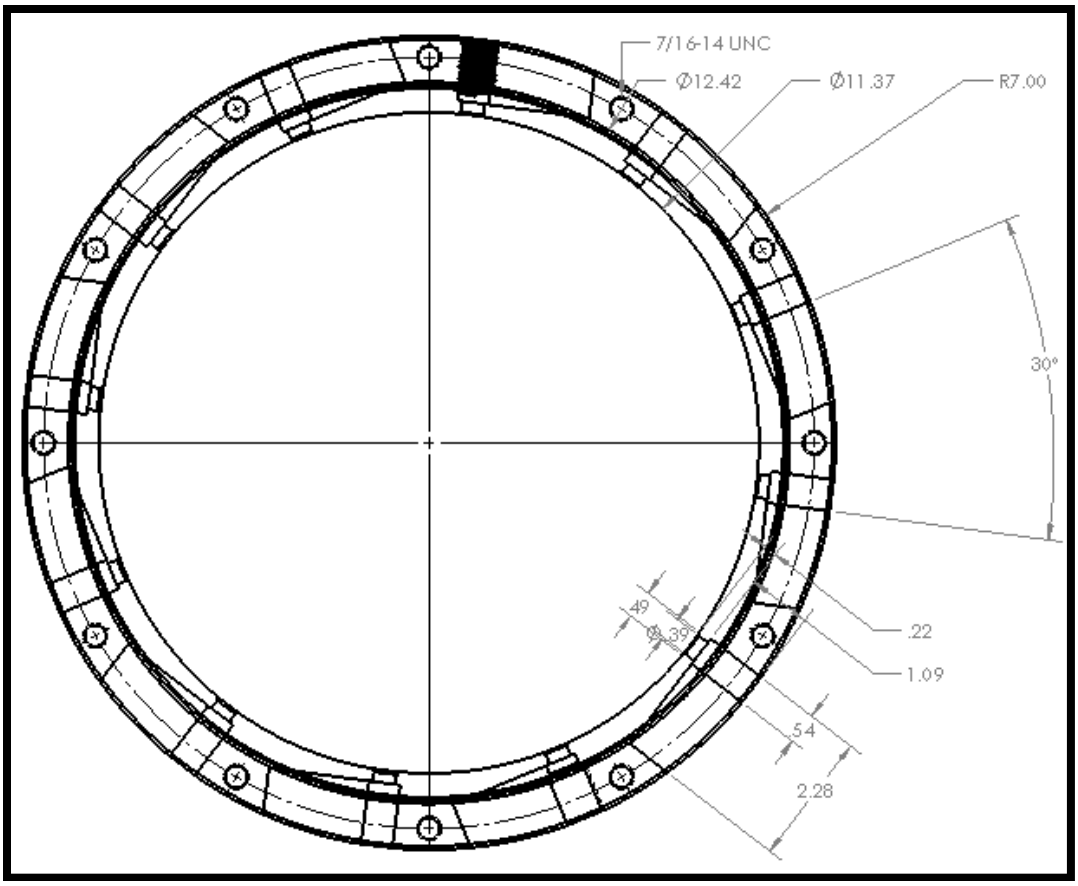

Figure 106. Tip Gap Casing Dimensions, Axial View.

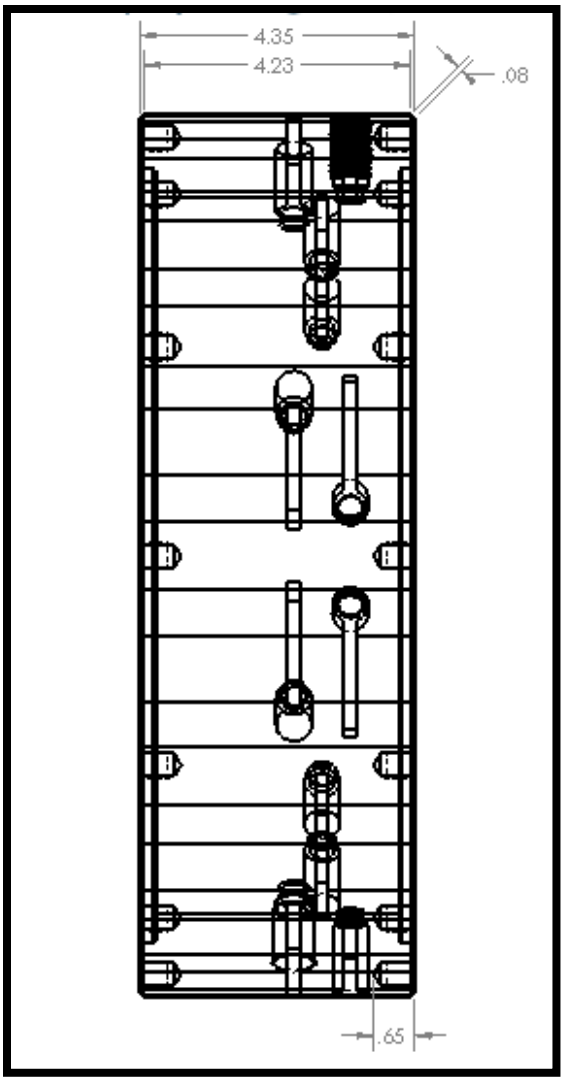

Figure 107. Tip Cap Casing Dimensions, Side View.

2. Velmex BiSlide Translation Stage and VRO Encoder

The translation stage needed to be replaced to account for the larger weight of the tip gap casing. The Thor Labs PD1 stage could only horizontally move objects weighing up to 3kg (6.61 lbs). The tip gap casing weighs approximately 21 lbs. A Velmex stepper motor operated BiSlide was used as a translation stage replacement. The stage operates by moving a mounting carriage via a precision lead screw controlled by a Vexta PK266 stepper motor. The BiSlide is also outfitted with a magnetic linear encoder with an accuracy of 0.025 mm/ 100 mm [26] and a repeatability of 0.01 mm. The encoder resolution is 0.001 μ. The encoder

is repeated to a VRO encoder display. T-slot slides provide mounting brackets to mount the stage onto the base plate. The stage features adjustable carriage limit switches. When the carriage reaches the limit switch, the carriage pushes down a button causing the carriage to stop movement. A serial port from the stage motor controller and from the VRO display enable the user to interface the devices via PC. For this experiment, both the VRO encoder display and the stage were remote controlled using MATLAB. Both serial port configurations are the same. Relevant specifications and serial configurations are provided in Table 35.

Table 35. BiSlide Translation Stage Specifications. Source [26].

Parameter	Specification
Max travel distance	2032 mm (80")
Carriage length	127 mm (5")
Dimensions	76.96 mm x 86.36 mm x 2294.89 mm (3.03" x 3.4" x 90.35")
Load capacity (static or dynamic)	1334.5 N (300 lbf)
Repeatability	5.08 μm (0.0002")
Screw lead accuracy	0.076 mm/25cm (0.003" /10")
Thread pitch	0.1 turns per mm (2.5 turns per inch)
Encoder accuracy	0.02 5mm / 100 mm (0.001"/3.94")
Encoder repeatability	0.01 mm (0.00039")
Encoder read rate	1.6 MHz
Encoder resolution	0.001 mm (0.000039")
Serial bits	8
Serial parity	None
Serial baudrate	9600
Serial stop bits	1

3. Tip Gap Casing Mount Grips and Slide

To couple the tip gap casing to the stage's carriage, a plastic (PLA) 3D printed gripping mount was created. To support the casing on the opposite side from the stage, a second casing grip mount was created in a similar way. A slide was created using 80/20 beams to guide the linear motion of the tip gap casing.

The stage's front casing grip mount is shown in Figure 108. Two 6.848 mm (0.27") holes in are cutout of the front of the coupler for two M6 x 1 (¼"-20) screws to fasten the

mount to the stage carriage. Two washers are used to distribute the pressure on the plastic couple and to prevent damage. The couple features 2 raised edges that follow the same curvature as the tip gap casing. These raised edges are used to clamp onto the casing. A 0.127 mm (0.005") clearance tolerance was given for the fit.

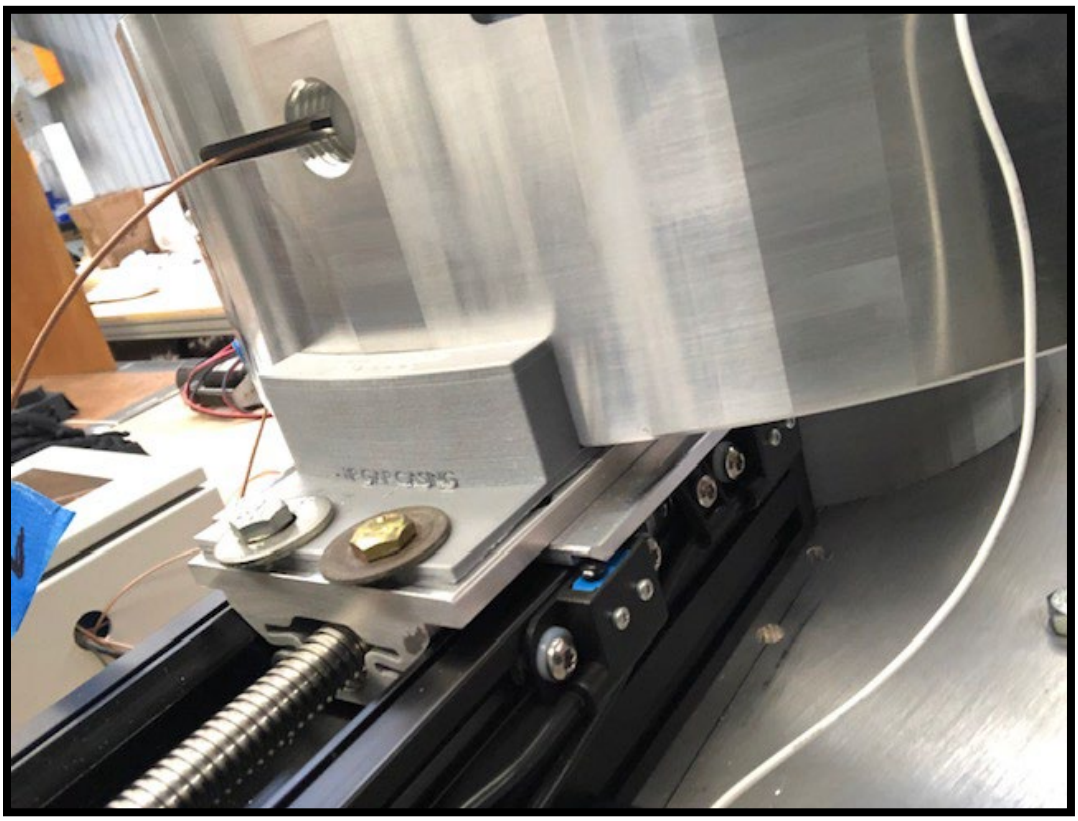

Figure 108. BCTR (Tip Gap Casing) Front Casing Grip Mount.

The rear mount and slide are shown in Figure 109. The rear mount also has the same clamp that hugs along the tip gap casing's width. The mount is fastened together with PLA 3D printed slide. The bottom of the slide is shaped after the pattern of a 10-series 80/20 beam, but with 0.254 mm (0.01") of tolerance. The slide was sanded for smoothness and lubricated for ease of movement. During movement, the slide is slotted along the 80/20 patterned T-slot to maintain alignment during motion. Two 80/20 10-series beams are stacked together to provide the height necessary to keep the casing level with the Velmex BiSlide.

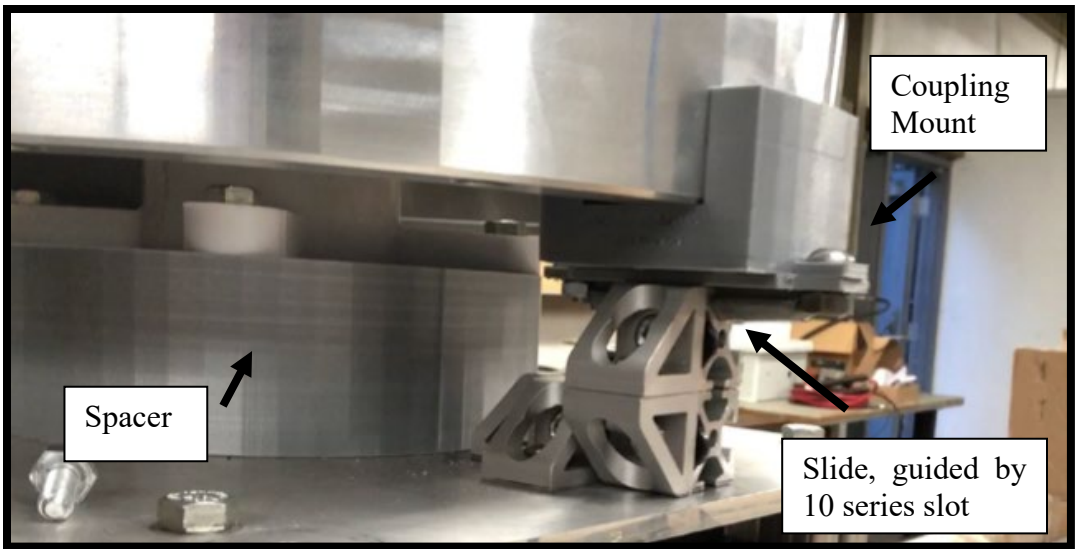

Figure 109. Rear Casing Grip Mount and Slide.

4. Bearing Housing Assembly Spacer

A cylindrical spacer, also shown in Figure 109, was 3D printed out of PLA to raise the bearing housing higher from the base plate to account for the added height provided by the Velmex BiSlide translation stage. The spacer is 52.07 mm (2.05") thick. Four 9.50 mm (0.374") diameter holes were cutout when printing to install eight M8 x 1.25 (5/16”-18) metal threaded inserts to mount on the bearing housing and fasten the spacer onto the base plate using the same holes as previously made. The threaded metal inserts were installed into the spacer by melting the inserts into premade holes using a soldering iron.

5. Power Turbine and Housing

Using the entire casing around the NPSMF removed the ability to effectively apply the driving air onto the rotor blades. Therefore, a separate air driven power turbine was needed to drive the shaft. A 3D printed power turbine and turbine housing were fabricated and installed at the bottom of the bearing housing as shown in Figure 110.

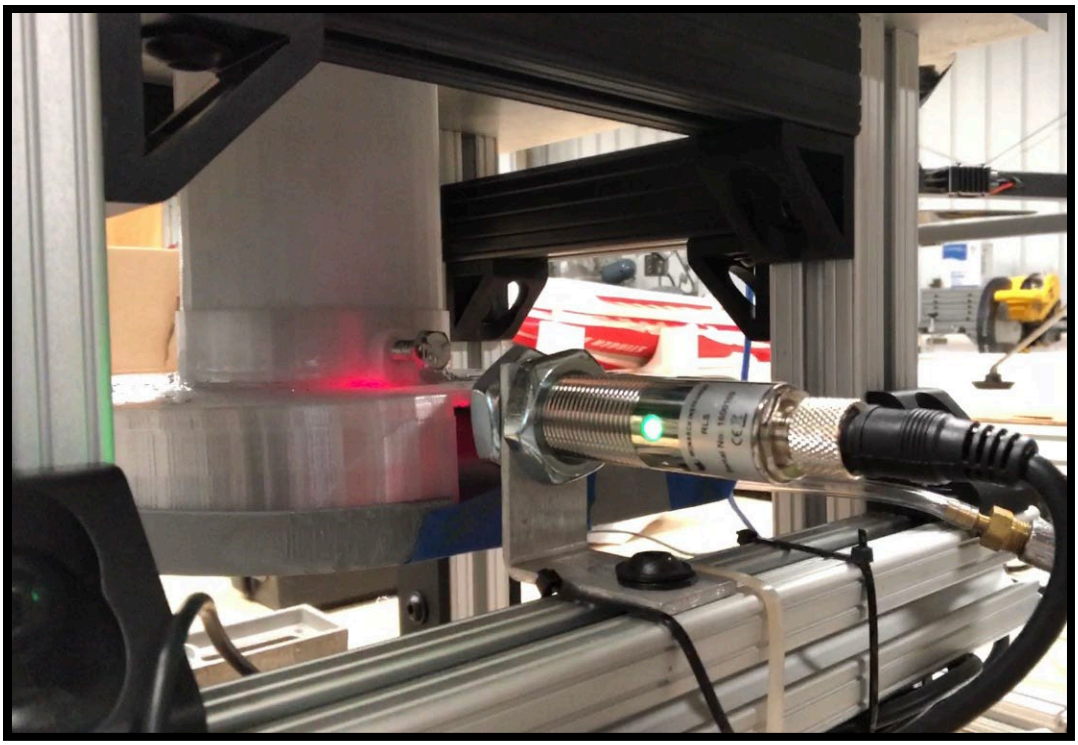

Figure 110. Turbine Assembly Mounted Onto Bottom of Bearing Housing.

The top half of the turbine is printed out of transparent PETG. The top of the upper housing has a sleeve that fits onto the outer wall of the bearing housing. M6 x 1 (¼" -20) screws are used as set screws to hold the bearing housing into place. The bottom half of the housing is made of PLA and snugly slides onto the upper half of the housing. M6 x 1 (¼" -20) screws are also used the hold the bottom and top half together. The upper housing contains a port for the flexible air hose to be inserted into. The port directs the air onto near the turbine tips for maximum torque. A viewing window is cut out for the laser tachometer to measure RPM. The bottom holding disc of the bearing housing assembly has the reflective tape used for measuring RPM. The viewing window also serves as the outlet for the air driving the turbine.

The power turbine is made of PLA. It is a 12.7 mm (½") thick disc with 8 blades. The blade shape is a simple cupped u-shaped profile. The blade to disc joint is fileted to remove sharp corners that could cause stress concentration points. A 6.35 mm (¼") hole is cut through the middle of the disc to mount onto the bottom of the shaft's holding screw. A hex

shaped key is cut from the middle to key onto the hex nut located at the bottom of the bearing housing assembly. Washers are used to provide adequate spacing of the power turbine from the top of the housing. The turbine is shown in Figure 111.

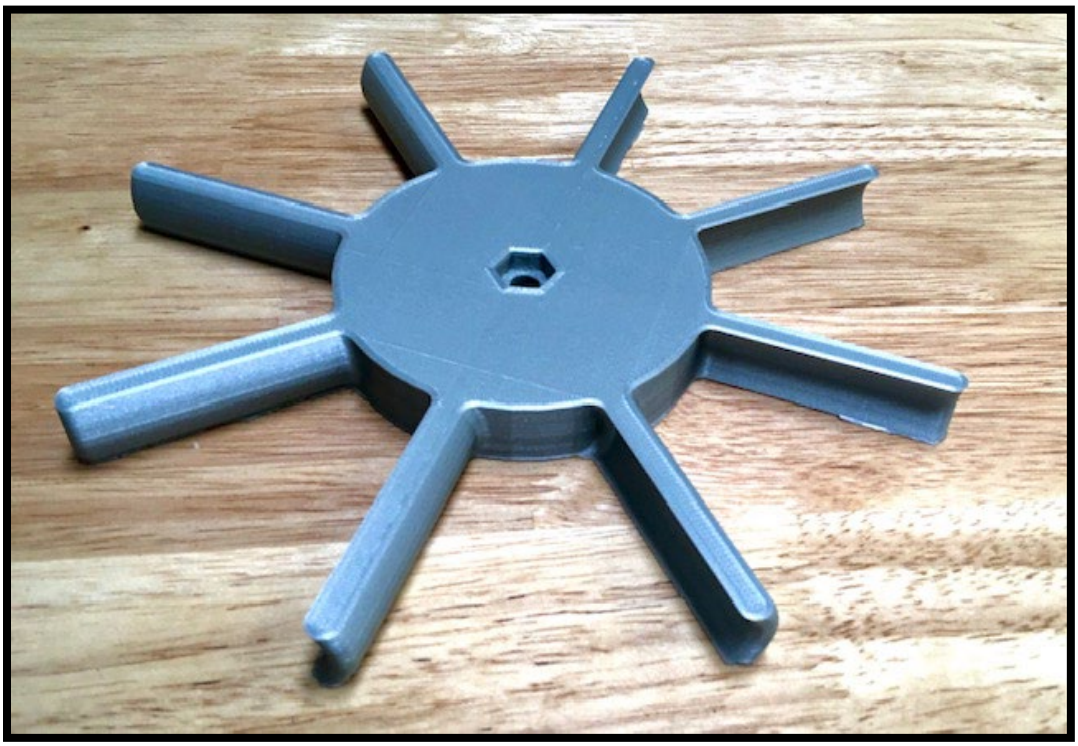

Figure 111. 3D Printed Power Turbine.

6. Encasing the DAS

The chassis and its power supply were installed into a metal box designed to be mounted on a wall in the TCR. The metal encasement was also to serve as a barrier to any EMI generated and background noise during the experiment. A hole is cutout of the side to allow entry for the probe wires, ethernet cable, and OPR line. The metal encasement of the DAS with its 24 VDC power source is shown in Figure 112. It was used with the BCTR (tip gap casing) calibration runs.

Figure 112. Casing for Data Acquisition Used on BCTR (Tip Gap Casing) and TCR Experiments.

THIS PAGE INTENTIONALLY LEFT BLANK

APPENDIX D. STANDARD OPERATING PROCEDURES

This appendix provides step-by-step standard operating procedures with accompanying figures for operators. The procedures included are the:

- BCTR (Mock Casing) Calibration Procedure
- BCTR (Tip Gap Casing) Calibration Procedure
- TCR Calibration Validation Procedure
- TCR Blade Tip Growth Measurement Procedure

A. BCTR (MOCK CASING) CALIBRATION PROCEDURE

This procedure is to conduct capacitive probe calibrations on the BCTR (mock casing). The procedure assumes the rotor is currently uninstalled, the bearing housing and the rig is assembled with no power or air connections connected. The procedure is meant to be followed in chronological to ensure safety.

1. Installing Rotor Blisk and Rig Setup

1. Ensure pressurized air source is not connected to flexible hose handle and that facility air cutout valve is shut prior to installation of rotor.
2. Place M6 (1/4") hex nuts into empty slots of the shaft to fan coupling piece for eventual blisk removal.
3. Insert polycarbonate coupling piece with M6 (1/4") hex nuts installed into the bottom of the NPSMF hub. Rotate as needed to ensure bolt holes are aligned.
4. Insert the 5 numbered M8 (5/16") hex bolts into the corresponding numbered bolt holes and hand tighten the bolts with their accompanying nuts.
5. When all bolts have been tightened by hand, starting at an arbitrary bolt, tighten each bolt in circular order, skipping over one bolt every tightening

using a socket wrench. This is to ensure even distribution of loading on rotor.

6. Ensure flexible nozzle air hose handle is secured on BCTR using 80/20 slot guides as a pincer (refer to Figure 91). Connect the flexible nozzle to the securing bolt, with the end pointing towards the rotor tips, tangent to the rotor blades. Verify air is pressurized and available.

2. Installing Translation Stage Mount and Mock Casing

1. Ensure 120 VAC power is off prior to starting. Ensure translation stage mount is tightly connected to rig base plate.
2. Using an Allen wrench secure the stage gripping mount onto the PD1 translation stage. There are 3 sets of tapped bolt holes on the PD1. Use the middle set.
3. Pick which mock casing you intend to use, either the Leading Edge (higher hole), Mid-Chord (middle height hole), or Lower Edge (lowest height hole).
4. Attach the rear piece (side with M20 x 2.5 (¾-10") tapped hole) of the mock casing onto the stage coupling mount. Secure the casing in place by using the two 8–32 bolts.
5. Slide the corresponding front piece of the mock casing in front of the rear piece, onto the mount. The two flat surfaces should be facing each other and the curved surface toward the NPSMF. Bolt the two pieces together using 8–32 bolts. Hand tighten first, then tighten down using Allen wrench to ensure even load distribution.
6. Place polycarbonate “C” clamp onto back of chosen capacitive probe. Carefully insert the probe into the back of the casing until the front of the probe is flush with the curved, front face of the mock casing. Ensure the wire is routed along the slot and not bent.
7. Using a M20 (3/4") Allen wrench, insert and lightly tighten plastic M20 x 2.5 (¾" -10) headless bolt behind the capacitance probe to hold in place.

8. Repeat with a second M20 x 2.5 (¾" -10) headless bolt to secure in place.

9. With user's hand, lightly slide the mock casing forward to where it is just touching the rotor blades.

10. Mount the electric dial indicator behind the mock casing. The measuring end should be in contact with the back of the mock casing, with enough room for the casing to slide back at least 4mm. Ensure that the dial indicator is perpendicular to the rear of the mock casing to prevent friction/cocking. Using the mount provided, tighten the dial indicator in place by sliding the clamp along the mount railing, pinching together the two sides of the clamp and tightening down the bolts using a 5/32" Allen wrench.

3. Instrumentation Setup and Wiring

1. Connect the end of the probe wire into its corresponding channel's SMA jack. Numbered probes are connected to their corresponding numbered jacks. Refer to Figure 113 for reference of channel locations.

2. Ensure OPR is not connected to PFI0 jack. Turn on DC power source for Laser Tachometer.

3. Ensure DC power source is 4.95 V. This must not exceed 5 V to not damage the data acquisition circuitry. Verify sensor is receiving power as noted by red laser emitting from front face. Hand spin rotor slowly and ensure sensor only senses one response per revolution as indicated by green light on side of sensor main body (refer to Figure 102).

4. Connect the OPR to the DAS via the PFI0 port, referencing Figure 113.

5. Ensure power source input is connected to DAS with the green grounding wire attached to the grounding stud.

6. Connect ethernet cable to PC. Power the DAS.

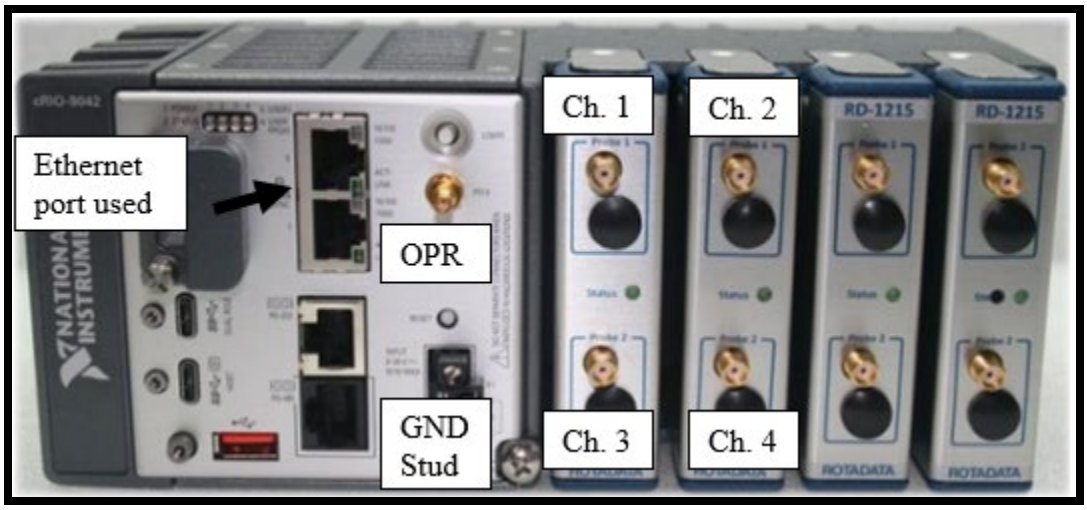

Figure 113. Data Acquisition Showing Numbered Channels and OPR Input Jack. Source [22].

7. Connect PD1 stage to PD1 motor controller. Connect PD1 motor controller to PC via USB cable. Power on motor controller.

4. Software Setup

1. The IPv4 address of the DAS is 192.168.18.81. This is needed to be configured prior to starting the RCap V program.
2. Start RCap V program and connect to DAS. Enable live data and ensure proper probe response in live data tab. Set number of averages in configuration tab to its maximum value. Specify recording location of data.
3. Start Kinesis software for the Thor Labs PD1 stage and connect to motor controller. Set jog step size to 1 for both the forward and aft direction.
4. Start MATLAB and start Tip Clearance App. On calibration recording tab specify date, rig, number of revolutions to record, file type, probe number, and probe position. Specify the location desired for file recording (should match the RCap V recording location). Press “Initialize Files.” Ensure a parent folder has been created for the calibration run. Do not press initialize stage/encoder button (only for tip gap casing version).

5. Active Calibration Procedure

1. Move casing forward until it touches the rotor then step casing back approximately 20 steps. Use spirit level to ensure casing is exactly upright.
2. Connect multimeter in “forward bias mode” to the NPSMF hub and the ground connecting of the mock casing. Slowly and lightly hand rotate the rotor while simultaneously slowly stepping the translation stage forward. The stage should be stepped one step closer once per revolution when nearing the zero position. Upon an audible alarm from the multimeter or an audible noise from the rotor tip slightly rubbing against the mock casing moving forward. The user’s hand must not be in contact with the rotor when the zero position is found to avoid creating a moment on the rotor. Zero the dial indicator. Check the checkbox for zeroing the casing with multimeter on Tip Clearance App for tracking purposes. Do not select zero encoder (only for tip gap casing version)
3. Step back the casing to the first calibration point (125 μm) by dial indicator measurement
4. Slowly crack open the air cutout valve and ensure the rotor begins to rotate. Ensure proper probe response and tachometer response on the live data tab of the RCap V software. Once proper movement has been noted, open air cutout valve, throttled to desired speed.
5. On Tip Clearance App select 125 μm calibration position in the drop-down menu. Do not press “go to position” button (only for tip gap casing version).
6. Verify correct RPM and probe response. Then press record. Record data for approximately 1 minute then stop.
7. Press rearrange data button on Tip Clearance App.
8. Press Time Stamp Check on Tip Clearance App. In status window verify no rows of data are lost. Ensure acceptable amount of difference between OPR

and Cap Probe data loss. Ensure acceptable synchronization of OPR and Cap Probe data. If unacceptable, delete data and re-record.

9. Once data is determined acceptable, check the corresponding checkbox in the Calibration Position Tracker section for tracking purposes. Select the next position in the drop-down menu. Use Kinesis software to move to next position, again as measured by the dial indicator. Repeat process until completed.

10. Switch probes referring to section 2 completing applicable steps. Then complete section 5 steps 1–9 again. Upon completion of all four probes in a probe monitoring position, switch casings referring again to section 2 through section 5.

11. Once all calibration positions for all probes are completed, view the Calibrate Files tab in the Tip Clearance App. Specify which folders to conduct calibration processing (normally start at 1 and end at 12).

B. BCTR (TIP GAP CASING) CALIBRATION PROCEDURE

This procedure assumes the NPSMF and Casing are currently not installed. The procedure assumes the Velmex stage, bearing housing spacer adapter, turbine assembly, and casing grip mounts are installed.

1. Installing Rotor Blisk and Rig Setup

1. Perform section 1, steps 1–5 of the BCTR (Mock Casing) calibration procedure.

2. Connect flexible nozzle air hose is connected into turbine housing port. To ensure it does not become loose during operation, bend the hose and fasten (tape) the hose to the housing. Verify air is pressurized and available.

2. Installing Translation Stage Mount and Tip Gap Casing

1. Ensure 120 VAC power is off prior to starting. Ensure translation stage mount is tightly connected to rig base plate using T-slot slides of Velmex casing.
2. Attach casing grip mounts onto carriage and 80/20 slide. Lubricate the slide as needed to ensure smooth operation.
3. Carefully and slowly mount the tip gap casing around the NPSMF and into the casing grip mounts. There is only 889 μm (0.035") of clearance space.
4. Place polycarbonate “C” clamp onto back of chosen capacitive probe. Choose probe monitoring position for calibration. Carefully insert all 4 probes into their corresponding ports of the casing until the front of the probe is flush with the curved, front face of the mock casing. Ensure the wire is routed along the slot and not bent. Use the naming convention label engraved on casing for mounting the probes in the correct position. The number indicates the probe number and the letter indicates the monitoring position. Refer to Figure 58.
5. Using a M20 (3/4") Allen wrench, insert and lightly tighten plastic ¾-10 headless bolt behind the capacitance probes to hold in place.
6. Repeat with a second round of M20 x 2.5 (¾" -10) headless bolt to secure in place.

3. Instrumentation Setup and Wiring

1. Perform section 3, steps 1–6 of the BCTR (Mock Casing) calibration procedure.
2. Connect Velmex BiSlide to its motor controller. Connect the BiSlide magnetic linear encoder line to the encoder readout. Connect the motor controller to the PC. Ensure the stage is connect to COM port 2 and the encoder is connected to COM port 7 on the PC for the MATLAB Tip Clearance App to function properly.

3. Connect a ground wire from the tip gap casing to the ground stud of the DAS (refer to Figure 113).

4. Software Setup

1. Perform section 4, steps 1–2 of the mock casing calibration procedure.
2. Start MATLAB and start Tip Clearance App. On calibration recording tab specify date, rig, number of revolutions to record, file type, probe number, and probe position. Specify the location desired for file recording (should match the RCap V recording location). Press "Initialize Files." Ensure a parent folder has been created for the calibration run. Press initialize stage/ encoder button. Verify stage control using jog controls on Tip Clearance App. Ensure encoder tracks stage movement. Check the checkbox to track that this step has been completed.

5. Active Calibration Procedure

1. Move casing forward using Tip Clearance App until it touches the rotor then step casing back approximately 10 steps. Use spirit level to ensure casing is exactly level.
2. Connect multimeter in "forward bias mode" to the NPSMF hub and the ground connecting of the mock casing. Slowly and lightly hand rotate the rotor while simultaneously slowly stepping the translation stage forward. The stage should be stepped one step closer once per revolution when nearing the zero position. Upon an audible alarm from the multimeter or an audible noise from the rotor tip slightly rubbing against the mock casing moving forward. The user's hand should not be touching the roto when the zero position is found to avoid causing a moment on the rotor. Zero the encoder using the app. Check the checkbox for zeroing the casing with multimeter on Tip Clearance App for tracking purposes.
3. Select 125 in the drop-down menu and move to position as measured by linear encoder either by manually jogging casing back, commanding the

casing to move to position using “go to selected position” button, or by manually rotating the lead screw by hand as needed.

4. Slowly crack open the air cutout valve and ensure the rotor begins to rotate. Ensure proper probe response and tachometer response on the live data tab of the RCap V software. Once proper movement has been noted, open air cutout valve, throttled to desired speed.

5. Verify correct RPM and probe response. Then press record. Record data for approximately 1 minute then stop.

6. Press rearrange data button on Tip Clearance App.

7. Press Time Stamp Check on Tip Clearance App. In status window verify no rows of data are lost. Ensure acceptable amount of difference between OPR and Cap Probe data loss. Ensure acceptable synchronization of OPR and Cap Probe data. If unacceptable, delete data and re-record.

8. Once data is determined acceptable, check the corresponding checkbox in the Calibration Position Tracker section for tracking purposes. Select the next position in the drop-down menu. Tip Clearance App to move to next position, again as measured by linear encoder. Repeat process until completed.

9. Repeat applicable steps to all probes in all probe monitoring positions.

10. Once all calibration positions for all probes are completed, view the Calibrate Files tab in the Tip Clearance App. Specify which folders to conduct calibration processing (normally start at 1 and end at 12).

C. TCR CALIBRATION VALIDATION PROCEDURE

This procedure begins assuming tip gap casing has been mounted onto TCR with probes connected to DAS and OPR sensor spliced and connected to DAS. This assumes that the casing is oriented per Figure 59.

1. Install all 4 probes to their mid-chord ports following the probe naming convention. Start the Allis air compressor system.

2. Referring to Figure 114, loosen bolts connecting the instrumented outlet casing to the power turbine housing and remove the bolts holding the front piping mount in place.

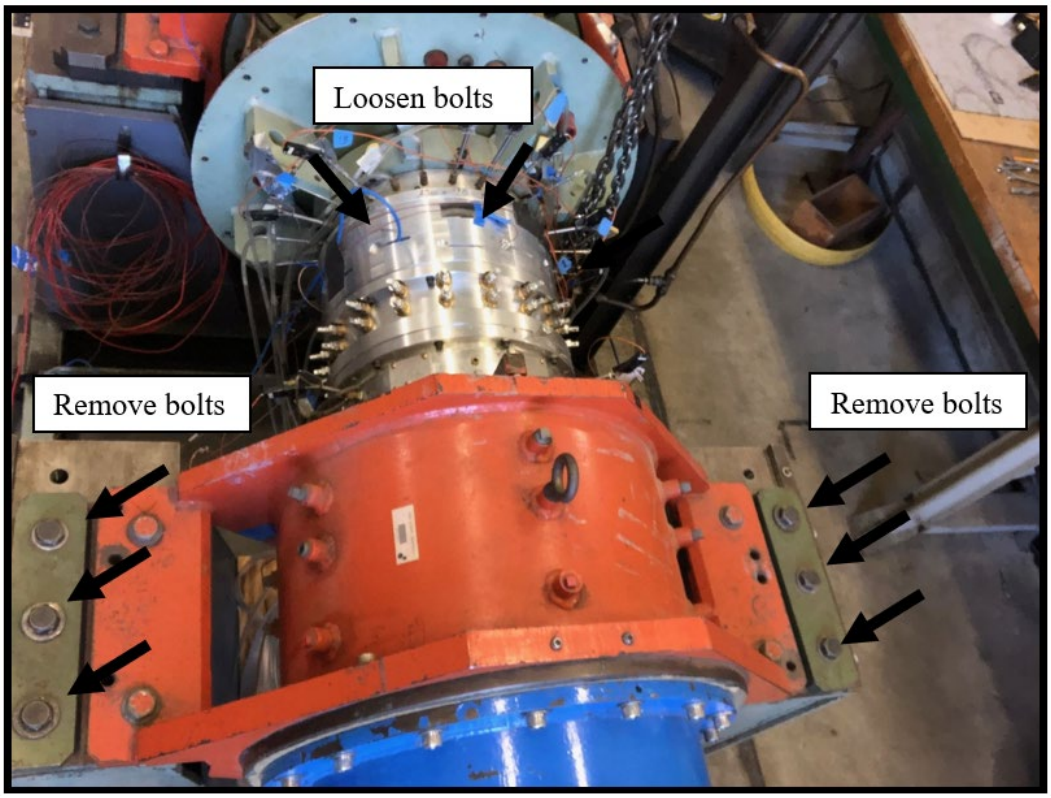

Figure 114. Overhead View of TCR Showing Referenced Bolts.

3. Referring to Figure 115, “nudge” the casing to the right until contact is prevents movement. With a feeler gauge measure the clearance space between the moveable portion of the mount and the stationary portion fixed to the deck. Measure at the corner closest to the tip gap casing. This should be approximately 457.2 mm (18") from the swivel point (where bolts were loosened).

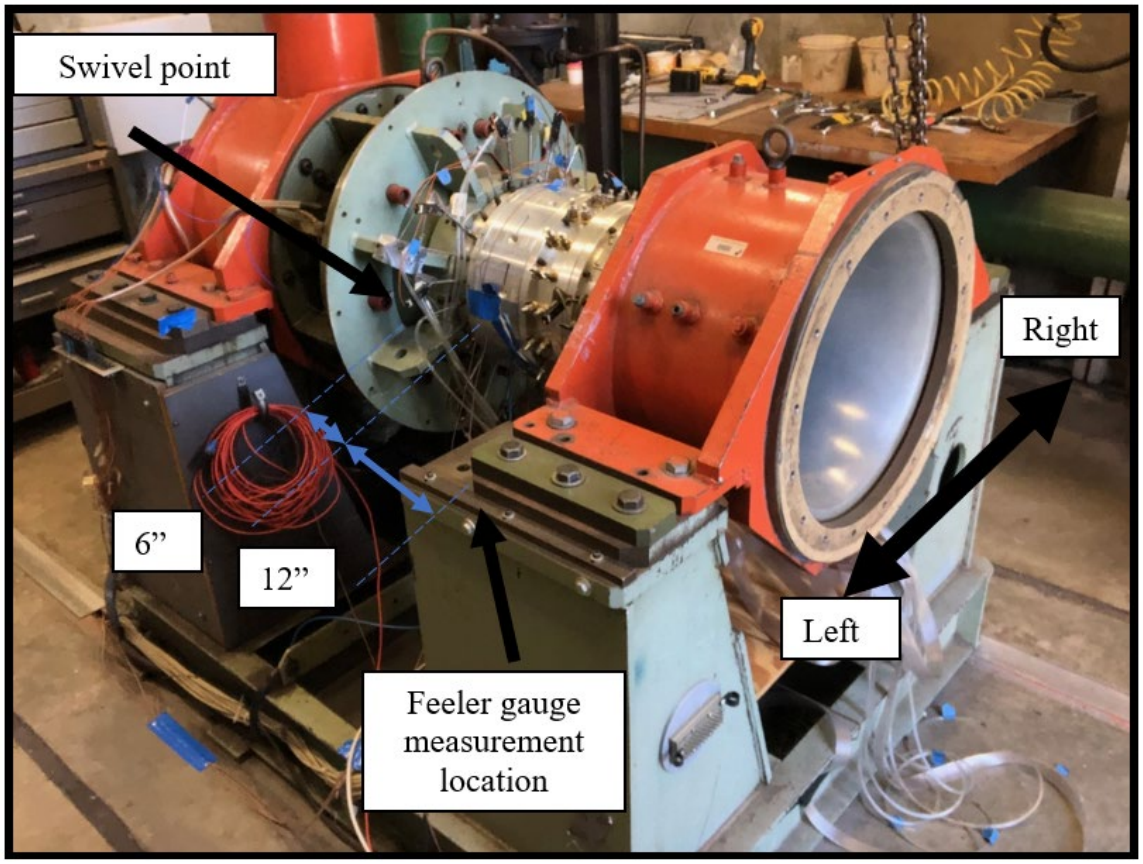

Figure 115. Measurement Location and Movement Orientation.

4. Throttle open air flow to the power turbine and bring TCR to approximately 3000–4000 RPM. Record data using RCap V program.
5. Stop the TCR.
6. “Nudge” the mount left until contact is again made. Start the TCR and record again.
7. Return the TCR to its normal center position and insert/tighten all bolts.
8. The movement of the plane of where the probes are located is 1/3 of the movement measured by the feeler gauge by similar triangles.

D. TCR TIP CLEARANCE MEASUREMENT PROCEDURE

1. Install the probes in either the leading edge, mid-chord, or trailing edge monitoring positions according to their naming convention per Figure 59.
2. Ensure OPR and capacitive probes are connected to DAS. Start instrumentation power to the TCR instruments from the TCR control panel.
3. Once the OPR is powered, turn on power to the DAS.
4. Start the RCap V program, specifying the recording folder location and the maximum RPM expected (set to 28,000 RPM).
5. For IP configuration refer to BCTR (Mock Casing) calibration procedure section 4.
6. Ensure all 4 probes are enabled in the configuration tab of the RCap V program. Verify proper signal response and OPR response.
7. Open Tip Clearance App. Navigate to TCR 4 Probe tab. Specify the recording location, date, mounting location, and target RPM (start with 3001).
8. Press initialize files and ensure the recording location matches the RCap V program's recording location.
9. Bring TCR up to speed. Once at desired speed, record using the RCap V program for approximately 10 seconds.
10. After recording, rearrange data using push button. Conduct time stamp check. If data is deemed unacceptable, delete folder and restart. If acceptable, specify next run (convention used is RPM = 3002), then repeat recording, rearranging, and data checking.
11. After 5 runs have been recorded at a specified speed, increase speed to next desired speed.
12. At bottom of tab, specify which folders to convert from DRO to micrometers. Press the push button to convert.

13. In the next tab, specify the calibration files folder location (location saved from calibration procedure). There should be 12 calibration files.

14. Specify the main folder of where all the data folders are located. Press the push button to begin to sort out data and create growth plot curves.

THIS PAGE INTENTIONALLY LEFT BLANK

APPENDIX E. MATLAB CODING

Only the main functions are presented in this paper. The entirety of the Tip Clearance App has been truncated for brevity.

A. CALIBRATION FUNCTION

```
function [CalMsg,TC_] =
TC_Cal(app,FolderNumber,CalPosition,NumRevs,FileType,...
            MainFolderPath,CalFilePath,FigFilePath)
%DESCRIPTION: Calibration function

%INPUTS
%app - needed for Tip Clearance App
%FolderNumber - can be a single number or range to be used in
%for loop. Folders from directory of .csv files
%Each data set should be kept in separate folders. 4 Probes in
%3 Positions (Leading Mid-Chord Trailing) should total 12
%folders.
%CalPosition - Single number or range of numbers. Specifies which calibration
point
%was used.
%NumRevs - Specifies number of revolutions to average over
%FileType - either .csv or .bin
%MainFolderPath is the path to where the raw data folders can be found as
specified
%CalFilePath is the path to where the calibration table is
%saved
%FigFilePath is the filepath to save the AFTBP figures.

%OUTPUTS
%CalMsg notifies user when complete.
%TC_ is a structure holding calibration tables and curves
for j = FolderNumber
   F = j+2;
   Folders=dir(MainFolderPath);
   ProbeFolder_ = Folders(F).name;
   fprintf('Started: %s %s\n',ProbeFolder_,datestr(now))
   fp=sprintf('%s\\%s',MainFolderPath,ProbeFolder_);
fd=sprintf('%s\\*%s',fp,FileType);
   fn = sprintf(' %s - Cal Table.mat',ProbeFolder_);
   fign = sprintf('%s - Cal Curve.fig',ProbeFolder_);
   if exist('TC_') ==0 %Initializes TC structure
       TC_.Cal = zeros(5,14);
       TC_.AFTBP = zeros(30, NumRevs);
       TC_.ProbeFolder = ProbeFolder_;
       disp('TC_ DNE. Initializing TC Structure')
   end

   for k = CalPosition
```

```
        fprintf('Started %s - File Number %d\n', ProbeFolder_, k)
        TC_.Cal(5,:) = [125,175,225,275,325,375,425,475,550,650,750, ...
            850,950,1050]; %calibration points used
        fprintf('Conducting Time Stamp Check')
        if FileType == '.csv'
            [~,Info,~,~,~] = TC_TimeStampCheck(app,fd,fp,k,FileType); %Uses
function to
            %display "Info" as TC_Cal processes.
        else
            Info = 'Binary file. No Info\n'; %Data unavailable in .bin form.
        end
        fprintf('Time Stamp Check Completed\n')
        TC_.Info{k} = Info; %Saves the info in structure for review as needed.
        [RD,OPR] = TC_GetData(app,fd,fp,k,FileType);
        fprintf('Get Data Complete\n');
        [dsRD,sFD,~,~,~,IL] = TC_IntFFTFilt(app,RD,OPR,k,FileType,NumRevs);
        fprintf('Filtering complete\n')
        [BPInt] = TC_OPR(app,NumRevs,IL);
        fprintf('Blade Pass Intervals Created\n');
        %% Find Longest Blade
        pkpkfiltered=zeros(NumRevs-1,20);
        for jjjj = 1:NumRevs-1
            for kkkk=1:20
                A = sFD(BPInt(jjjj,kkkk):BPInt(jjjj,kkkk+1));
                pkpkfiltered(jjjj,kkkk)=max(A)-min(A);
            end
        end
        pkpkavg=mean(pkpkfiltered);
        LB = find(pkpkavg==max(pkpkavg));
        clear RD OPR IL %saves space
        %% Filtered Calibration Only
        TC_.Cal(1,k)=pkpkavg(LB);
        TC_.Cal(2,k) = std(pkpkfiltered(:,LB),1);
        %stdev weighted with "1" Divides by N-1 instead of N.
        TC_.pkpkfiltered=pkpkfiltered;
        TC_.LB=LB;
        fprintf('%s\n',TC_.Info{k})
        %% Non Filtered Calibration Only
%         pkpk=zeros(NumRevs-1,20);
%         for jjjj = 1:NumRevs-1
%             for kkkk=1:20
%                 A = dsRD(BPInt(jjjj,kkkk):BPInt(jjjj,kkkk+1));
%                 pkpk(jjjj,kkkk)=max(A)-min(A);
%             end
%         end
%         pkpkavg=mean(pkpk);
%         TC_.Cal(1,k)=mean(pkpkavg(LB));
%         TC_.Cal(2,k) = std(pkpk(:,LB),1);%stdev weighted with "1" Divides by
N-1 instead of N.
%         fprintf('%s\n',TC_.Info{k})

    end
    cd(CalFilePath);pause(1)
    close all
```

```
   %Clear all data to conserve RAM
   clear CalPlot A B BN BPInt CalMsg dsRD dsMD Folders FBP Info IntDiff IntMax
IntMin;pause(1);
   clear j k LBMM LB MD OPR PointClosestToAvg_max PointClosestToAvg_min RD
ProbeFolder  sFD;pause(1);
   clear sOPR ValueAtFBP_Max ValueAtFBP_Min; pause(1);
   %Save TC for later as needed.
   save(fn,'TC_');pause(3);
end
CalMsg = sprintf('\n\nAll Done\n\n');
end
```

B. TIME STAMP CHECKING FUNCTION

```
function  [Error,Info,files,RDTimeError,OPRTimeError] =
TC_TimeStampCheck(app,fd,fp,CP,FileType)
%Conducts a check of time stamps to verify there isn't sufficient data
%loss.
%% Initialization
files=dir(fd);
NumFiles = length(dir(fd)); %needed to divide OPR files and Raw files
fname = fullfile(fp, files(CP).name);
A=dlmread(fname); %extract data
unix = A(:,2); %usually on order of 10^9 seconds
microsecs = A(:,3)/1e6; %units of seconds
timestamps = unix+microsecs; %csv file has them in two columns. This combines.
Units are in seconds
DROMax = max(max(A(:,6:end)));
DROMin = min(min(A(:,6:end)));
pkpk = DROMax - DROMin; %used to see if data trends well.
%% Timestamp Loss Determination
X = diff(timestamps); %Seconds. Should be 0.01
Y=X*1e6; %units of microseconds. 10,000 nominally
  Z = Y(Y<12e3); %takes all non-row skips
 Z=Z-10e3;% non row skip data loss
 uSecLost = sum(Z); %total microseconds lost on uncertainty in time
 RowsSkipped = round(sum((Y(Y>12e3)-10e3)/10e3));%total rows skipped
if isempty(find(Y>12e3)) == 0 %anything greater then 12 thousand microseconds
       RDTimeError = 1;
       RDRowsSkipped = RowsSkipped;
else
        RDTimeError=0;
        RDRowsSkipped = 0;
end

%% OPR Time Stamp Check
j=CP+NumFiles/2; %second half of files in the folder
OPRfiles=dir(fd);
OPRfname = fullfile(fp, OPRfiles(j).name);
OPRA=dlmread(OPRfname);
OPRunix = OPRA(:,2);
OPRmicrosecs = OPRA(:,3)/1e6;
OPRtimestamps = OPRunix+OPRmicrosecs;
```

```
OPRX = diff(OPRtimestamps);
OPRY=OPRX*1e6;
OPRZ = OPRY(OPRY<22e3);
OPRZ=OPRZ-20e3;
uSecLostOPR = sum(OPRZ);
OPRRowsSkipped1 = round(sum((OPRY(OPRY>22e3)-20e3)/20e3));
if isempty(find(OPRY>2.5e4)) == 0
   OPRTimeError = 1;
   OPRRowsSkipped = OPRRowsSkipped1;
else
   OPRTimeError=0;
   OPRRowsSkipped = 0;
end

%% Summary Info Readout
A_OPR=OPRA(:,6:end);
mmm=numel(A_OPR);
OPR= zeros([1 mmm]);
for jjj = 1:size(A_OPR) %rearrange data
   OPR(10000*(jjj-1)+1:10000*jjj) = A_OPR(jjj,1:10000);
end
%NumUpPulses = length(diffOPR(diffOPR>0)); %number revs
UpPulseLocate = find(diff(OPR)>0); %finds the start of a revolution
TotalRevs = length(UpPulseLocate); %total revs recorded in the set raw.
AvgTBP = mean(diff(UpPulseLocate))*2/20; % average period of blade passing.
%units of microseconds. *2 to account for 2 microseconds per data point
TimeLossPercentRD_AvgBP = 100*uSecLost/AvgTBP;
TimeLossPercentOPR_AvgBP =100* uSecLostOPR/AvgTBP;
RDOPRTimeLossDifference = uSecLost - uSecLostOPR;

Error = RDTimeError + OPRTimeError;
Info = sprintf(['%s\n\nRAW DATA\nTime Error in Raw Data? (T/F):   %d\nRows
skipped of Raw Data:   %d\n microsec of Raw Data Lost:   %d\n'...
   '\nONCE PER REV\nTimeError in OPR? (T/F):   %d\n'...
   'Row Skipped of OPR Data: %d\nmicrosec of OPR Data Lost:   %d\n'...
   '\nBLADE PASSING INTERVAL INFO\n'...
   'Total Revs Recorded:   %d\n'...
   'Average Period of Blade Pass:   %d microsec\n'...
   'Raw Data Percent Time of Lost of the Average Blade Period:   %d%%\n' ...
   'Once-Per-Rev Percent Time of Lost of the Average Blade Period: %d%%\n' ...
   'Raw Data Time Lost - OPR Time Lost = %d (microsec). If positive RD shifts
to right relative to OPR intervals.\n' ...
   '\nPeak to Peak Value:   %d.'],...

files(CP).name,RDTimeError,RDRowsSkipped,uSecLost,OPRTimeError,OPRRowsSkipped,
uSecLostOPR,TotalRevs,AvgTBP,TimeLossPercentRD_AvgBP,...
   TimeLossPercentOPR_AvgBP,RDOPRTimeLossDifference,pkpk);

%% Plotting Peaks over revolutions
% Does a rough filter using a moving mean. Plots location of peaks as a
% fraction of blade pass event. User to verify it is "flat" and not
% erroneous or trending up or down.
if FileType == '.csv'
```

```
A = A(:,6:end); %gets rid of time and RPM columns
nnn = numel(A);
RD= zeros([1 nnn]);

for iii = 1:size(A,1) %size(A,1) is the number of rows A.
   RD(5000*(iii-1)+1:5000*iii) = A(iii,1:5000); %puts all the A rows into one
continuous row
end

MD=movmean(RD,100);
elseif FileType == 'bin'
files=dir(fd);
NumFiles = length(files);
k=CP;
j=(NumFiles/2) + CP;
MN=100;
fname=fullfile(fp,files(k).name);
fid=fopen(fname,'r','b');
RD=fread(fid,'uint16');
oprfname=fullfile(fp,files(j).name);
oprfid=fopen(oprfname,'r','b');
OPR=fread(oprfid,'uint16');
MD=movmean(RD,MN);

end
MD=movmean(MD,100);
MD=movmean(MD,100); %rough filtering

NumRevs=(TotalRevs-10);BN=15; %blade number doesn't matter for this rough
check.
BPInt = zeros(NumRevs,21); %opr start indices
up = find(diff(OPR)>0,NumRevs+1);
for j = 1:NumRevs
BPInt(j,1:21) = linspace(up(j),up(j+1),21);
end
BPInt = floor(BPInt);

for j=1:NumRevs %location of max's
   ExpBounds = floor((BPInt(j,BN+1) - BPInt(j,BN))*.05); %capture maxs that
occur outside of intervals
   B = MD((BPInt(j,BN)):(BPInt(j,BN+1)+ExpBounds));
   FracLength.Max(j)=find(B==max(B),1)/length(B);  %fraction of the interval
that max occurs
end
for j=1:NumRevs %locations of min's
   ExpBounds = floor((BPInt(j,BN+1) - BPInt(j,BN))*0.05);
   B = MD((BPInt(j,BN)):(BPInt(j,BN+1)+ExpBounds));
   FracLength.Min(j)=find(B==min(B),1)/length(B);  %fraction of the interval
that max occurs
end
FracLengthMaxRMOUT = rmoutliers(FracLength.Max); %remove erroneous points
FracLengthMinRMOUT = rmoutliers(FracLength.Min);
H=std(FracLengthMaxRMOUT,1);
H=3*H; %show remoutlier line.
```

```
I=std(FracLengthMinRMOUT,1);
I=3*I;
AFTBPCheck = figure(1);
% figure(AFTBPCheck)
x = (1:length(FracLength.Max)); %length is NumRevs
scatter(x, FracLength.Max,3,'o');hold on
scatter(x, FracLength.Min,3,'o');
G=mean(FracLengthMaxRMOUT);
F=mean(FracLengthMinRMOUT);
line([1 length(FracLength.Max)],[G G]) %format for older MATLAB codes if
needed.
line([1 length(FracLength.Min)],[F F])
line([1 length(FracLength.Max)],[G+H G+H],'Color','r')
line([1 length(FracLength.Max)],[G-H G-H],'Color','r')

line([1 length(FracLength.Max)],[F+I F+I],'Color','r')
line([1 length(FracLength.Max)],[F-I F-I],'Color','r')

ylim([-0.1 1.1]);

end
```

C. EXTRACTING DATA FROM CSV OR BIN FILES

```
function  [RD,OPR] = TC_GetData(app,fd,fp,CP,FileType)
%DESCRIPTION: Extracts and rearranges RCAP V raw data .csv or .bin files
%from specified file path, fp, to create a raw data vector, RD and an OPR
signal
%vector to be used in the follow-on functions.

%INSTRUCTION
%--Using TC_Script: fd, fp, CP, and FileType are defined in TC_Cal and
%TC_Script. In TC_Script: define which calibration point(s) to process
%Folder specified should have raw data files first in the ascending tip
clearance
%order.

%INPUTs
%--fd is used to create a directory "dir(fd)".
%--fp is the filepath to the raw data.
%--CP is the calibration position, 1 through 14
%FileType is either 'csv' or 'bin' for the type of file to be processed

%OUTPUTs
%RD is the raw data from csv file, reordered to be one row vector
%OPR is the OPR signal in a row vector

files=dir(fd);
NumFiles = length(files); %kept as lever for different amounts of calibration
points
k=CP;
if NumFiles > 5
```

```
j=(NumFiles/2)+CP;
elseif NumFiles == 5
   j=5;
end
fname = fullfile(fp, files(k).name); %Raw Data File
OPRfname=fullfile(fp, files(j).name); %OPR File

if FileType == '.csv'
A = dlmread(fname);
A_OPR=dlmread(OPRfname);
A = A(:,6:end); %gets rid of time and RPM columns
A_OPR=A_OPR(:,6:end); %gets rid of time and RPM columns
nnn = numel(A);
mmm=numel(A_OPR);
RD= zeros([1 nnn]);
OPR= zeros([1 mmm]);
for iii = 1:size(A,1) %size(A,1) is the number of rows A.
   RD(5000*(iii-1)+1:5000*iii) = A(iii,1:5000); %puts all the A rows into
   %one continuous row
end
for jjj = 1:size(A_OPR)
   OPR(10000*(jjj-1)+1:10000*jjj) = A_OPR(jjj,1:10000); %same for OPR
end

elseif FileType == 'bin'
fid=fopen(fname,'r','b');
RD=fread(fid,'uint16'); %already stored as a row vector.
oprfid=fopen(OPRfname,'r','b');
OPR=fread(oprfid,'uint16');
end
end
```

D. RESAMPLING, FFT, FILTERING FUNCTION

```
function  [dsRD,sFD,Y1,Y2,f,IL] =
TC_IntFFTFilt(app,RD,OPR,CP,FileType,NumRevs)
%DESCRIPTION: Take RD and OPR from TC_GetData, normalizes revolutions
%to uniform interval length, IL, runs it through an FFT that uses a blackman
%window. It then applies a lowpass filter based on FFT. Cross correlation
%is conducted to find and then eliminate lag induced by filter. Outputs the
%interpolated>detrended>lag shifted data for raw and filtered data. Also
%outputs FFT data for analysis.

%INPUTS
%RD and OPR from TC_Get Data. CP, FileType, NumRevs specified in
%TC_Script .

%OUTPUTS
%dsRD is detrended and phase shifted raw data
%sFD is the delay shifted lowpass filtered signal
%Y1,Y2, and f are outputs of FFTCalc to be used for graphing and analysis.
```

```
up=find(diff(OPR)>0,NumRevs+1);%Find all the up pulses in OPR data. This
%is the start of each revolution.
% IL_0 = 2.5 *max(diff(up));
IL_0 = 1/27000*60e6/2;
IL = IL_0 + 20 - rem(IL_0,20);%More then doubles new Fs
%and ensure it is divisible by 20 blades
RDInterp = zeros(1,NumRevs*IL);
for j = 1:NumRevs
x = up(j):up(j+1); %Raw OPR revolution length. Starts all data at first OPR
pulse.
Int = ((j-1)*IL+1):(j*IL); %Creates interval for interpolated raw data.
RDInterp(Int) = interp1(x, RD(x), linspace(up(j),up(j+1), IL));
%This extends out each revolution to be "IL" points of data, for all revs.
end
RD=RDInterp; %Replace raw data with interpolated data
%% FFT
Time = 1/IL*(1:length(RD))'; %Artificial time vector based on new Fs.
if FileType == '.csv'
RD=RD'; %turn into column vector for FFT use.
end
dRD=detrend(RD);  %Remove DC  bias
%% FFT If Needed
% Time = 1/IL*(1:length(RD))'; %Used for FFT
% NFFTN=1; %padding
% [Y2, ~, f,~,Y1] = FFTCalc(Time, dRD, NFFTN);
Y2 = 'skipped';
Y1 = 'skipped';
f = 'skipped';
%% Filter
if CP < 13
   Fpass = 400;
else
   Fpass = 250;
end
Fstop = Fpass*1.3;        % Stopband Frequency
Apass = 1;           % Passband Ripple (dB)
Astop = 100;          % Stopband Attenuation (dB)
match = 'passband';  % Band to match exactly
Fs=IL; %Artificial sampling freq in samples per revolution (shaft order)
% Construct an FDESIGN object and call its BUTTER method.
h  = fdesign.lowpass(Fpass, Fstop, Apass, Astop, Fs);
Hd = design(h, 'butter', 'MatchExactly', match);
FD=filter(Hd,dRD); %applies filter
%% Lag Correction
[r,lag]=xcorr(dRD,FD); %find lag
[~,I]=max(abs(r));
delay=lag(I)*-1;
dsRD=dRD(1:end-delay); %correct for delay from lag
sFD=FD(delay+1:end);
end
```

E. CREATING INDEX LOOKUP TABLE

```
function [BPInt] = TC_OPR(app,NumRevs,IL)
%DESCRIPTION: Creates an artificial OPR signal based on revolution size
%specified in TC_FFT's interpolation section. Then creates 20 equally
%spaced intervals to isolate each blade for blade-by-blade analysis.

%INPUTS
%NumRevs - Number of revolutions specified in TC_Script
%IL - the interval length as determined under TC_IntFFTFilt

%OUTPUTS
%BPInt - Blade pass interval lookup table.

BPInt = zeros(NumRevs,21);
up = 1:IL:(NumRevs+1)*IL;
for j = 1:NumRevs
BPInt(j,1:21) = linspace(up(j),up(j+1),21);
end
BPInt = floor(BPInt);
end
```

F. CONVERTING TCR DATA FROM DRO TO MICROMETERS

```
% Button pushed function: Convertall4toMicrometersButton
function Convertall4toMicrometersButtonPushed(app, event)
tic;fprintf('Conversion Loop Started\n')
%% Initialize
fpc= app.CalFilePath4RunEditField.Value;
if app.MountingLocationDropDown.Value=="1 - Leading"
CalFileAdd = 0;
elseif app.MountingLocationDropDown.Value=="2 - Middle"
CalFileAdd=4;
elseif app.MountingLocationDropDown.Value=="3 - Trailing"
CalFileAdd=8;
end

fpd=app.RunDataPathEditField.Value;
BladeNo='Longest';
for qq=app.DataFileStartEditField.Value:app.DataFileEndEditField.Value
folders = dir(fpd);
fp1 = sprintf('%s\\%s',fpd,folders(qq+2).name);
for FileNo = 1:4
%% Create calibration curve
CalFileNo=FileNo+CalFileAdd;
cd(fpc); %go to cal file
fd = sprintf('%s\\*.mat',fpc); %find all the mat files in the cal folder
files = dir(fd); %put them into a string vector
cname = files(CalFileNo).name; %name of the cal file
load(cname);
close all;
fprintf('Beginning conversion using\nCalFile:%s\n\n',cname)
%INSERT CFTOOL RESULTS HERE
```

```
[xData, yData] = prepareCurveData( TC_.Cal(1,:), TC_.Cal(5,:) );
% Set up fittype and options.
ft = fittype( 'exp2' );
opts = fitoptions( 'Method', 'NonlinearLeastSquares' );
opts.Display = 'Off';
opts.StartPoint = [226.551875237484 -0.000421970891327102 1873.62771497954 -
0.00024879381329672];
% Fit model to data.
[fitresult, gof] = fit( xData, yData, ft, opts );
coeffs=coeffvalues(fitresult);
a=coeffs(1);b=coeffs(2);c=coeffs(3);d=coeffs(4);
x=linspace(0,TC_.Cal(1,1),10e3);
f = a*exp(b*x)+c*exp(d*x);
%% Plot Calibration Curve and Arrange Data to Output Table
TipClearance.CalCurve = figure('Name','CalCurveFit','Color',[1 1 1]);
hold on
plot(x,f,'r');
for k = 1:14 %create std dev converted
x=TC_.Cal(1,k); %start with mean DRO
A = a*exp(b*x)+c*exp(d*x); %convert the mean DRO
x = TC_.Cal(1,k)+TC_.Cal(2,k); %add in st dev
B = a*exp(b*x)+c*exp(d*x); %convert the added st dev
TC_.Cal(6,k) = abs(B-A); %subtract to obtain st dev converted
end
TipClearance.Cal=TC_.Cal;
TipClearance.Cal=TipClearance.Cal';
TipClearance.Cal(:,3) = TipClearance.Cal(:,6); %sets up table for use in
thesis
coeffs=coeffs';
TipClearance.Cal(2:5,4) = coeffs(1:4);
TipClearance.Cal(1,4) = gof.rsquare; %this sets up tables for thesis
errorbar(TC_.Cal(1,1:14),TC_.Cal(5,1:14),TC_.Cal(6,1:14),'blue')
ylim([0 1100])
% Fixup Figure
lgd = legend('Fitted Calibration Curve','Calibration Curve with St Dev');
lgd.FontSize = 11.5;
lgd.FontName = 'Times New Roman';
xlabel(sprintf('Digital Readout\n'),'FontName','Times New
Roman','FontSize',11.5);
ylabel(sprintf('Tip Clearance (\\mum)'),'FontName','Times New
Roman','FontSize',11.5);
ax = gca;
ax.FontSize = 11.5;
ax.FontName = 'Times New Roman';
grid on;
title(sprintf('%s',cname),'FontSize',10)
%% Take raw data and process
%Receive data
cd(fp1);
fd = sprintf('%s\\*.csv',fp1);
files=dir(fd);
fname = files(FileNo).name;
OPRfname = files(5).name;
[RD,OPR] = TC_GetData(app,fd,fp1,FileNo,FileType);
```

```
%Resample and Filter
up = find(diff(OPR)>0);
Revs = length(up);
Revs = round(0.95*Revs);
[dsRD,sFD,~,~,~,IL] = TC_IntFFTFilt(app,RD,OPR,12,FileType,Revs+1);
%Create Intervals
fprintf('Creating Blade-by-Blade Intervals\n\n')
[BPInt] = TC_OPR(app,Revs,IL);
%Store data for later viewing if needed
TipClearance.sFD=sFD;
TipClearance.dsRD=dsRD;
TipClearance.BPInt=BPInt;
%% Conversion w/ Filtered Calibration Use Only with Fraction Blade Passing
Considered
%                   %Time Fraction Individual Blades
%                   fprintf('Finding average location of peaks\n\n')
%                   FBP.Min = zeros(Revs,20);
%                   FBP.Max=FBP.Min;
%                   for jj=1:Revs
%                   for kk= 1:20
%                       %Accounts for outliers outside of BPInt bounds
%                       A = sFD(BPInt(jj,kk):BPInt(jj,kk+1)+ExpandBounds);
%uses the
%                       %filtered data to find FBP of peaks
%                       FBP.Min(jj,kk)=find(A==min(A),1)/length(A);
%                       %fraction of the interval that min occurs
%                       FBP.Max(jj,kk)=find(A==max(A),1)/length(A);
%                       %fraction of the interval that max occurs
%                   end
%                   end
%                   %Time Fraction Average minus outliers using 'mean' method
%                   FBP.MinAvg = zeros(1,20); FBP.MaxAvg = FBP.MinAvg;
%                   for k=1:20
%                       A=mean(rmoutliers(FBP.Min(:,k),'mean'));
%                       B=mean(rmoutliers(FBP.Max(:,k),'mean'));
%                       %find the min/max closest to min/max
%                       PointClosestToAvg_min = find(abs(FBP.Min(:,k)-A) ==
min(abs(FBP.Min(:,k)-A)),1);
%                       PointClosestToAvg_max= find(abs(FBP.Max(:,k)-
B)==min(abs(FBP.Max(:,k)-B)),1);
%                       FBP.MinAvg(k)=FBP.Min(PointClosestToAvg_min,k);
%                       FBP.MaxAvg(k)=FBP.Max(PointClosestToAvg_max,k);
%                   end
%                   for jj=1:Revs
%                   for kk=1:20
%                       B = dsRD(BPInt(jj,kk):BPInt(jj,kk+1)+ExpandBounds);
%                       DROmin(jj,kk) = B(round(FBP.MinAvg(kk)*length(B)));
%                       DROmax(jj,kk)= B(round(FBP.MaxAvg(kk)*length(B)));
%                   end
%                   end
%% Conversion
fprintf('Converting to micrometers using equation\n\n')
%Find longest blade using filtered signal
pkpkfiltered=zeros(Revs,20);
```

```
for jjjj = 1:Revs
for kkkk=1:20
A = sFD(BPInt(jjjj,kkkk):BPInt(jjjj,kkkk+1));
pkpkfiltered(jjjj,kkkk)=max(A)-min(A);
end
end
pkpkavg=mean(pkpkfiltered);
LB = find(pkpkavg==max(pkpkavg));
%% Filtered Conversions Only
pkpk=pkpkfiltered;
%% Raw Conversion Only
%                   %Obtain all pkpk's for all blades all revs
%                   pkpk=zeros(Revs,20);
%                   for jj=1:Revs
%                   for kk=1:20
%                       B = dsRD(BPInt(jj,kk):BPInt(jj,kk+1));
%                       pkpk(jj,kk)=max(B)-min(B);
%                   end
%                   end

%% Convert pkpk DRO to micrometers
TipClearance.pkpk=pkpk;
TipClearance.values=zeros(Revs,20);
for j = 1:Revs
for k = 1:20
x=pkpk(j,k);
f = a*exp(b*x)+c*exp(d*x); %plug in that rev's blade's pkpk to conversion eq.
TipClearance.values(j,k) = f; %store it
end
end

%Indiv Blade Plot
fprintf('Creating plots\n\n')
savefilename = sprintf('%s',fname);
TipClearance.LongestBladePlot = figure('Name',savefilename,'Color',[1 1 1]);
scatter(1:Revs,TipClearance.values(1:Revs,LB),10,'b','filled')
xlabel(sprintf('Revolutions\n'), 'FontSize',11.5,'FontName','Times New Roman')
ylabel(sprintf('Tip Clearance (\\mum)'), 'FontSize',11.5,'FontName','Times New
Roman')
title(sprintf('Tip Clearance Plot for Longest Blade\n'))
tipclearanceavg = mean(TipClearance.values(:,LB));
yline(tipclearanceavg,'-',sprintf('%s - Avg',tipclearanceavg))
yline(tipclearanceavg+std(TipClearance.values(:,LB)),'-','St Dev')
yline(tipclearanceavg-std(TipClearance.values(:,LB)),'-','St Dev')
TipClearance.File = fname;
TipClearance.std = std(TipClearance.values);
TipClearance.avg = tipclearanceavg;
TipClearance.RevolutionsRecorded=Revs;
TipClearance.LongestBladeFound = LB;
limx = Revs + 50;
xlim([1 limx+500])
cd(fp1)
figfilename = sprintf('%s-LongestBladeTipClearance.fig',savefilename);
savefig(TipClearance.LongestBladePlot,figfilename)
```

```
pause(2)

%Tip Clearance Blade by Blade
TipClearance.AllBlades = figure('Name',savefilename,'Color',[1 1 1]);
clf;hold off; hold on;
for j = 1:20
x=zeros(1,Revs);
x=x+j;
scatter(x,TipClearance.values(:,j),2,'black','filled')
end
xlabel(sprintf('Blade Number\n'), 'FontSize',14,'FontName','Times New Roman')
ylabel(sprintf('Tip Clearance (\\mum)'), 'FontSize',14,'FontName','Times New
Roman')
figfilename = sprintf('%s-AllBlades.fig',savefilename);
savefig(TipClearance.AllBlades,figfilename)
pause(2)

%Saving Stuff
fprintf('Saving\n\n')
assignin('base','TipClearance',TipClearance)
save(sprintf('%s -
TipClearanceConverted.mat',savefilename),'TipClearance','TC_')
pause(2)
fprintf('Completed\n%s\n%s\n \n \n \n ',fname,OPRfname)

end
end
fprintf('Conversion Loop Ended Total Elapsed Time: %s',toc)
end
```

G. CREATING GROWTH PLOTS

```
savepath = 'specify path';
savefile='specify.mat';
TCRfilesLE='specify path';
TCRfilesME='specify path';
TCRfilesTE='specify path';
cd(savepath);pause(1)
%%
cd(savepath);pause(1)
save(savefile,'BTC');pause(2)
%% Initialize Tables for L,M,andT

%  BTC(1).ME = cell(14,8);
row1 = {'Run','500','3k','12k','21k','24k','25.5k','27k'};
row12={'','','500-3k','3k-12k','12k-21k','21k-24k','24k-25.5k','25.5k-27k'};
for k = 1:8
BTC(1).ME{1,k}=row1(k);
BTC(1).ME{12,k}=row12(k);
end
col1 =
{'Run','1','2','3','4','5','6','7','8','Avg(um)','Avg(in)','SpeedRange','BTC
Change(um)','BTC Change(in)'};
```

```
for k = 1:14
    BTC(1).ME{k,1} = col1(k);
end
for j = 1:4
    for k=1:8
    BTC(j).LE{1,k} = BTC(1).ME{1,k};
    BTC(j).LE{12,k} = BTC(1).ME{12,k};
    BTC(j).ME{1,k} = BTC(1).ME{1,k};
    BTC(j).ME{12,k} = BTC(1).ME{12,k};
    BTC(j).TE{1,k} = BTC(1).ME{1,k};
    BTC(j).TE{12,k} = BTC(1).ME{12,k};
    end
    for k=1:14
    BTC(j).LE{k,1} = BTC(1).ME{k,1};
    BTC(j).ME{k,1} = BTC(1).ME{k,1};
    BTC(j).TE{k,1} = BTC(1).ME{k,1};
    end
end
 row2 = {'','500','3k','12k','21k','24k','25.5k','27k',''};
 col1LE = {'Averages','Probe/Position','1L','2L','3L','4L','Avg (um)','Avg
(in)','Average Growth','BTC Change(um)','BTC Change(in)','Blade Growth (Curve
Fit Adjusted)'};
 col1ME = {'Averages','Probe/Position','1M','2M','3M','4M','Avg (um)','Avg
(in)','Average Growth','BTC Change(um)','BTC Change(in)','Blade Growth (Curve
Fit Adjusted)'};
 col1TE = {'Averages','Probe/Position','1T','2T','3T','4T','Avg (um)','Avg
(in)','Average Growth','BTC Change(um)','BTC Change(in)','Blade Growth (Curve
Fit Adjusted)'};
 row9 = {'','','500-3k','3k-12k','12k-21k','21k-24k','24k-25.5k','25.5k-
27k','Total'};
 BTC(5).ME{1,1} = 'Averages';
for k =1:9
    BTC(5).LE{2,k} = row2(k);
    BTC(5).ME{2,k} = row2(k);
    BTC(5).TE{2,k} = row2(k);
    BTC(5).LE{9,k} = row9(k);
    BTC(5).ME{9,k} = row9(k);
    BTC(5).TE{9,k} = row9(k);
end
for k=1:12
    BTC(5).LE{k,1}=col1LE(k);
    BTC(5).ME{k,1}=col1ME(k);
    BTC(5).TE{k,1}=col1TE(k);
end
BTC(5).LE{10,2}=0;
BTC(5).ME{10,2}=0;
BTC(5).TE{10,2}=0;
BTC(5).TE{9,2}='0-500RPM';
%% Extract Data to Table Get Avg Convert to Inches (Middle Chord)
%Open each converted tip clearance file one by one and run this

F={'*500*','*300*','*1200*','*2100*','*2400*','*2550*','*2700*'};
for i = 1:length(F)
cd(TCRfilesME)
```

```
datafolder = dir(F{i});
numfolder = length(datafolder);
for j=1:numfolder
cd(TCRfilesME)
cd(datafolder(j).name);
files = dir(sprintf('%s\\*.mat',cd));
numfiles = length(files);
for k= 1:numfiles
   fprintf('\nloading %s',files(k).name)
   load(files(k).name)
   BTC(k).ME{j+1,i+1}=TipClearance.avg;
   close all
end
end
cd(TCRfilesME)
for j = 1:4
BTC(j).ME{10,i+1}=mean([BTC(j).ME{2:numfolder+1,i+1}]);
BTC(j).ME{11,i+1}=BTC(j).ME{10,i+1}/25.4/1000;
end
end
for j=1:4
   for k =3:8
       BTC(j).ME{13,k} = BTC(j).ME{10,k}-BTC(j).ME{10,k-1};
       BTC(j).ME{14,k} = BTC(j).ME{13,k}/1000/25.4;
   end
end

%% Process Data to Make Average Data and Make Curves
% Transfer Information Into Average Table
for j = 1:4
   for k = 2:8
       BTC(5).ME{j+2,k} = BTC(j).ME{10,k};
   end
end
%Probe Averages
for k = 2:8
   BTC(5).ME{7,k} = mean([BTC(5).ME{3:4,k},BTC(5).ME{6,k}]);
   BTC(5).ME{8,k} = BTC(5).ME{7,k}/25400;
end
%Tip Clearance Reduction Based on Change in Averages
for k=3:8
   BTC(5).ME{10,k} = BTC(5).ME{7,k} - BTC(5).ME{7,k-1};
   BTC(5).ME{11,k} = BTC(5).ME{10,k}/(1000*25.4);
end
BTC(5).ME{11,9}=sum([BTC(5).ME{11,2:8}]);
%Total Blade Growth
z = zeros(4,7);
for j = 1:4
   for k = 1:7
       z(j,k) = sum([BTC(j).ME{13,2:k+1}])/-24500;
   end
end
zz = mean(z);
%Curve Fit
```

```
xx=[500,3e3,12e3,21e3,24e3,25500,27e3];
[xData, yData] = prepareCurveData( xx, zz );
ft = fittype( 'poly2' );
opts = fitoptions( 'Method', 'LinearLeastSquares' );
opts.Lower = [-Inf -Inf 0];
opts.Upper = [Inf Inf 0];
[fitresult, gof] = fit( xData, yData, ft, opts );
coeffs=coeffvalues(fitresult);
p1=coeffs(1);p2=coeffs(2);p3=coeffs(3);
x=linspace(0,27e3,27e3);
f=p1*x.^2 + p2*x + p3;
%correct for growth from 0 - 500 RPM
z=z+f(500);
zz=zz+f(500);
for k = 1:7
   BTC(5).ME{12,k+1} = zz(k);
end
close all

%Plot Blade Growth
BTC(5).GrowthPlotMEInches=figure('Name','GrowthPlotMEInches','Color',[1 1
1]);hold on;
for j = 1:4
   plot(xx,z(j,:))
end
plot(xx,zz,'--')
plot( x,f );
lgd = legend('1M','2M','3M','4M','Avg','Avg Fit');
lgd.Location='northwest';
xlabel(sprintf('TCR RPM'),'FontName','Times New Roman','FontSize',11.5);
ylabel(sprintf('Rotor Blade Radial Growth (in)'),'FontName','Times New
Roman','FontSize',11.5);
ax = gca;
ax.XTick = [0,500,3000,12000,21000 24000 25500 27000];
ax.XTickLabel = [0,500, 3000, 12000, 21000, 24000, 25500, 27000];
ax.XTickLabelRotation=55;
ax.FontSize = 11;
ax.FontName = 'Times New Roman';
xlim([-1000 27e3])
% set(gca, 'YDir','reverse')
set(gcf,'OuterPosition',[0 50 810 415]);
set(gca, 'Position', [.13 .21 .78 .72])
outerpos = ax.OuterPosition;
ti = ax.TightInset;
left = outerpos(1) + ti(1);
bottom = outerpos(2) + ti(2);
ax_width = outerpos(3) - ti(1) - ti(3);
ax_height = outerpos(4) - ti(2) - ti(4);
ax.Position = [left bottom ax_width ax_height];
grid on

BTC(5).ME{10,2} =f(500)*25400;
BTC(5).ME{10,9}=sum([BTC(5).ME{10,2:8}]);
BTC(5).ME{11,9}=BTC(5).ME{10,9}/25400;
```

```
%%
% %% Extract Data to Table Get Avg Convert to Inches (Leading Edge)
% %Open each converted tip clearance file one by one and run this
% clc
% F={'*500*','*300*','*1200*','*2100*','*2400*','*2550*','*2700*'};
% for i = 1:length(F)
% cd(TCRfilesLE)
% datafolder = dir(F{i});
% numfolder = length(datafolder);
% for j=1:numfolder
% cd(TCRfilesLE)
% cd(datafolder(j).name);
% files = dir(sprintf('%s\\*.mat',cd));
% numfiles = length(files);
% for k= 1:numfiles
%     fprintf('\nloading %s',files(k).name)
%     load(files(k).name)
%     BTC(k).LE{j+1,i+1}=TipClearance.avg;
%     close all
% end
% end
% cd(TCRfilesLE)
% for j = 1:4
% BTC(j).LE{10,i+1}=mean([BTC(j).LE{2:numfolder+1,i+1}]);
% BTC(j).LE{11,i+1}=BTC(j).LE{10,i+1}/25.4/1000;
% end
% end
% for j=1:4
%     for k =3:8
%         BTC(j).LE{13,k} = BTC(j).LE{10,k}-BTC(j).LE{10,k-1};
%         BTC(j).LE{14,k} = BTC(j).LE{13,k}/1000/25.4;
%     end
% end
%% Process Data to Make Average Data and Make Curves
%Probe Averages
for k = 2:8
   BTC(5).LE{7,k} = mean([BTC(5).LE{3:5,k}]); %leave out probe 4
   BTC(5).LE{8,k} = BTC(5).LE{7,k}/25400;
end
%Tip Clearance Reduction Based on Change in Averages
for k=3:8
   BTC(5).LE{10,k} = BTC(5).LE{7,k} - BTC(5).LE{7,k-1};
   BTC(5).LE{11,k} = BTC(5).LE{10,k}/(25400);
end
BTC(5).LE{11,9}=sum([BTC(5).LE{11,2:8}]);
%Total Blade Growth
z = zeros(3,7);
for j = 1:3 %omit 4
   for k = 1:7
       z(j,k) = sum([BTC(j).LE{13,2:k+1}])/-24500;
   end
end

zz = mean(z);
```

```
%Curve Fit
xx=[500,3e3,12e3,21e3,24e3,25500,27e3];
[xData, yData] = prepareCurveData( xx, zz );
ft = fittype( 'poly2' );
opts = fitoptions( 'Method', 'LinearLeastSquares' );
opts.Lower = [-Inf -Inf 0];
opts.Upper = [Inf Inf 0];
[fitresult, gof] = fit( xData, yData, ft, opts );
coeffs=coeffvalues(fitresult);
p1=coeffs(1);p2=coeffs(2);p3=coeffs(3);
x=linspace(0,27e3,27e3);
f=p1*x.^2 + p2*x + p3;
%correct for growth from 0 - 500 RPM
z=z+f(500);
zz=zz+f(500);
for k = 1:7
   BTC(5).LE{12,k+1} = zz(k);
end
close all

%Plot Blade Growth
BTC(5).GrowthPlotLEInches=figure('Name','GrowthPlotLEInches','Color',[1 1
1]);hold on;
for j = 1:3
   plot(xx,z(j,:))
end
plot(xx,zz,'--')
plot( x,f );
lgd = legend('1L','2L','3L','Avg','Avg Fit');
lgd.Location='northwest';
xlabel(sprintf('TCR RPM'),'FontName','Times New Roman','FontSize',11.5);
ylabel(sprintf('Rotor Blade Radial Growth (in)'),'FontName','Times New
Roman','FontSize',11.5);
ax = gca;
ax.XTick = [0,500,3000,12000,21000 24000 25500 27000];
ax.XTickLabel = [0,500, 3000, 12000, 21000, 24000, 25500, 27000];
ax.XTickLabelRotation=55;
ax.FontSize = 11;
ax.FontName = 'Times New Roman';
xlim([-1000 27e3])
% set(gca, 'YDir','reverse')
set(gcf,'OuterPosition',[0 50 810 415]);
set(gca, 'Position', [.13 .21 .78 .72])
outerpos = ax.OuterPosition;
ti = ax.TightInset;
left = outerpos(1) + ti(1);
bottom = outerpos(2) + ti(2);
ax_width = outerpos(3) - ti(1) - ti(3);
ax_height = outerpos(4) - ti(2) - ti(4);
ax.Position = [left bottom ax_width ax_height];
grid on

BTC(5).LE{10,2} =f(500)*25400;
BTC(5).LE{10,9}=sum([BTC(5).LE{10,2:8}]);
```

```
BTC(5).LE{11,9}=BTC(5).LE{10,9}/25400;
%% Extract Data to Table Get Avg Convert to Inches (Trailing Edge)
%Open each converted tip clearance file one by one and run this
clc
F={'*500*','*300*','*1200*','*2100*','*2400*','*2550*','*2700*'};
for i = 1:length(F)
cd(TCRfilesTE)
datafolder = dir(F{i});
numfolder = length(datafolder);
for j=1:numfolder
cd(TCRfilesTE)
cd(datafolder(j).name);
files = dir(sprintf('%s\\*.mat',cd));
numfiles = length(files);
for k= 1:numfiles
   fprintf('\nloading %s',files(k).name)
   load(files(k).name)
   BTC(k).TE{j+1,i+1}=TipClearance.avg;
   close all
end
end
cd(TCRfilesTE)
for j = 1:4
BTC(j).TE{10,i+1}=mean([BTC(j).TE{2:numfolder+1,i+1}]);
BTC(j).TE{11,i+1}=BTC(j).TE{10,i+1}/25.4/1000;
end
end
for j=1:4
   for k =3:8
       BTC(j).TE{13,k} = BTC(j).TE{10,k}-BTC(j).TE{10,k-1};
       BTC(j).TE{14,k} = BTC(j).TE{13,k}/1000/25.4;
   end
end
% Transfer Information Into Average Table
for j = 1:4
   for k = 2:8
       BTC(5).TE{j+2,k} = BTC(j).TE{10,k};
   end
end
%% Process Data to Make Average Data and Make Curves
%Probe Averages
for k = 2:8
   BTC(5).TE{7,k} = mean([BTC(5).TE{3:4,k},BTC(5).TE{6,k}]);
   BTC(5).TE{8,k} = BTC(5).TE{7,k}/25400;
end
%Tip Clearance Reduction Based on Change in Averages
for k=3:8
   BTC(5).TE{10,k} = BTC(5).TE{7,k} - BTC(5).TE{7,k-1};
   BTC(5).TE{11,k} = BTC(5).TE{10,k}/(1000*25.4);
end
BTC(5).TE{11,9}=sum([BTC(5).TE{11,2:8}]);
%Total Blade Growth
z = zeros(3,7);
for j = 1:2
```

```
   for k = 1:7
       z(j,k) = sum([BTC(j).TE{13,2:k+1}])/-24500;
   end
end
   for k =1:7 %Because we omit probe 3
       z(3,k) = sum([BTC(4).TE{13,2:k+1}])/-24500;
   end
zz = mean(z);
%Curve Fit
xx=[500,3e3,12e3,21e3,24e3,25500,27e3];
[xData, yData] = prepareCurveData( xx, zz );
ft = fittype( 'poly2' );
opts = fitoptions( 'Method', 'LinearLeastSquares' );
opts.Lower = [-Inf -Inf 0];
opts.Upper = [Inf Inf 0];
[fitresult, gof] = fit( xData, yData, ft, opts );
coeffs=coeffvalues(fitresult);
p1=coeffs(1);p2=coeffs(2);p3=coeffs(3);
x=linspace(0,27e3,27e3);
f=p1*x.^2 + p2*x + p3;
%correct for growth from 0 - 500 RPM
z=z+f(500);
zz=zz+f(500);
for k = 1:7
   BTC(5).TE{12,k+1} = zz(k);
end
close all

%Plot Blade Growth
BTC(5).GrowthPlotTEInches=figure('Name','GrowthPlotTEInches','Color',[1 1
1]);hold on;
for j = 1:3
   plot(xx,z(j,:))
end
plot(xx,zz,'--')
plot( x,f );
lgd = legend('1T','2T','4T','Avg','Avg Fit');
lgd.Location='northwest';
xlabel(sprintf('TCR RPM'),'FontName','Times New Roman','FontSize',11.5);
ylabel(sprintf('Rotor Blade Radial Growth (in)'),'FontName','Times New
Roman','FontSize',11.5);
ax = gca;
ax.XTick = [0,500,3000,12000,21000 24000 25500 27000];
ax.XTickLabel = [0,500, 3000, 12000, 21000, 24000, 25500, 27000];
ax.XTickLabelRotation=55;
ax.FontSize = 11;
ax.FontName = 'Times New Roman';
xlim([-1000 27e3])
% set(gca, 'YDir','reverse')
set(gcf,'OuterPosition',[0 50 810 415]);
set(gca, 'Position', [.13 .21 .78 .72])
outerpos = ax.OuterPosition;
ti = ax.TightInset;
left = outerpos(1) + ti(1);
```

```
bottom = outerpos(2) + ti(2);
ax_width = outerpos(3) - ti(1) - ti(3);
ax_height = outerpos(4) - ti(2) - ti(4);
ax.Position = [left bottom ax_width ax_height];
grid on

BTC(5).TE{10,2} =f(500)*25400;
BTC(5).TE{10,9}=sum([BTC(5).TE{10,2:8}]);
BTC(5).TE{11,9}=BTC(5).TE{10,9}/25400;
%% Average Plot Comparison
close all
BTC(5).AvgGrwPlt = figure('Name','Average Growth Plot','Color',[1 1 1]);
xx=[500,3e3,12e3,21e3,24e3,25500,27e3];
for k = 1:7
   Z(k) =   BTC(5).LE{12,k+1};
   zz(k) =  BTC(5).ME{12,k+1};
   zzz(k) = BTC(5).TE{12,k+1};
end
hold on
plot(xx,Z)
plot(xx,zz)
plot(xx,zzz)
lgd = legend('Leading Edge','Mid Chord','Trailing Edge');
lgd.Location='northwest';
xlabel(sprintf('TCR RPM'),'FontName','Times New Roman','FontSize',11.5);
ylabel(sprintf('Rotor Blade Radial Growth (in)'),'FontName','Times New
Roman','FontSize',11.5);
ax = gca;
ax.XTick = [0,500,3000,12000,21000 24000 25500 27000];
ax.XTickLabel = [0,500, 3000, 12000, 21000, 24000, 25500, 27000];
ax.XTickLabelRotation=55;
ax.FontSize = 11;
ax.FontName = 'Times New Roman';
xlim([-1000 27e3])
set(gcf,'OuterPosition',[0 50 810 415]);
set(gca, 'Position', [.13 .21 .78 .72])
outerpos = ax.OuterPosition;
ti = ax.TightInset;
left = outerpos(1) + ti(1);
bottom = outerpos(2) + ti(2);
ax_width = outerpos(3) - ti(1) - ti(3);
ax_height = outerpos(4) - ti(2) - ti(4);
ax.Position = [left bottom ax_width ax_height];
grid on
%% Model Data to Measured Data Comparison
fig1=figure('Name','GrowthPlotComparison','Color',[1 1 1]);hold on;
xx=[500,3e3,12e3,21e3,24e3,25500,27e3];
LEModel = [0 2.9e-5 4.65e-4 1.42e-3 1.86e-3 2.1e-3 2.35e-3];
MCModel = [0 7.9e-5 1.26e-3 3.87e-3 5.06e-3 5.71e-3 6.4e-3];
Adj = 0.009214/0.0108;
TEModel=[0 1.34e-4 2.14e-3 6.56e-3 8.57e-3 9.68e-3 1.08e-2];
TEModelAdj=TEModel.*Adj;
MC = zeros(1,7);TE=MC;LE=MC;
for k = 1:7
```

```
LE(k) = BTC(5).LE{12,k+1};
MC(k) = BTC(5).ME{12,k+1};
TE(k) = BTC(5).TE{12,k+1};
end

hold on
% plot(xx,LEModel,'--r')
% plot(xx,MCModel,'--black')
plot(xx,TEModel,'--black')
plot(xx,TEModelAdj,'--r')
% plot(xx,LE,'r')
% plot(xx,MC,'black')
plot(xx,TE,'b')
TE1 = TE + 0.00114;
TE2 = TE - 0.00101;
plot(xx,TE1,'-.b')
plot(xx,TE2,'-.b')

lgd = legend('Trailing Edge Model','Adjusted Trailing Edge Model','Measured
Trailing Edge','Error Band');
lgd.Location='northwest';
xlabel(sprintf('TCR RPM'),'FontName','Times New Roman','FontSize',11.5);
ylabel(sprintf('Blade Radial Growth (in.)'),'FontName','Times New
Roman','FontSize',11.5);
ax = gca;
ax.XTick = [0,500,3000,12000,21000 24000 25500 27000];
ax.XTickLabel = [0,500, 3000, 12000, 21000, 24000, 25500, 27000];
ax.XTickLabelRotation=55;
ax.FontSize = 11;
ax.FontName = 'Times New Roman';
xlim([0 27e3])
set(gcf,'OuterPosition',[0 50 810 415]);
set(gca, 'Position', [.13 .21 .78 .72])
outerpos = ax.OuterPosition;
ti = ax.TightInset;
left = outerpos(1) + ti(1);
bottom = outerpos(2) + ti(2);
ax_width = outerpos(3) - ti(1) - ti(3);
ax_height = outerpos(4) - ti(2) - ti(4);
ax.Position = [left bottom ax_width ax_height];
grid on
```

H. TCR CALIBRATION VERIFICATION

```
%% BCTR Calibration validation for use on TCR
cd('specify')
close all
folderpath = 'specify';
cd(folderpath)
folders = dir(folderpath);
fpc='Specify';
for j = 2:3
filepath = sprintf('%s\\%s',folderpath,folders(j+2).name);
```

```
for k = 1:4
cd(filepath)
[RD,OPR] = TC_GetData(sprintf('%s\\*.csv',cd),filepath,k,'.csv');
up = find(diff(OPR)>0);
Revs = length(up);
Revs = round(0.95*Revs);
[dsRD,sFD,~,~,~,IL] = TC_IntFFTFilt(RD,OPR,k,'.csv',Revs);
[BPInt] = TC_OPR(Revs,IL);
CalFileNo=4+k;
cd(fpc); %go to cal file
fd = sprintf('%s\\*.mat',fpc); %find all the mat files in the cal folder
files = dir(fd); %put them into a string vector
cname = files(CalFileNo).name; %name of the cal file
load(cname);
close all;
fprintf('Beginning conversion using\nCalFile:%s\n\n',cname)
[xData, yData] = prepareCurveData( TC_.Cal(1,:), TC_.Cal(5,:));
ft = fittype( 'exp2' );
opts = fitoptions( 'Method', 'NonlinearLeastSquares' );
opts.Display = 'Off';
opts.StartPoint = [226.551875237484 -0.000421970891327102 1873.62771497954 -
0.00024879381329672];
[fitresult, gof] = fit( xData, yData, ft, opts );
coeffs=coeffvalues(fitresult);
a=coeffs(1);b=coeffs(2);c=coeffs(3);d=coeffs(4);
x=linspace(0,TC_.Cal(1,1),10e3);
f = a*exp(b*x)+c*exp(d*x);
plot(x,f,'r');title(sprintf('%s',cname))
fprintf('Converting to micrometers using equation\n\n')
%Find longest blade using filtered signal
pkpkfiltered=zeros(Revs,20);
for jjjj = 1:Revs-1
for kkkk=1:20
A = sFD(BPInt(jjjj,kkkk):BPInt(jjjj,kkkk+1));
pkpkfiltered(jjjj,kkkk)=max(A)-min(A);
end
end
pkpkavg=mean(pkpkfiltered);
LB = find(pkpkavg==max(pkpkavg));
%Find Longest Blade Average and Convert it Using Equation 2
pkpkavgLB = mean(pkpkfiltered(:,LB));
x=pkpkavgLB;
f = a*exp(b*x)+c*exp(d*x);
ANSWER(j,k)=f;

end
end
ProbeTC = ANSWER';
%%
ProbeTCinches = ProbeTC/25400
ProbeTCDiff=(ProbeTC(:,3)-ProbeTC(:,2))./25400
% ProbeAvg=mean(ProbeTC)
% Growth = abs(ProbeAvg(1)-ProbeAvg(2))
```

THIS PAGE INTENTIONALLY LEFT BLANK

LIST OF REFERENCES

[1] A. Londoño, "Near-stall modal disturbances within a transonic compressor rotor," M.S thesis, Dept. of Mech. And Aero. Eng. NPS, Monterey, CA, USA, 2011. [Online.] Available: http://hdl.handle.net/10945/10641

[2] B. Yu, H. Ke, E. Shen and T. Zhang, "A review of blade tip clearance - measuring technologies for gas turbine engines," *Measurement and Control,* vol. 53, no. 2020, pp. 339–357, 2020. [Online.] Available: https://journals.sagepub.com/doi/full/10.1177/0020294019877514

[3] P. Lampart, "Tip leakage flow in turbines," Institute of Fluid-Flow Machinery, Polish Academy of Sciences, Gdansk, Poland, 2006. [Online.] Available: Research Gate

[4] J. J. Adamczyk, M. L. Celestina and E. M. Greitzer, "The role of tip clearance in high-speed fan stall," *Journal of Turbomachinery,* vol. 115, no. 1, pp. 28–38, 1993. [Online.] Available: Research Gate

[5] G. R. Miller and E. E. Bailey, "Static pressure contours in the blade passage at the tip of several high Mach number rotors," National Aeronautics and Space Administration, Washington, D.C., USA, 1971. [Online.] Available: NASA

[6] M. W. Leitner, M. Zippel and S. Staudacher, "The interaction of tip leakage with incoming flow in a compressor cascade," Institute of Aircraft Propulsion Systems Stuttgart University, Suttgart, Germany, 2016. [Online.] Available: https://www.dglr.de/publikationen/2016/420023.pdf

[7] I. Garcia, R. Przysowa, J. Amorebieta and J. Zubia, "Tip-clearance in the first stage of the compressor of an aircraft engine," *Sensors (Basel, Switzerland),* vol. 16, no. 11, p. 1897, 2016. [Online.] Available: https://www.ncbi.nlm.nih.gov/pmc/articles/PMC5134556/

[8] M. J. Ford, R. E. Honeycutt, R. E. Nordlund and W. W. Robinson, "Advanced optical blade tip clearance measurement system," National Aeronautics and Space Administration, Washington, D. C., USA, 1978. [Online.] Available: NASA

[9] H. R. Simmons, D. L. Michalsky, K. E. Brewer and A. J. Smalley, "Measuring rotor and blade dynamics using an optical blade tip sensor," *The American Society of Mechanical Engineers,* 1990. [Online.] Available: ASME

[10]] J. Wu, B. Wen, Y. Zhou, Q. Zhang, S. Ding, F. Du and S. Zhang, "Eddy current sensor system for blade tip clearance measurement based on a speed adjustment model," Basel, Switzerland. MDPI, 2019. [Online.] Available: https://www.mdpi.com/1424-8220/19/4/761

[11] J. W. H. Chivers, "A technique for the measurement of blade tip clearance in a gas turbine," Imperial College, London, UK, 1989. [Online.] Available: https://spiral.imperial.ac.uk/bitstream/10044/1/7408/1/John_William_Hender_Chivers-1989-PhD-Thesis.pdf

[12] A. G. Sheard and B. Killeen, "A blade by blade tip clearance measurement system for gas turbine applications," *Journal of Engineering for Gas Turbines and Power,* vol. 117, no. 2, pp. 326–331, 1995. [Online.] Available: ASME

[13] D. Muller, A. G. Sheard, S. Mozumdar and E. Johann, "Capacitive measurement of compressor and turbine blade tip to casing running clearance," *The American Society of Mechanical Engineers,* vol. 96, 1996. [Online.] Available: ASME

[14] A. G. Sheard, "Blade by blade tip clearance measurement," *International Journal of Rotating Machinery,* vol. 2011, 2011. [Online.] Available: ASME

[15] J. D. Stubbs and M. A. Shahid, "Blade tip clearance measurement system for high speed turbomachinery applications and the potential for blade tip timing applications," in *Proceedings of ASME Turbo Expo 2020*, Virtual, Online, 2020. [Online.] Available: ASME

[16] S. J. Gill, M. Ingallinera and A. G. Sheard, "Turbine tip clearance system measurement system evaluation on an industrial gas turbine," in *International Gas Turbine and Aeroengine Congress and Exhibition*, Orlando, FL, 1997. [Online.] Available: ASME

[17] A. G. Sheard, S. G. O'Donnell and J. F. Stringfellow, "High temperature proximity measurement in aero and industrial turbomachinery," *Journal of Engineering for Gas Turbines and Power,* vol. 121, no. 1, pp. 167–173, 1997. [Online.] Available: ASME

[18] Rotadata, "Rotadata" Accessed 8 November 2021. [Online]. Available: https://www.rotadata.com

[19] G. D. Thornton, "Fluid-structure analysis of a transonic rotor," M.S thesis, Dept. of Mech. And Aero. Eng. NPS, Monterey, CA, USA, 2019. [Online.] Available: https://calhoun.nps.edu/handle/10945/62704

[20] B. L. Meinster, “Stall characteristic prediction in a single passage of a transonic axial compressor rotor,” M.S thesis, Dept. of Mech. And Aero. Eng. NPS, Monterey, CA, USA, 2021. [Online.] Available: https://calhoun.nps.edu/handle/10945/67780

[21] D. M. Magno, A. J. Gannon and W. C. Smith, “Analytical methods for transonic compressor rotor blade tip clearance measurements using capacitive probes,” *Turbo Expo,* June 2022. [Online.] Available: ASME

[22] Rotadata Ltd., “RCap V blade tip clearance system user manual v 1.0”, Derby, UK: Rotadata, Ltd., 2020.

[23] National Instruments, “Specifications cRIO – 9042,” National Instruments, 2018. [Online.] Available: ni.com

[24] Thor Labs, Inc., “Thor Labs,” Accessed 12 April 2022. [Online]. Available: https://www.thorlabs.com/

[25] Mitutoyo, “Mitutoyo,” Mitutoyo America Corp. Accessed 9 April 2022. [Online]. Available: https://www.mitutoyo.com/products/small-tool-instruments-and-data-management/indicators/digimatic-indicators/absolute-digimatic-indicator-id-c

[26] Velmex, Inc., “Velmex, Inc.,” 2016. [Online]. Available: https://www.velmex.com/Index.html

[27] W. D. Callister and D. G. Rethwisch, “Properties of selected engineering materials,” in *Material Science and Engineering, An Introduction*, 9th Ed., New York: John Wiley & Sons, Inc., 2014. pp. 882-910.

[28] R. D. Zucker and O. Biblarz, “Introduction to compressible flow,” in *Fundamentals of Gas Dynamics*, 2nd Ed., Hoboken, New Jersey, USA: John Wiley & Sons, Inc., 2002. pp. 83-102.

[29] Rotadata, Ltd., “Capacitance probe data sheet,” Data Sheet. Derby, UK: Rotadata, Ltd., 2020.

[30] GMN Bearing USA, “ High precision ball bearings,” Accessed 12 April 2021. Data Sheet. Houston, TX. GMN Bearing USA. [Online.] Available: gmnbt.com

[31] Monarch Instruments, “Monarch instruments data sheet,” Data Sheet. Amherst, NH: Monarch Instruments, 2020. [Online.] Available: https://monarchinstrument.com/

[32] P. Hill and C. Peterson, “Axial compressors,” in *Mechanics and Thermodynamics of Propulsion*, 2nd Ed., Reading, MA, USA: Addison-Wesley. 1992. pp. 275-366.

[33] D. Japikse and N. C. Baines, *Introduction to Turbomachinery*, Norwich, Vermont, USA: Concepts ETI, Inc. and Oxford University Press, 1994.

[34] K. Harman, “Continued modernization of the NPS transonic compressor test rig,” M.S thesis, Dept. of Mech. And Aero. Eng. NPS, Monterey, CA, USA, 2019. [Online.] Available: https://calhoun.nps.edu/handle/10945/63456

[35] R. Eckert, “Performance analysis and initial tests of a transonic turbine test rig,” M.S thesis, Dept. of Mech. And Aero. Eng. NPS, Monterey, CA, USA, 1966. [Online.] Available: https://calhoun.nps.edu/handle/10945/9605

[36] S. W. Smith, *The Scientist and Engineer’s Guide to Digital Dignal Processing*, San Diego, CA, USA: California Technical Publishing, 1997. [Online.] Available: http://www.dspguide.com/pdfbook.htm

INITIAL DISTRIBUTION LIST

1. Defense Technical Information Center
   Ft. Belvoir, Virginia

2. Dudley Knox Library
   Naval Postgraduate School
   Monterey, California